Final Technical Report

10/14/2015

Combined Heat and Power Systems Technology Development and Demonstration 370 kW High Efficiency Microturbine

DOE Project ID # DE-EE0004258

Capstone Turbine Corporation

DISCLAIMER

This report was prepared as an account of work sponsored by an agency of the United States Government. Neither the United States Government nor any agency thereof, nor any of their employees, makes any warranty, express or implied, or assumes any legal liability or responsibility for the accuracy, completeness, or usefulness of any information, apparatus, product, or process disclosed, or represents that its use would not infringe privately owned rights. Reference herein to any specific commercial product, process, or service by trade name, trademark, manufacturer, or otherwise does not necessarily constitute or imply its endorsement, recommendation, or favoring by the United States Government or any agency thereof. The views and opinions of authors expressed herein do not necessarily state or reflect those of the United States Government or any agency thereof.

Table of Contents

List of Figures

List of Tables

1. Executive Summary

The C370 Program was awarded in October 2010 with the ambitious goal of designing and testing the most electrically efficient recuperated microturbine engine at a rated power of less than 500 kW. The aggressive targets for electrical efficiency, emission regulatory compliance, and the estimated price point make the system state-of-the-art for microturbine engine systems. These goals will be met by designing a two stage microturbine engine identified as the low pressure spool and high pressure spool that are based on derivative hardware of Capstone's current commercially available engines.

The development and testing of the engine occurred in two phases. Phase I focused on developing a higher power and more efficient engine, that would become the low pressure spool which is based on Capstone's C200 (200kW) engine architecture. Phase II integrated the low pressure spool created in Phase I with the high pressure spool, which is based on Capstone's C65 (65 kW) commercially available engine. Integration of the engines, based on preliminary research, would allow the dual spool engine to provide electrical power in excess of 370 kW, with electrical efficiency approaching 42%. If both of these targets were met coupled with the overall CHP target of 85% total combined heating and electrical efficiency California Air Resources Board (CARB) level emissions, and a price target of $600 per kW, the system would represent a step change in the currently available commercial generation technology.

Phase I of the C370 program required the development of the C370 low pressure spool. The goal was to increase the C200 engine power by a minimum of 25% — 250 kW — and efficiency from 32% to 37%. These increases in the C200 engine output were imperative to meet the power requirements of the engine when both spools were integrated. An additional benefit of designing and testing the C370 low pressure spool was the possibility of developing a stand-alone product for possible commercialization.

The low pressure spool design activity focused on an aeropath derivative of the current C200 engine. The aeropath derivative included changes to the compressor section —compressor and inducer — and to the turbine nozzle. The increased power also necessitated a larger, more powerful generator and generator controller to support the increased power requirements. These two major design changes were completed by utilizing both advanced 3D modeling and computational fluid dynamics modelling. After design, modeling, and analysis, the decision was made to acquire and integrate the components for testing.

The second task of Phase I was to integrate and test the components of the low pressure spool to validate power and efficiency. Acquisition of the components for the low pressure spool was completed utilizing Capstone's current supplier base. Utilization of Capstone's supply base for integration of the test article would allow — if the decision was made —expedited commercialization of the product. After integration of the engine components, the engine was tested and evaluated for performance and emissions. Test data analysis confirmed that the engine met all power and efficiency requirements and did so while maintaining CARB level emissions. The emissions were met without the use of any post processing or catalyst. After testing was completed, the DOE authorized — via a milestone review — proceeding to Phase II: the development of the integrated C370 engine.

The C370 high pressure spool design activity required significant changes to the C65 engine architecture. The engine required a high power density generator, completely redesigned compressor stage, turbine section, recuperator, controls architecture, and intercooler stage as well aerodynamic interconnects between stages. The design of the engine was completed by utilizing both expert internal resources and contracting industry experts.

The two most critical design challenges were the turbine section (the nozzle and turbine) and the controls architecture. The design and analysis of all of the components was completed and integrated into a system model. The system model — after numerous iterations — indicated that, once integrated, the engine will meet or exceed all system requirements. Unfortunately, the turbine section's life requirements remain a technical challenge and will require continued refinement of the bi-metallic turbine wheel design and manufacturing approach to meet the life requirement at theses high temperatures. The current controls architecture requires substantial effort to develop a system capable of handling the high-speed, near real-time controls requirement, but it was determined not to be a technical roadblock for the project.

The C370 Program has been a significant effort with state-of-the-art technical targets. The targets have pushed Capstone's designers to the limits of current technology. The program has been fortunate to see many successes: the successful testing of the low pressure spool (C250), the development of new material processes, and the implementation of new design practices. The technology and practices learned during the program will be utilized in Capstone's current product lines and future products. The C370 Program has been a resounding success on many fronts for the DOE and for Capstone.

2. Award No. and Name of Recipient

DOE Award # DE- EE0004258 to Capstone Turbine Corp.

3. Project Title and Name of Project Director

High Efficiency 370kW Microturbine with Integral Heat Recovery — Steve Gillette (initial) and Dan Vicario (final)

4. Date of Report and Period Covered

Final Technical Report dated July 31, 2015 for project work during the period of October 1, 2010 through August 31, 2015.

5. Comparison of Accomplishments with Goals/Objectives

<u>Task #1: Early Technology Validation and Risk Mitigation</u>

The primary goal of this task was to transform the current C200 engine into the low pressure spool of the C370 engine and validate the C370 cycle. This task was completed and was successful in achieving target performance goals.

<u>Task #2: C370 Low Pressure Sub-system Design</u>

The primary goal of this task was to build prototype hardware of the C370 low pressure assembly as a C250 engine to allow complete assembly testing. This prototype would also serve as a potential uprated design of the current C200 engine. Prototype testing of this assembly was successfully accomplished in the laboratory with the assembly meeting target performance goals set out to support the C370 requirements.

Task #3: C370 Two Shaft Engine Development

The primary goal of this task was to complete the detail design of the C370 system — including controls, electronics assemblies, and package. Capstone completed the conceptual design of the system but did not include the package at this stage. This exclusion was due to the initial prototype engine hardware configuration not being in the final, compact form it would likely take once in production. A decision was made to do initial prototype testing in a slightly altered configuration to allow for better performance measurement capability. The high-risk hardware was procured and tested per the goals of the task. This included the higher capacity power electronics controllers and a scaled bi-metallic transient liquid phase bonded turbine wheel that was tested in a slave C65 engine.

6. Project Activity Summary

6.1. C370 Initial Cycle Definition & Initial Development Testing

6.1.1. Cycle Sensitivity Studies

Initial studies resulting from the DOE-sponsored C200 AMTS program provided critical analysis for the start of the C370 program. A detailed engineering report shows the analysis of the following configurations:

1) Single Shaft, Single Generator, Single Burner [1S1G1B], baseline case
2) Single Shaft, Single Generator, Single Burner [1S1G1B], high pressure ratio
3) Single Shaft, Single Generator, Single Burner [1S1G1B], high pressure ratio and TIT
4) Two Shaft, Two Generator, Two Burner [2S2G2B]
5) Two Shaft, Two Generator, One Burner [2S2G1B]
6) Two Shaft, One HP Generator, One Burner [2S1HPG1B]
7) Two Shaft, One LP Generator, One Burner [2S1LPG1B]
8) Two Shaft, One HP Generator, One Burner, Medium Pressure Heat Exchanger [2S1HPGMPQX]
9) Three Shaft, One LP Generator on Free Power Turbine, One Burner [3S1G1B]
10) C30-C200, (special case of 2S2G2B) [C30-C200].

Initial performance studies were done to evaluate the potential of each configuration. The results of these studies can be seen in Table 1. The first three cases were the cases of the C200 AMTS running at different pressure and temperature conditions.

Case No	Configuration	mdot	LP Ratio	HP Ratio	HP Eratio	LP Eratio	HP TIT
1	1S1G1B	2.2	4.0			3.80	
2	1S1G1B	2.2	16.0			15.2	
3	1S1G1B	2.2	16.0			15.2	
4	2S2G2B	2.2	4.0	4.0	3.84	3.84	1750
5	2S2G1B	2.2	4.0	4.0	3.88	3.88	2330
6	2S1HPG1B	2.2	4.0	4.0	7.18	2.10	2330
7	2S1LPG1B	2.2	4.0	4.0	1.70	8.84	2330
8	2S1HPGMPQX	2.2	4.0	4.0	4.20	3.59	2330
9	3S1G1B	2.2	4.0	4.0	1.73/1.70	5.12	2330/2042
10	C30-C200	2.9	4.2	3.6	3.40	3.95	1550

Case No	Configuration	LP TIT (°F)	LP TET (°F)	LP Power (kW)	HP Power (kW)	Total Power (kW)	Efficiency (%)
1	1S1G1B	1750	1230	148		148	34.6
2	1S1G1B	1750	841	146		146	24.4
3	1S1G1B	2330	1183	289		289	36.5
4	2S2G2B	1750	1227	152	136	289	37.4
5	2S2G1B	1664	1158	143	223	365	43.3
6	2S1HPG1B	1428	1165	0	362	362	43.1
7	2S1LPG1B	2042	1169	359	0	359	42.9
8	2S1HPGMPQX	712	447	0	239	239	41.4
9	3S1G1B	1777	1156	367	0.0/0.0	367	43.4
10	C30-C200	1750	1205	211	128	339	35.4

Table 1: Performance Predictions of Various Turbine Engine Configurations

Case No	Configuration	Attractive	Comments
4	2S2G2B	Yes	Requires high speed, high power generator
5	2S2G1B	No	HP TIT too high at simulated conditions
6	2S1HPG1B	No	HP expansion ratio too high
7	2S1LPG1B	No	LP expansion too high, two ceramic turbines
8	2S1HPGMPQX	No	Recuperator inlet temperature too high
9	3S1G1B	Yes	Two ceramic turbines, one metallic
10	C30-C200	Yes	Requires high speed, high power generator

Table 2: Summary of Finding for the Different Engine Configurations

At the time that the C200 AMTS report was written, the recommendation was to go forward with Case 10. At the start of the C370 program — approximately five years after the C200 AMTS report — the goal had shifted to achieve much higher efficiencies. Looking at the tradeoff analysis in Table 1, it was clear that only three configurations would achieve the efficiencies desired — cases 5, 6, and 7. As noted, both cases 6 and 7 had expansion ratios that were too high to be practically realized in a single stage. Therefore case 5 was targeted as the best go-forward configuration for the C370 engine. This approach required determining a technical solution to the HP stage elevated turbine inlet temperatures that were above the limits of the available technology. The rest of the cycle was not technically difficult for Capstone to achieve.

6.1.2. Mechanical Configuration Selection

Figure 1 shows the layout of the primary components in the engine cycle chosen. This is a representation of case 5.

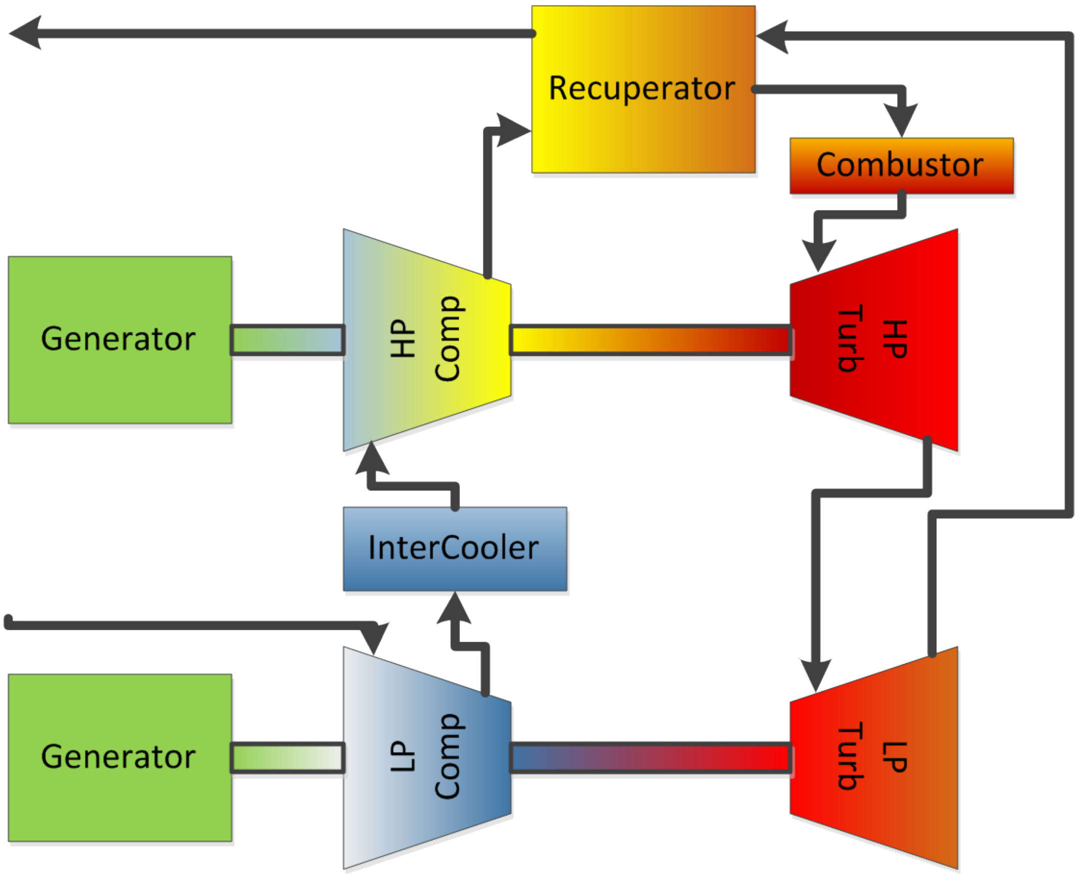

Figure 1: Initial Cycle for C370 Engine

Initial Cycle Analysis determined that it might be possible to upsize the current C200 engine and use it as the LP (low pressure) assembly in the C370 engine. This approach had the added benefit of providing an additional commercial product that could replace the current C200 engine. The power and efficiency goals for each engine based on the initial analysis were:

- CARB-compliant C250 system: 250kW and 37% efficiency
- CARB-compliant C370 engine: +370kW, +42% efficiency and +85% thermal efficiency

6.1.3. Cycle Performance and Component Concept Approach

The first step in identifying the component performance requirements was to baseline the C200 engine maximum performance. To accomplish this, a test was run with a modified C200 system that would allow the operation of the engine at much higher speeds to discover the performance limitations. The engine stopped making power and lost efficiency at speeds above 63 krpm. This was determined to be a result of the compressor stage flow capacity limitations.

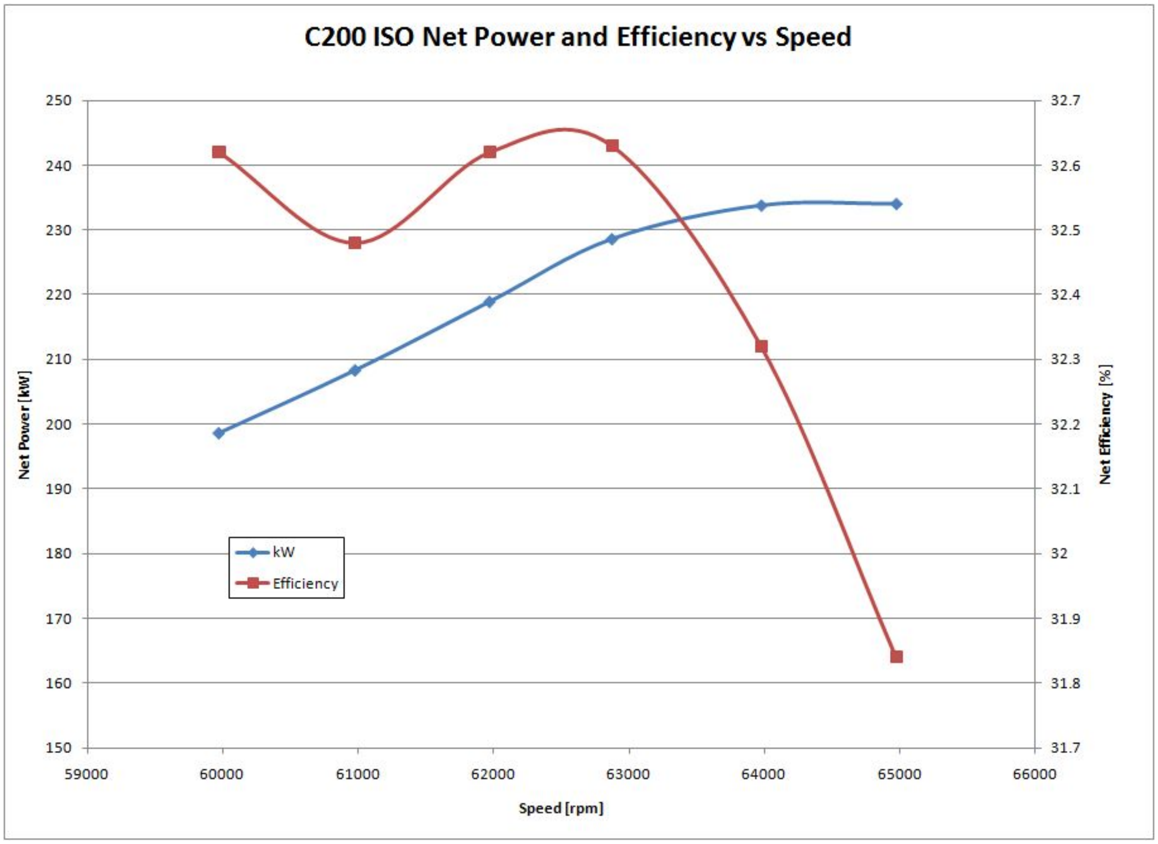

Figure 2: C200 Engine Over Speed Test Results

Reviewing the C200 design with a change to the compressor resulted in a potential increase of pressure ratio and airflow from 1.2 kg/sec at a pressure ratio of 4.0 to 1.5 kg/sec at a pressure ratio of 4.8 for the design speed of 60 krpm. The performance of the engine with this modified compressor is as follows:

- 270 kW system power
- 34.7% system efficiency
- 60 krpm engine speed
- 1.54 kg/sec mass flow
- 1780 °F TIT (turbine inlet temperature)

Since this analysis showed that this operating condition essentially met our goals, it was selected and used to determine which components would have to change. The engine components identified for redesign are:

- Compressor wheel and diffuser
- Turbine nozzle
- Combustor and injectors

- Generator

While the detailed design of the C370 LP design was underway, further refinements and studies were done to outline the performance of the complete C370 engine with the new C250 engine configuration components as a function of the HP (high pressure) TIT. As the initial results predicted, the HP TIT would need to be above 2275 °F to reach the target efficiency of greater than 42% at the system level.

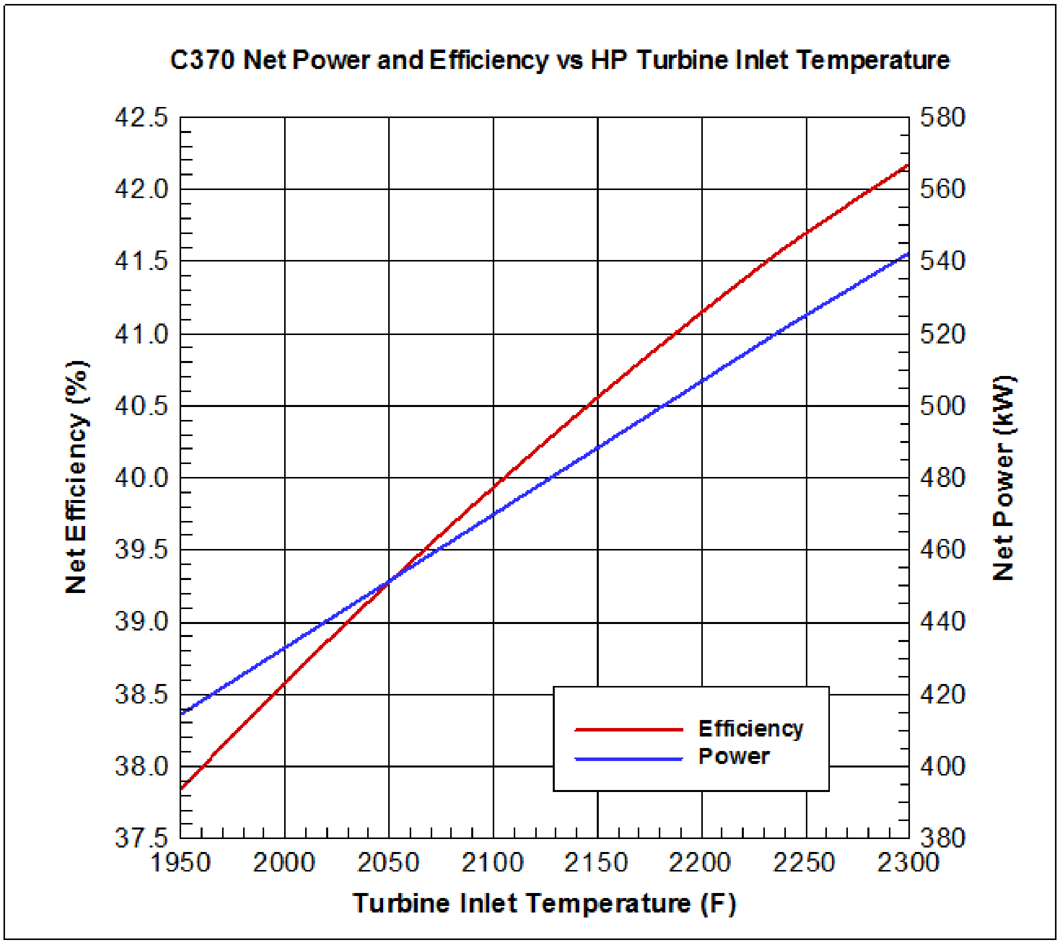

Figure 3: C370 Power and Efficiency vs TIT

With the LP spool components determined, and based on the results shown in Figure 3, the updated C370 target cycle was defined as the basis for identifying the specific design requirements of the C370 components. A target was chosen as the cycle that met 42% engine efficiency — only system efficiency is shown in cycle analysis — at an operating point with as low a TIT as possible (2200 °F) and under conditions at which the C250/C370 LP spool was capable of running.

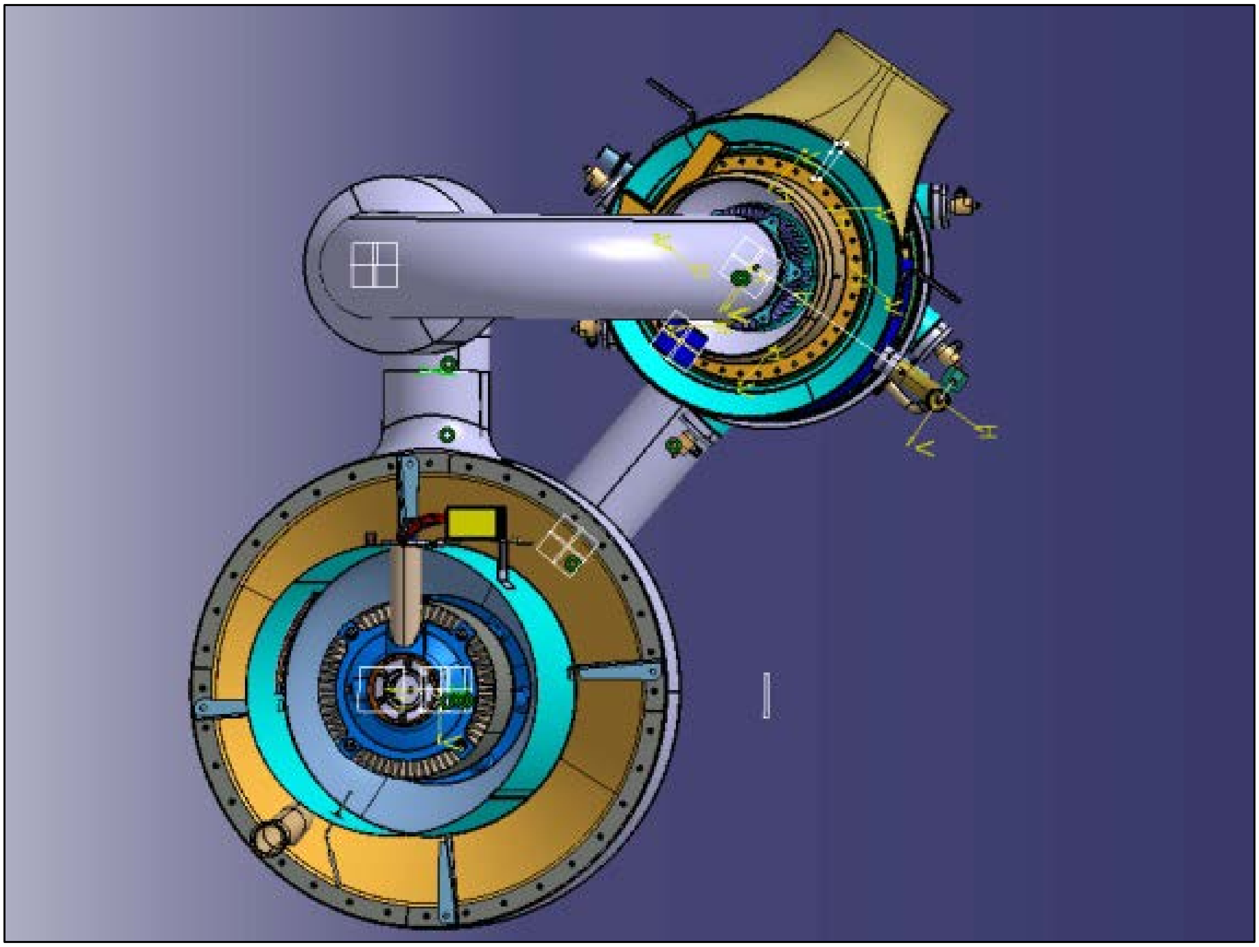

Figure 4: C370 Concept Drawing

Figure 4 is a rendering of the anticipated appearance of the chosen configuration. The key technical component developments for the C370 system — based on the concept drawing and the cycle analysis — were identified to be:

- High temperature in high pressure turbine wheel
- High temperature turbine nozzle
- High pressure and effectiveness recuperator – 11:1
- Dual high power generators – both LP and HP spool
- Dual spool controls
- High temperature low emissions combustor
- Inter stage compressor intercooler
- Higher power electronics controllers
- Water cooling/heat exchange system
- HP/LP turbine and compressor volutes

6.1.4. High Pressure Turbine Wheel Concept Approach

In order to mitigate the foremost technical risk early in development, significant effort was expended on the design of a C370 high pressure turbine wheel. This effort was in parallel with the C250 hardware design. Two potential methods were identified to operate the wheel at the speeds and temperatures required.

The first was to use a ceramic (Silicon Nitride) wheel. While the ceramic wheel was a viable option, it was rejected due to the extremely low yield rates of current manufacturing capabilities. Capstone was looking for a solution that was consistently reproducible using proven manufacturing processes.

The other option was to use a single crystal alloy metal, but this approach also had issues. Larger turbines grow individual axial turbine blades out of single crystal alloys, but a single radial turbine wheel was too complex a shape to grow. To address this problem, Capstone decided to grow just the blade tips that see the highest heat and stress due to high speed rotation and bond them to a high-temperature nickel alloy turbine hub. With this approach — illustrated in Figure 5 — Capstone believed that they could manufacture a wheel able to operate at or near the C370 design point without melting.

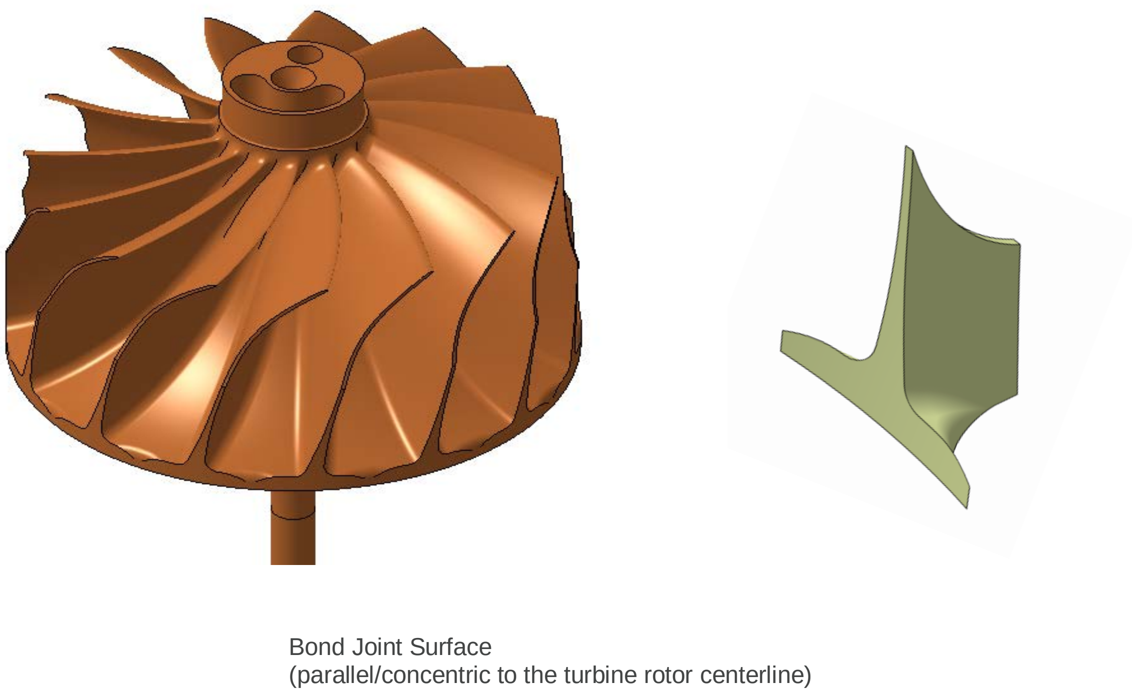

Figure 5: C370 High Pressure Turbine Wheel Bi-Metallic Design Concept

6.2. Low Pressure Spool Design (C250)

6.2.1. C250 Cycle Model

A C250 cycle model was developed. This model was based on cycle analysis conducted in the early stages of the program. The objective of the cycle model was to evaluate final C250 performance and provide design targets for subcomponents at ISO conditions — sea level, 60% relative humidity, and 59 °F ambient temperature. The key results of the C250 cycle model are listed in Table 3.

It was determined that the C250 will generate 294.2 kW and have 36.7% efficiency at generator lead. The compressor stage is expected to provide 5:1 pressure ratio with 82.5% stage efficiency. The recuperator will provide an effectiveness of 0.88, with a pressure drop of 1.6% on the air side and 3.8% on the gas side. The turbine stage is targeted at 87.4% efficiency and the generator at 98%.

C250 Key Performance – System		
Description	**Unit**	**Value**
Engine Speed	rpm	60000
Control TET	°F	1150
Ambient Temperature	°F	59
Ambient Pressure	psi	14.696
Relative Humidity	%	60
Power Output at Inverter	kW	278.7
System Efficiency Based on Inverter Power	%	34.75
Power Output at Generator Lead	kW	294.2
System Efficiency Based on Generator Power	%	36.7
Compressor Pressure Ratio		5
Compressor Stage Efficiency	%	82.5%
Recuperator Effectiveness		0.8809
Recuperator Pressure Drop - Air Side	%	1.6%
Recuperator Pressure Drop - Gas Side	%	3.8%
Fuel Flow Rate	lb/hr	133.532
Pressure Expansion Ratio		4.45
Turbine Stage Efficiency	%	87.4%
Generator Efficiency	%	98.0%

Table 3: C250 Key Performance Parameters (ISO Conditions)

The same cycle model also provided off-design performance predictions at less ideal conditions — sea level, 70 °F — for a more realistic set of operating conditions. The results of this predictive model are shown in Table 4. Under these conditions, generator power output drops to 278 kW and efficiency to 36.1.

C250 Key Performance - System		
Description	**Unit**	**Value**
Engine Speed	rpm	60000
Control TET	°F	1150
Ambient Temperature	°F	70
Ambient Pressure	psi	14.696
Relative Humidity	%	60
Power Output at Inverter	kW	263.1
System Efficiency Based on Inverter Power	%	34.21
Power Output at Generator Lead	kW	278
System Efficiency Based on Generator Power	%	36.1

Table 4: C250 Performance Prediction (Sea Level, 70 °F)

A complete performance prediction at different ambient temperature is shown in Figure 6.

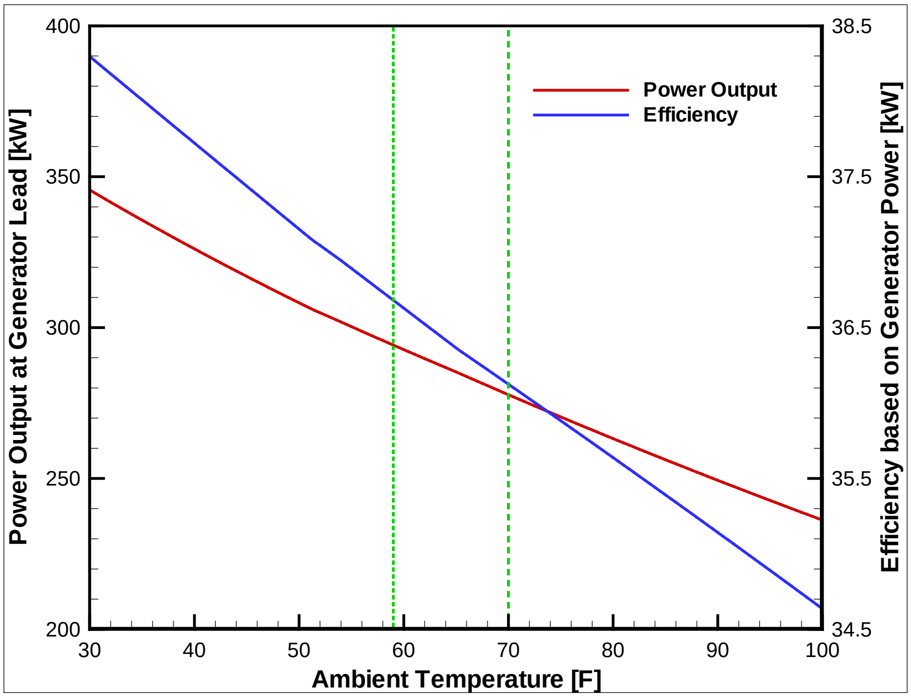

Figure 6: C250 Performance Prediction at Different Ambient Temperatures (at Sea Level)

6.2.2. Motor/Generator Design

The motor/generator design was one of the most critical components to design on the C250 due to the constraints on size. After initial rotor analysis and testing was done, it was determined that the rotor length could only be increased by 10% due to the rotor dynamics associated with this design. Figure 7 is a graphical representation of the rotor dynamic analysis.

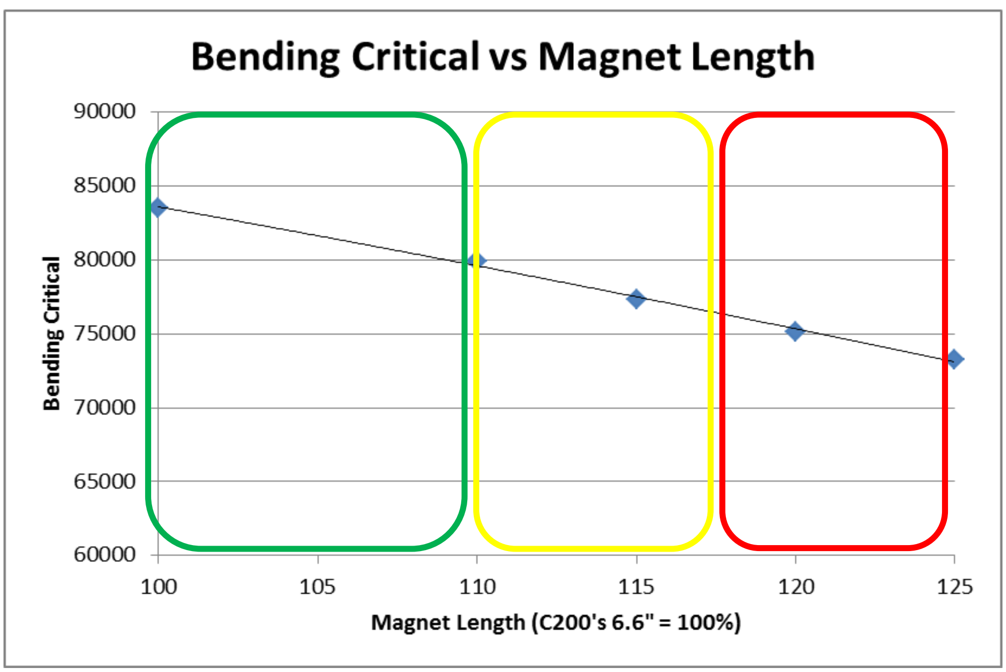

Figure 7: C250 Rotor Bending Analysis as a Function of Rotor Length

Since the diameter was fixed and the length was limited, another solution was needed to increase the stator power from the C200 220 kW specification level to the predicted C250 296 kW specification. This was accomplished with a change of material to a newer Samarium Cobalt material that was recently introduced. This material has a higher flux density than the C200 rotor magnet material. This allowed completion of the rotor design with an unchanged diameter. With the rotor design finalized, specification and design of the stator began.

STATOR DESIGN REQUIREMENTS

The dimensional constraints to which the new stator was subject are shown in Figure 8. Accounting for these dimensional constraints, performance design constraints were derived from cycle analysis and controls design inputs. See Table 5.

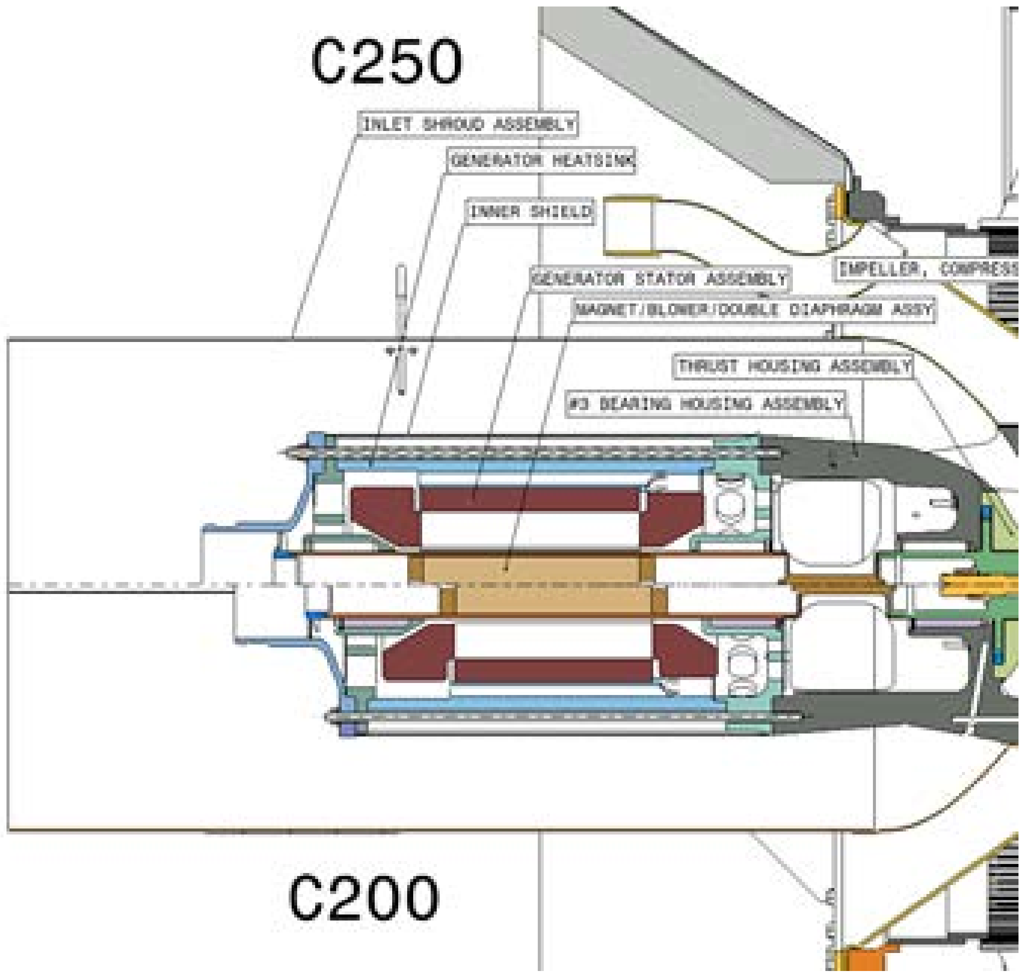

Figure 8: C250 Stator Dimensional Constraints Relative to the C200 Stator

Parameter	Value
Machine Type	Permanent magnet synchronous
Power	296 kW for -4°F to 59 °F
Line-to-line Terminal Voltage	0 – (480 +5/-10) V_{AC}
Rated Line-to-line Terminal Voltage	480 +5/-10 V_{AC} at rated speed
Current	Maximum 390 A_{RMS} @ 296 kW, 59 °F
Speed	0 – 60,000 rpm
Rated Speed	60,000 rpm
Required Speed Ramp Time from/to Standstill	0 – 18,000 rpm in less than 1.2 s
Maximum Current During Speed Ramp from/to	600 A_{peak}
Rated Electrical Frequency	1000 Hz
Efficiency	≥ 97 % at full power
Converter DC bus range	720 – 840 V_{DC}
Converter Modulation Scheme	Symmetrical bus clamped PWM
Converter Switching Frequency	10 kHz
Corona Inception Voltage	Minimum 3000 $V_{L\text{-}G}$ and $_{L\text{-}L}$
Insulation Class of Stator Materials	Class N (392 °F)
Maximum Stator Winding Temperature	329 °F
Rotor Magnet Material Specified Maximum	Minimum 652 °F
Maximum Rotor Sleeve Temperature	572 °F
Cooling	Air Cooled with total 0.40 lbm/s mass flow rate
Agency standards	Compliant with UL 1004 and UL1446

Table 5: C250 Stator Performance Specification Values

DESIGN DETAILS

The design of the stator was done by an external company contracted by Capstone. The results of the first article unit testing are shown in Table 6 below.

Test Title	Qual Requirement	Acceptance Criteria	Test Results
Resistance	Resistance of leads is within tolerance	6.50 ± 5% mΩ(1)	A-B 6.34 mΩ B-C 6.42 mΩ A-C 6.41 mΩ
Inductance	Inductance is within tolerance	A-B 142 ± 1.5% B-C 148 ± 1.5% A-C 156 ± 1.5% all at 1 kHz	A-B 126 µH B-C 133 µH A-C 140 µH
Hi-pot	Ground Insulation is suitable	3.325 V_{DC} for 1 second, leakage current < 5 mA	PASS
Winding Temperature	Hot spot temperature of windings is within insulation system limits	T ≤ 165 °C at 275 kW at generator at 25 °C	T > 190 °C for 15 °C ambient

Table 6: C250 Stator Qualification Results

The stator met all design criteria at the rated performance, except the winding temperature. The stator temperature test uncovered a flaw in either the design of the generator and its cooling or a manufacturing flaw. The generator cooling mass flow rate was verified to be at or above the minimum that was specified. It is possible that the cooling air flow path is not optimum or that the cooling air mass flow is not sufficient at the full power condition. Running at temperatures above the specification level will not result in an immediate failure, but will result in a reduction of stator life. The cooling system design must be re-evaluated prior to production, but the stator life should be more than adequate for the life of the prototype engine.

6.2.3. Combustion System Design

ENGINEERING DESIGN REQUIREMENTS

Capstone internal Engineering Requirements Specifications apply to the design of the combustion system for C250 POC engine. The specific requirements for the combustion system are listed in Table 7.

MEM Requirement	MEM Parameter	Notes
NOx	Not Required	Measurement required for supporting Beta phase design work
CO	Not Required	Measurement required for supporting Beta phase design work
VOC	Not Required	Not required to measure at current phase
Life Igniter	Min. 200 EOH	
Life Injector	Min. 200 EOH	
Life Combustor	Min. 200 EOH	
Fuel Energy	802 kW at ISO or 797 kW at 70 °F	Cycle Deck Analysis for 59 °F and 70 °F
Combustion System Pressure Drop	2.3% – Target	Risk — Using C200 hardware with much higher flow, meeting dP target is risky.
Combustion Exhaust Characteristics	No pattern factor requirement	

Table 7: C250 POC Combustion Design Requirements

DESIGN BASIS

For the C250 POC engine, there are two specifications that might have been the design basis for its combustion system. A detailed comparison of the assumptions and results was performed. While there are small differences in power output between the two analyses, the efficiency differences are much greater due to different underlying assumptions. For example, the engine efficiency measured at the generator leads is predicted / specified to be 36.80% / 36.12% respectively which yields a disparity of 0.68%.

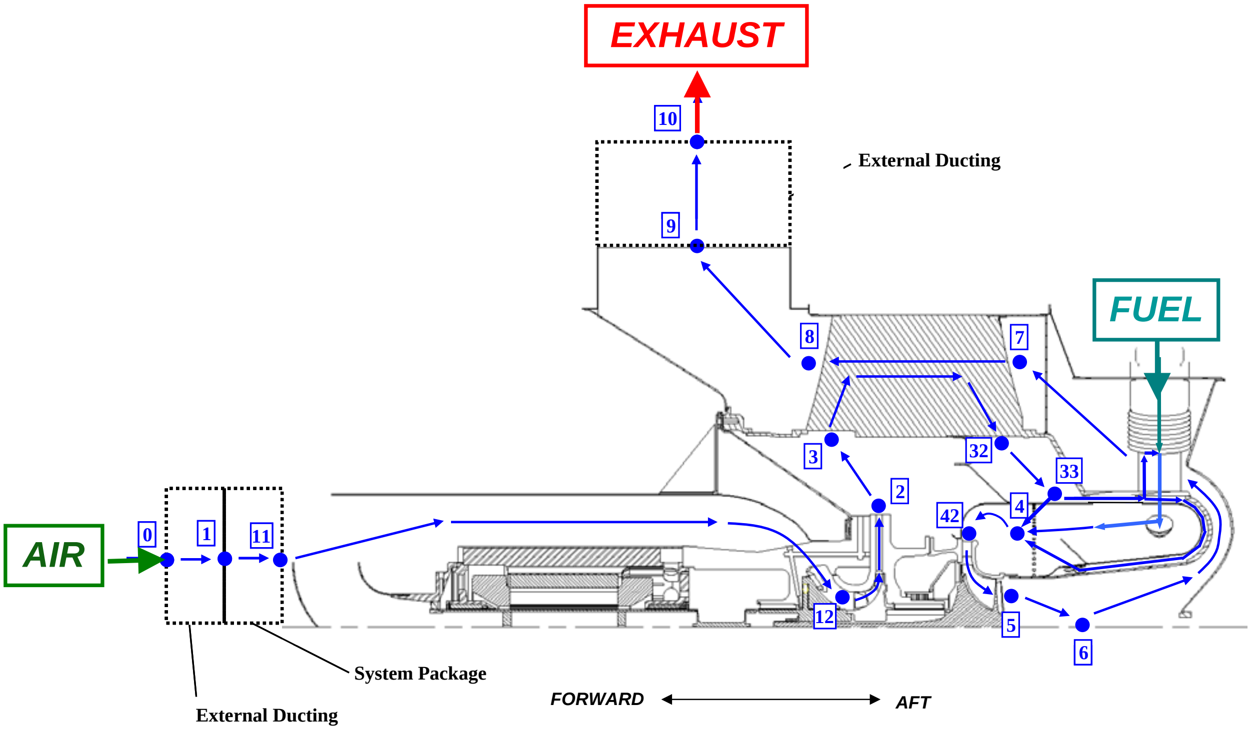

Figure 9: Schematic of Cycle Stations (C200 Shown)

DESIGN DETAILS

The requirements for the C250 POC engine are significantly reduced from a final C250 design. Generally, requirements are based on modifications to an existing C200 system and should be interpreted as such, unless otherwise specified.

Combustion Specification Analysis

Table 8 compares the C250 design Target Cycle parameters to the other Capstone Microturbine systems, including C200 at ISO conditions.

	Unit	C200	C250
Combustion Energy	kW	615	802
Mass Flow – Air	lb/s	2.84	3.59
Mass Flow – Fuel	lb/hr	102.42	133.53
AFR		99.83	96.83
FAR		0.0100	0.0103
Phi Overall		0.1720	0.1774
Combustor Inlet Temperature	°F	1055.8	1074.2
Combustor Exit Temperature	°F	1744.1	1780.6
Max Combustor Exit T (PF=0.20)	°F		
Combustor Pressure	PSIA	58.7	71.9
Combustor Pressure Drop	%	2.0	2.3

Table 8: C250 Target Cycle Top Level Specifications with Comparison

Based on the C250 Design Target Cycle full power parameters, the results were then extrapolated to a wider operating range and to much lower power output by assuming the following:

1. C200 performance and operating parameters are reasonably represented by a set of parametric studies completed in January 2009
2. The C250 engine will perform similarly to the C200, i.e. the C250 will follow similar “trends” — not absolute values — demonstrated in the C200 engine in terms of air pressure, air temperature, efficiency, and power output as a function of engine speed
3. At ISO conditions, the engine power output is directly correlated to engine speed

Combustion Conditions

The combustion conditions of the microturbine are defined by the fuel type/fuel composition, fuel flow rate, air flow rate, and the initial conditions (P33, T33 per Figure 9) of fuel and air before reactions.

Cycle Deck data showed that the C250 has a compression ratio of 4.89 while the C200 system has a compression ratio of 4.00. At steady state, the C250 will operate at much higher pressures and higher temperatures, as shown in Figure 10. Due to the C250’s higher power output requirement, higher flow rates of air and fuel are also observed. At station #33 (See Figure 9), the C250 air flow rate is 126.5% of that of C200. However, due to higher overall efficiency, the fuel flow rate of the C250 is only 30.4% higher than the C200 while producing 39% more electrical power. The air and fuel flow rate trends for both systems are shown in Figure 11.

The fuel used in the C250 POC phase demonstration will be the pipeline natural gas at Capstone’s Stagg test facility which typically has a lower heating value of approximately 20,500 BTU/lbm and 90-96% methane content.

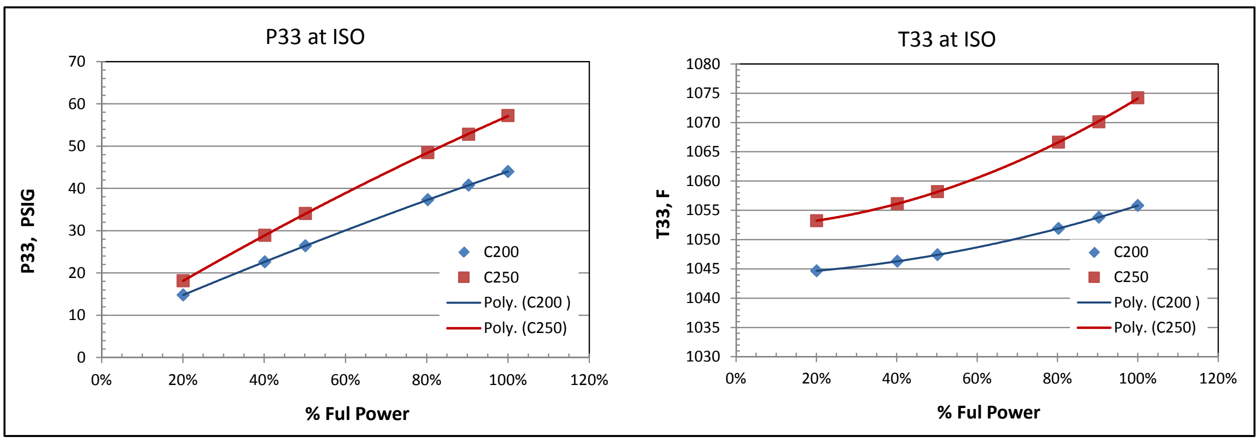

Figure 10: Combustion Air Temperature and Pressure — C200 vs C250

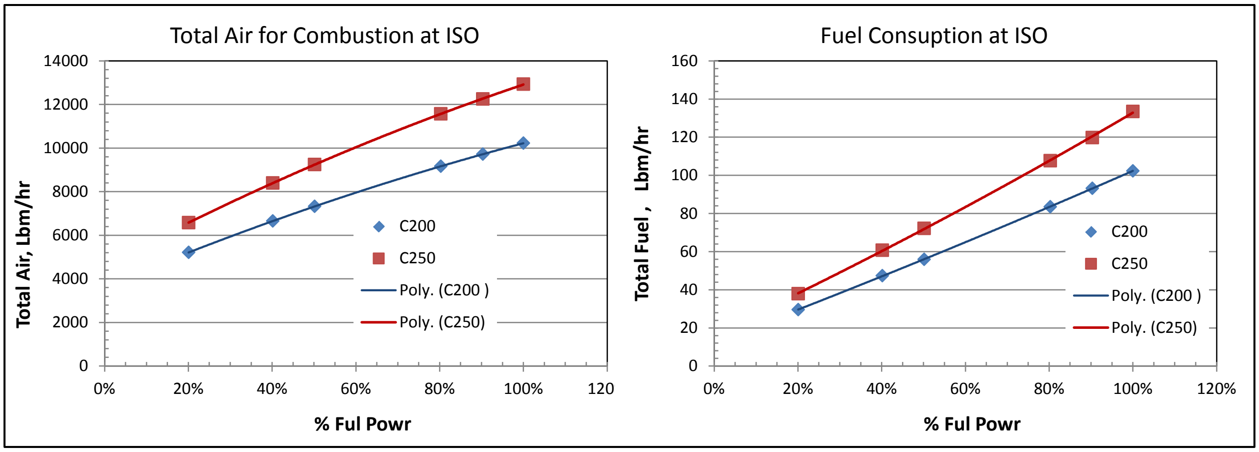

Figure 11: Fuel and Air Flow Rate for C200 and C250

Flow Area and Geometry Analysis

The compressed recuperator air is used as: (1) combustion air — as an oxidizer, (2) cooling air to achieve the desired component — liner and injector, for example — temperature, and (3) dilution air to mix with high temperature combustion exhaust to generate desired pattern factor (PF), velocity profile, and momentum distribution for the turbine stage. Flow area and geometry analysis will help to understand the C200 and give direction on how to modify the C200 injector and combustion liner for C250 POC demonstration purposes. Flow analysis coupled with other analysis, such as combustion chemical kinetics, will determine a combustion system geometry that will

- achieve desired airflow split to primary zone for achieving optimal emissions
- achieve cooling desired to maintain component temperature at levels that will achieve designed operating life
- limit pressure drop to the design target — for C250 combustion system, for example, the design target is 2.3% — to achieve designed performance
- have jet penetration for dilution air which will achieve desired pattern factor for optimal turbine stage performance
- effectively control flow via orifices to give system variability
- partially define combustor, injectors, and casing geometries

Ideally, a comprehensive study would have been carried out using 3D CFD simulation or more detailed 1D flow network tools to characterize the extant C200 system. C65, C200, and C250 POC engines share the same combustion architecture. Figure 12 shows the 1D flow network common to these three engines. The model calculates flow resistances — i.e., pressure drops — for a number of discrete flow elements, such as wall friction, flow around a bend, and flow through an orifice. However, due to resource and schedule limitations, flow network analysis for the C250 POC phase was conducted based on an “effective flow area” approach which assumes an isothermal condition — 1D incompressible/ideal gas fluid networks. Flow rate splits were determined by effective passage area which is the smallest geometric area along a passage.

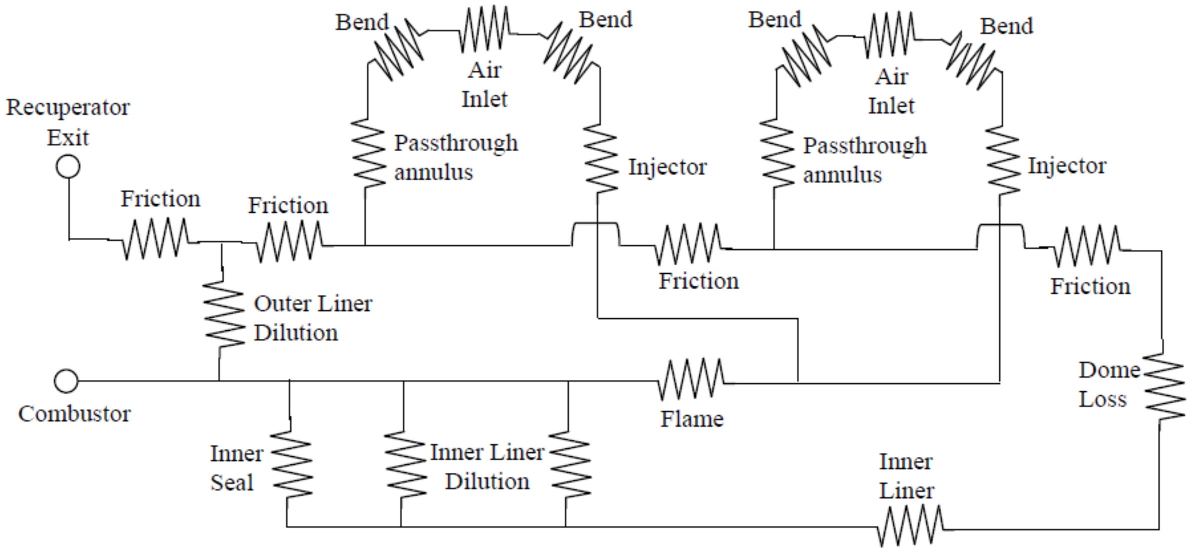

Figure 12: Schematic of 1D Flow Network for C65/C200/C250 POC

The major combustion system components of a Capstone Microturbine system include (1) a combustion liner, (2) a set of injectors or fuel/air mixers, and (3) an igniter. Figure 13 is a cross-sectional view of the C200 combustion sub-module. It is important to note that the recuperated high pressure air flows through the space between the outside wall of the combustion liner and the inside wall of the recuperator casing before being introduced to the combustion chamber via injectors, cooling holes, and dilution holes at the desired splitting ratio.

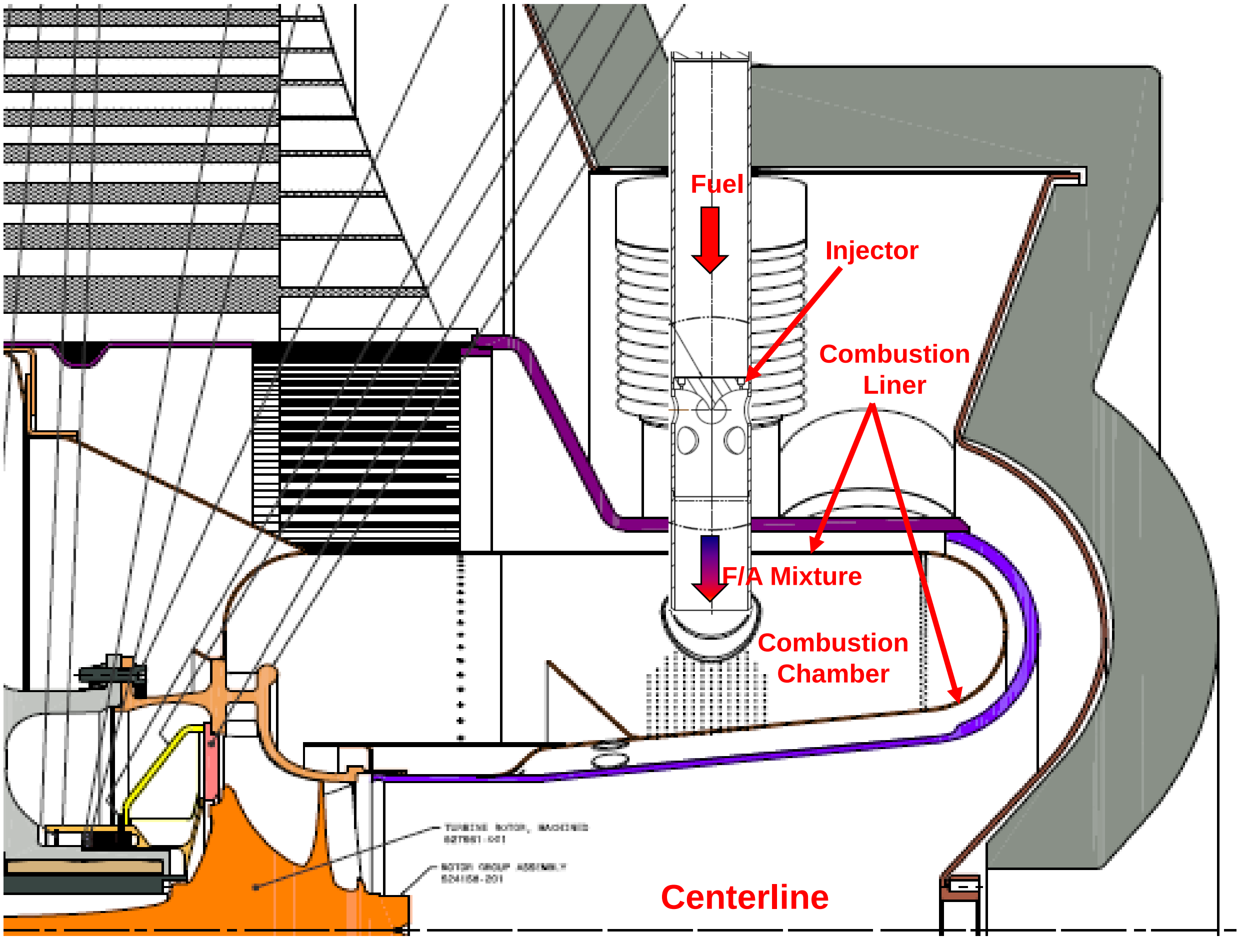

Figure 13: C200 Combustion System Cross-Sectional View

Table 9 is a flow area analysis for the C200 natural gas system which uses combustion liner part number 527163-100 and injector part number 522669-101. Without including the floating seals at the interface of injectors and liner, the total effective opening area for the C200 flow passage is only 19.55 inch^2. If the floating seals are taken into consideration, the effective area is smaller. By area approximation, the air split of effusions holes, outer dilution holes, the injectors, inner dilution holes, and inner dilution slots are 2.0%, 5.0%, 45.2%, 46.7% and 1.1% respectively. For the injectors, the effective area is the injector exit — or the inner diameter — which makes it difficult to direct more air to the primary combustion zone of the liner without closing holes at other locations which would introduce extra pressure drop across the combustion system.

Effusion Opening	Unit	Area	% of Total
Effusion Holes	**in.^{2}**	**0.38**	**2.0**
Outer Dilution Holes	**in.^{2}**	**0.98**	**5.0**
Effective Area for Annulus, Injectors, and Inner Liner	**in.^{2}**	**18.19**	**93.0**
Liner Annulus Area	in.^{2}	21.99	93.0
Effective Area – All Injectors	**in.^{2}**	**8.84**	**45.2**
ALL Injectors Annulus Area	in.^{2}	18.73	
ONE Injector – Exit Area	in.^{2}	1.47	
ONE Injector – Effusion Area	in.^{2}	1.47	
Number of Injectors	ea.	6.00	
Effective Post Dome Area	in.^{2}	9.34	47.8

Effusion Opening	Unit	Area	% of Total
Annulus Area – Lower Dome	$in.^2$	11.34	47.8
Annulus Area Be4 In. Dilution Holes	$in.^2$	12.13	47.8
Inner Dilution Holes and Slots	$in.^2$	9.34	
Inner Dilution Holes	**$in.^2$**	**9.13**	**46.7**
Inner Dilution Slots	$in.^2$	0.21	1.1
Total Effusion Opening Area	**$in.^2$**	**19.55**	**100.0**

Table 9: Flow Area Analysis for Production C200 Natural Gas Engine

Combustion Analysis

The predicted overall air-to-fuel ration (AFR) is shown in Figure 14. This prediction is based on the C250 Target Cycle and the C200 parametric study and assumes that the C250 will follow the same trend of fuel air ratio. The predicted AFR indicates that the C250 will exhibit combustion performance similar to or better than the C200.

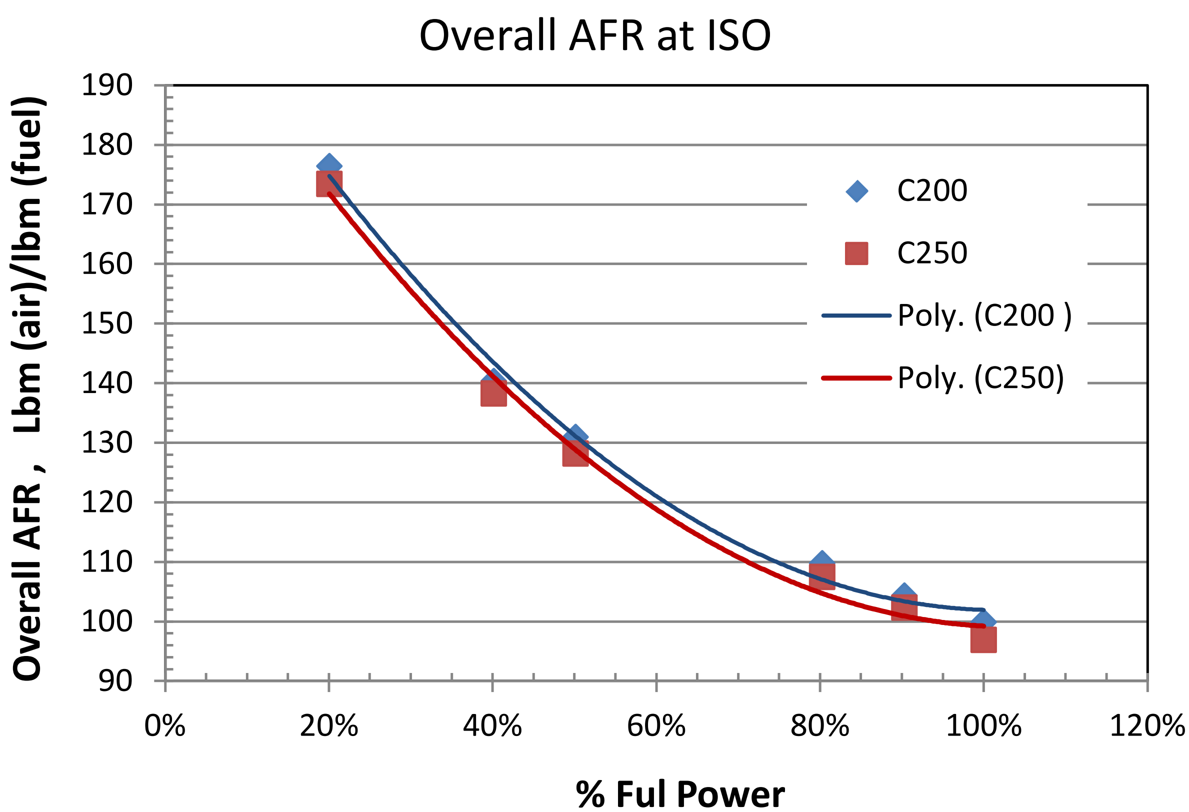

Figure 14: Overall AFR for Both C200 and C250 Target Cycle

For a lean premixed combustion system like that employed in Capstone microturbine systems, combustion design challenges and possible issues include flashback, stability, and auto-ignition. While C200 systems have been proven a solid design and the C250 POC engine retains similar combustion architecture, the criteria used for the current design would be a “scaling” based on the C200 system.

Auto-Ignition

Auto-ignition is a spontaneous chemical reaction between fuel and air without an external ignition source. Higher temperature, higher pressure, and longer residence time make it easier for a fuel-air mixture within the flammability range to auto-ignite. At a fixed temperature, pressure, and fuel-air mixture, there is a minimum amount of residence time that is needed for the mixture to auto-ignite which is called auto-ignition delay time. For Capstone microturbine engines, auto-ignition within the injector must be prevented because it will lead to injector hardware damage and combustion system failure. At full power condition of C250 operation, chemical kinetics simulations predicted that the air-fuel mixture has an auto ignition delay time of more than 80 ms, while the residence time of the fuel/air mixture in the injector is much less — 2-3 ms. As a result, even at C250 conditions — higher temperature and higher pressure — the risk of autoignition within the injector is low and there is no concern of auto-ignition in the injector.

Flashback

Flashback has been a concern for any lean premixed combustion system due to fuel variation and other operational variations. The same is true in Capstone systems. The general methods employed to combat flashback include:

1. Injector mixture design optimization to avoid creating or minimize a recirculation zone
2. Increase bulk velocity within the injector to give higher flashback resistance margin
3. Reduce fuel concentration in low velocity zone

Since the C200 natural gas injector was selected for the C250 POC engine, the shortcomings and merits of the injector design were also inherited. Options (1) and (3) listed were difficult to implement in the C250 POC phase. However, the team was able to design a good air flow split to increase the bulk velocity within the injector (option 2) to provide increased flashback resistance margin. Previous experience established that the injector will have good flashback-resistance margin when the average velocity of fuel/air mixture in the injector is 50 times of that of the laminar flame speed of the fuel/air mixture.

Chemical kinetics analysis found that the laminar flame speed of the C250 fuel/air mixture at full power is on the order of approximately 80 cm/s, hence a bulk velocity of 40 m/s in the injector should provide good flashback resistance margin. A study of the impact of the primary zone (PZ) air split on injector velocity and PZ equivalence ratio (ER) was performed. The results of this study are presented in Figure 15. As shown, the injector bulk velocity increases as more air is introduced to PZ via the injectors. At the same time, the fuel/air mixture will be leaner. It was found that the air split to PZ needs to be greater than 27% in order to achieve an injector bulk velocity of 40 m/s and to have a reasonable flashback resistance margin. At 27% PZ air split, the ER of the PZ will be 0.657.

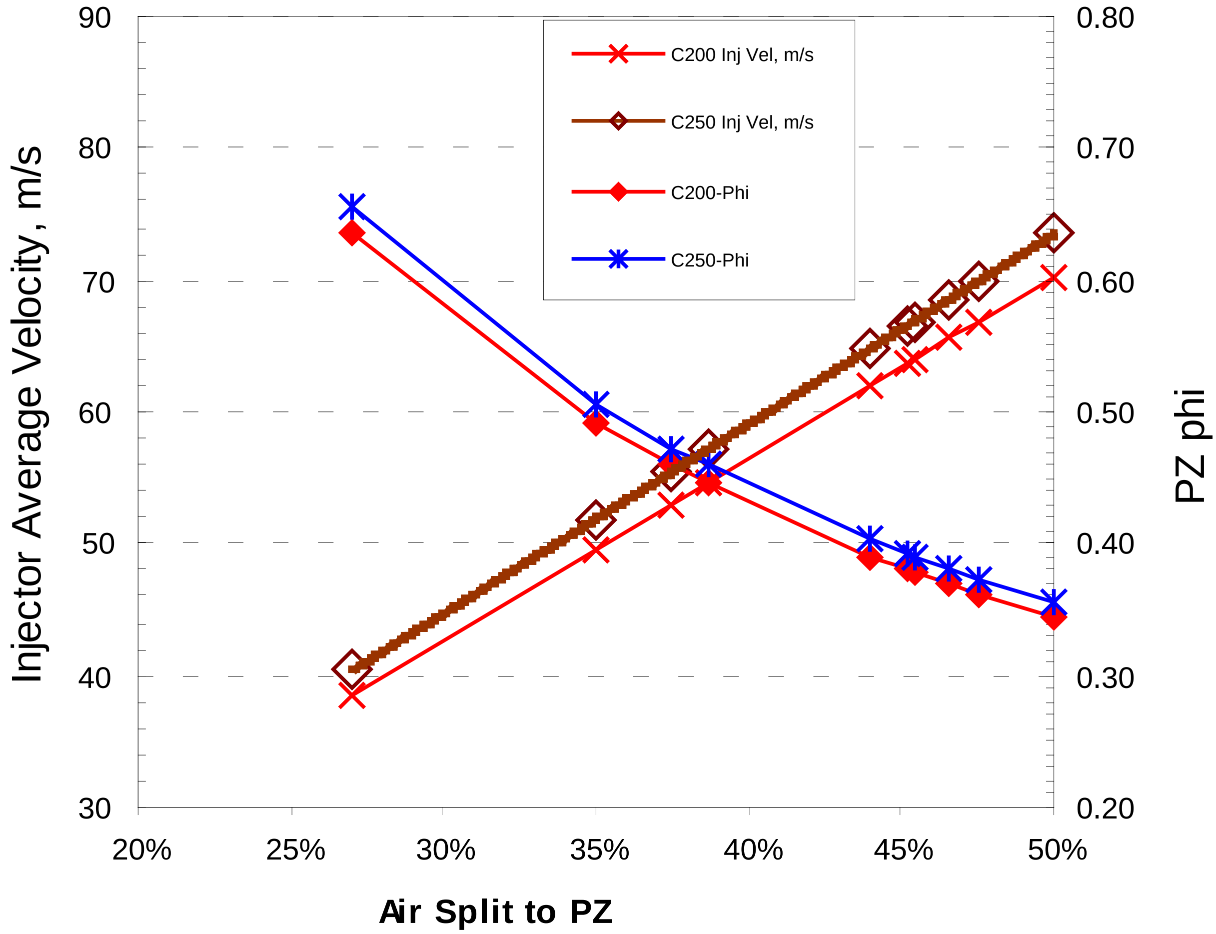

Figure 15: PZ Air % vs Injector Average Velocity and PZ ER

Emissions

Although the POC engine has no emission requirements, it was desirable to characterize emissions performance to provide guidance for the next phase design. As a result, one combustion submodule for the POC engine was designed to achieve low levels of pollutant emissions, including NO_x and CO. The target of these levels shall be as close as possible to those of C200 natural gas system. For natural-gas-burning, lean premixed microturbine combustion systems, emissions strongly depend on the temperature in the PZ. This is particularly true for NO_x, because thermal NO_x mechanisms account for the majority of NO_x production. Thus, in order to maintain low NO_x levels, it is necessary to maintain a low PZ temperature. However, lower PZ temperature reduces stability and causes high CO emissions. Hence, the temperature — or ER — “sweet zone” range is relative narrow for lean premixed combustion system. Figure 16 charts the relationship between NO_x and CO with respect to PZ temperature. Using a 0-D model by assuming a perfect stirred reactor (PSR) model for the primary zone of the combustor, the adiabatic flame temperature (AFT) is calculated as a function of the primary zone air amount (air split % to PZ). Figure 18 is the predicted AFTs at full power operation (System power - 200 kW for C200, 278 kW for C250 at ISO conditions).

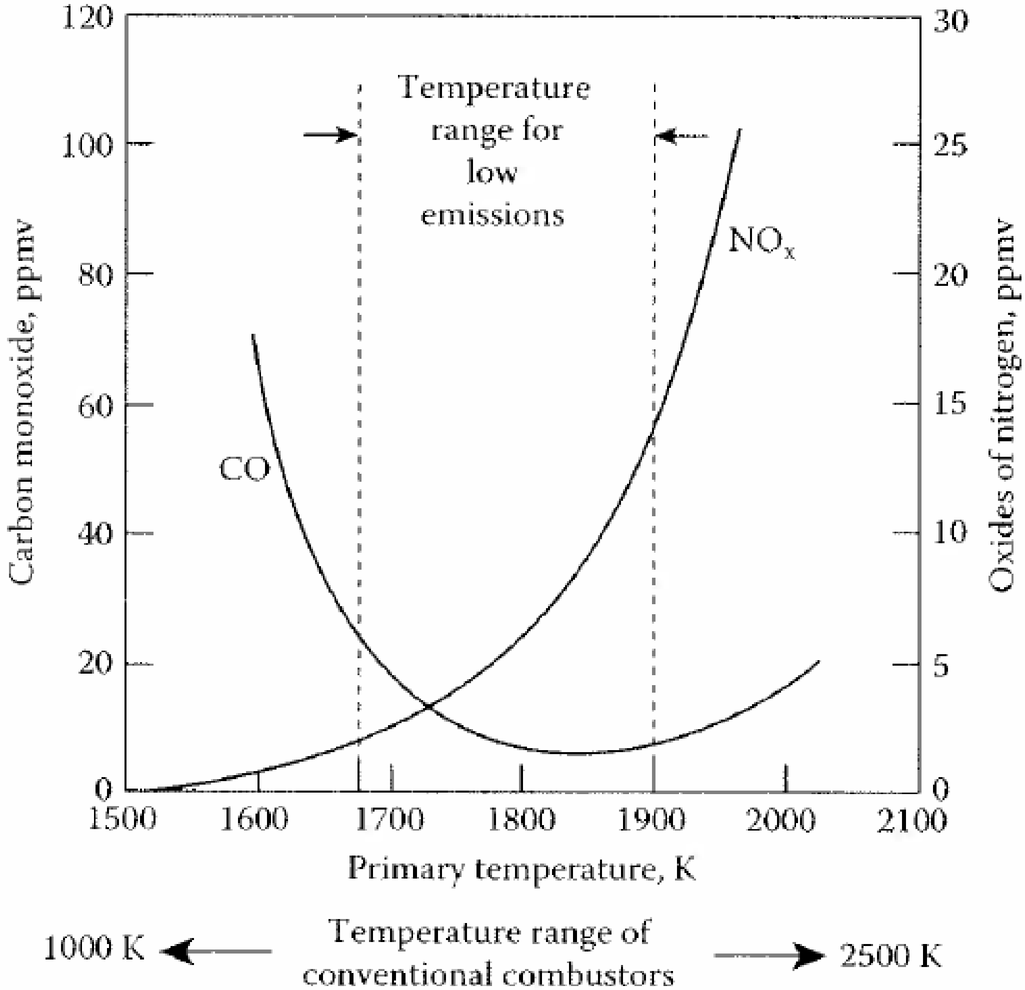

Figure 16: Influence of PZ Temperature on CO and NOx Emissions
(Ref. Gas Turbine Combustion: Alternative Fuels and Emissions, 3rd Edition)

It is believed that both spatial and temporal variation in the fuel/air mixing will impact the emissions of NO_x. As a result, significant effort was expended in developing strategies for rapid and complete mixing of fuel and air in lean premixed injectors like those used in the C200. Although systems have different achievable emission levels due to design differences, there is a highly-cited NO_x "entitlement" emissions chart assuming "perfect" mixing for premixed natural gas combustion systems shown in Figure 17.

In order for the Capstone C200/C250 to achieve 9 ppm NO_x emissions at 15% O_2, the PZ AFT must be maintained at 2960 °F (1900 K) or lower, which corresponds to a PZ air split of 37% or higher. At 42 – 45% air split — assuming that fuel and air temperature at the exit of injectors is maintained at T33 — the C200 PZ AFT is 2600 – 2700 °F. See Figure 18. This AFT is potentially an underestimate. The actual AFT for C200 may be higher than 2600 – 2700 °F.

In order to maintain similar level of NO_x emissions for the C250, the PZ AFT must be maintained at the same level as the C200 since the overall fuel to air ratio is higher. In other words, the PZ ER must be maintained at the same levels, assuming the fuel/air mixing level and the PZ heat losses are the same. As a result, more air should be driven to the PZ via the injectors.

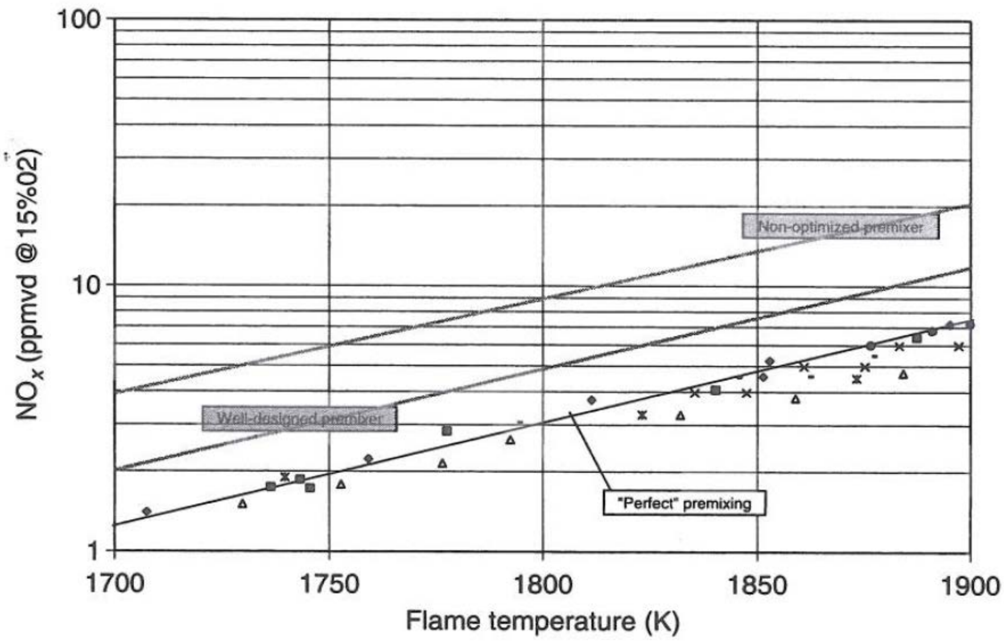

Figure 17: Minimum NOx Achievable for Lean Premixed Combustion (per Leonard and Stegmaier, 1994)

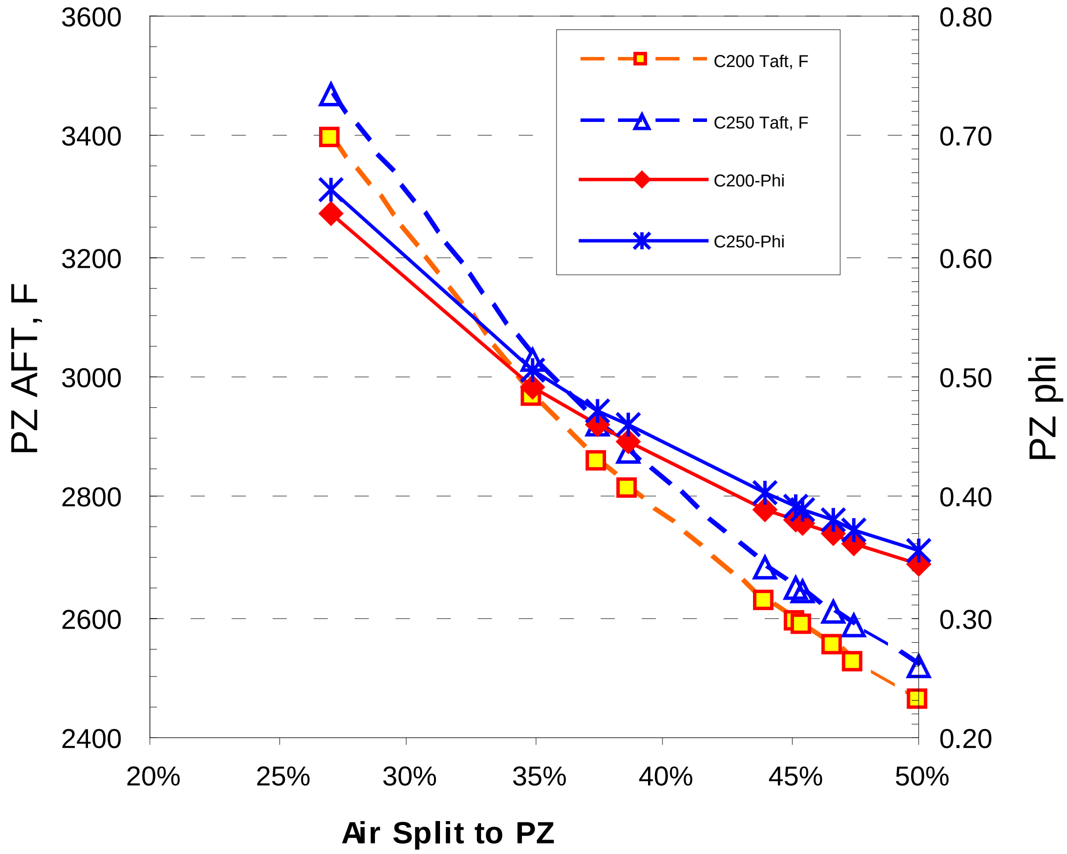

Figure 18: PZ Air % vs AFT and PZ ER for Full Power Operation

Combustion System Pressure Drops

One of the high level requirements for the C250 POC engine is to maintain high system efficiency which passes down to the microturbine engine module (MEM) level as a requirement of generator efficiency of 36.12% per Target Cycle or 36.80%, without restriction at the exhaust exit. At 70 °F, there is a 0.68% generator efficiency discrepancy between the two specifications.

Microturbine efficiency is impacted by the effectiveness or efficiency of all the sub-modules and components, which include the compressor, recuperator group, combustion system, turbine rotor group, exhaust duct design, and others. However, the impact of combustion system pressure drop on the overall system efficiency is relatively small, according to C200 data and analysis. For a C200 microturbine system, it was predicted that a 1% change in pressure drop — for example, combustion system pressure increase from 2% to 3% — would result in nearly 3 kW change in power and 0.2% change in efficiency.

If the C200 combustion system hardware — maintaining the geometries with no changes — were used for C250 operation at higher pressure, higher temperature, and higher air flow rate, the pressure drop ratio would be:

$$\frac{\Delta P_{POC}}{\Delta P_{C200}} \sim \left(\frac{\dot{m}_{POC}}{\dot{m}_{c200}}\right)^2 \left(\frac{T_{POC}}{T_{c200}}\right)\left(\frac{P_{c200}}{P_{POC}}\right)$$

When this equation is populated with the values from the C250 Target Cycle and C200 cycle number for full power at ISO conditions, the result is a 30% higher pressure drop for the C250 POC combustion system compared to the C200 natural gas system. Therefore, in order to maintain a pressure drop level similar to that of the C200, the combustion liner and/or injector design must change.

C250 POC Design Configurations

Basic Configuration

For the C250 POC phase, it was determined that the C200 combustion system shall be adopted without changes to the igniter, combustion liner envelope, injector envelope, or injector arrangement. The interfaces with other modules, except for the interface between nozzle and seal, shall also not be changed. The features that shall not change include:

- Combustion liner general geometry. The bolted C200 blank combustor, similar to 530207-100, shall be used to generate the C250 POC liner with modified hole patterns.
- Combustion liner shall be mounted in the same way as in C200.
- Injectors shall be of the same type as the flexible C200 natural gas injector (Figure 19) — while distribution holes and mixing holes may vary.
- Six injectors shall be arranged in two planes like those used in C200 and with the same orientations.

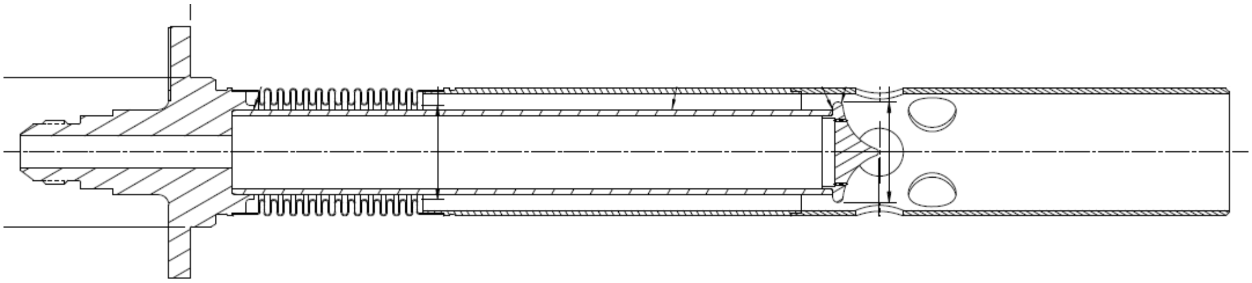

Figure 19: C200 Natural Gas Injector

Since the other combustion components are not changed from the C200, the combustion configuration or design cases referred to hereafter is defined as a combination of liner and injectors with the other unchanged components.

Design for Emissions: Design Case # POC-1

The final production C250 engine is required to have emissions at levels similar to those of the C200 at full power conditions for much wider operating conditions and load ranges. This makes the C250 combustion system design much more challenging. Although the major focus for the POC engine is the demonstration of power output and engine (generator) efficiency, it is highly desirable to have an estimate of the emissions flexibility of applying C200 engine — with minor changes — to C250 POC operation. To match the C200 full power emissions, the approach is to match the ER or AFT as well as the residence times of the primary and dilutions zones.

	C200 NG system, full power, ISO conditions, Cycle Deck v7.6	C250 NG system, full power, ISO conditions, Cycle Deck v7.7
Overall AFR	**99.88**	**96.85**
PZ Air %	**ER in PZ**	
40.0	0.430	0.444
42.0	0.410	0.422
44.0	0.391	0.403
45.2	**0.381**	0.393
46.6	0.369	**0.381**
47.5	0.362	0.374
50.0	0.344	0.355

Table 10: PZ ER as a Function of PZ Air Split

By geometry approximation, it was found that the C200 has 45.2% effective flow area for the injectors which leads to 45.2% air flow split and gives an ER of 0.381 for the C200 PZ at ISO conditions, as shown in Table 10. Since the C250 overall FAR is higher than the C200 combustion system, more air — 46.6% — must be delivered to the C250 POC PZ in order to match the ER of the C200. Also, due to the overall injector flow passage being limited by the injector exit — the inner diameter of the injector — per analysis in Table 9, one or more of the other flow passages have to be closed slightly to drive more air to the PZ. The configuration of this proposed design case is shown in Table 11. For this C250 POC injector — denoted as POC-Inj-1 —the changes from Production C200 NG injector will include:

- Bigger fuel distribution holes — all distribution holes (24) increase from 0.036 in. ID to 0.040 in. ID
- Bigger mixing holes — all mixing holes (8) increase from 0.5625 in. ID to 0.625 in. ID

For this design case, the combustion liner — denoted POC-liner-1 — decreases the inner dilution hole diameters from 17.68 to 17.11 mm compared to the C200 natural liner. Because of this change, the distribution of effective passage areas and the air flow distribution among them will change as shown in Table 11. In this POC-liner-1, the only change is the diameter of the inner dilution holes. It is possible to use production C200 liner with inner dilution hole seaming to match the opening area.

		C200 NG Production PN 522669-101		**C250 POC-1 46.6% to PZ unreleased**	
Effusion Opening	**Unit**	**Area**	**% Total**	**Area**	**% Total**
Effusion Holes	**inch^2**	**0.38**	**2.0**	**0.38**	**2.0**
Outer Dilution Holes	**inch^2**	**0.98**	**5.0**	**0.98**	**5.2**
Effective Area for Annulus, Injectors, and Inner Liner	**inch^2**	**18.19**	**93.0**	**17.61**	**92.8**
Liner Annulus Area	inch^2	21.99	93.0	21.99	92.8
Effective Area – All Injectors	**inch^2**	**8.84**	**45.2**	**8.84**	**46.6**
ALL Injectors Annulus Area	inch^2	18.73		18.73	
ONE Injector – Exit Area	inch^2	1.47		1.47	
ONE Injector – Effusion Area	inch^2	1.47		1.47	
Number of Injectors	each	6.00		6.00	
Effective Post Dome Area	inch^2	9.34	47.8	8.77	46.2
Annulus Area – Lower Dome	inch^2	11.34	47.8	11.34	46.2
Annulus Area Be4 In. Dilution Holes	inch^2	12.13	47.8	12.13	46.2
Inner Dilution Holes and Slots	inch^2	9.34		8.77	
Inner Dilution Holes	**inch^2**	**9.13**	**46.7**	**8.56**	**45.1**
Inner Dilution Slots	inch^2	0.21	1.1	0.21	1.1
Total Effusion Opening Area	**inch^2**	**19.55**	**100.0**	**18.97**	**100.0**
dP vs C200-C200 condition	**%**	**100**		**106**	
dP vs C200-C250 POC condition	**%**	**130**		**138**	
PZ % range (based on area approximation)	**%**	**27 – 45.2**		**27 – 46.6**	

Table 11: Design Case Configuration POC-1

While this design case is intended to have emissions similar to the C200, it is expected that higher pressure loss — approximately 38% higher than the C200 — will be observed for the following reasons:

1. Different operation conditions – higher flow rate and higher temperature
2. Closing-up of the opening of inner dilution holes to drive the desired flow split to the PZ

Design for Lower Pressure Drop

As described previously, the POC engine is to demonstrate desired levels of power output and efficiency. As a result, the other design criteria are to minimize combustion system pressure drops. Given all other conditions, such as temperature, pressure, friction and similar geometry among others, are the same, pressure drop of a system is reversely proportionally to the area-squared, that is, $dP \sim 1/A^2$

A few design cases have been developed based on:

1. Maintain sufficient flashback resistance by keeping primary zone air at 27% or higher;
2. Maintain low enough AFT for liner life;
3. Increase effective flow area to be more than that of C200 NG baseline liner (19.55 inch^2) to minimize pressure drop for combustion system;
4. Configuration flexibility – for development tests, able to seam the combustion liner and/or injector.

Based on pressure drop analysis, it would be require 22.28 inch^2 effective passage area for the C250 POC combustion system to match the same pressure drop as C200 natural gas combustion system. These design configurations are listed in Table 12 and Table 13.

		C200 NG Production PN 522669-101		C250 POC-2A 27% to PZ (~40 m/s)		C250 POC-2B		C250 POC-3A 36.9% to PZ	
Effusion Opening	**Unit**	**Area**	**% Total**	**Area**	**% Total**	**Area**	**% Total**	**Area**	**% Total**
Effusion Holes	**inch^2**	**0.38**	**2.0**	**1.38**	**6.2**	**1.38**	**5.5**	**1.12**	**4.7**
Outer Dilution Holes	**inch^2**	**0.98**	**5.0**	**3.55**	**15.9**	**3.55**	**14.1**	**2.63**	**11.0**
Effective Area for Annulus, Injectors, and Inner Liner	**inch^2**	**18.19**	**93.0**	**17.36**	**77.9**	**20.19**	**80.4**	**20.19**	**84.3**
Liner Annulus Area	inch^2	21.99	93.0	21.99	77.9	21.99	80.4	21.99	84.3
Effective Area – All Injectors	**inch^2**	**8.84**	**45.2**	**6.02**	**27.0**	**8.84**	**35.2**	**8.84**	**37.0**
ALL Injectors Annulus Area	inch^2	18.73		18.73		18.73		18.73	
ONE Injector – Exit Area	inch^2	1.47		1.47		1.47		1.47	
ONE Injector – Effusion Area	inch^2	1.47		1.00		1.47		1.47	
Number of Injectors	each	6.00		6.00		6.00		6.00	
Effective Post Dome Area	inch^2	9.34	47.8	11.34	50.9	11.34	45.2	11.34	47.4
Annulus Area – Lower Dome	inch^2	11.34	47.8	11.34	50.9	11.34	45.2	11.34	47.4
Annulus Area Be4 In. Dilution Holes	inch^2	12.13	47.8	12.13	50.9	12.13	45.2	12.13	47.4
Inner Dilution Holes and Slots	inch^2	9.34		14.09	50.9	14.09	45.2	13.10	47.4
Inner Dilution Holes	**inch^2**	**9.13**	**46.7**	**13.88**	**50.1**	**13.88**	**44.5**	**12.89**	**46.6**
Inner Dilution Slots	inch^2	0.21	1.1	0.21	0.8	0.21	0.7	0.21	0.8
Total Effusion Opening Area	**inch^2**	**19.55**	**100.0**	**22.29**	**100.0**	**25.11**	**100.0**	**23.94**	**100.0**
dP vs C200-C200 condition	**%**	**100**		**77**		**61**		**67**	
dP vs C200-C250 POC condition	**%**	**130**		**100**		**79**		**87**	
PZ % range (based on area approximation)	**%**	**27 – 45.2**		**27 – 35.2**		**27 – 35.2**		**27 – 37**	

Table 12: C250 POC Configurations – 2A, 2B, 3A

Effusion Opening	Unit	C250 POC-3B 27% to PZ (~40 m/s)		C250 POC-4A 39.7% to PZ		C250 POC-4B 30.9% to PZ	
		Area	% Total	Area	% Total	Area	% Total
Effusion Holes	**inch^2**	**1.12**	**5.3**	**0.74**	**3.3**	**0.74**	**3.8**
Outer Dilution Holes	**inch^2**	**2.63**	**12.4**	**1.36**	**6.1**	**1.36**	**7.0**
Effective Area for Annulus, Injectors, and Inner Liner	**inch^2**	**17.36**	**82.2**	**20.19**	**90.6**	**17.36**	**89.2**
Liner Annulus Area	inch^2	21.99	82.2	21.99	90.6	21.99	89.2
Effective Area – All Injectors	**inch^2**	**6.02**	**28.5**	**8.84**	**39.7**	**6.02**	**30.9**
ALL Injectors Annulus Area	inch^2	18.73		18.73		18.73	
ONE Injector – Exit Area	inch^2	1.47		1.47		1.47	
ONE Injector – Effusion Area	inch^2	1.00		1.47		1.00	
Number of Injectors	each	6.00		6.00		6.00	
Effective Post Dome Area	inch^2	11.34	53.7	11.34	50.9	11.34	58.3
Annulus Area – Lower Dome	inch^2	11.34	53.7	11.34	50.9	11.34	58.3
Annulus Area Be4 In. Dilution Holes	inch^2	12.13	53.7	12.13	50.9	12.13	58.3
Inner Dilution Holes and Slots	inch^2	15.12	53.7	12.21	50.9	12.21	58.3
Inner Dilution Holes	**inch^2**	**14.91**	**53.0**	**12.00**	**50.0**	**12.00**	**57.3**
Inner Dilution Slots	inch^2	0.21	0.7	0.21	0.9	0.21	1.0
Total Effusion Opening Area	**inch^2**	**21.10**	**100**	**22.28**	**100.0**	**19.46**	**100.0**
dP vs C200-C200 condition	**%**	**86**		**77**		**101**	
dP vs C200-C250 POC condition	**%**	**112**		**100**		**131**	
PZ % range (based on area approximation)	**%**	**27 – 37**		**30.9 – 39.7**		**30.9 – 39.7**	

Table 13: C250 POC Configurations – 3B, 4A, 4B

<u>Lower Pressure Case: POC-2A and 2B</u>

In design cases POC-2A and -2B, the effective area for the combustion system is 22.29 and 25.11 in.^{2} respectively. Both design cases share the same liner configuration — POC-liner-2 — but the injectors are slightly different in their mixing hole diameters. The changes to the POC-Liner-2 from the C200 natural gas liner are:

- Larger inner dilution holes —total opening of 13.88 in.^{2} — which requires each of the 24 inner dilution holes to be changed to 21.79 mm in diameter
- Larger outer dilution holes —total opening of 3.55 in.^{2} — which requires each of the 120 outer dilution holes to be changed to 4.93 mm in diameter
- Increased total effusion cooling hole area —total 1.382 in.^{2} — which requires an increase of the total number of effusion holes from 1214 to 4400 at the same diameter of 0.020 in

The injector for Design Case POC-2B is the same as those used in Design Case POC-1, viz., POC-inj-1.

The injector for Design Case POC-2A — POC-inj-2 — differs from POC-inj-1 in that POC-inj-2's 8 mixing holes have a diameter of 0.400 in.

For both design cases, one liner — POC-liner-2 — and one set of six injectors — POC-inj-1 — are needed. With proper seaming to the injectors, the same set can be used to test PZ air from 27 – 35.2%, based on analysis, with pressure drop ranging from 79 – 100% of that of the C200.

Lower Pressure Case: POC-3A and 3B

In design cases POC-3A and -3B, the effective area is 23.95 and 21.10 in.^{2} respectively. Both design cases share the same liner configuration — POC-liner-3 — but the injectors are slightly different in their mixing hole diameters. The changes to the POC-Liner-3 from the C200 natural gas liner are:

- Larger inner dilution holes — total opening of 12.88 in.^{2} — which requires each of the 24 inner dilution holes to be changed to 21.00 mm in diameter
- Larger outer dilution holes — total opening of 2.626 in.^{2} — which requires each of the 120 outer dilution holes to be changed to 4.24 mm in diameter
- Increased total effusion cooling hole area — total 1.122 in.^{2} — which requires an increase of the total number of effusion holes from 1214 to 3570 at the same diameter of 0.020 in.

The injector for Case POC-3A is POC-inj-1. The injector for Case POC-3B is POC-inj-2.

For these two designs, only one liner — POC-3 — and one set of six injectors are needed. With proper seaming to the liner and injectors, this set of hardware can test PZ air from 27 – 37%, based on analysis, with pressure drop ranging from 87 – 112% of that of the C200.

Lower Pressure Case: POC-4A and 4B

In design cases POC-4A and -4B, the effective area is 22.28 and 19.46 in.^{2} respectively. Both cases share the same liner — POC-4. The liner has the following changes from the C200 natural gas liner:

- Larger inner dilution holes — total opening of 12.00 in.^{2} — which requires each of the 24 inner dilution holes to be changed to 20.26 mm in diameter
- Larger outer dilution holes — total opening of 1.36 in.^{2} — which requires each of the 120 outer dilution holes to be changed to 3.05 mm in diameter
- Increased total effusion cooling hole area — total 0.74 in.^{2} — which requires an increase to the total number of effusion holes from 1214 to 2350 with the same diameter of 0.020 in.

The injector for Design Case POC-4A is POC-inj-1. The injector for Design Case POC-4B is POC-inj-2.

For these two design cases, only one liner — POC-Liner-4 — and one set of six injectors — POC-inj-1 — are needed. With proper seaming to the liner and injectors, the set of hardware can test PZ air from 27 – 37%, based on analysis, with pressure drop ranging from 100 – 131% of that of the C200.

Design Case Summary

As a result of the previous calculation and analysis, two types of design case have been developed: design for emissions and design for lower pressure drops. Two approaches may be considered:

1. Study the impacts of different effusion cooling in POC phase with the configurations defined in Table 14.
2. Do not study impact of different effusion cooling, therefore make no change to effusion cooling hole pattern. These configurations are listed in Table 15.

		C200 NG		POC-1		POC-2A		POC-2B		POC-3A		POC-3B		POC-4A		POC-4B	
		Production		46.6% to PZ		27% to PZ				36.9% to PZ		27% to PZ		39.7% to PZ		30.9% to PZ	
1.0 FUEL SECTION - INJECTOR		528677-100		POC-inj-1		POC-inj-2		POC-inj-1		POC-inj-1		POC-inj-2		POC-inj-1		POC-inj-2	
1.2 FUEL DISTRIBUTOR																	
Nominal Fuel Exit Diameter	in.	0.036		0.040		0.040		0.040		0.040		0.040		0.040		0.040	
Number of Holes		24		24		24		24		24		24		24		24	
2.1 AIR – MIXING HOLES																	
Nominal Mixing Hole Diameter	in.	0.5625		0.6250		0.3995		0.6500		0.6250		0.3995		0.6250		0.3995	
Number of Mixing Holes		8		8		8		8		8		8		8		8	
Nominal Mixing Hole Area	$in.^2$	1.988		2.454		1.003		2.655		2.454		1.003		2.454		1.003	
5.0 COMBUSTION LINER		**530207-100**		**POC-liner-1**		**POC-liner-2**				**POC-liner-3**				**POC-liner-4**			
5.1 INNER DILUTION HOLES																	
Number of Holes		24		24		24				24				24			
Hole Diameter	mm	17.68		17.11		21.79				21.00				20.26			
Total Hole Area	$in.^2$	9.13		8.56		13.88				12.89				12.00			
5.3 OUTER DILUTION HOLES																	
Number of Holes		120		120		120				120				120			
Hole Diameter	mm	2.59		2.59		4.93				4.24				3.05			
Total Hole Area	$in.^2$	0.981		0.981		3.547				2.629				1.361			
5.4 EFFUSION HOLES																	
Number of Holes		1214		1214		4400				3570				2350			
Hole Diameter	mm	0.020		0.020		0.020				0.020				0.020			
6.0 TOTAL EFF OPENING AREA		19.55	100%	18.97	100%	22.29	100%	25.11	100%	23.94	100%	21.10	100%	22.28	100%	19.46	100%
Effusion Holes	$in.^2$	0.38	2.0%	0.38	2.0%	1.38	6.2%	1.38	5.5%	1.12	4.7%	1.12	5.3%	0.74	3.3%	0.74	3.8%
Outer Dilution Holes	$in.^2$	0.98	5.0%	0.98	5.2%	3.55	15.9%	3.55	14.1%	2.63	11.0%	2.63	12.4%	1.36	6.1%	1.36	7.0%
Effusion Area for Annulus, Injectors, and Inner Liner	$in.^2$	18.19	93.0%	17.61	92.8%	17.36	77.9%	20.19	80.4%	20.19	84.3%	17.36	82.2%	20.19	90.6%	17.36	89.2%
Effective Area – All Injectors	$in.^2$	8.84	45.2%	8.84	46.6%	6.02	27.0%	8.84	35.2%	8.84	37.0%	6.02	28.5%	8.84	39.7%	6.02	30.9%
Inner Dilution Holes	$in.^2$	9.13	46.7%	8.56	45.1%	13.88	50.1%	13.88	44.5%	12.89	46.6%	12.88	52.9%	12.00	50.0%	12.00	57.3%
Inner Dilution Slots	$in.^2$	0.21	1.1%	0.21	1.1%	0.21	0.8%	0.21	0.7%	0.21	0.8%	0.21	0.9%	0.21	0.9%	0.21	1.0%
dP vs. C200-C250 POC Condition	%	130		138		100		79		87		112		100		131	
PZ% Range (per Area Approx.)	%	27 – 45.2		27 – 46.6		27 – 35.2				27 – 37				30.9 – 39.7			

Table 14: Effusion Hole Design Case Summary

<table>
<tr><td colspan="2"></td><td colspan="2">C200 NG</td><td colspan="2">POC-1</td><td colspan="2">POC-2A</td><td colspan="2">POC-2B</td><td colspan="2">POC-3A</td><td colspan="2">POC-3B</td><td colspan="2">POC-4A</td><td colspan="2">POC-4B</td></tr>
<tr><td colspan="2"></td><td colspan="2">Production</td><td colspan="2">46.6% to PZ</td><td colspan="2">27% to PZ</td><td colspan="2"></td><td colspan="2">36.9% to PZ</td><td colspan="2">27% to PZ</td><td colspan="2">39.7% to PZ</td><td colspan="2">30.9% to PZ</td></tr>
<tr><td colspan="2">1.0 FUEL SECTION - INJECTOR</td><td colspan="2">528677-100</td><td colspan="2">POC-inj-1</td><td colspan="2">POC-inj-2</td><td colspan="2">POC-inj-1</td><td colspan="2">POC-inj-1</td><td colspan="2">POC-inj-2</td><td colspan="2">POC-inj-1</td><td colspan="2">POC-inj-2</td></tr>
<tr><td colspan="18">1.2 FUEL DISTRIBUTOR</td></tr>
<tr><td>Nominal Fuel Exit Diameter</td><td>in.</td><td colspan="2">0.036</td><td colspan="2">0.040</td><td colspan="2">0.040</td><td colspan="2">0.040</td><td colspan="2">0.040</td><td colspan="2">0.040</td><td colspan="2">0.040</td><td colspan="2">0.040</td></tr>
<tr><td>Number of Holes</td><td></td><td colspan="2">24</td><td colspan="2">24</td><td colspan="2">24</td><td colspan="2">24</td><td colspan="2">24</td><td colspan="2">24</td><td colspan="2">24</td><td colspan="2">24</td></tr>
<tr><td colspan="18">2.1 AIR – MIXING HOLES</td></tr>
<tr><td>Nominal Mixing Hole Diameter</td><td>in.</td><td colspan="2">0.5625</td><td colspan="2">0.6250</td><td colspan="2">0.3995</td><td colspan="2">0.6250</td><td colspan="2">0.6250</td><td colspan="2">0.3995</td><td colspan="2">0.6250</td><td colspan="2">0.3995</td></tr>
<tr><td>Number of Mixing Holes</td><td></td><td colspan="2">8</td><td colspan="2">8</td><td colspan="2">8</td><td colspan="2">8</td><td colspan="2">8</td><td colspan="2">8</td><td colspan="2">8</td><td colspan="2">8</td></tr>
<tr><td>Nominal Mixing Hole Area</td><td>in.^{2}</td><td colspan="2">1.988</td><td colspan="2">2.454</td><td colspan="2">1.003</td><td colspan="2">2.454</td><td colspan="2">2.454</td><td colspan="2">1.003</td><td colspan="2">2.454</td><td colspan="2">1.003</td></tr>
<tr><td colspan="2">5.0 COMBUSTION LINER</td><td colspan="2">530207-100</td><td colspan="2">POC-liner-1</td><td colspan="4">POC-liner-2</td><td colspan="4">POC-liner-3</td><td colspan="4">POC-liner-4</td></tr>
<tr><td colspan="18">5.1 INNER DILUTION HOLES</td></tr>
<tr><td>Number of Holes</td><td></td><td colspan="2">24</td><td colspan="2">24</td><td colspan="4">24</td><td colspan="4">24</td><td colspan="4">24</td></tr>
<tr><td>Hole Diameter</td><td>mm</td><td colspan="2">17.68</td><td colspan="2">17.11</td><td colspan="4">21.79</td><td colspan="4">21.00</td><td colspan="4">20.26</td></tr>
<tr><td>Total Hole Area</td><td>in.^{2}</td><td colspan="2">9.13</td><td colspan="2">8.56</td><td colspan="4">13.88</td><td colspan="4">12.89</td><td colspan="4">12.00</td></tr>
<tr><td colspan="18">5.3 OUTER DILUTION HOLES</td></tr>
<tr><td>Number of Holes</td><td></td><td colspan="2">120</td><td colspan="2">120</td><td colspan="4">240</td><td colspan="4">240</td><td colspan="4">240</td></tr>
<tr><td>Hole Diameter</td><td>mm</td><td colspan="2">2.59</td><td colspan="2">2.59</td><td colspan="4">3.95</td><td colspan="4">3.40</td><td colspan="4">2.43</td></tr>
<tr><td>Total Hole Area</td><td>in.^{2}</td><td colspan="2">0.981</td><td colspan="2">0.981</td><td colspan="4">4.550</td><td colspan="4">3.370</td><td colspan="4">1.720</td></tr>
<tr><td colspan="18">5.4 EFFUSION HOLES</td></tr>
<tr><td>Number of Holes</td><td></td><td colspan="2">1214</td><td colspan="2">1214</td><td colspan="4">1214</td><td colspan="4">1214</td><td colspan="4">1214</td></tr>
<tr><td>Hole Diameter</td><td>mm</td><td colspan="2">0.020</td><td colspan="2">0.020</td><td colspan="4">0.020</td><td colspan="4">0.020</td><td colspan="4">0.020</td></tr>
<tr><td>Total Hole Area</td><td>in.^{2}</td><td colspan="2">0.381</td><td colspan="2">0.381</td><td colspan="4">0.381</td><td colspan="4">0.381</td><td colspan="4">0.381</td></tr>
<tr><td colspan="2">6.0 TOTAL EFF OPENING AREA</td><td>19.55</td><td>100%</td><td>18.97</td><td>100%</td><td>22.29</td><td>100%</td><td>25.12</td><td>100%</td><td>23.94</td><td>100%</td><td>21.11</td><td>100%</td><td>22.29</td><td>100%</td><td>19.46</td><td>100%</td></tr>
<tr><td>Effusion Holes</td><td>in.^{2}</td><td>0.38</td><td>2.0%</td><td>0.38</td><td>2.0%</td><td>0.38</td><td>1.7%</td><td>0.38</td><td>1.5%</td><td>0.38</td><td>1.6%</td><td>0.38</td><td>1.8%</td><td>0.38</td><td>1.7%</td><td>0.38</td><td>2.0%</td></tr>
<tr><td>Outer Dilution Holes</td><td>in.^{2}</td><td>0.98</td><td>5.0%</td><td>0.98</td><td>5.2%</td><td>4.55</td><td>20.4%</td><td>4.55</td><td>18.1%</td><td>3.37</td><td>14.1%</td><td>3.37</td><td>16.0%</td><td>1.72</td><td>7.7%</td><td>1.72</td><td>8.8%</td></tr>
<tr><td>Effusion Area for Annulus, Injectors, and Inner Liner</td><td>in.^{2}</td><td>18.19</td><td>93.0%</td><td>17.61</td><td>92.8%</td><td>17.36</td><td>77.9%</td><td>20.19</td><td>80.4%</td><td>20.19</td><td>84.3%</td><td>17.36</td><td>82.2%</td><td>20.19</td><td>90.6%</td><td>17.36</td><td>89.2%</td></tr>
<tr><td>Effective Area – All Injectors</td><td>in.^{2}</td><td>8.84</td><td>45.2%</td><td>8.84</td><td>46.6%</td><td>6.02</td><td>27.0%</td><td>8.84</td><td>35.2%</td><td>8.84</td><td>37.0%</td><td>6.02</td><td>28.5%</td><td>8.84</td><td>39.7%</td><td>6.02</td><td>30.9%</td></tr>
<tr><td>Inner Dilution Holes</td><td>in.^{2}</td><td>9.13</td><td>46.7%</td><td>8.56</td><td>45.1%</td><td>13.88</td><td>50.1%</td><td>13.88</td><td>44.5%</td><td>12.89</td><td>46.6%</td><td>12.88</td><td>52.9%</td><td>12.00</td><td>50.0%</td><td>12.00</td><td>57.3%</td></tr>
<tr><td>Inner Dilution Slots</td><td>in.^{2}</td><td>0.21</td><td>1.1%</td><td>0.21</td><td>1.1%</td><td>0.21</td><td>0.8%</td><td>0.21</td><td>0.7%</td><td>0.21</td><td>0.8%</td><td>0.21</td><td>0.9%</td><td>0.21</td><td>0.9%</td><td>0.21</td><td>1.0%</td></tr>
<tr><td>dP vs. C200-C250 POC Condition</td><td>%</td><td colspan="2">130</td><td colspan="2">138</td><td colspan="2">100</td><td colspan="2">79</td><td colspan="2">87</td><td colspan="2">111</td><td colspan="2">100</td><td colspan="2">131</td></tr>
<tr><td>PZ% Range (per Area Approx.)</td><td>%</td><td colspan="2">27 – 45.2</td><td colspan="2">27 – 46.6</td><td colspan="4">27 – 35.2</td><td colspan="4">27 – 37</td><td colspan="4">30.9 – 39.7</td></tr>
</table>

Table 15: No Effusion Hole Design Case Summary

COMBUSITON DESIGN CONCLUSIONS

A preliminary design for C250 POC combustion system has been completed. The completed tasks include:

- Upper level requirements analysis
- Combustion analysis
- Top level flow split analysis and analysis of impact on combustion performance — including AFT, emissions, flashback and stability
- Proposed design cases for C250 POC engine combustion system, including a design case for matching C200 emissions and several cases for achieving lower pressure drop, while maintaining combustion performance

6.2.4. Rotor dynamics and Bearing Design

LP Spool RBS Requirements

Definition

The rotor and bearings assembly provides the location and structure for the rotating components and the interface between rotating and static components. This includes:

- bladed rotating components — for example, compressor and turbine wheels
- bearing journals
- connecting shafting within the rotor
- bearings
- rotor dynamics analysis

The rotor is the only rotating component of the MEM. In the typical Capstone design, there is a single rotor, made up of several components, such as an impeller, turbine wheel, and generator magnet shaft. However, any rotating component within the MEM is considered to part of the rotor group. Bearings allow relative motion between the rotating and non-rotating components. In the typical Capstone design, the bearings are oil-free, air foil bearings with distinctly separate thrust and radial bearings. Due to the similarity of applicable analyses, seals are considered together with the bearings.

Requirements

Design requirements were derived from thermodynamic cycle model predictions. Key requirements identified were:

- oil-free bearings
- RBS life of 20,000 hours
- rated speed of 54,284 rpm at 194 kW Net Output Power at LP generator lead
- desired over speed margin of 10%
- RBS to provide dynamic load support at all engine operating conditions, such as during start and stop, steady state, and transient load cycles

LP Spool RBS Design

The C250 design is a scaled up modification of the C200 which required the following changes to the C200 rotating group hardware in order to meet the power demand of the C250:

- generator magnet shaft
- compressor wheel

Since power is proportional to air flow, adjustments were made in the compressor wheel aerodynamic blade profile and tip diameter to provide more air flow. Similarly, magnet size on the generator shaft was increased to provide magnetic flux needed to generate the required power at the generator lead. These changes in the rotating group hardware necessitated re-evaluation of LP Spool RBS rotor dynamics.

Detailed electromagnetic FEAs were performed for magnet re-sizing to achieve 250 kW at the LP spool generator lead. Based on several trade studies performed, it was decided that an increase to magnet length was preferred over a change in diameter to minimize changes to

- magnet retaining sleeve
- rotor bearing system

- rotor windage

The following approach was employed during the design effort:

1. Reevaluate the rotor dynamics of the generator magnet shaft
2. Design and build a rotor dynamics test rig to verify generator magnet shaft with new magnet design
3. Test and validate the generator magnet shaft on the rotor dynamics rig
4. Test generator magnet shaft in an actual engine for design verification

Generator Magnet Shaft Rotor Dynamics

A detailed rotor dynamics model was built using commercial FEA code. The model included the turbine rotor, generator rotor, and the shaft coupling. Figure 20 shows the model's Undamped Critical Speed (UCS) map. All rigid body modes are below 20,000 rpm at various bearing stiffness values depicted in black, red, green, and blue lines. Four radial bearings — two each at the turbine and generator shafts — were modeled, resulting in four rigid body modes. The gray line shows first bending mode at 71,111 rpm, which would provide 31% critical speed design margin.

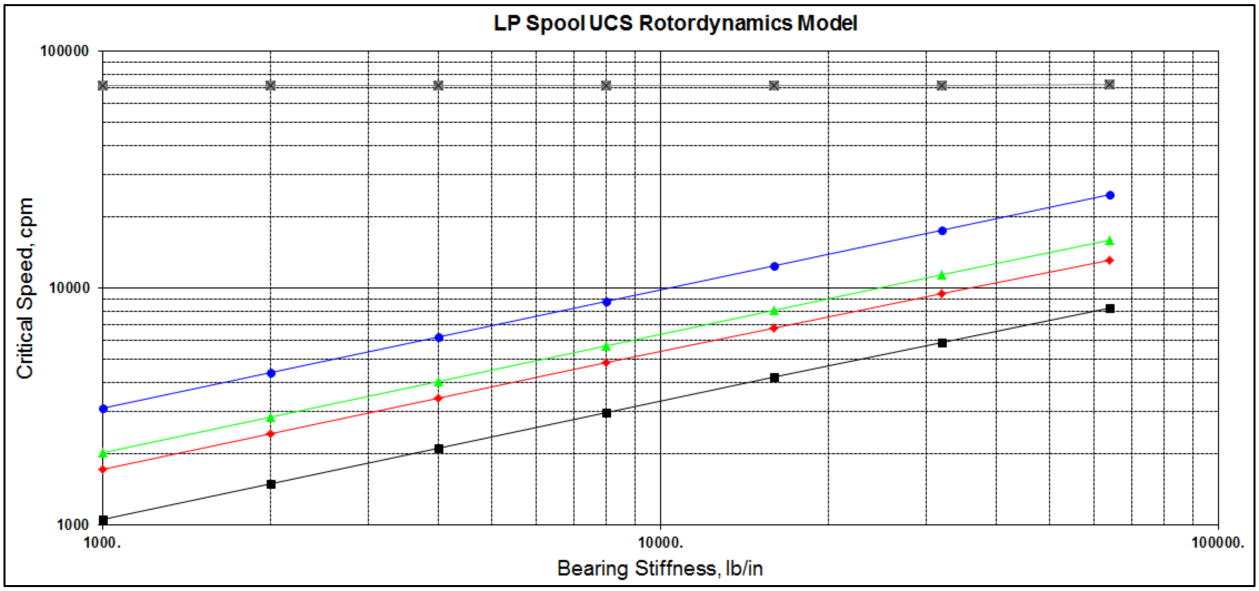

Figure 20: LP Spool UCS Model

Bearing dynamic force coefficients were used as an input in the rotor dynamic model to perform stability analysis — Damped Eigen Value. Synchronous forced response analysis was also performed, per ISO G2.5 balance standard for in and out of phase imbalance conditions for synchronous response and bearing dynamic loads. All analyses showed satisfactory rotor group performance results at all operating conditions.

Rotor Dynamics Test Rig

A high speed, motor driven rotor dynamics test rig was designed and built to verify the generator magnet shaft with longer magnet. This test rig used the same generator shaft and bearings as the engine. The rig was fully instrumented with thermocouples at various locations, see Figure 21 below. Orthogonal proximity probes were installed at each bearing location to monitor rotor vibration. The rig ran to progressively higher speeds to verify the generator magnet shaft rotor dynamics.

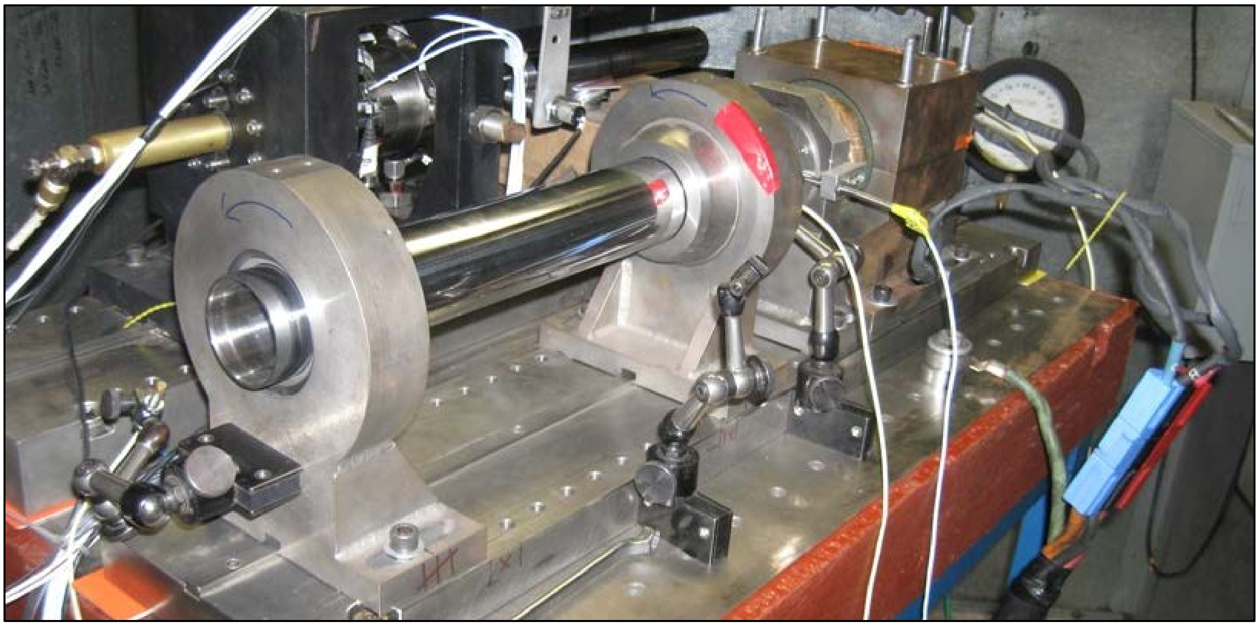

Figure 21: Generator Shaft Rotor dynamics Test Rig

The Bode plot in Figure 22 shows rotor dynamic model correlation with actual test data collected at FWD bearing location during the rig test. This FWD bearing location is at the non-coupling end of the test rig — toward left, as shown in Figure 21 above. The solid red line in Figure 22 depicts predicted rotor response and the blue line shows data from actual test following the same trend. The difference in vibration amplitude is attributed to the variance between the predicted and actual system damping present. This also emulates successful demonstration of generator shaft operation up to 75,000 rpm, well above design speed of 60,000 rpm.

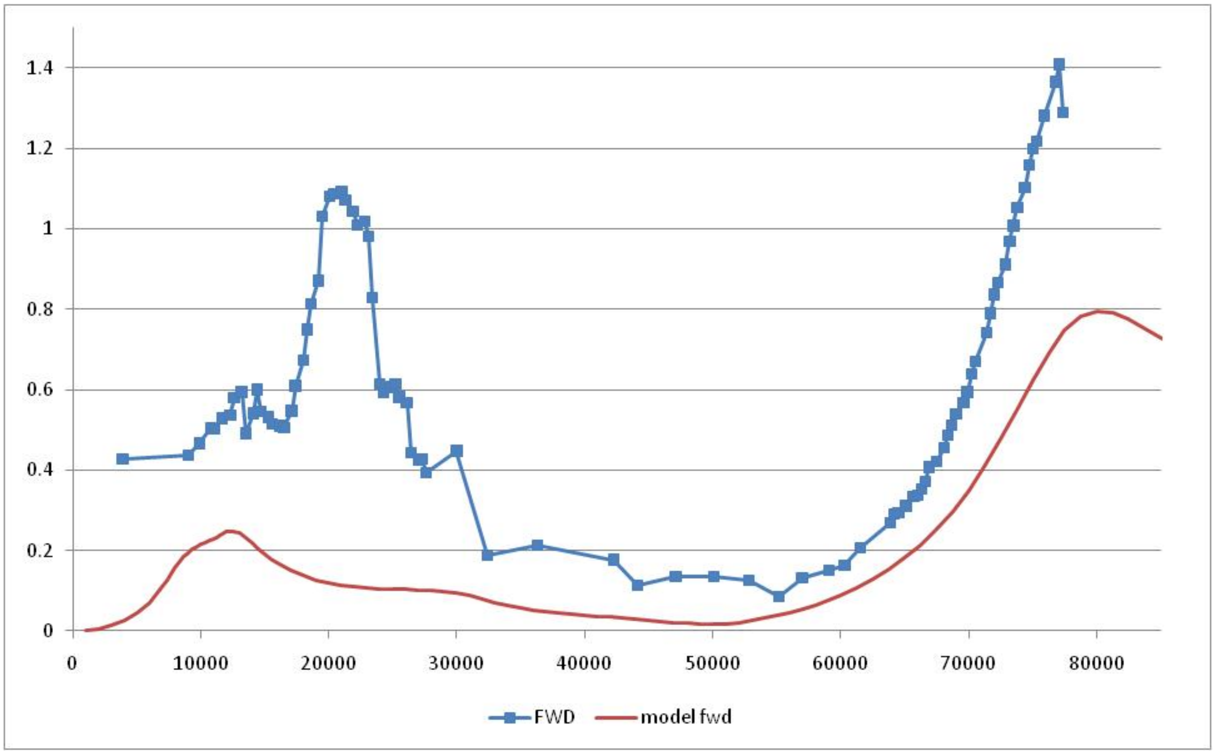

Figure 22: Rotor dynamics Model Validation on the Test Rig

Engine Level Test

Completion of component level testing on the rotor dynamics test rig was followed by testing on the actual product — viz., a C250 microturbine engine. The engine was built and successfully tested at 60,000 rpm with all of the updated static and rotating group hardware, producing 250 kW plus power at the generator lead. Figure 23 is a waterfall plot of the generator shaft vibration response at one of the bearing locations while rotating at 60,000 rpm. Synchronous response observed during testing was low. Sub-synchronous response, although not shown, was almost negligible. This data validated the generator shaft design with longer magnet.

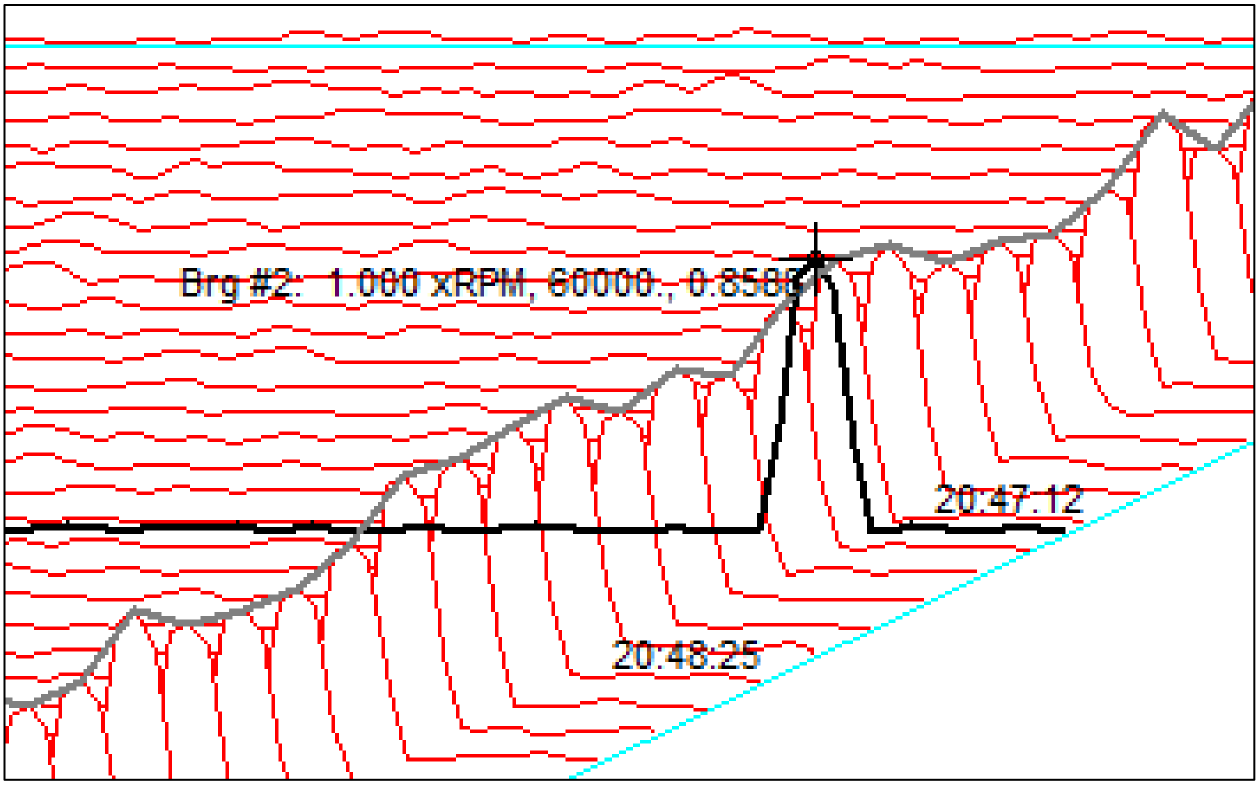

Figure 23: Generator Shaft Design Validation at Engine Level

6.2.5. Compressor Design

Compressor Stage Design Objectives and Requirements

The C250 compressor stage design targets — shown in Table 16 — were developed based on a C250 cycle study. The general design approach is to develop a centrifugal impeller — flank-milled impeller — with a wedge diffuser. The performance target is to obtain a mass flow rate of 3.6 lbs. /s and a pressure ratio of 5.

Parameter	Unit	Value
Mass Flow	lbs./s	3.6
Inlet Temperature	°F	66.7
Inlet Pressure	psia	14.617
Pressure Ratio	—	5
Target Peak Efficiency	%	83
Minimum Efficiency	%	81
Shaft Speed	krpm	30 – 60

Table 16: C250 Compressor Stage Design Objectives

Compressor Stage Design – Impeller

A centrifugal impeller was developed and key impeller dimension defined. See Table 17. The impeller is a 9 (main blades) + 9 (splitter blades) configuration. See Figure 24. Main blade thickness of the impeller was set at 0.069 in. at the leading edge (LE), rising to approximately 0.096 in. at mid-chord, then thinning to 0.071 in. at the trailing edge (TE). The splitter blade was slightly thinner than the main blade with a maximum thickness of 0.087 in. Both blades have “cut-off” designs and the same trailing edge thickness. The impeller wheel diameter is 6.988 in.

Due to flank-milling manufacturing requirements, impeller blades are specified on hub and shroud sections whereas intermediate sections are interpolated. With assumed vane clearance, the shroud diameter over the inducer is 4.72 in. and axial width at the outlet is 0.39 in.

Parameter	Unit	Value
Inlet hub diameter	in.	2.096
Inlet tip diameter	in.	4.704
Radial clearance at inlet	in.	0.010
Axial Clearance at Outlet	in.	0.005
Outlet Tip diameter	in.	6.988
Vane count	ea.	9 + 9

Table 17: Key Impeller Dimensions

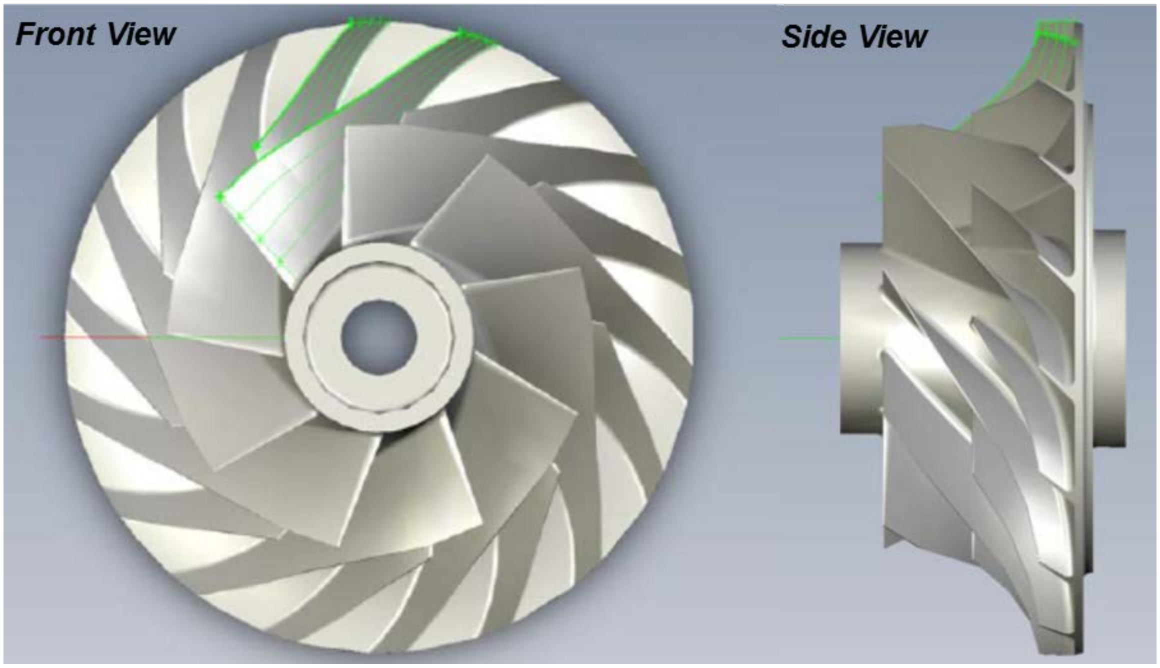

Figure 24: C250 Impeller Design

Compressor Stage Design – Diffuser

The diffuser vane is a wedge design. Diffuser LE is located at a radius ratio of 1.17 from the impeller TE. This relatively large gap minimizes the potential interaction between the diffuser and impeller and avoids problems of forced response vibration. The final diffuser geometry is illustrated in Figure 25 and key dimensions are shown in Table 18.

Parameter	Unit	Value
Inlet Diameter	in.	8.150
Outlet Diameter	in.	13.992
Throat Area	in.^{2}	2.813
Channel Width	in.	0.315
Inlet Vane Angle	°	76.5
Divergence Angle (2θ)	°	8.9
Vane Count	ea.	19

Table 18: Key C250 Diffuser Dimensions

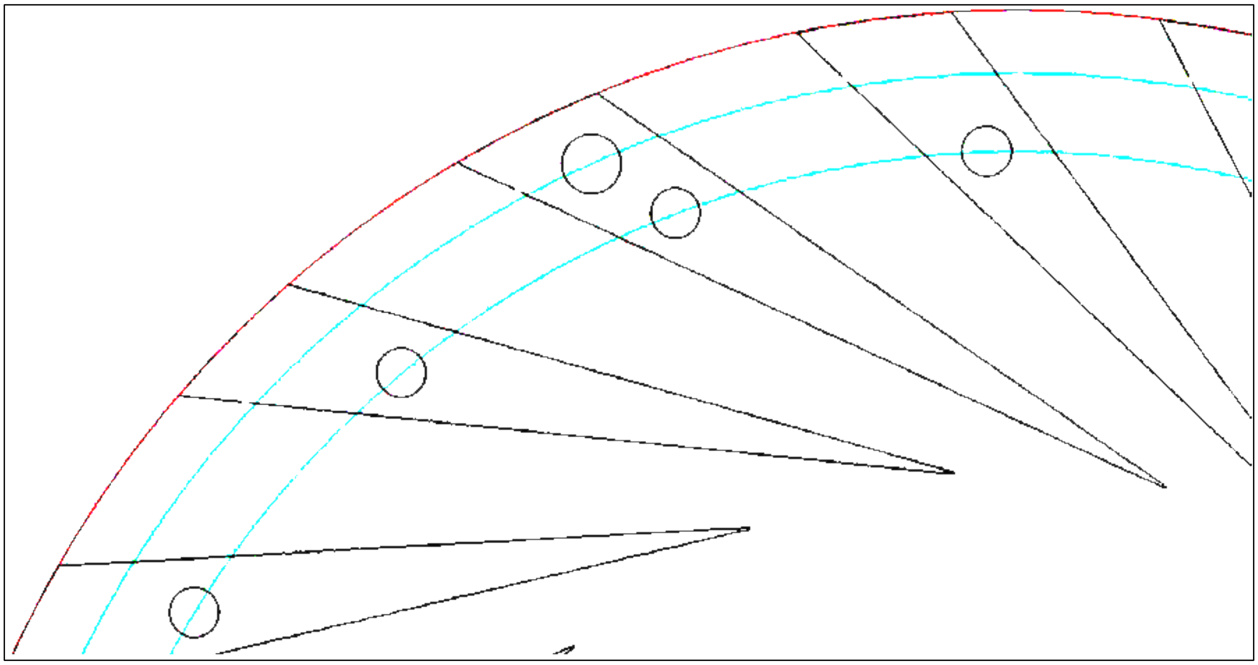

Figure 25: C250 Diffuser Design

Compressor Stage Performance

A multi-stage aerodynamic simulation was performed to evaluate and validate compressor stage design. The simulation was conducted by using ANSYS CFX version 12. The computation domain includes a single passage of impeller and diffuser as shown in Figure 26.

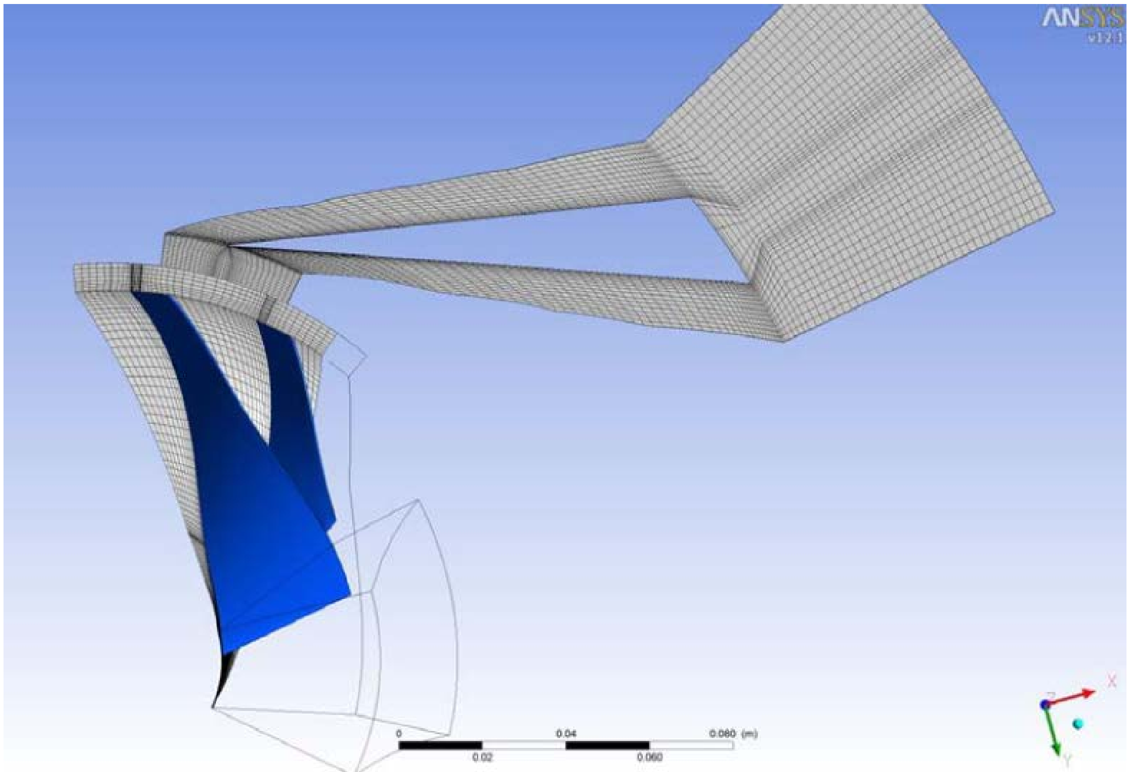

Figure 26: C250 Simulation Computation Domains for Compressor Stage

When simulation results are distilled to 1D values — see Figure 27 and Figure 28 — it is observed that the current design satisfies design target.

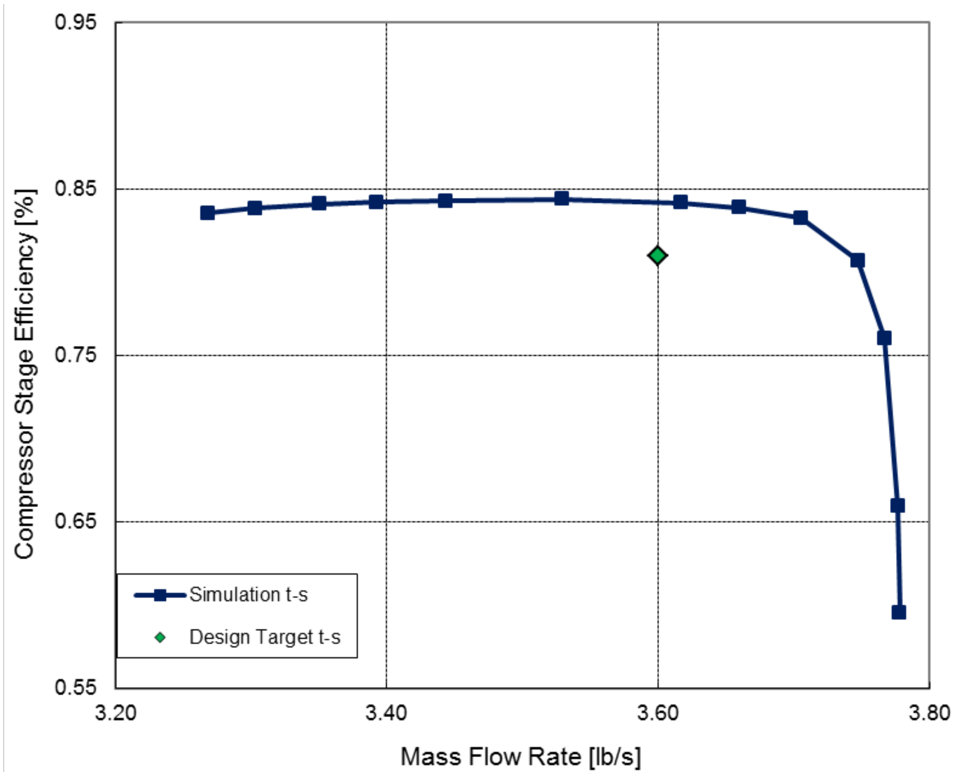

Figure 27: C250 Stage Efficiency Simulation Results

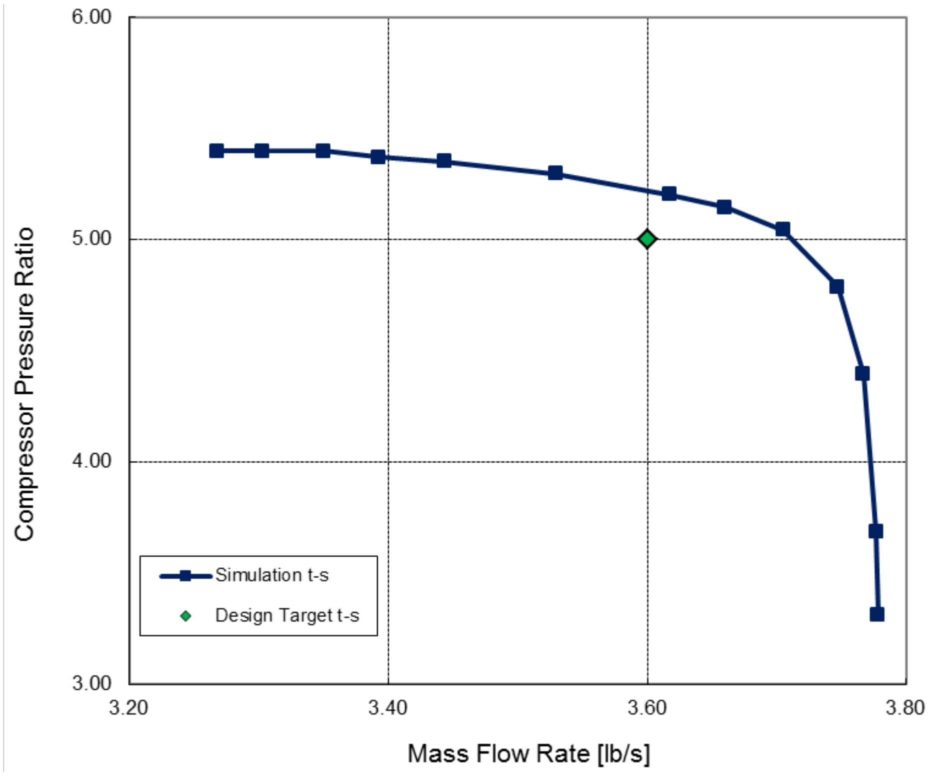

Figure 28: C250 Pressure Ratio Simulation Results

Impeller contour plots of relative Mach number (Mn) from simulation results at 20%, 50%, and 80% for three operating conditions — near surge (3.40 lbs./s), near impeller peak efficiency (3.66 lbs./s), and near choke (3.77 lbs./s) — are shown in Figure 29.

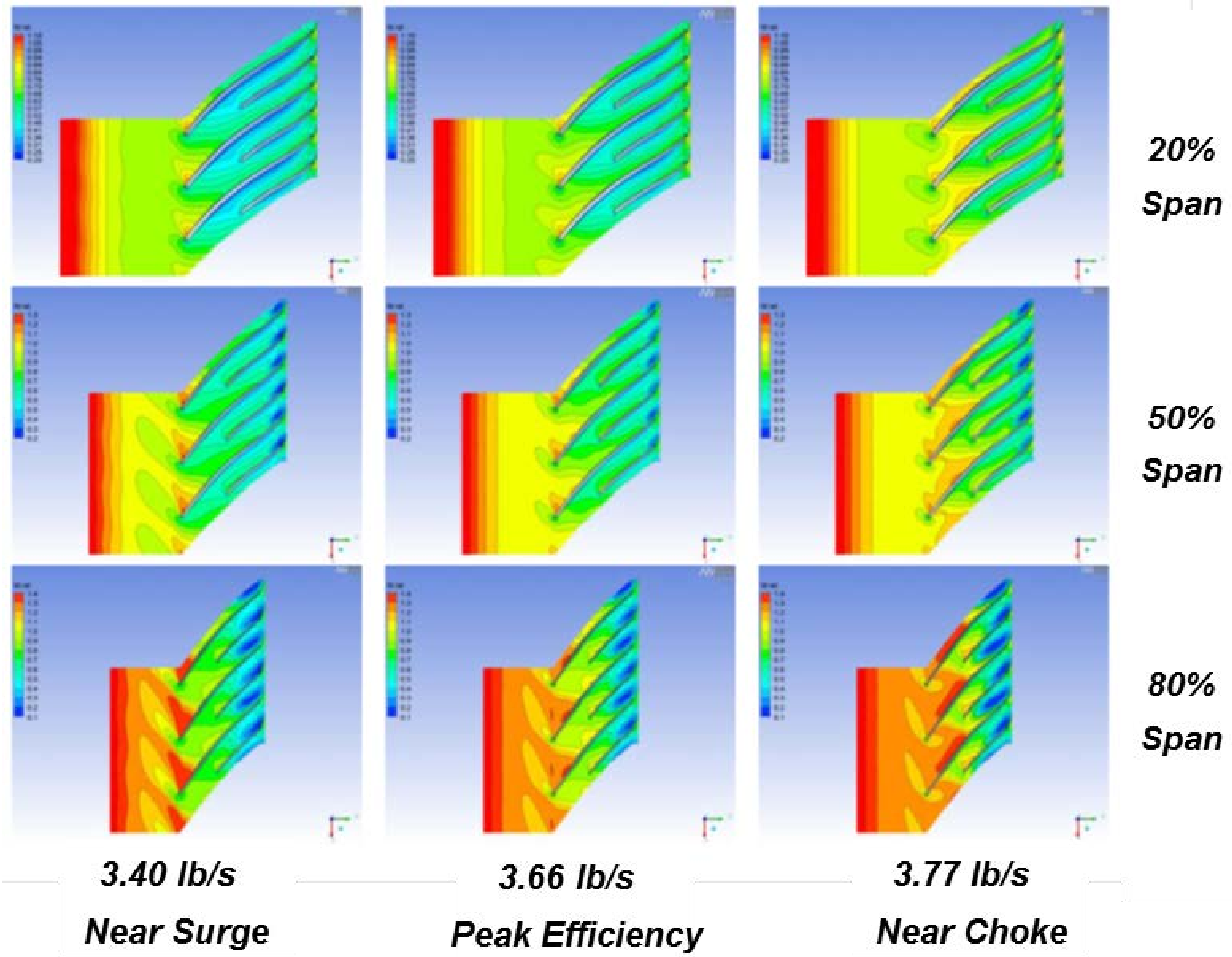

Figure 29: C250 Impeller Relative Mach Number Contour

Simulation results indicate that the impeller has a supersonic patch in the inducer which has been controlled in camber to keep an almost constant relative Mn ahead of the start of the covered passage. As the stage is throttled towards stall, the shock becomes expelled. The shock falls back inside the covered passage towards choke. The recambering of the splitter avoids local overspeed successfully. There is no apparent separation at the sections. Blade loading distribution is shown in Figure 30. Figure 30 also shows the corresponding static pressure distribution on the impeller blade surface. The blades look to be well-matched radially judging by the leading edge incidence as shown by the gap between the pressure on suction and pressure surfaces.

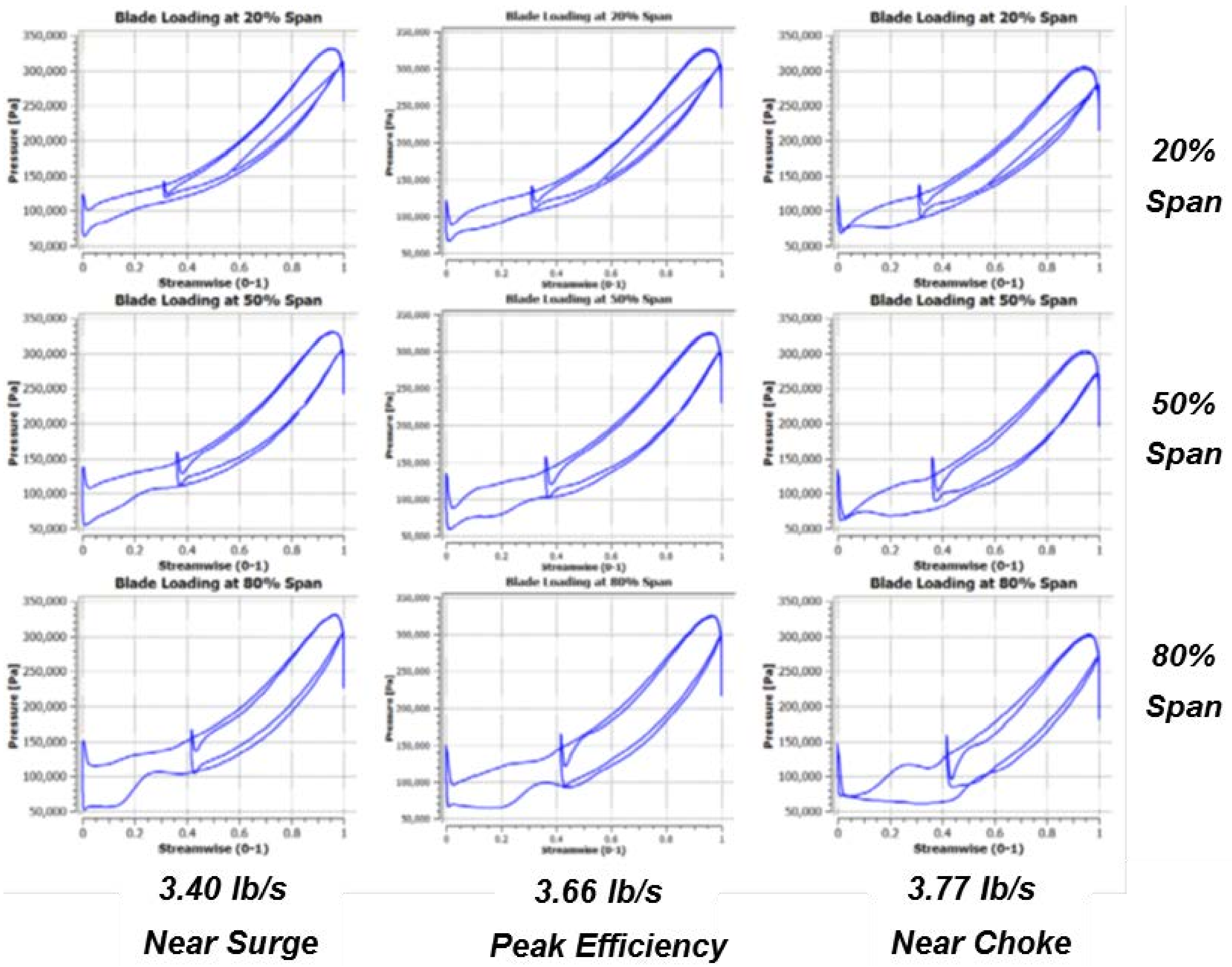

Figure 30: C250 Impeller Blade Loading

Similar plots are given for the diffuser domain in Figure 31 and Figure 32. The incidences based on full passage, area-averaged inlet gas angles are approximately -2.8°, -4.7°, and -6.9°. The thick wakes from the wedges are a dominant feature.

There is a slight tendency for the diffuser to be closer to separation within the passage at 20% span in the mid-map and toward stall results, otherwise the flow seems well attached. There is a strong shock inside the passage at near choke condition which results in flow separation. The pressure distribution — see Figure 32 — shows well low incidence in the mid-map location. There is some incidence evident towards stall as the gap between surface and pressure at the LE shows a local increase in loading.

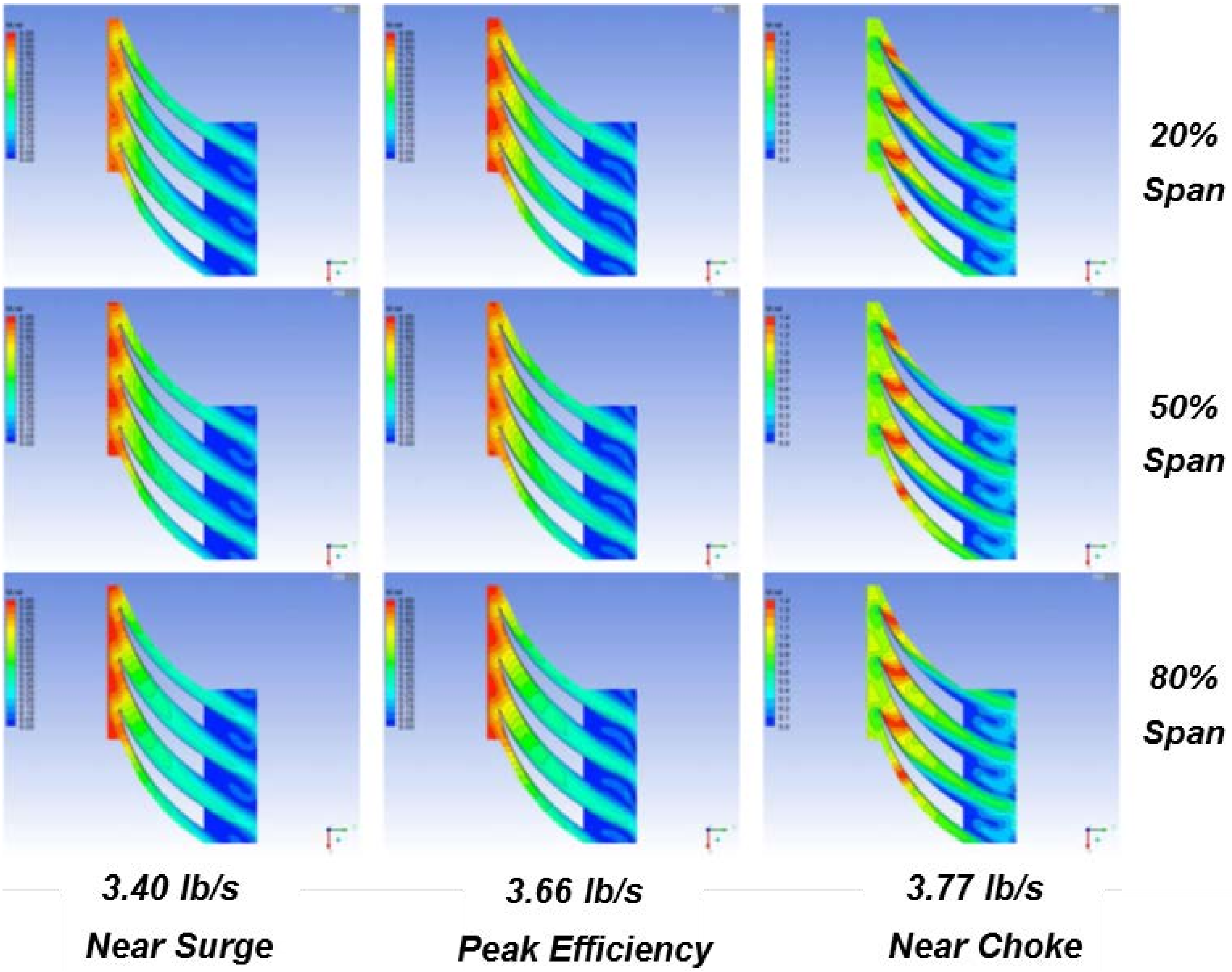

Figure 31: C250 Diffuser Relative Mach Number Contour

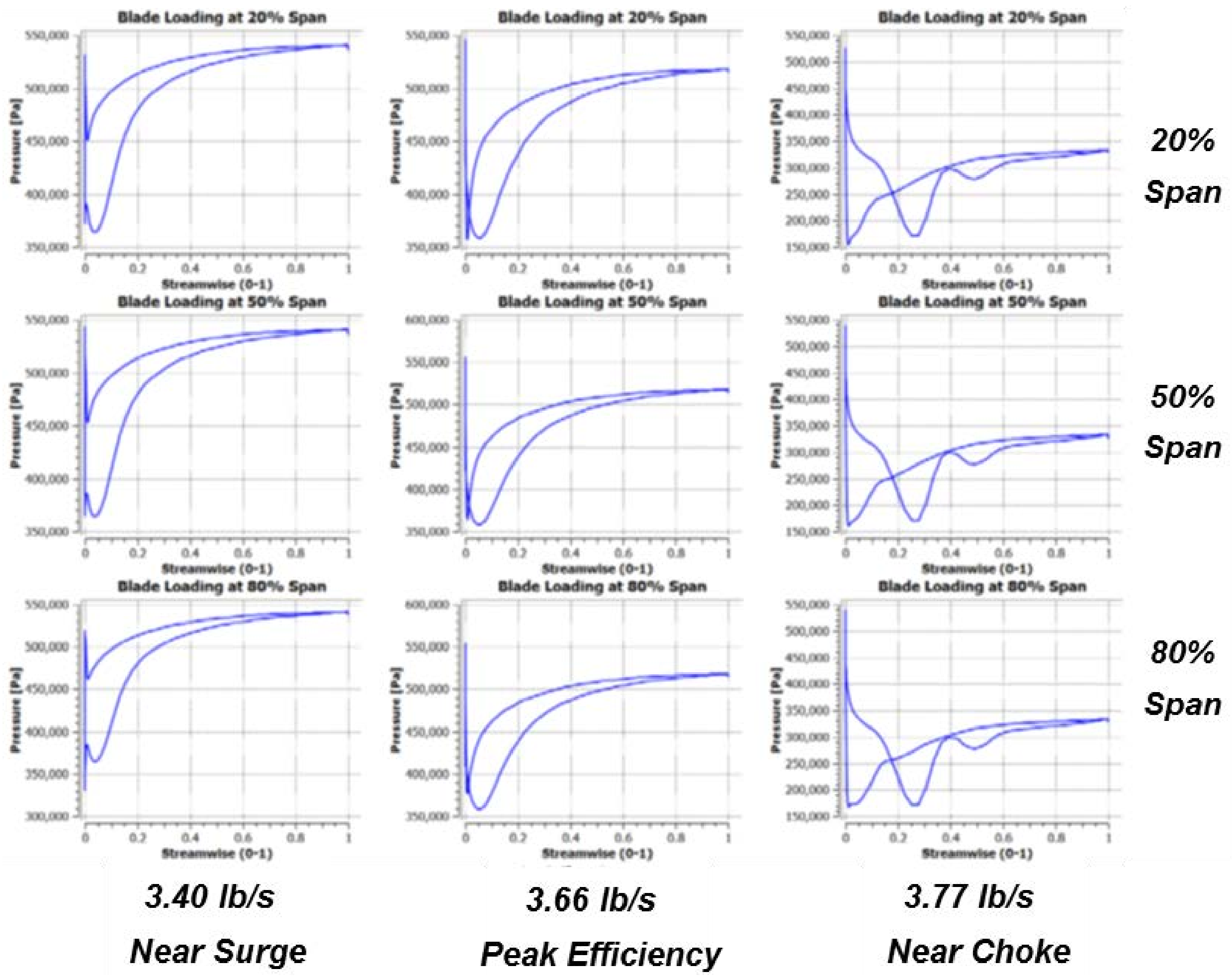

Figure 32: C250 Diffuser Blade Loading

Impeller Geometry and FEA Model

The mechanical analysis was based on the finalized blade profile and disk profile illustrated in Figure 33. The vane-to-hub fillet radius was set to .079 in. The chosen material is Ti6lAl4V and its assumed mechanical properties are given in Table 19. Elastic analysis is performed at a speed of 60,000 rpm.

Temperature (°F)	68	212	392	572	752
Young's Modulus E ($\times 10^6$) psi	16.5	16.1	15.5	15.0	144.2
Poisson's Ratio	0.3255	0.3255	0.3255	0.3255	0.3255
Density (lbm/in.^{3})	0.160	0.160	0.160	0.160	0.160
0.2% Yield Strength ksi	134.85	117.45	101.5	92.51	83.375
Ultimate Tensile Strength (UTS) ksi	148.915	132.675	117.015	107.88	100.485
Coefficient of Thermal Expansion ($\times 10^{-6}$) in./in./°F	15.5	16.0	16.6	17.2	18.0
Thermal Conductivity (BTU/hr-°F-ft)	2.43	3.06	3.81	4.56	5.26

Table 19: Ti6Al4V Material Mechanical Properties for Elastic FEA

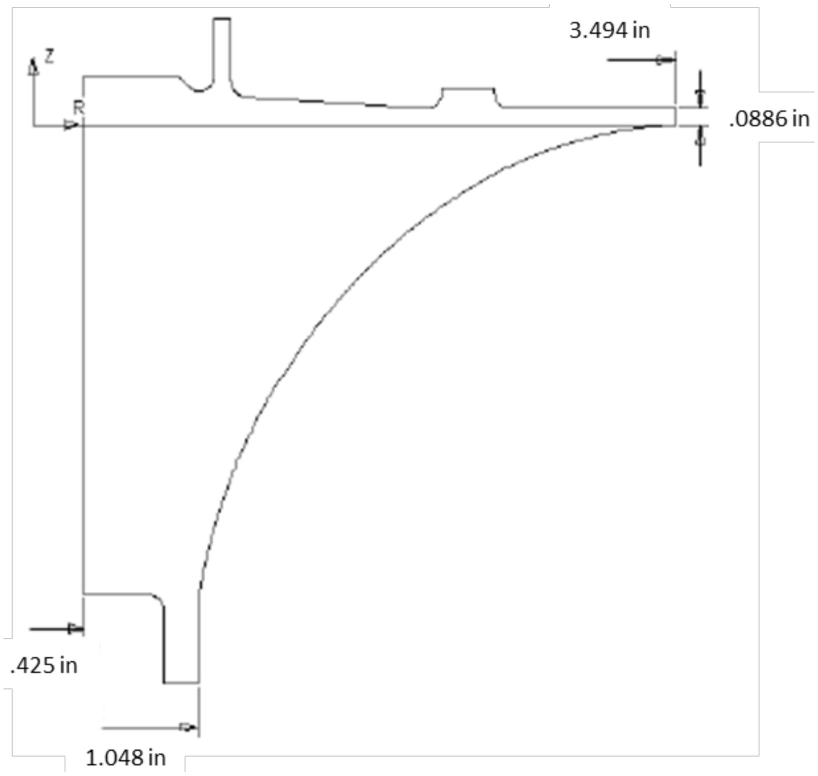

Figure 33: C250 Impeller Disk Profile

Due to cyclic symmetry of the impeller (9 main + 9 splitter blades), a cyclic sector FE model — see Figure 34 — was developed for the elastic analysis. The impeller weighs 4.28 lbm.

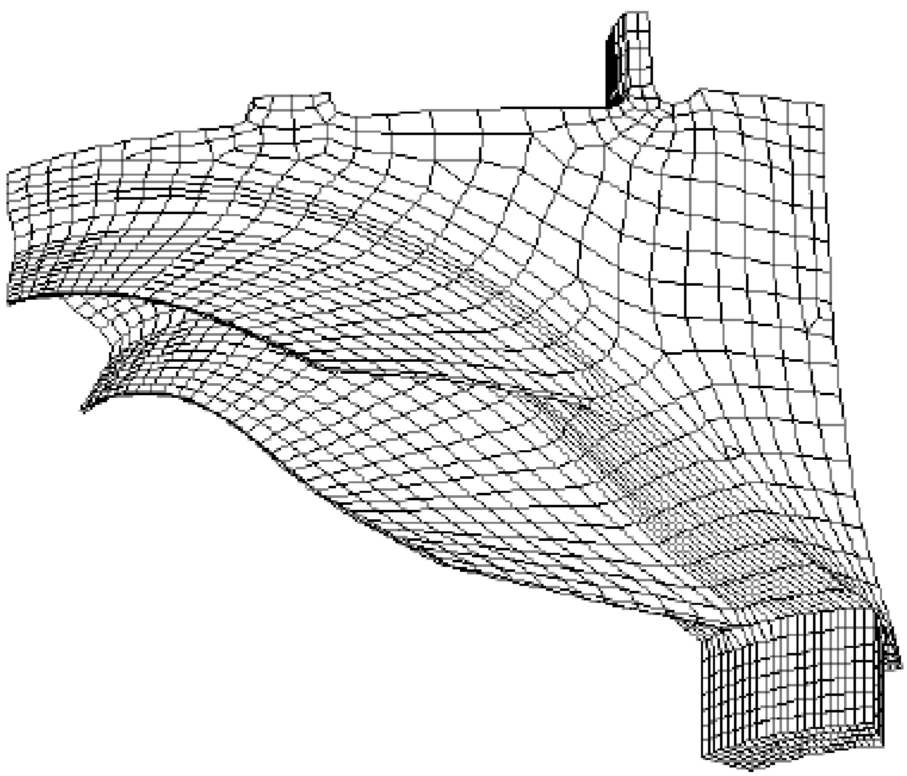

Figure 34: C250 Finite Element Model for a Cyclic Sector Impeller

Impeller Temperature

A steady-state temperature conduction analysis was performed with the following boundary conditions — face letters reference Figure 35:

1. Temperature distribution on the main and splitter vane surfaces and the gas-swept surfaces at the impeller hub, obtained by mapping the static temperature distribution computed from the CFD analysis at the nominal operating point on the FE model.
2. Temperature of 167 °F on face 'A'.
3. Temperature of 320 °F on faces 'B' and 'C'.

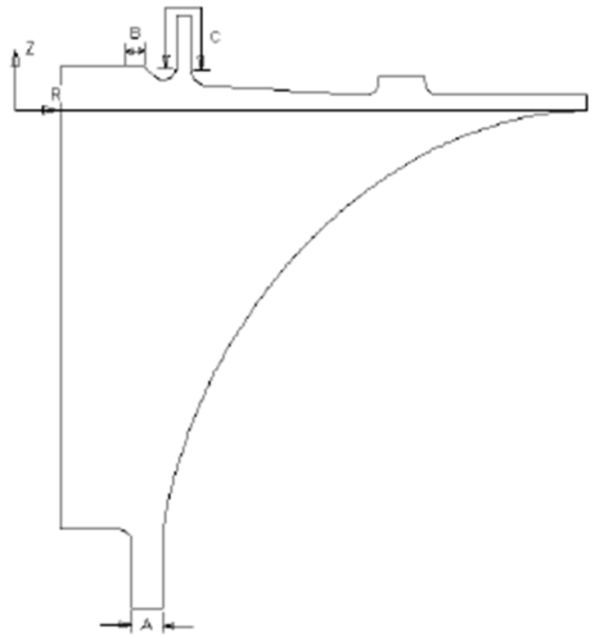

Figure 35: Specified Temperature Boundaries on the Impeller Disk

The computed steady-state temperature distribution is illustrated in Figure 36 and indicates that the impeller rim reaches a temperature of approximately 320 °F while the bore reaches 257 °F.

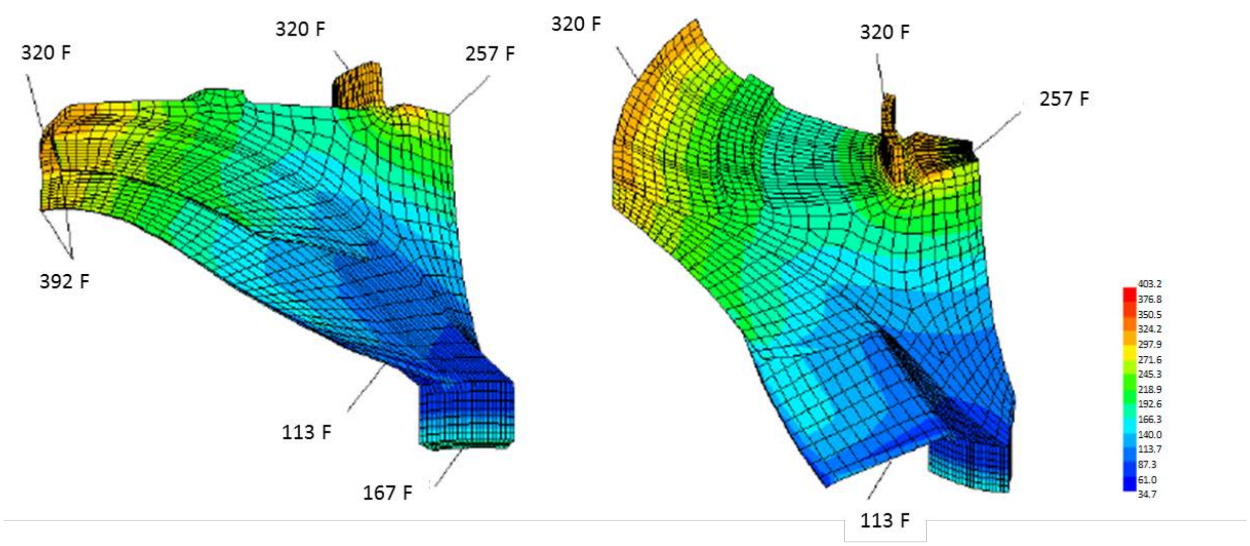

Figure 36: C250 Impeller Steady-State Temperature Distribution

Impeller Stress Analysis

The boundary conditions for the elastic stress analysis are summarized as follows — face letters reference Figure 35:

1. Cyclic symmetry displacement boundaries on the faces defining the disk sector
2. Axial and tangential displacement constraints on face 'A'
3. Tangential displacement constraint on face 'B'
4. Rotational speed of 60,000 rpm
5. Temperature body force presented above

The von-Mises stress distribution is illustrated in Figure 37 and discrete values are given in Table 20. The maximum stress occurs in the bore at 101 ksi.

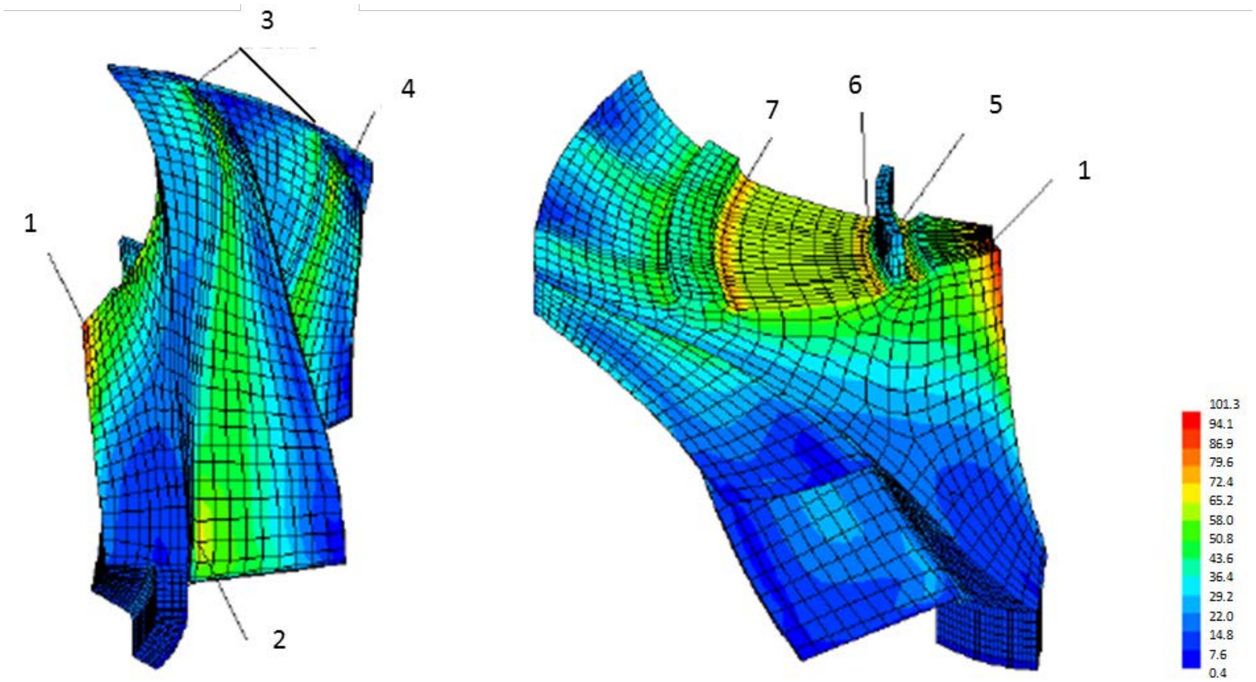

Figure 37: C250 Impeller von-Mises Stress Diagram

Position		Von-Mises Stress (ksi)
1	Bore	101
2	Main vane, leading edge – hub	70
3	Main and splitter vane, trailing edge – hub	51
4	Main and splitter vane, trailing edge – approx. 30% span	62.4
5	Fillet under rear stub shaft	72.5
6	Fillet above rear stub shaft	74
7	Balancing ring filler radius	77.6

Table 20: von-Mises Stresses

Using the volume-weighted mean, equivalent stress was calculated to be 33 ksi giving a burst margin at design speed of 1.625. This is based on 70% of the ultimate tensile strength of 124 ksi, at an estimated disk temperature of 302 °F.

The displacements of the impeller main vane at selected position are given in Table 21. The positions in the table reference Figure 38.

	Position	U-Radial Displacement (in.)	V-Tangential Displacement (in.)	W-Axial Displacement (in.)
1	Main vane LE shroud	0.0057	0.0265	0.0321
2	Main vane LTE shroud	0.0106	0.0076	-0.0084
3	Main vane disk rim	0.0088	0.0001	-0.0143
4	Splitter vane LE shroud	0.0048	0.0120	0.0079
5	Splitter vane TE shroud	0.0108	0.0078	-0.0083
6	Splitter vane disk rim	0.0088	0.0001	-0.0143

Table 21: C250 Impeller Vane Displacements

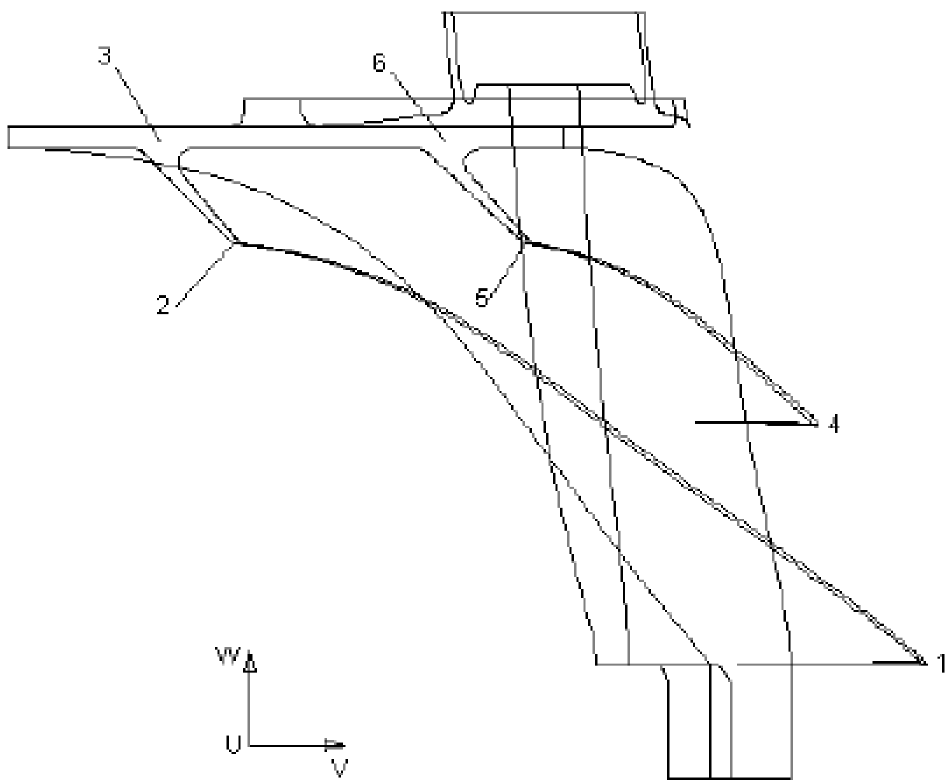

Figure 38: Key Points of Vane Displacement

Impeller Modal Analysis

A modal analysis was conducted to compute the natural frequencies of the impeller vane modes. The analysis was based on a running speed of 60,000 rpm, where effects of stress stiffening and inertia are included.

Since there are 19 diffuser vanes downstream of the impeller, 1 nodal diameter family of modes was selected as it may be aliased to 19 nodal diameters with a cyclic sector model of 1/9 of the impeller containing 9 main vanes and 9 splitter vanes. The relationship between aliased nodal diameters is summarized as follows:

For a given number of cyclic sectors, N, the nodal diameters that are aliased to each other are: $N-n$, $N+n$, $2N-n$, $2N+n$, etc. where n is the phase angle multiplier, or nodal diameter, that takes on values of 0, 1, $2 \ldots N/2$ if N is even, or $(N-1)/2$ if N is odd.

According to the above formula, 8ND, 9ND, 17ND, and 19ND are all aliased to each other for 1ND case ($n=1$). 19/rev passing frequency from the diffuser vane will excite the 19ND modes, which is aliased to 1ND.

The computed natural frequencies for the 1ND family — which is aliased to the 19/rec excitation resulting from the number of diffuser vanes — are presented in Table 22. These results and the Campbell diagram — Figure 39 — show that the 19/rev excitation corresponding to 19,000 Hz at the running speed is close to modes 22 to 24, which occur in the range from 18,530 Hz to 19,705 Hz.

However, these are high order modes with frequencies that are difficult to accurately predict due to material and manufacturing variability and inaccuracies in the modal analysis. To reduce the aerodynamics excitation forces developed by the diffuser vanes, it is common practice to limit the radial proximity of the vane leading edge to the impeller tip. The length of this radial, vane-less space is typically 15% of the impeller tip radius.

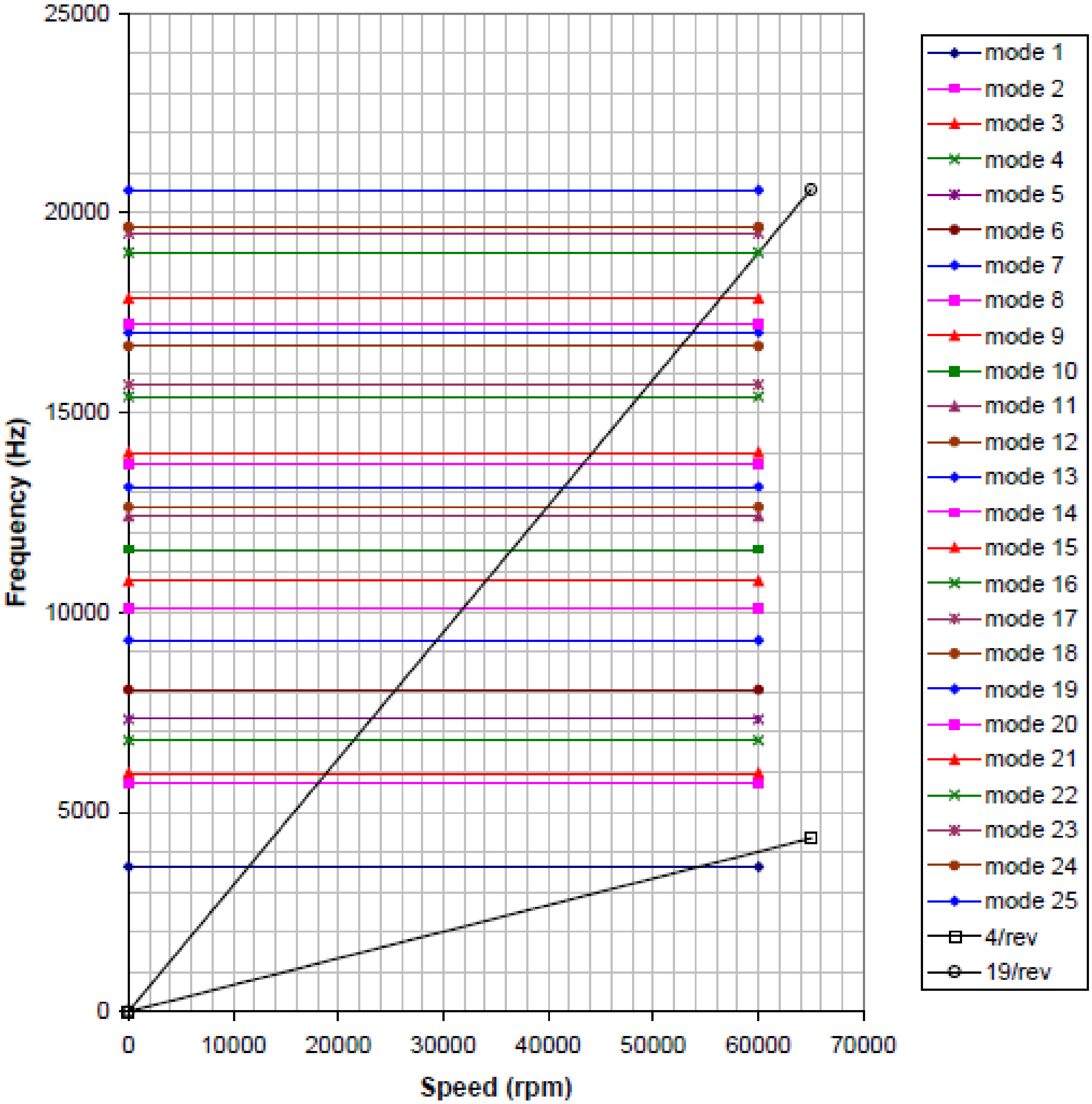

Figure 39: C250 Impeller Campbell Diagram - 1ND Family

Mode	f – Hz
1	3627
2	5720
3	5969
4	6789
5	7317
6	8064
7	9302
8	10081
9	10780
10	11577
11	12397
12	12632
13	13139
14	13700
15	14005
16	15397
17	15695
18	16665
19	17012
20	17223
21	17857
22	19005
23	19492
24	19651
25	20574

Table 22: Computed 1ND Family Natural Frequencies

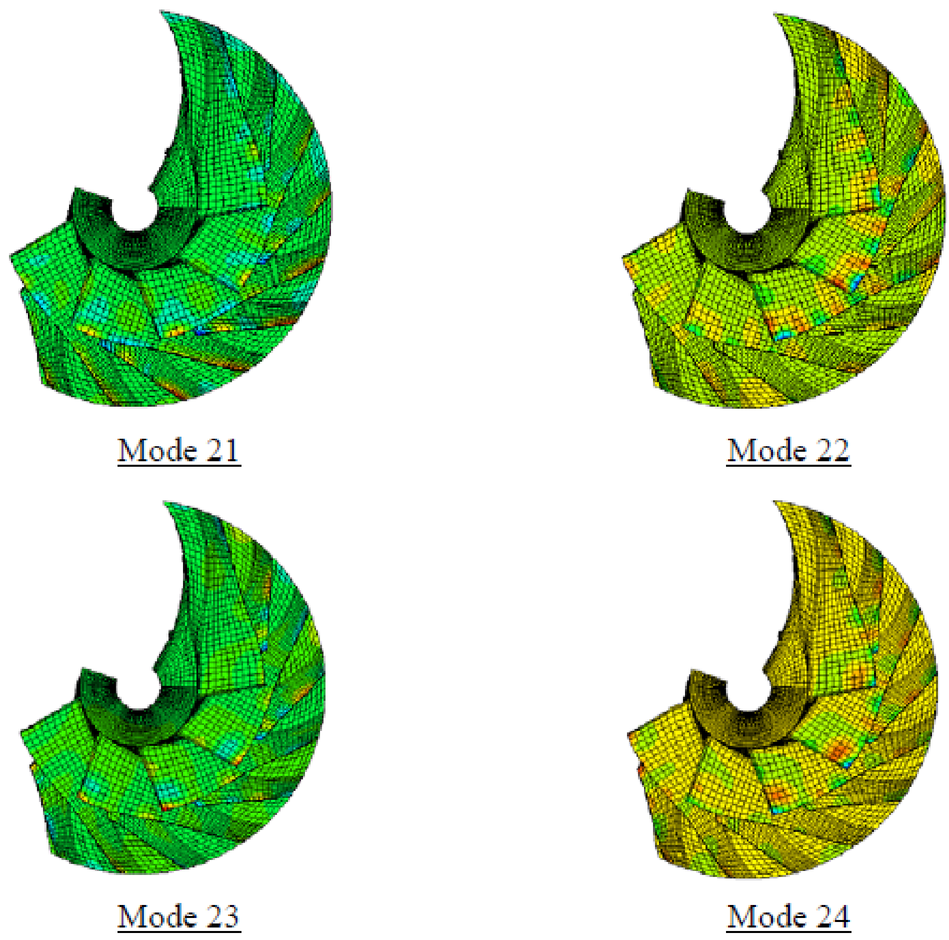

Figure 40: 1NF Family Modes 21 to 24

A 4ND family of natural frequencies was also computed since it is common to design the impeller so that the first mode is above a 4/rev passing frequency. The computed natural frequencies are listed in Table 23. The impeller first mode is below the 4/rev — 4 kHz — but above the 3/rev — 3 kHz. The first natural frequency occurs approximately midway between the 3/rev and 4/rev excitation, which is deemed to be acceptable.

Mode	f – Hz	Mode	f – Hz
1	3643	7	9495
2	5911	8	10420
3	7072	9	11254
4	7923	10	12105
5	8711	11	13136
6	9293	12	13822

Table 23: Computed 4ND Family Natural Frequencies

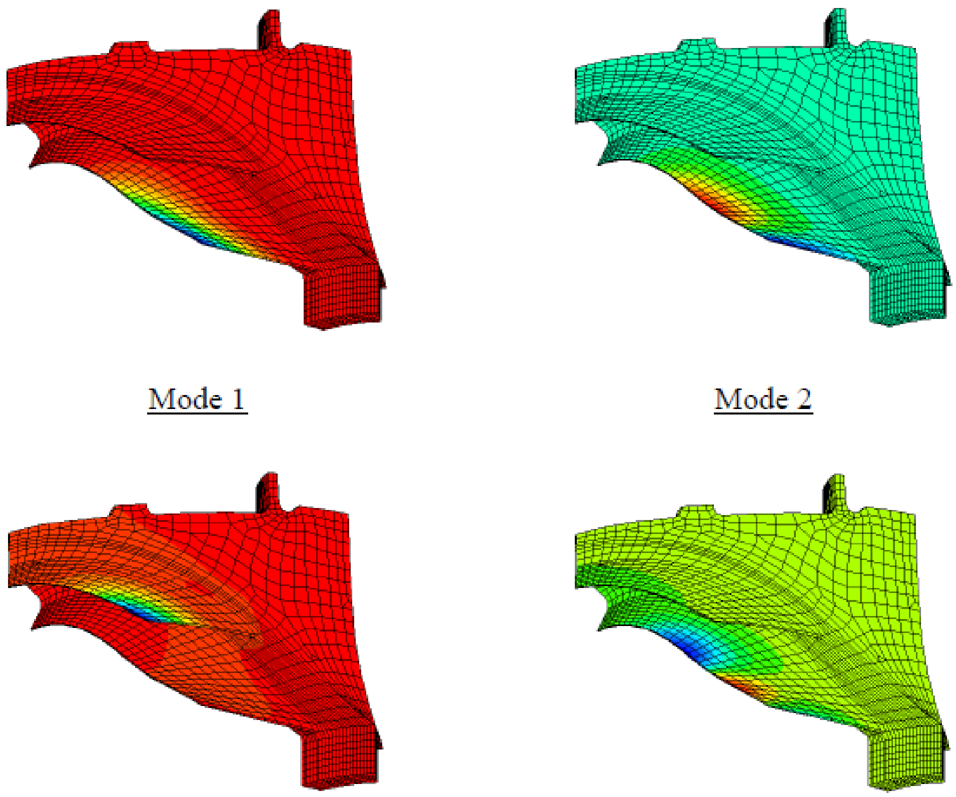

Figure 41: 4ND Family Modes 1 to 4

Figure 42 shows the low cycle fatigue (LCF) life data from MIL-HDBK-5H for annealed extrusion Ti6Al4V material at room temperature. Based on the maximum von-Mises stress of 101 ksi in the impeller bore, the mean LCF life is approximately 370,000 cycles.

There is significant scatter in the data and temperature effects were not considered, so actual LCF life may be significantly lower. Even if the LCF life is an order of magnitude lower than predicted — for example, 37,000 cycles — it still satisfies typical impeller LCF fatigue requirement. Therefore, the current design and stress level is deemed acceptable in terms of LCF life capability.

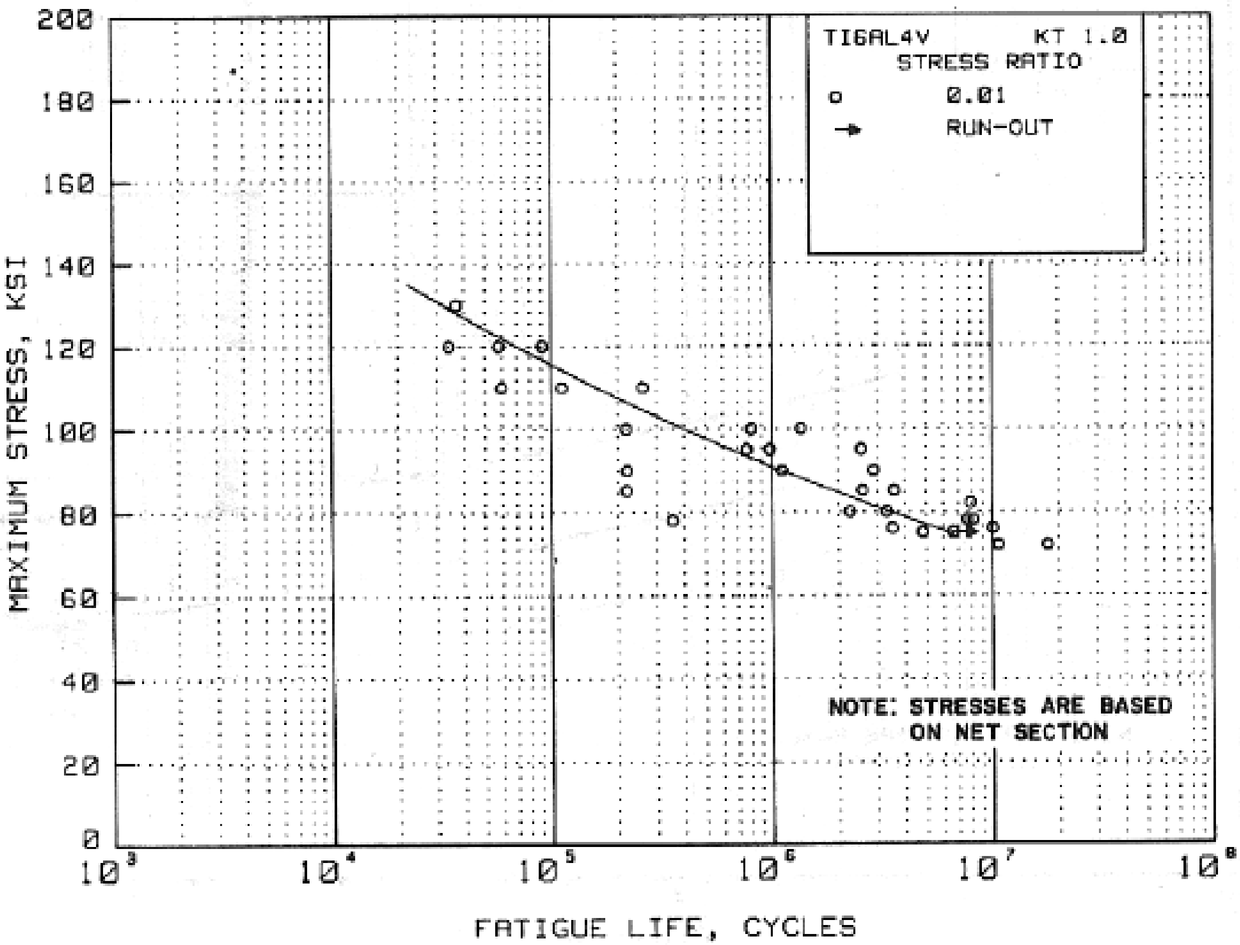

Figure 42: Annealed Ti-6Al-4V Extrusion at Room Temperature

6.2.6. Turbine Nozzle Design

The turbine nozzle design effort for the C250 has been undertaken to achieve a performance gain of approximately 1% in efficiency over the original C200. Initially, a conjugate CFD analysis of a 180° sector of the C200 combustor was modeled to provide accurate representation of the turbine stage inlet profiles. The combustor model solved for the metal temperatures of the combustor liner. The model included a two-step reacting flow mixture of methane and air as well as radiation to non-conjugate components. Results showed several hot streaks propagating to the combustor exit with a single pronounced hot streak — 2 for the full 360° — which was approximately 200 °F higher than the average profile entering the turbine stage. See Figure 43. The peak hot streak was determined to be the effect of aerodynamic blockage from the rear staggered injectors propagating forward and affecting the forward row of injectors. Peak metal temperature for the combustor liner reached 1885 °F.

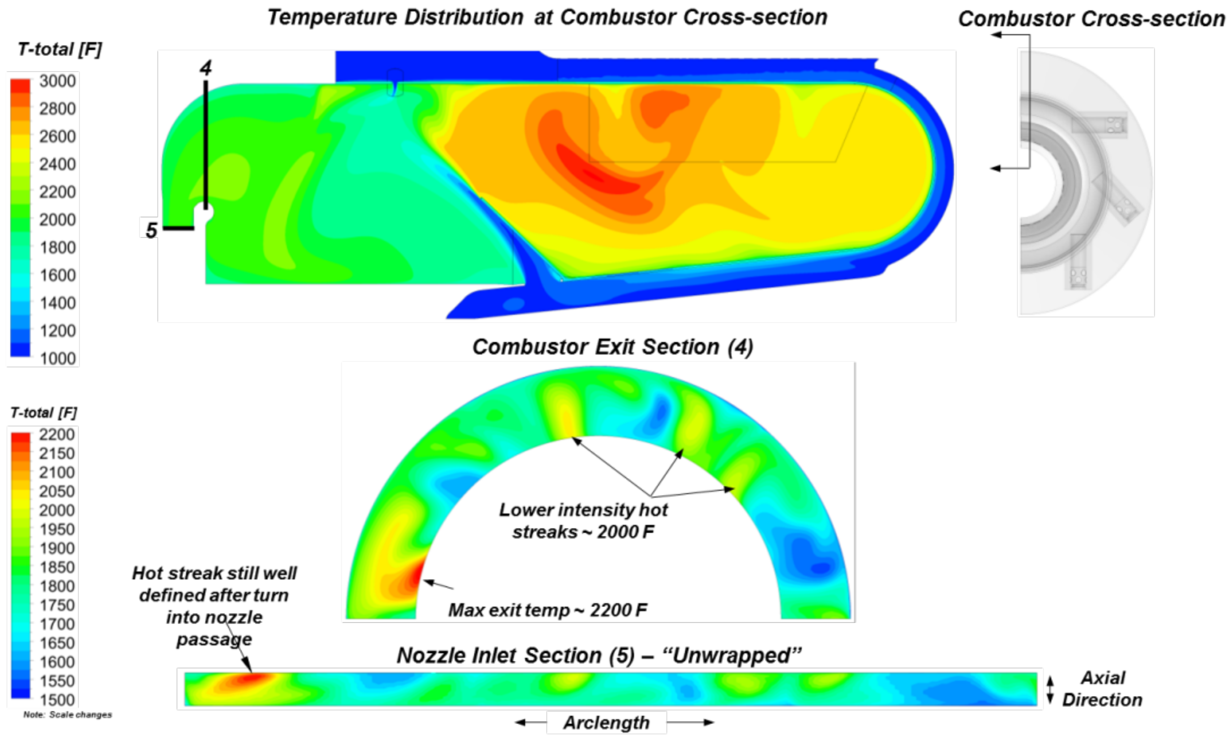

Figure 43: C250 Combustor Temperature Distribution

A CFD model of the turbine stage, with conjugate modeling for the turbine wheel, was performed on both C200 and C250 engine models and included the turbine wheel space leakage. See Figure 44. C200 average combustor exit profiles were then applied to the C200 turbine stage nozzle inlet and C200 profiles were scaled to match cycle conditions for the C250 turbine stage. See Figure 45.

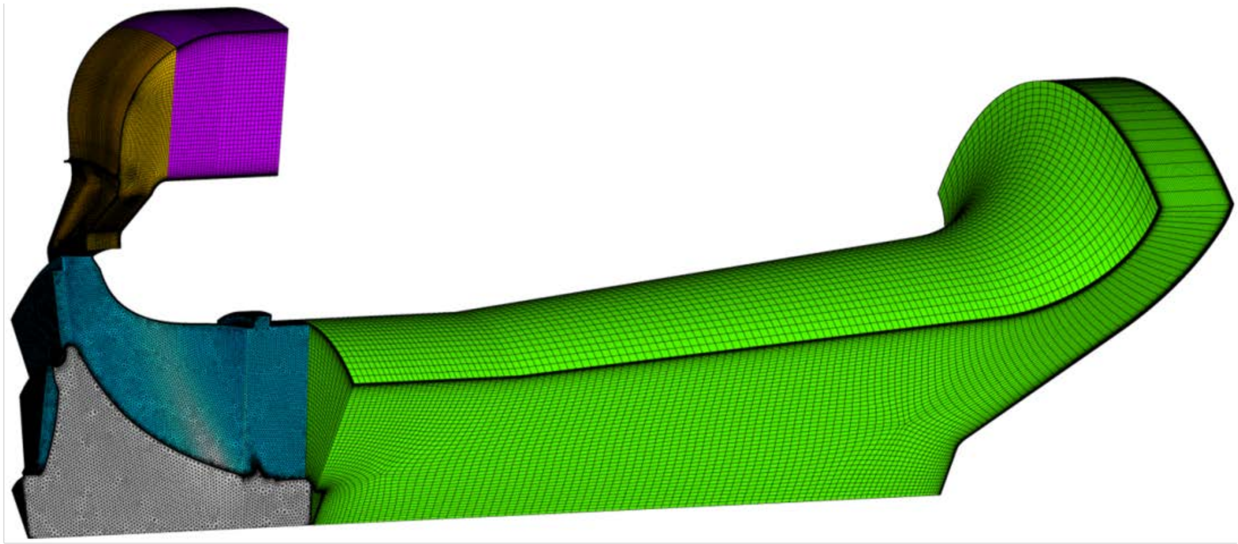

Figure 44: C250 Turbine Nozzle Computation Domain

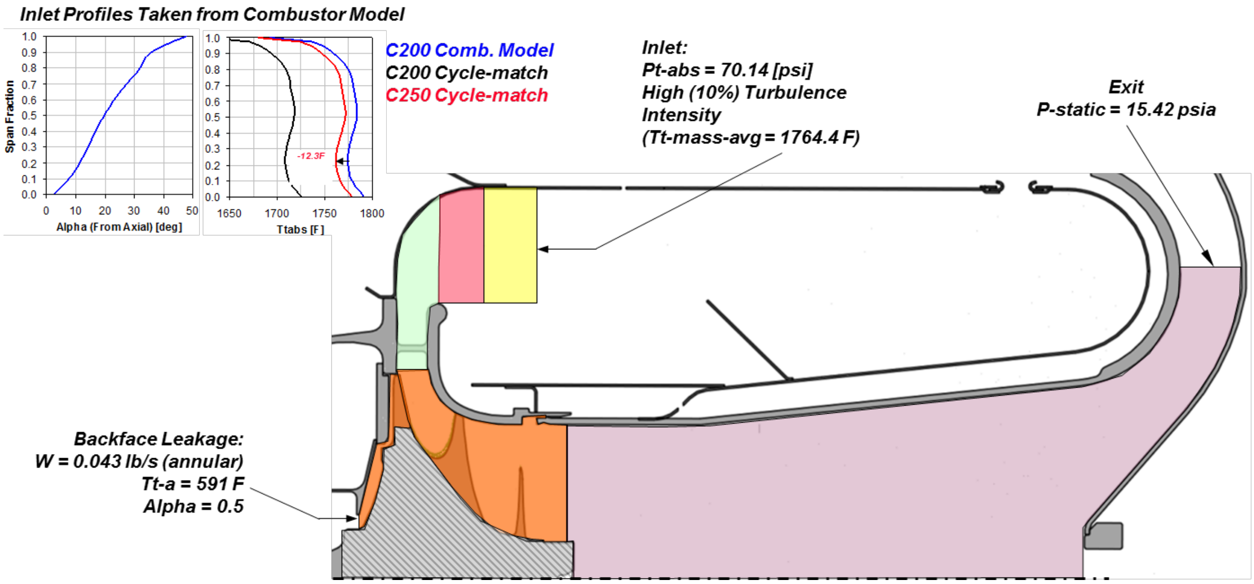

Figure 45: C250 Turbine Nozzle Simulation Boundary Condition

Turbine nozzle design iterations were performed on a vane only model at C250 conditions to quickly sort through designs. Several design iterations were completed on the turbine nozzle profile to remove the SS over-speed by adding camber to the profile, matching the vane solidity to the base vane design — as shown in Figure 46 and Figure 47, and reduce inlet separation with a smooth curve transition on the aft casing nose — as shown in Figure 48.

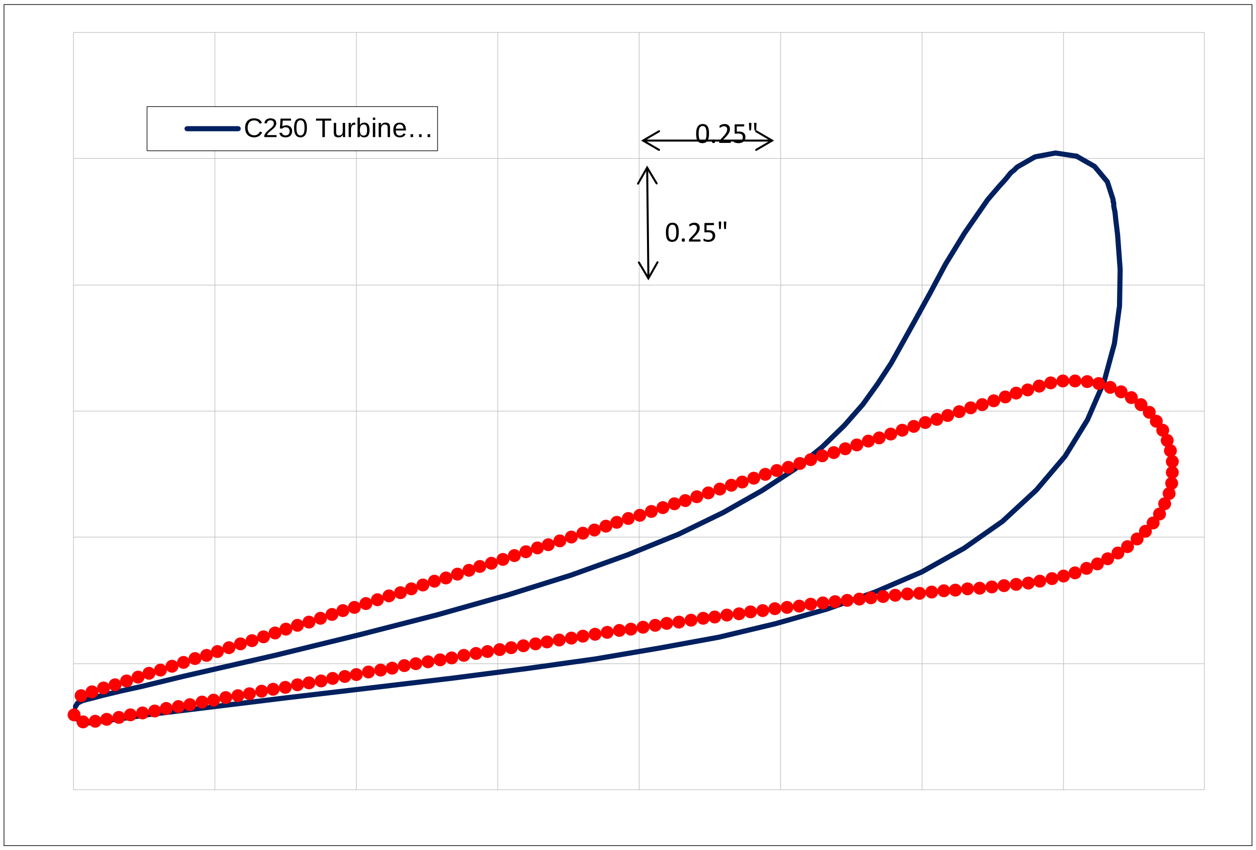

Figure 46: C250 vs. C200 Turbine Nozzle Airfoil Comparison

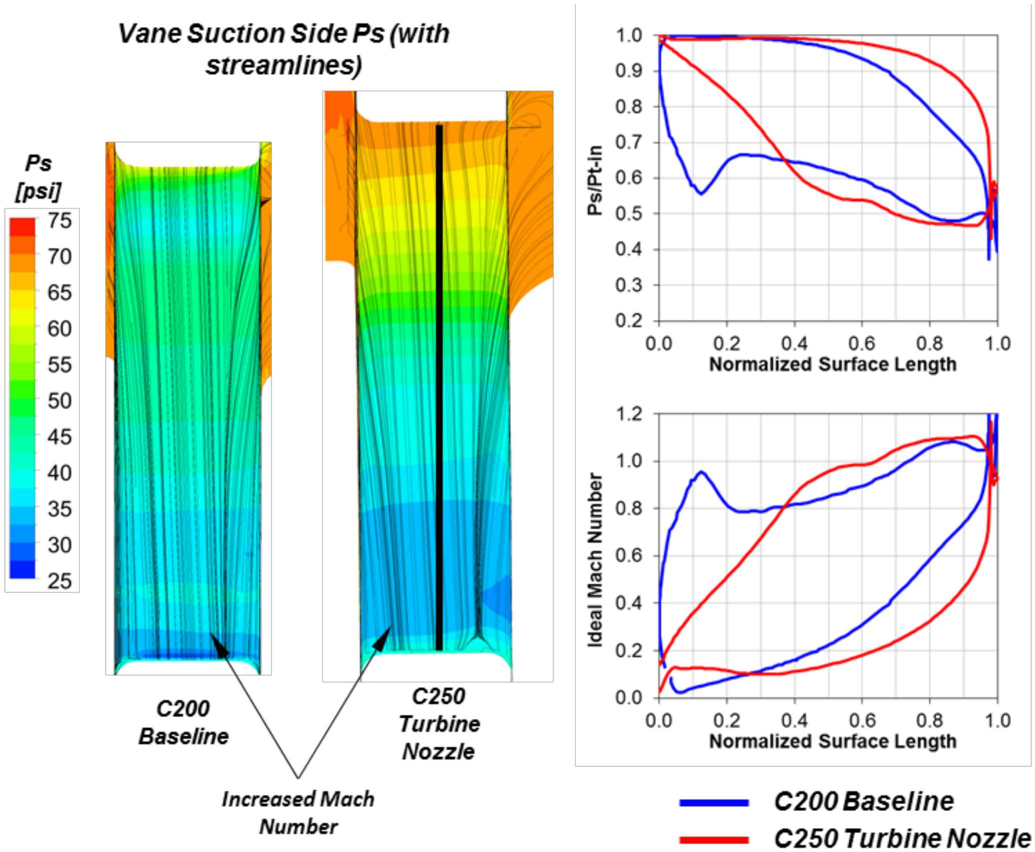

Figure 47: C250 vs. C200 Turbine Nozzle Vane Loading Comparisons

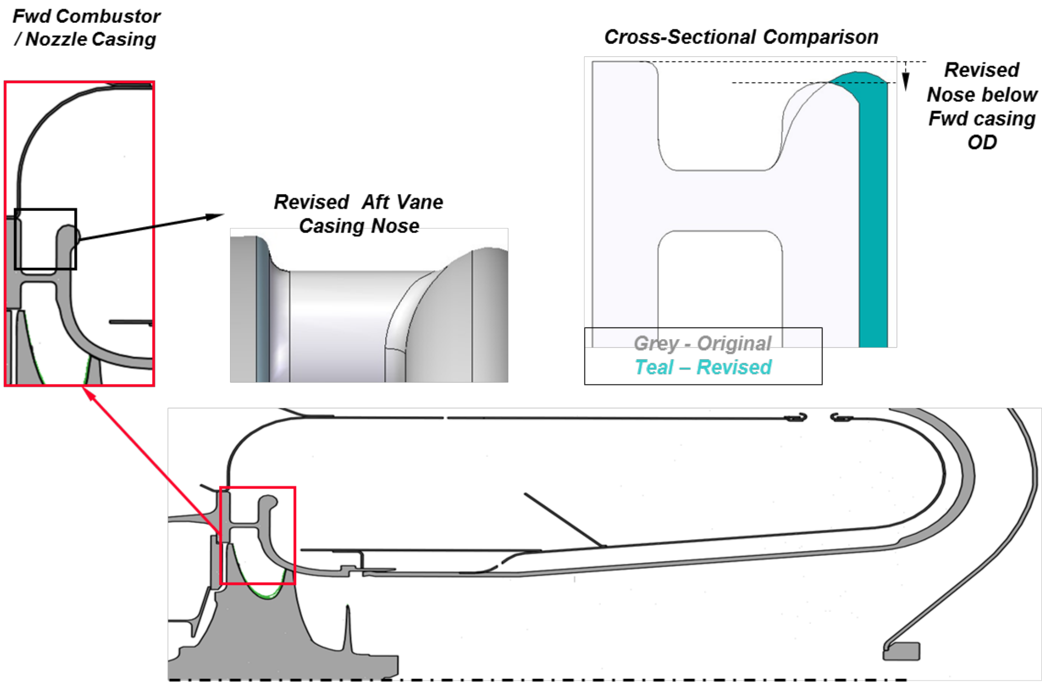

Figure 48: C250 vs. C200 Turbine Nozzle Lip Design Comparisons

These design modifications enabled the performance of the C250 turbine stage to be increased by 1.2 points over the C200 baseline design — from 88.8% to 90% T-T stage efficiency, as shown in Figure 49 — which exceeded the design target of 1 point. Additionally, turbine wheel temperatures were not predicted to change in magnitude — 1325 °F — or general location from the C200 design, as shown in Figure 50.

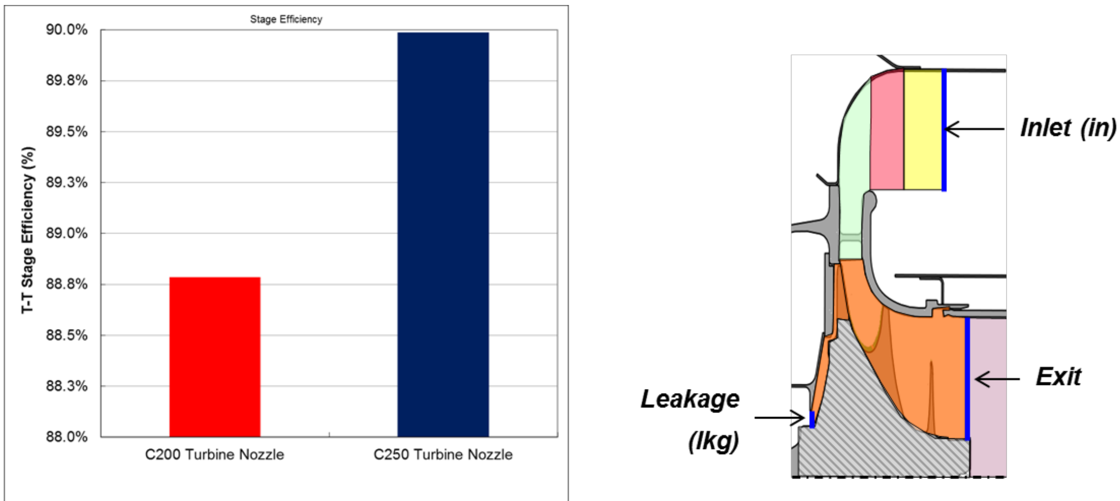

		W-in	W-lkg	W-exit	Q-conj	Tt-in	Pt-in	Pt-ex	ΔH-ideal	η-stage	Power	P-Spec
	Casing Design	pps	pps	pps	W	F	psi	psi	J/kg	–	kW	kW/kg
C200 Turbine Nozzle	Original Nose	2.81	0.034	2.84	-1600.20	1709.74	56.81	16.09	–	88.8%	–	–
C250 Turbine Nozzle	Revised Nose	3.53	0.043	3.57	-1638.81	1761.64	70.14	16.45	438712.6	90.0%	626	386.6

Figure 49: C250 Efficiency Simulation Results

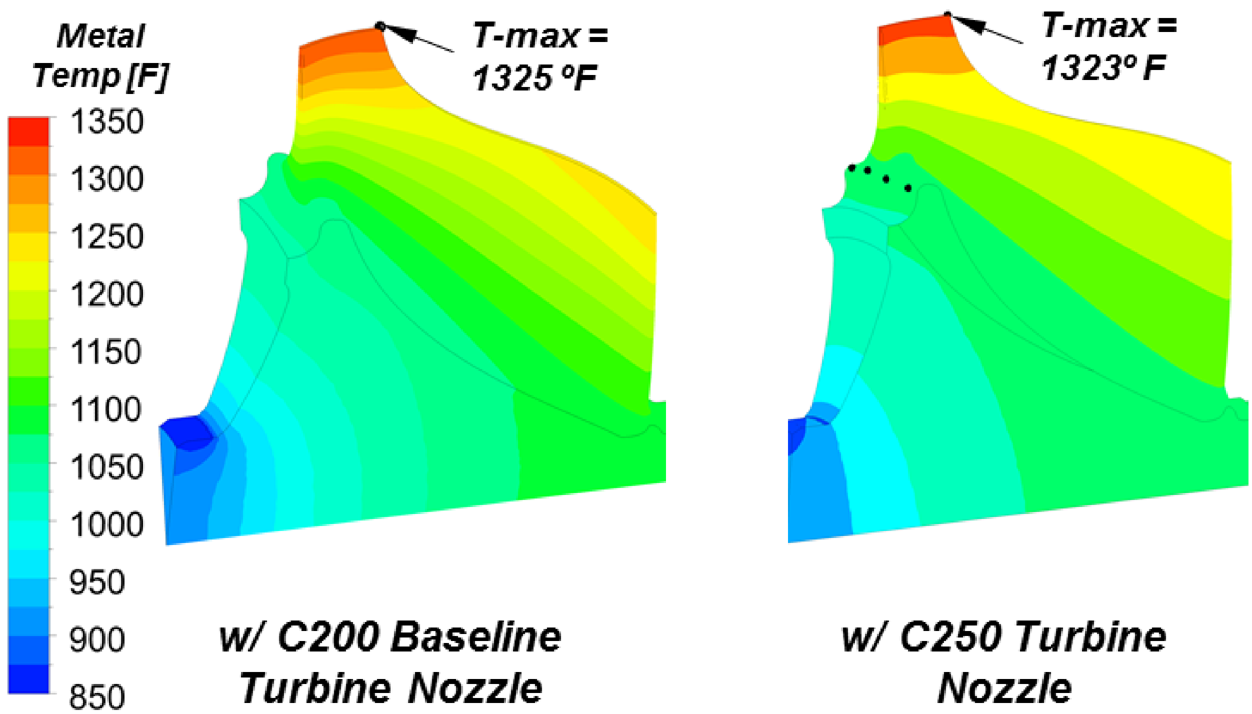

Figure 50: C250 Turbine Metal Temperature Contour

6.2.7. Static Structure Design

The static structure design of the C250 POC engine was based on Capstone Turbine's production C200 engine. The changes made to the static structure for the C250 POC engine were limited to the powerhead section. Modifications were to accommodate the C250-specific compressor stage, turbine nozzle, and generator stator.

Items redesigned or modified for the C250 POC engine include:

- Impeller, Compressor (not static)
- Inducer
- Center Housing Assembly
- #3 Bearing Housing Assembly
- Thrust Housing Assembly
- Turbine Nozzle
- Generator Stator Assembly
- Generator Heatsink
- Magnet / Blower / Double Diaphragm Assembly (not static)
- Inlet Shroud Assembly
- Inner Shield

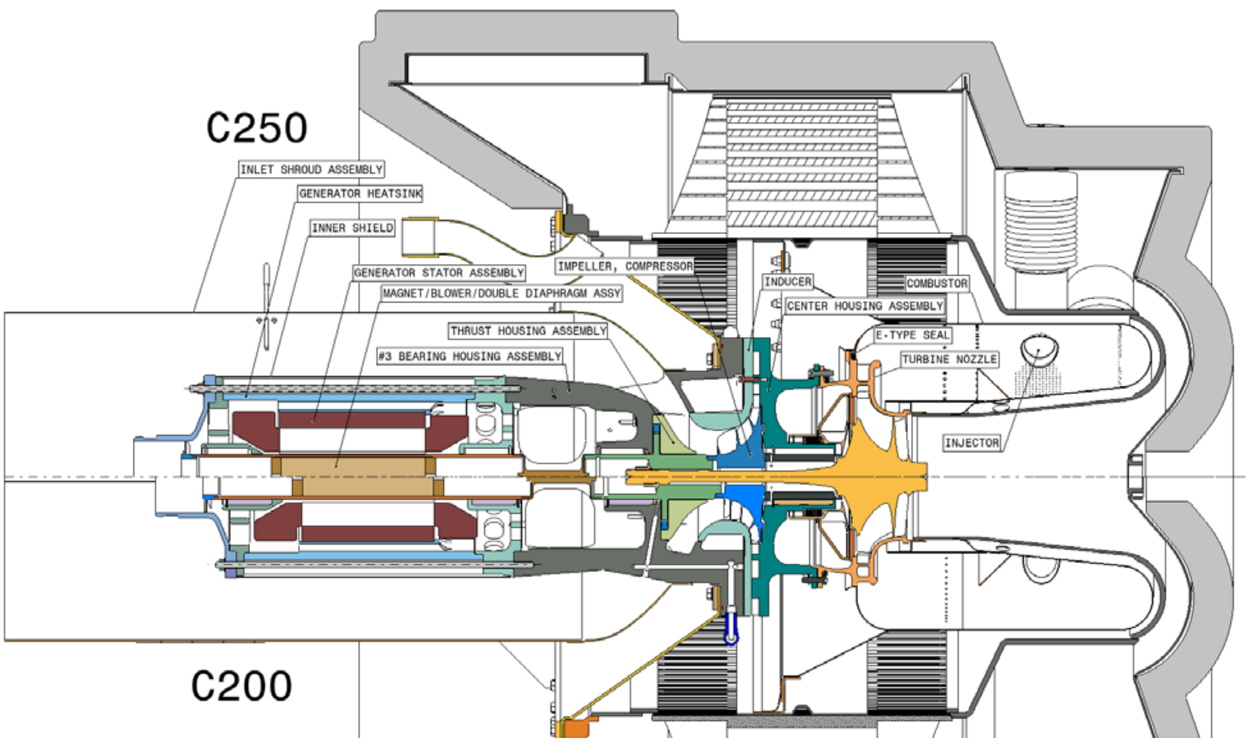

Figure 51: C250 vs. C200 Static Structure Design

6.3. Low Pressure Spool Performance Demonstration (C250)

6.3.1. Hardware Procurement and Manufacturing Tooling Plan

All parts for the LP spool — C250 — were quoted and procured from Capstone's current supply base. The decision to utilize Capstone's current vendor base was made in order to support future commercialization and reduce tooling cost for the performance testing of the C250. An important note is that 94% of Capstone's manufacturing and supply base is located within the in the United States.

6.3.2. Engine Assembly Requirement

One of the key engine assembly requirements for efficient engine operation is maintaining a small axial clearance between the impeller and inducer shroud line. See Figure 52. This clearance should be made as small as possible to maximize engine efficiency yet large enough to avoid rubbing during engine operation.

To determine and verify the cold build and operating clearances, a series of engine builds with varying cold clearances were created and tested to determine the relationship between the cold build clearance and the operating clearance.

The testing was conducted with two aluminum rub pins installed at the gage point of the inducer shroud line at the 6 and 12 o'clock locations. The rub pins are installed with enough length protruding from the inducer shroud that they were cut shorter by the impeller blades while the engine is operating. The portion of the rub pin that remains sticking out of the inducer shroud after the engine operation is the actual operating clearance. The testing consisted of fast accelerations, fast decelerations, and steady-state operation to find the minimum operating axial clearance.

The test data showed that minimum clearance and nominal clearance during fast start and steady-state operation respectively are similar to those of the production C200 engine with the same cold axial build clearance. Therefore, the requirement for the C250 engine impeller cold build clearance is the same as the production C200 engine.

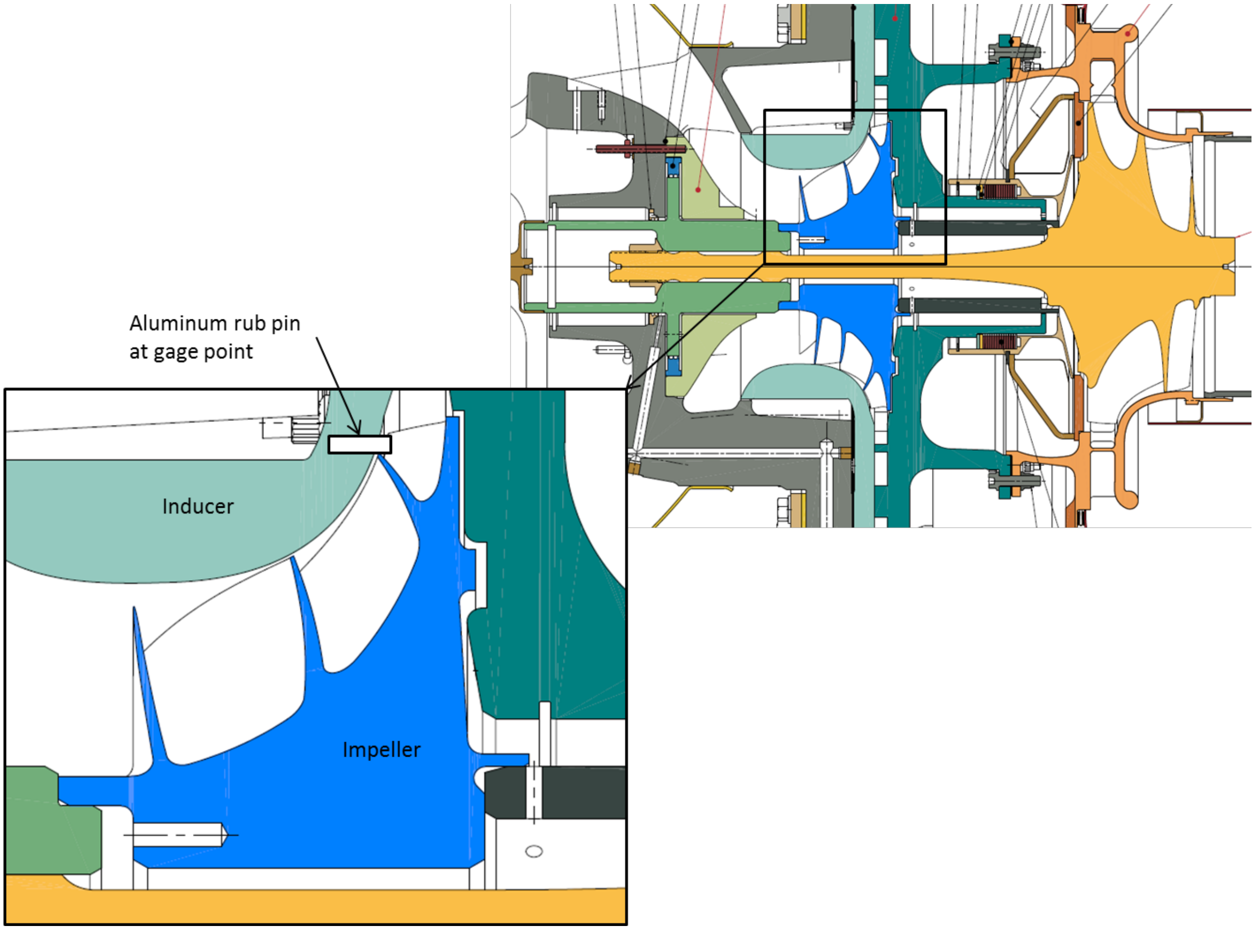

Figure 52: Cross-Section of C250 Rotor Group and Impeller/Inducer Detail

6.3.3. Performance Testing Results

A performance test was conducted to test C250 POC engine. The objectives of the test include:

1. Collect key engine performance data
2. Evaluate overall engine performance
3. Investigate and validate key engine design variables

The test was conducted on January 23, 2013. Test results from C250 POC engine are near target power output at generator leads in all test conditions. Two (2) trend lines were generated from these test results. Both lines parallel the design target derate slope. See Figure 53.

Electrical efficiencies at the generator leads are discrepant — 3.04% lower at 1150 °F TET and 2.61% lower at 1170 °F TET. See Figure 54. A series of investigations were initiated to determine the cause. These revealed that the exhaust gas temperature is higher than predicted which that the recuperator component was out of specification for effectiveness. An inspection was conducted and it was determined that the recuperator failed to operate at design conditions due to mechanical failure. The mechanical failure was later identified as a manufacturing defect. If the recuperator operates at design conditions and efficiency then the POC engine could meet its electrical efficiency targets

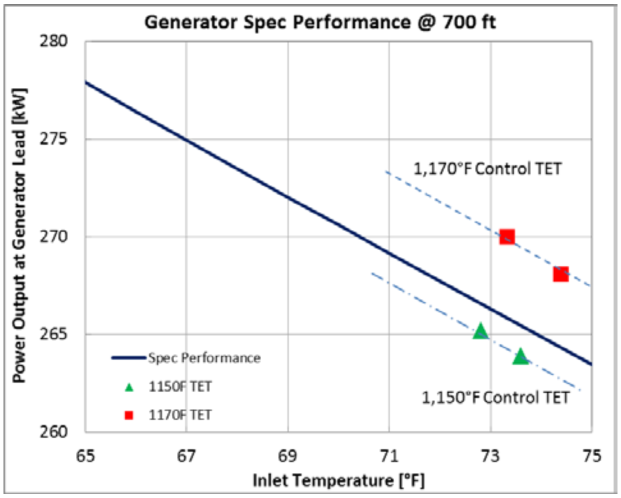

Figure 53: C250 POC Derate Test Results

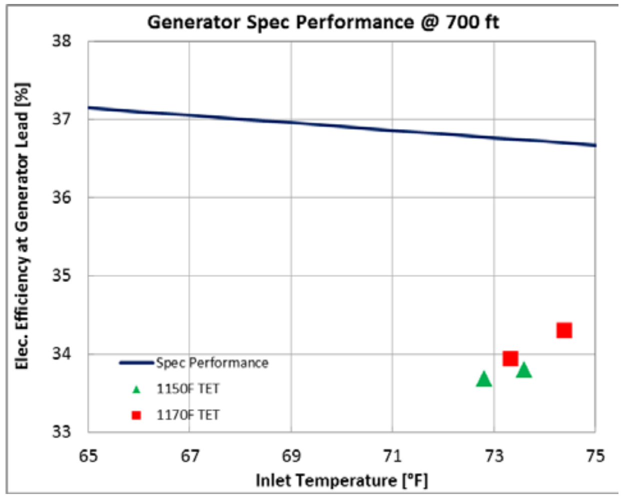

Figure 54: C250 POC Electrical Efficiency Test Results

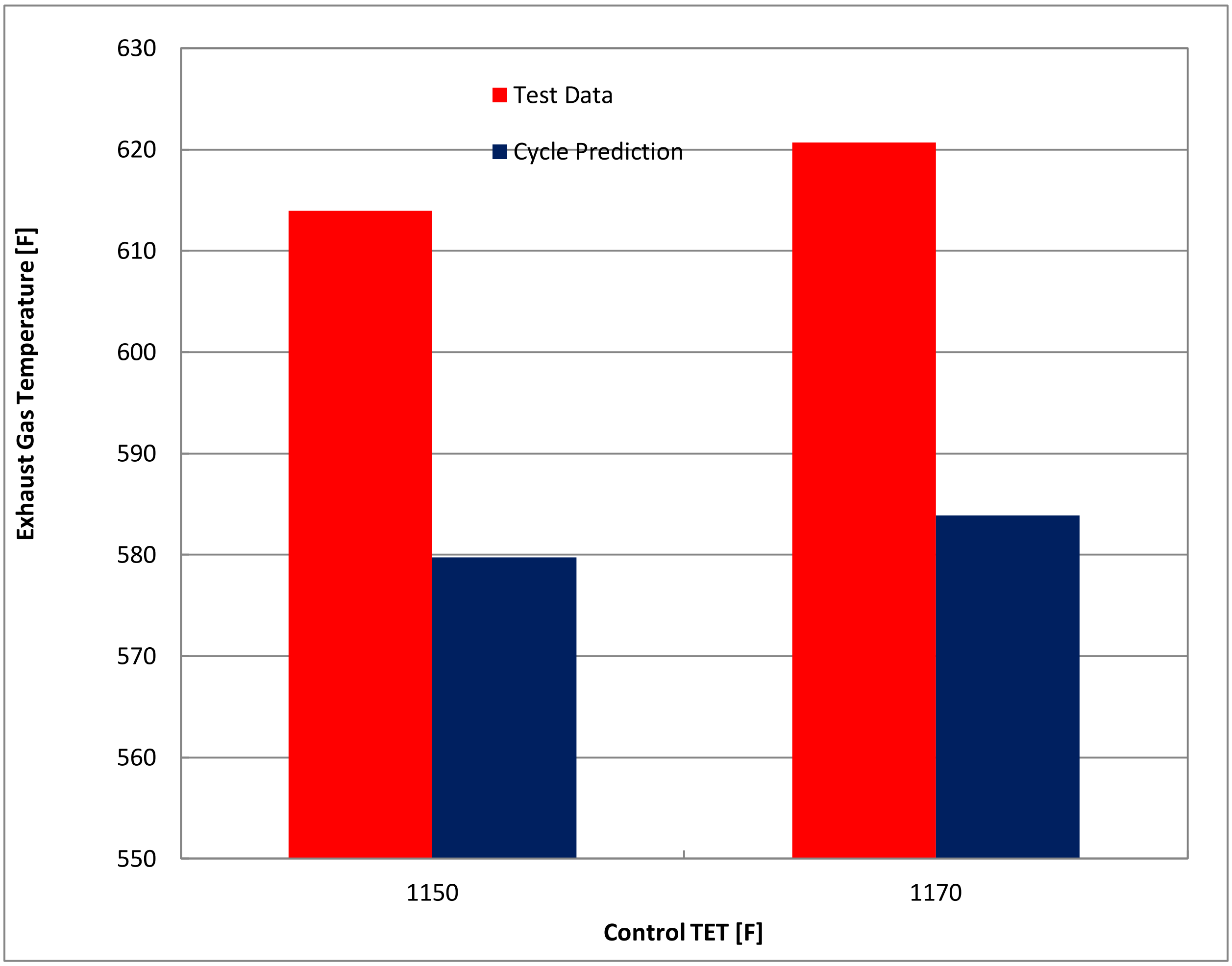

Figure 55: C250 Engine EGT Comparisons

6.3.4. C250 POC Engine Combustion Test Results

The C250 POC engine was tested and demonstrated in January 2013 at Capstone's Stagg test facility. In addition to engine and power measurements, emissions were also measured. This section summarizes the findings of combustion performance of the engine.

Test Item Description

The combustion configuration for the C250 POC engine #1 was Design Case POC-1 as defined in the earlier combustion section

- Liner: C250 prototype
- Injector C250 prototype
- Test Fuel: Pipeline Natural Gas at Stagg Facility.
- Emissions equipment: Capstone Horiba Emission Bench.
- Emissions reported in this report were measured with an ambient temperature ranging from 72 – 78 °F on January 23, 2013 at Stagg.

Test Results

Post Test Inspection

Post-test visual inspection did not reveal any obvious abnormal deformation or discoloration to combustion components — i.e., liner and injectors. Figure 56 shows that the components were still in excellent condition with only normal "wear-and-tear".

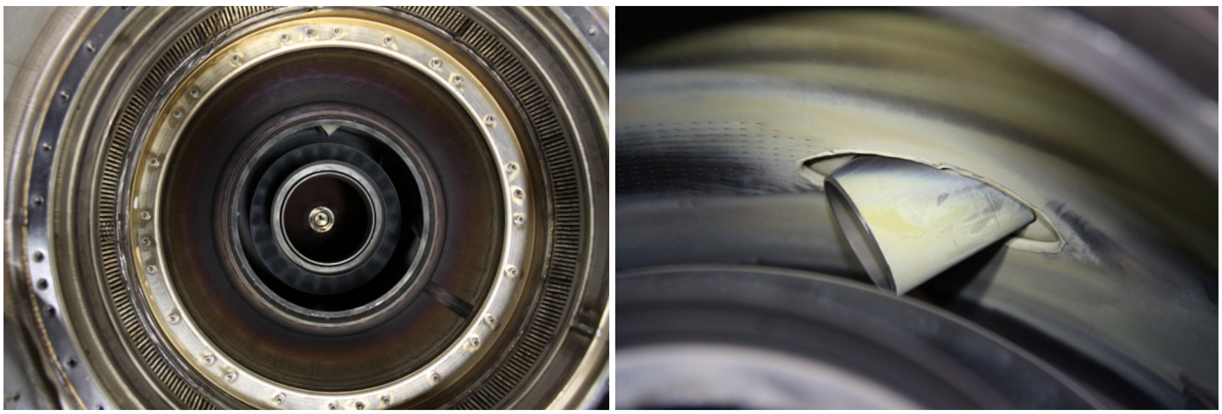

Figure 56: Post-Test Visual Inspection

Emissions

The emissions of the C250 POC engine are listed in Table 24. These values are after data reduction, which includes (1) background emission correction and (2) unit conversion. The emissions are presented in three formats.

Format 1: ppmVd 15% O_2
Format 2: lb/MW-hr.

This format is the required unit for CARB Distribution Generation (DG) certification. In the emission calculation process, the power output used was the "Yoka Power after GCM/LCM", which is close to the microturbine system power output. However, this power data set is expected to be higher than the power output from a packaged system due to extra pressure losses resulting from packaging.

Format 3: grams-per-brake-horsepower-hr or g/bhp-hr.
This is the required unit for CARB hybrid electric vehicle (HEV) certification. In the emissions calculation process, the power output used was "Yoka Power at Generator".

		Engine Speed	TET	Tamb.	Generator Power	Power after GCM/LCM	Raw Data, Not Background corrected, ppm			Emissions, ppmV@15%O2, Background Corrected (a)			Emissions, lb/MW-h, Background corrected (a)(c)			HEV Emissions, g/bop-hr, Based on HEV power (a)(b)(c)		
Test No.	Test Cond.	°F	°F	°F	W	W	CO	NOx	THC	CO	NOx	THC	Mco	Mnox	Mthc	Mco	Mnox	Mthc
1	Without Venturi	59977	1151	72.4	263911	246732	1.24	0.68	-0.09	1.37	0.82	-6.56	0.04	0.04	-0.10	0.012	0.012	-0.034
2		59978	1171	74.0	268098	250770	0.32	0.84	-0.27	-0.21	1.10	-6.87	-0.01	0.05	-0.10	-0.002	0.016	-0.035
3		57918	1173	73.8	239016	223633	1.46	0.56	-0.20	1.80	0.64	-7.00	0.05	0.03	-0.11	0.016	0.010	-0.036
4		58030	1150	73.8	234719	219712	4.79	0.45	0.43	7.82	0.45	-5.96	0.21	0.02	-0.09	0.072	0.007	-0.031
5	With Venturi	59975	1151	76.1	264482	247449	1.45	0.69	-0.03	1.72	0.84	-6.47	0.05	0.04	-0.10	0.016	0.012	-0.033
6		59976	1171	77.9	269471	252432	0.36	0.87	-0.26	-0.14	1.14	-6.84	0.00	0.05	-0.10	-0.001	0.017	-0.035
7		57903	1170	77.5	241097	225545	2.10	0.57	-0.03	2.93	0.65	-6.67	0.08	0.03	-0.10	0.027	0.010	-0.035
8		58004	1150	77.4	237959	222716	4.84	0.48	0.44	7.96	0.50	-5.98	0.21	0.02	-0.09	0.073	0.008	-0.031
9	Without Venturi	59978	1151	72.5	265204	248109	1.18	0.71	-0.10	1.29	0.90	-6.71	0.03	0.04	-0.10	0.012	0.013	-0.035
10		59976	1171	73.6	269995	252474	0.31	0.90	-0.24	-0.23	1.19	-6.82	-0.01	0.05	-0.10	-0.002	0.018	-0.035
11		57867	1170	72.7	238968	223572	1.77	0.61	-0.10	2.36	0.73	-6.83	0.06	0.03	-0.10	0.021	0.011	-0.035
12		57991	1150	71.9	236714	221586	4.81	0.48	0.42	7.84	0.50	-5.96	0.21	0.02	-0.09	0.072	0.008	-0.031
	Min=	57867	1150	71.9	234719	219712	0.31	0.45	-0.27	-0.23	0.45	-7.00	-0.01	0.02	-0.11	-0.002	0.007	-0.036
	Max=	59978	1173	77.9	269995	252474	4.84	0.90	0.44	7.96	1.19	-5.96	0.21	0.05	-0.09	0.073	0.018	-0.031
	Avg=	58964	1161	74.5	252469	236227	2.05	0.65	0.00	2.88	0.79	-6.56	0.08	0.03	-0.10	0.026	0.012	-0.034
Regulation Standard:		CARB 2007											0.1	0.07	0.02			
		CARB HEV 2010														5.0/15.50	0.2	0.14

NOTE:

(a). Negative exhaust emission values - exhaust gas has lower emissions than those of the ambient air (background).

(b). For HEV application, power is drawn directly from generator, without GCM/LCM losses (~7%).

(c). Color coded based on comparison to CARB 2007 DG or CARB HEV 2010: Green - pass; Red - fail.

Table 24: C250 Emission Test Data from 1/23/2013vs. Regulation Standards

As shown in Figure 57, the NO_x emissions of the C250 POC engine was around 1 ppmVd, corrected to 15% O_2, from 220 – 250 kW power — post LCM and GCM — for both TET settings — 1150 °F or 1170 °F. NO_x emissions were shown not to be sensitive to power change.

At the TET set point of 1150 °F, CO emissions were 1.29 ppmVd and 7.8 ppmVd, after being corrected for full power — 248 kW — and lower power — approximately 220 kW — respectively. At higher the TET set point of 1170 °F, CO emissions were near 0 ppmVd and 2.36 ppmVd, after being corrected to 15% O_2 for 252.5 kW and 223.6 kW respectively. This demonstrates that CO emissions were very sensitive to both TET set point and power level for the tested conditions. This sensitivity is related to the combustion flame temperature differences.

The THC emission values after background correction were all negatives. This indicates that the engine exhaust gas had lower hydrocarbon content than the surrounding air. In essence, the engine “cleaned” the hydrocarbons in the atmosphere.

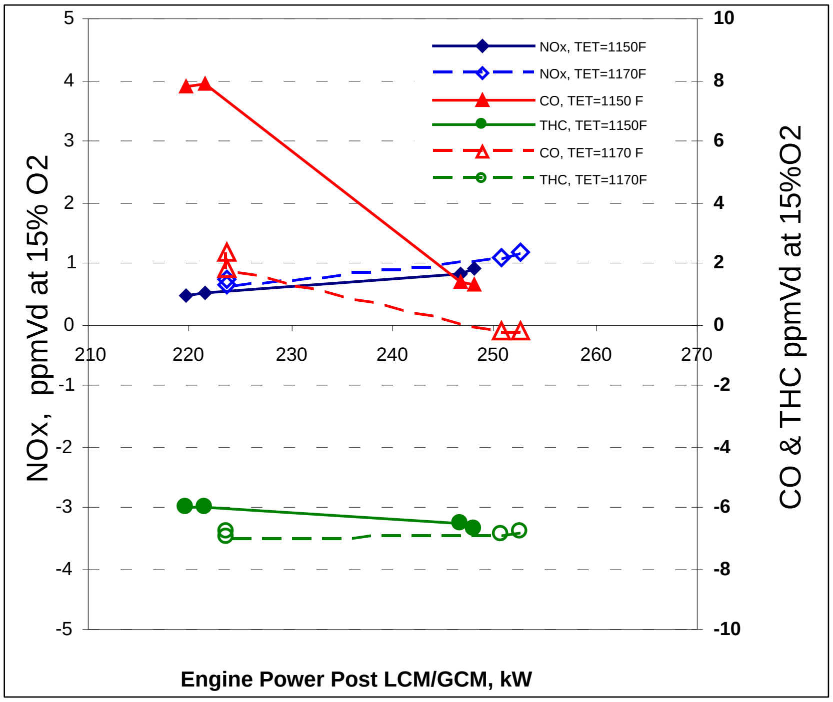

Figure 57: C250 POC Engine Emissions in ppmV at 15% O_2

Figure 58 shows the emissions (NO_x, CO, and THC) in lb/MW-hr.

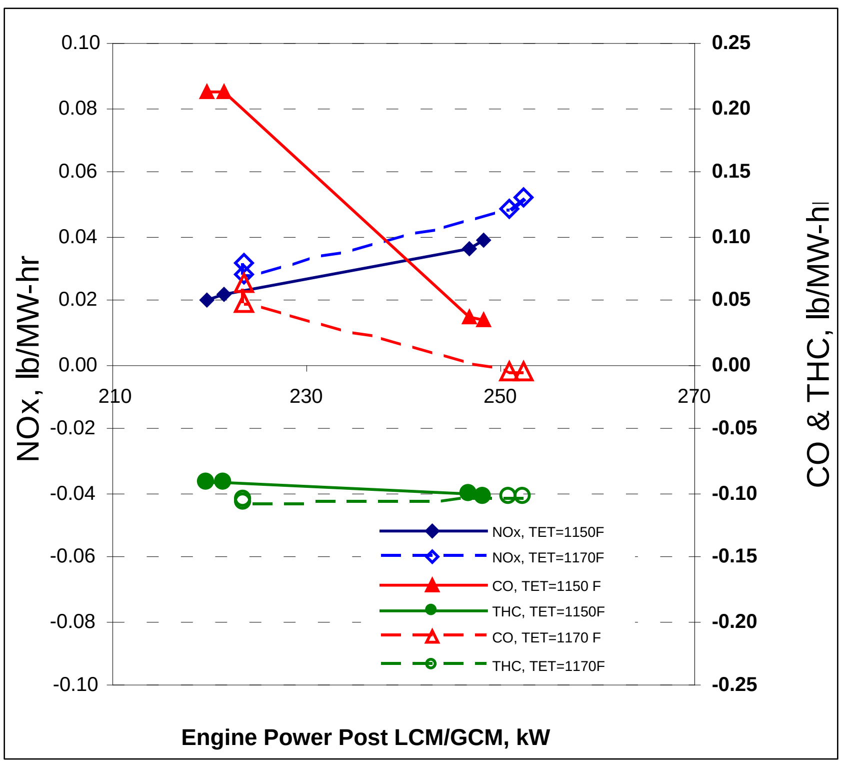

Figure 58: C250 POC Engine Emissions in lb/MW-hr

Analysis

C250 POC Engine Emission Comparison to C200 and CARB DG 2007

CARB 2007 DG standards for fossil fuels are listed in Table 25. Capstone's current C200 iCHP natural gas product was certified to CARB 2007 DG standards under the following conditions

- Integrated combine heat and power application, with 177.9 kW electrical power output and 240 kW heat recoveries.
- CO catalyst was installed.

Pollutant	Emission Standard (lb/MW-hr)
NO_x	0.07
CO	0.10
VOCs	0.02

** California Code of Regulations, Title 17, Division 3, Chapter 1, Subchapter 8, Article 3, § 94200 – § 94214*

** Final regulation order as approved by OAL. Effective 2007-09-07.* http://www.arb.ca.gov/energy/dg/2006regulation.pdf.

Table 25: CARB 2007 DG Certification Standards for Fossil Fuel

An emissions comparison — NO_x, CO and THC/VOC — between the C250 POC engine, the C200 natural gas system, and the C200 iCHP system was made.

As shown in Figure 59, NO_x emissions from the C250 POC engine — TET set point of 1150 or 1170 °F —meets CARB 2007 DG standards without heat recovery credit. However, NO_x emissions of the C200 natural gas system do not meet the CARB 2007 DG standards without the 243 kW heat recovery credit.

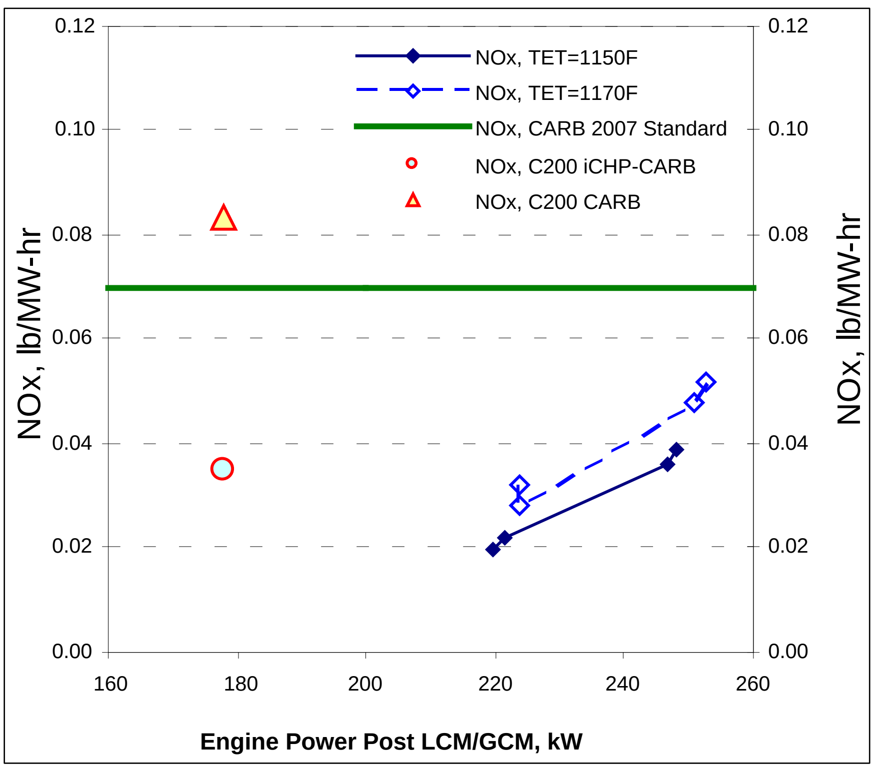

Figure 59: NO_x Comparison

The CO emissions of the C250 POC engine — TET set point of 1150 or 1170 °F — at full power also meet CARB 2007 DG standards without heat recovery credit and without a CO catalyst module. However, it was only with both a CO catalyst and heat recovery module that CO emissions of the C200 natural gas system met the CARB 2007 DG standards. See Figure 60.

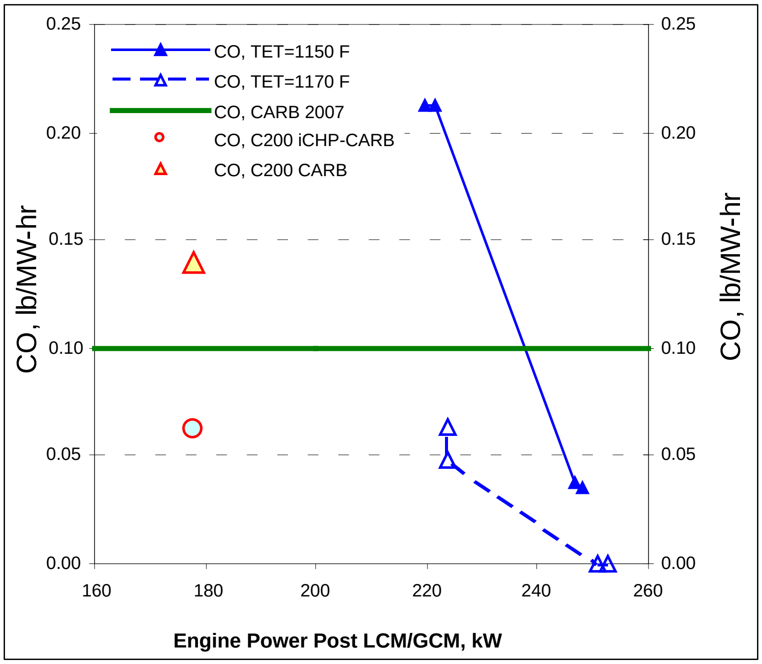

Figure 60: CO Comparison

As shown in Figure 61, the C250 POC engine — TET set point of 1150 or 1170 °F — produces lower than background total hydrocarbon emissions. This resulted in the THC levels being negative values. The C200 system VOC — a sub-set of THC — only met the CARB 2007 DG standards when used in an integrated CHP application with 243 kW heat recovery credit.

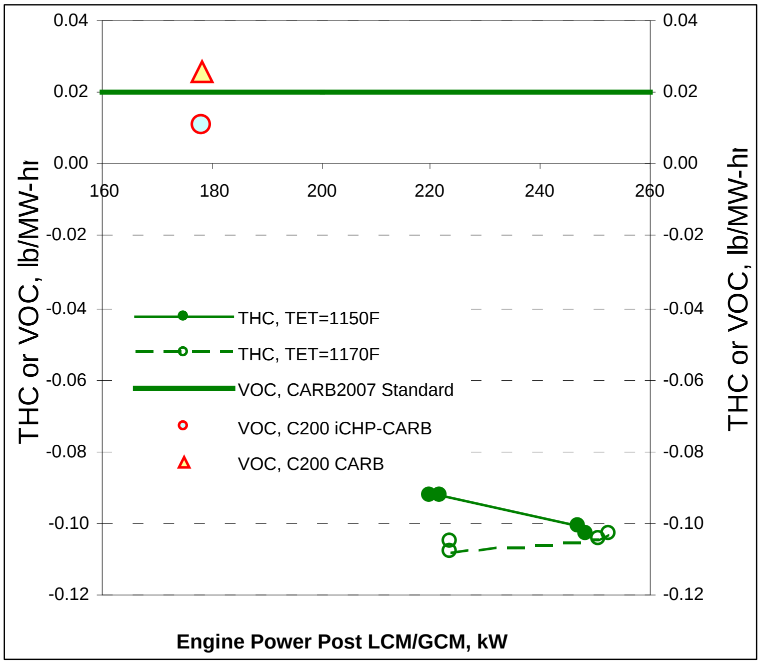

Figure 61: THC/VOC Comparison

Test Result Conclusions and Recommendations

The following summary can be drawn after the combustion design and test work from the current C250 POC project:

- Preliminary design for the C250 POC combustion system is complete, which includes:
  - Requirement analysis
  - Combustion calculation
  - Injector and liner split ratio trade-off studies
  - Design configurations completed for emissions and lower pressure drop.
- POC combustion performance and emissions test results:
  - None to limited tests performed for combustion system.
  - No obvious combustion issues have been discovered so far.
  - For the tested C250 POC configuration, better than CARB 2007 standard emissions have been demonstrated at full power, without heat recovery credit and without CO catalyst.
  - For HEV applications, full power emissions meet the CARB HEV 2010 standards. Partial load data may not meet the standards and the system may need further optimization.
- Test results demonstrate current combustion design approaches were effective and well established.

A few recommendations are also offered as follows:

1. Since very limited to no combustion testing has been performed for the C250 POC engine, further evaluation of the combustion system is recommended. Since this is only the first iteration of combustion design for the C250 POC engine, further optimization may lead to improved performance.
2. At full power, current C250 POC engine has demonstrated lower than CARB 2007 DG and CARB HEV 2010 standards emissions.
3. Current C250 POC combustion architecture may be further revised for better staging or control for partial load emission improvement.

6.4. Refined C370 Cycle Analysis

6.4.1. Introduction of C370 Cycle Analysis

A study was conducted to optimize C370 cycle model. The performance target of the study includes the following:

1. Total power output at generator lead: >370 kW
2. Electrical efficiency based on total power output at generator leads: >42%
3. Combine heat and power efficiency: >85%
   a. Sources of combined heat and power efficiency;
      i. Thermal recovery from intercooler module
      ii. Thermal recovery from heat recovery module (HRM)
      iii. Electrical power at generator leads.
   b. HRM will not be included in the proof of concept engine demonstration.
   c. Combined heat and power efficiency will be demonstrated through computation only and is based on 130 °F water inlet temperature
4. Constraint on turbine inlet temperature to lower value.

A 2-spool cycle analysis code was developed at Capstone Turbine for this study. This code performs cycle prediction, design evaluation, and performance analysis for C370 designs. Through the analysis process, a C370 cycle model will be developed with component requirements defined. The recommended C370 cycle model will meet both power and efficiency requirements. It will also satisfy overall thermal efficiency requirement with a specified HRM design.

An initial cycle model was established by using initial component definitions shown in Table 26 and the pressure drop model shown in Figure 62.

Key Parameters				
Category	**No.**	**Description**	**Unit**	**Default**
Package	1	Package Inlet Heating	°F	0
Generator	2	LP Generator Efficiency	%	97.5
	3	HP Generator Efficiency	%	97.5
	4	Generator Blower Power	kW	0
	5	Generator Blower Power	kW	0
Leakage	6	Bearing Leakage Mass Flow Rate	%	2
Compressors	7	LP Compressor Pressure Ratio	—	4.8
	8	HP Compressor Pressure Ratio	—	2.5
Intercooler	9	Intercooler Air Exit Temperature	°F	150
	10	Intercooler Fluid Inlet Temperature	°F	140
	11	Intercooler Fluid Flow Rate	GPM	30
	12	Intercooler Pressure Drop	%	1.5
	13	Intercooler Effectiveness	—	0.963
Combustion	14	Combustion Efficiency	%	100
	15	Combustion Pressure Drop	%	2.5
Recuperator	16	Recuperator Effectiveness	—	0.89
	17	Recuperator Pressure Drop – Cold	%	1.5
	18	Recuperator Pressure Drop – Hot	%	3
Internal Heating	19	Temperature Rise across LP Generator	°F	5
	20	Temperature Rise across HP Generator	°F	5
	21	Temperature Rise from Compressor to Recuperator	°F	25
Mechanical Efficiency	22	LP Spool Mechanical Efficiency	%	99.2
	23	HP Spool Mechanical Efficiency	%	99.2
HRM	24	HRM Effectiveness	—	0.846
	25	HRM Water Inlet Temperature	°F	182
	26	HRM Water Flow Rate	GPM	115
	27	HRM Pressure Drop	%	1.5

Table 26: C370 Initial Cycle Definitions

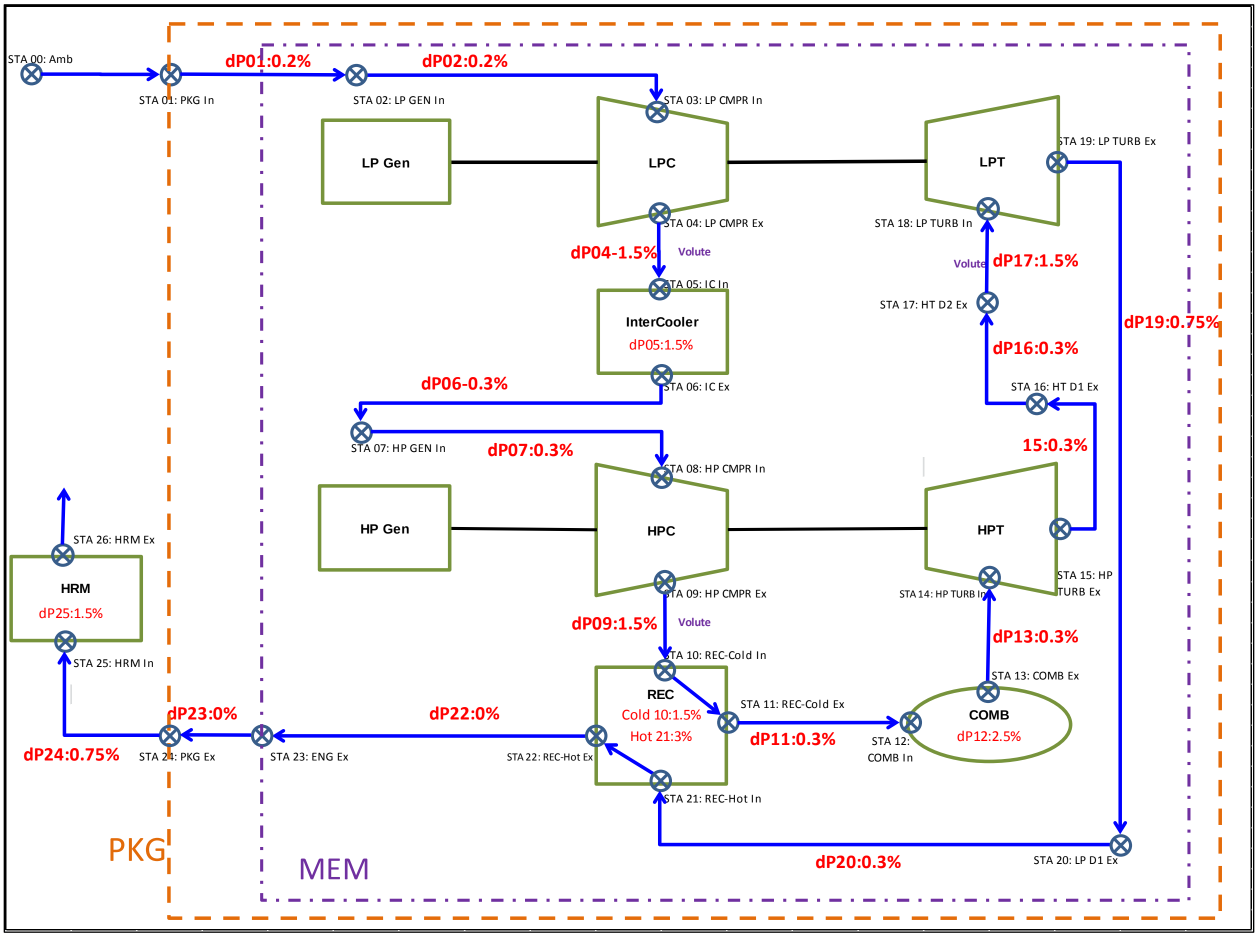

Figure 62: C370 Pressure Drop Model

Cycle prediction indicates a Gen Power of 477.9 kW and a Gen Efficiency of 41.29%. See Figure 63. The HP turbine tip relative temperature is 1880 °F at a TIT of 2050 °F, which is the maximum allowable TIT.

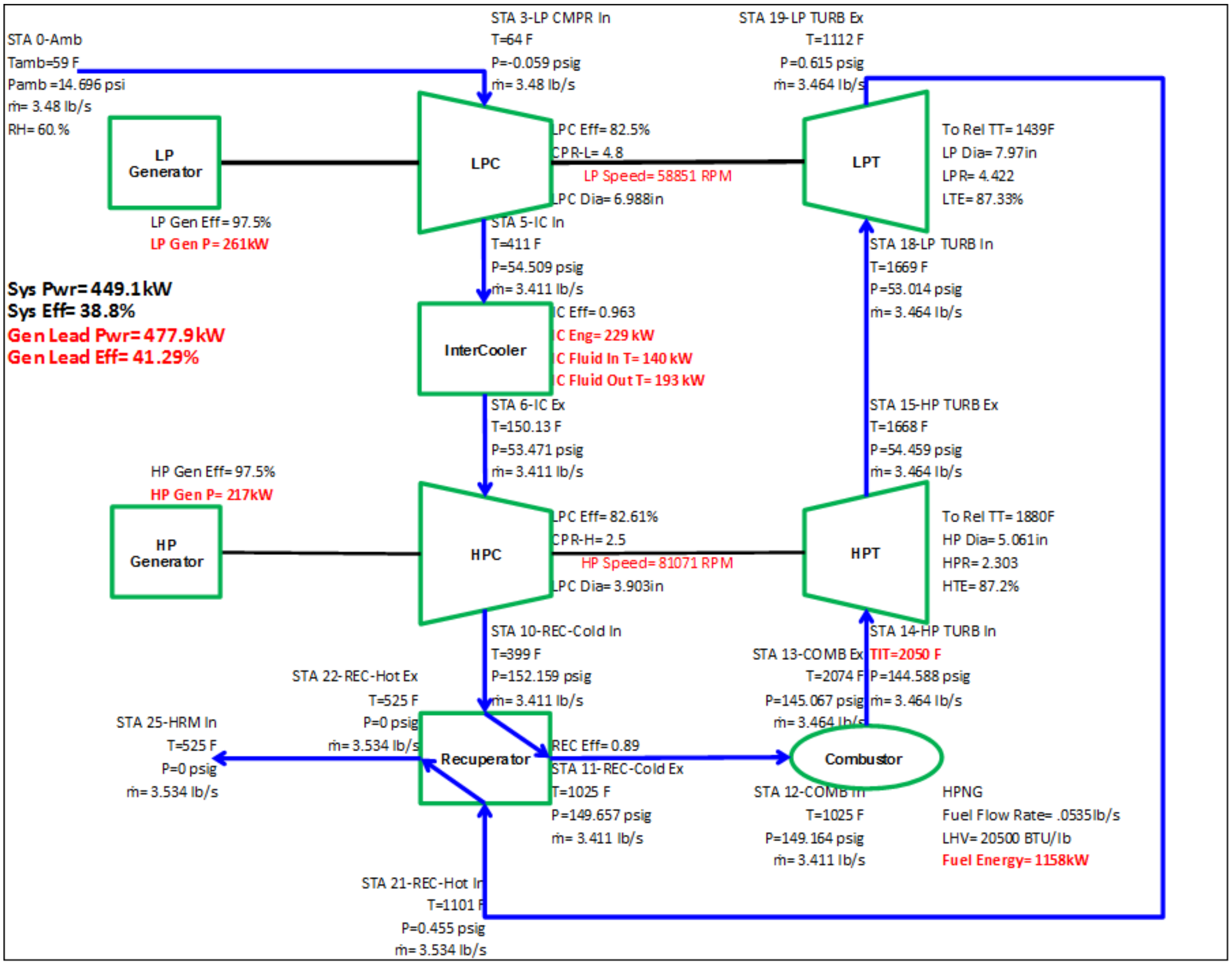

Figure 63: C370 Cycle Prediction (TIT=2050 °F)

Two (2) additional cycle predictions were performed to identify an increased TIT that meets performance requirements. It was found that the MEM will satisfied both power and efficiency requirements at a TIT of 2110 °F. At this TIT, the predicted power is 501.3 kW at generator lead and efficiency is 42.1% based on generator power. The corresponding HP turbine tip relative temperature is 1937 °F. For the MEM with an HRM, thermal efficiency is 85% (HRM effectiveness is 0.846). All C370 models used show the potential of the C370 to meet performance targets. However, extra power output and high TIT indicate the cycle may not be optimized.

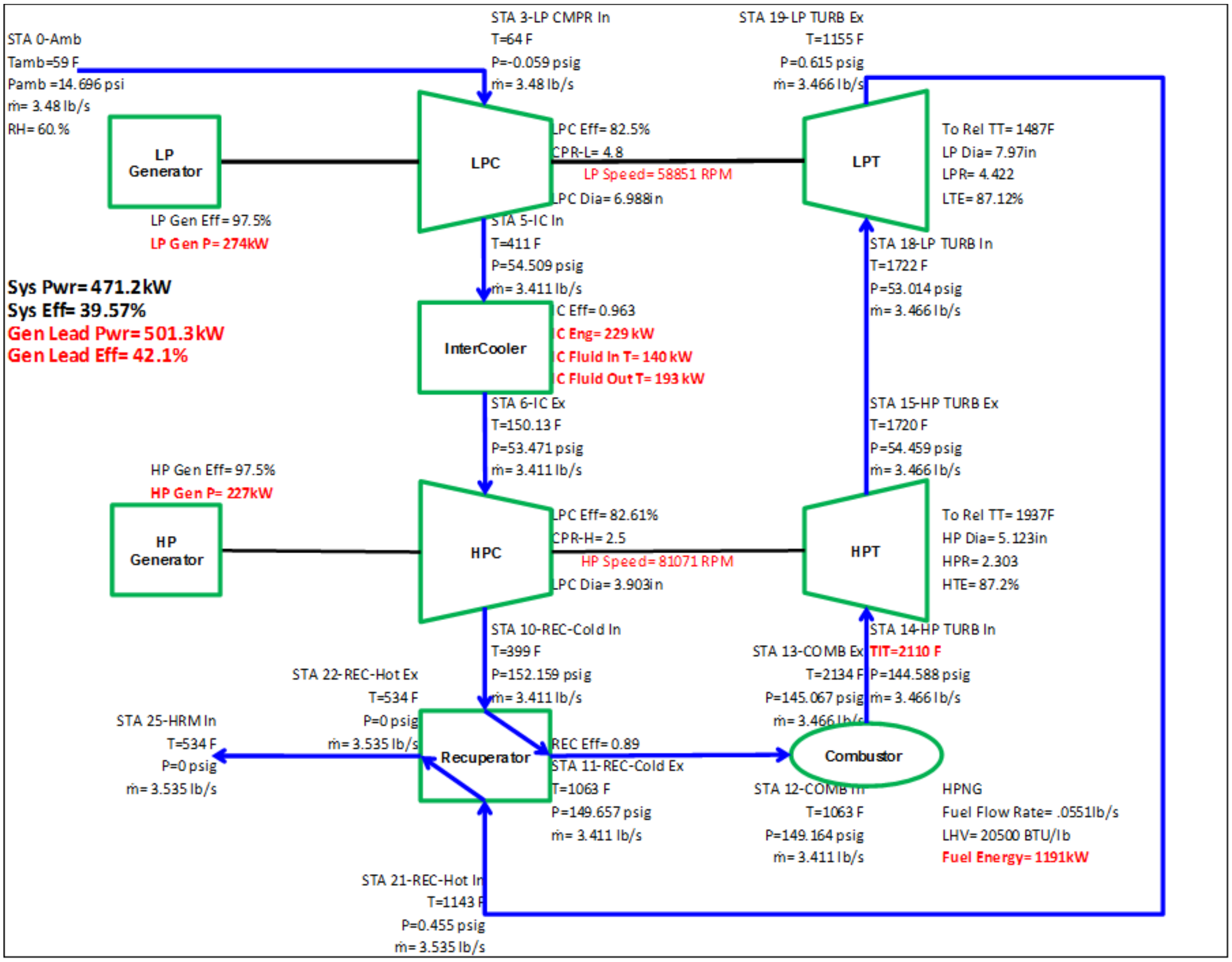

Figure 64: C370 Cycle Prediction (TIT=2110 °F)

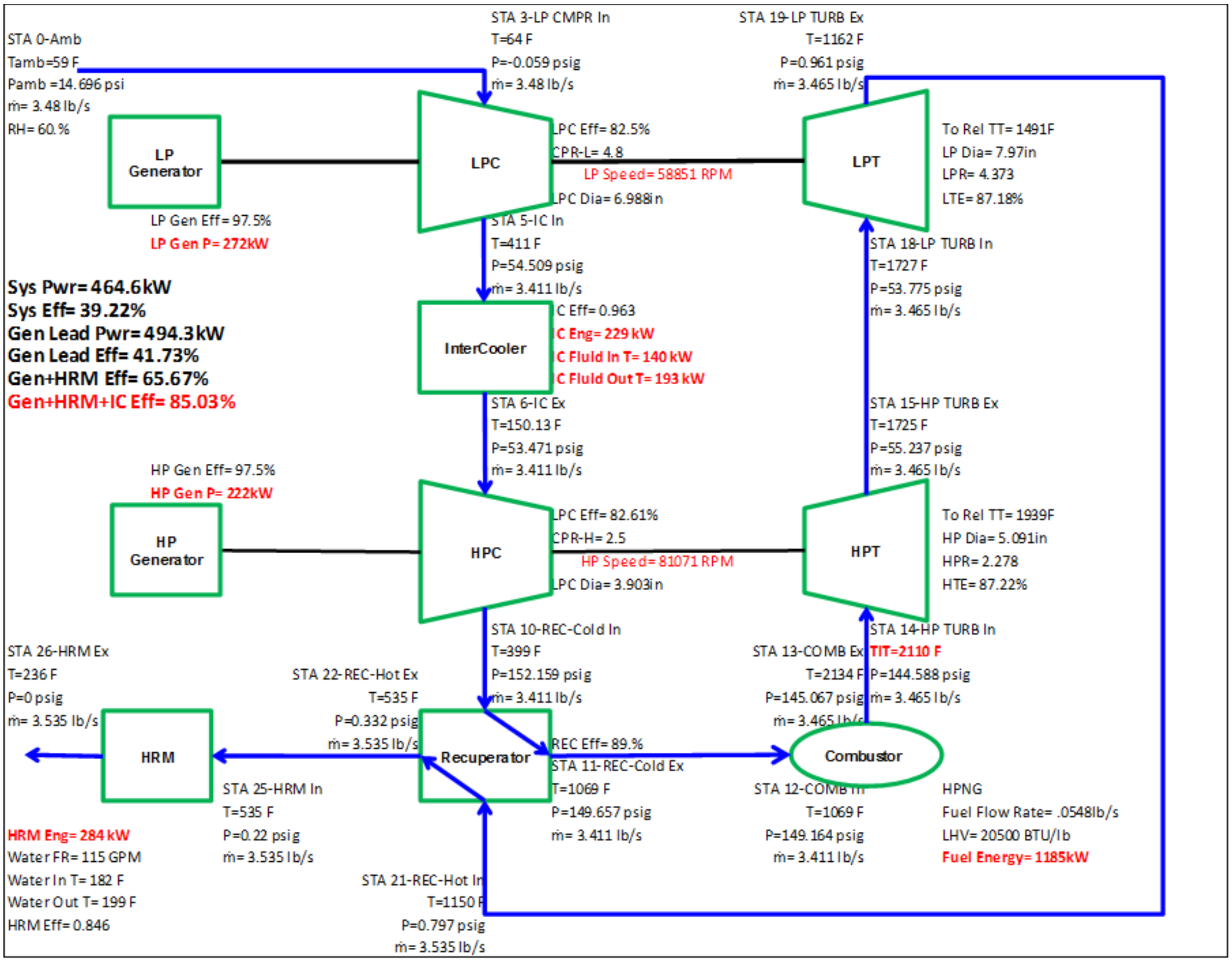

Figure 65: C370 CHP Cycle Prediction (TIT=2110 °F)

6.4.2. C370 Cycle - Component Design

A C370 component performance evaluation was conducted to improve and optimize system performance. The target of the design is to reach 42% efficiency and 370 kW power output targets. An initial C370 cycle model predicted 449 kW and 41.29% with a TIT of 2050 °F. An upgraded C370 cycle model increased TIT to 2110 °F to meet the 42% efficiency requirement.

The component design study was based either on existing technologies used in Capstone Turbine products or the best available technology developed in the industry. The study was focus on following components:

1. Compressor
2. Intercooler
3. Recuperator

Compressor Stage Optimization

A study was conducted to evaluate compressor operating conditions at both low pressure (LP) and high pressure (HP) compressor stages. Results are shown in Figure 66. It was observed that the initial cycle model does not operate at the optimal condition. The maximum efficiency was reached in the following ranges of 3.6 – 3.8 LP ratio and 2.3 – 2.5 HP ratio.

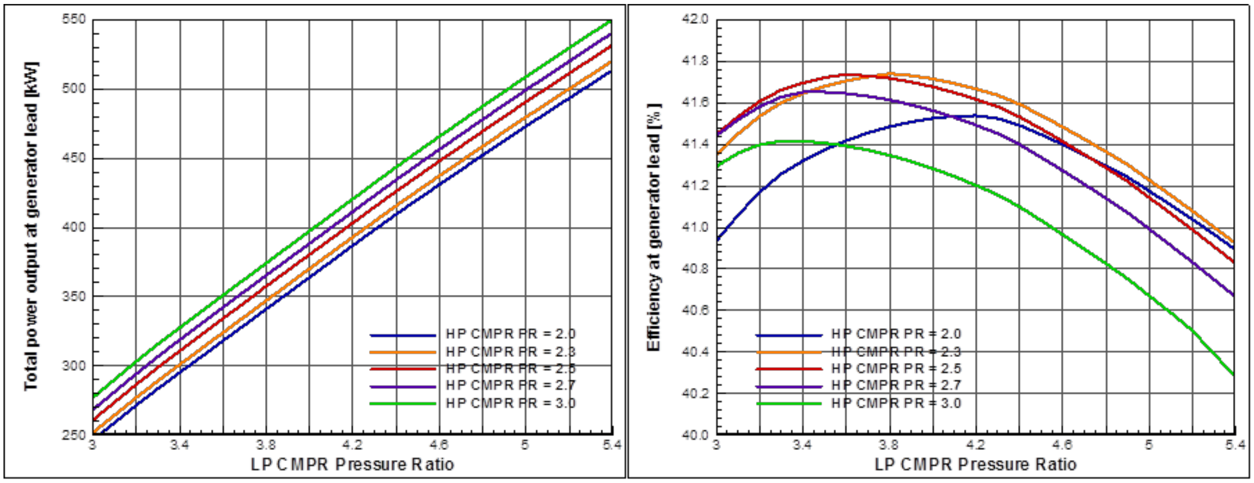

Figure 66: Impact from Compressor Operating Conditions

However, the optimal efficiency range does not meet generator power requirement at 370 kW. An optimal compressor operating condition was defined as 3.9 – 4.0 LP ratio and 2.4 – 2.6 HP ratio.

Intercooler Design Requirement Study

A study of the intercooler design reveals that intercooler fluid inlet temperature, intercooler effectiveness, and intercooler pressure drop have an impact on overall system performance, as illustrated in Figure 67 and Figure 68.

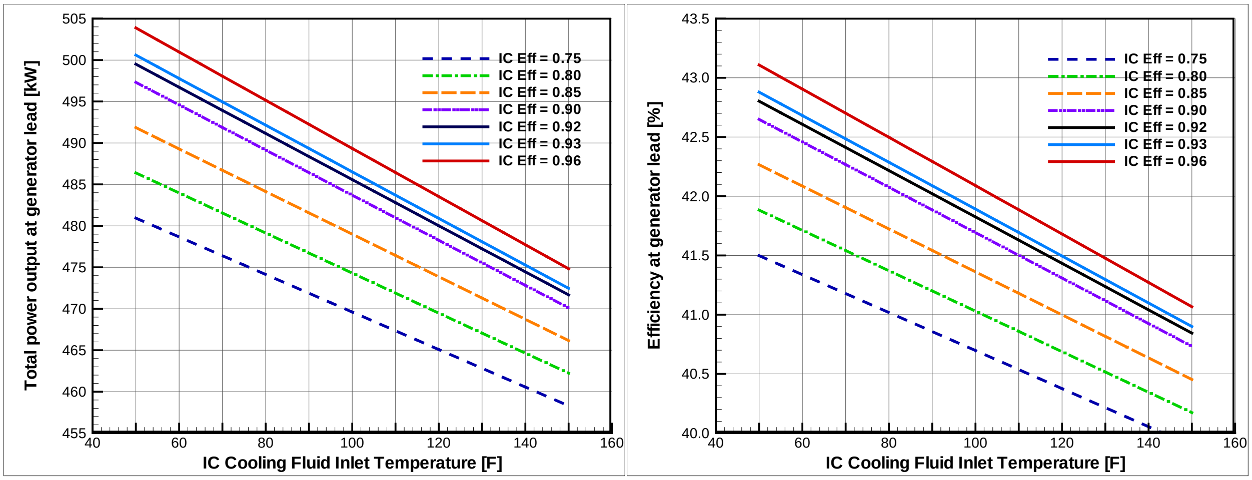

Figure 67: Intercooler Effectiveness and Cooling Flow Inlet Temperature Study

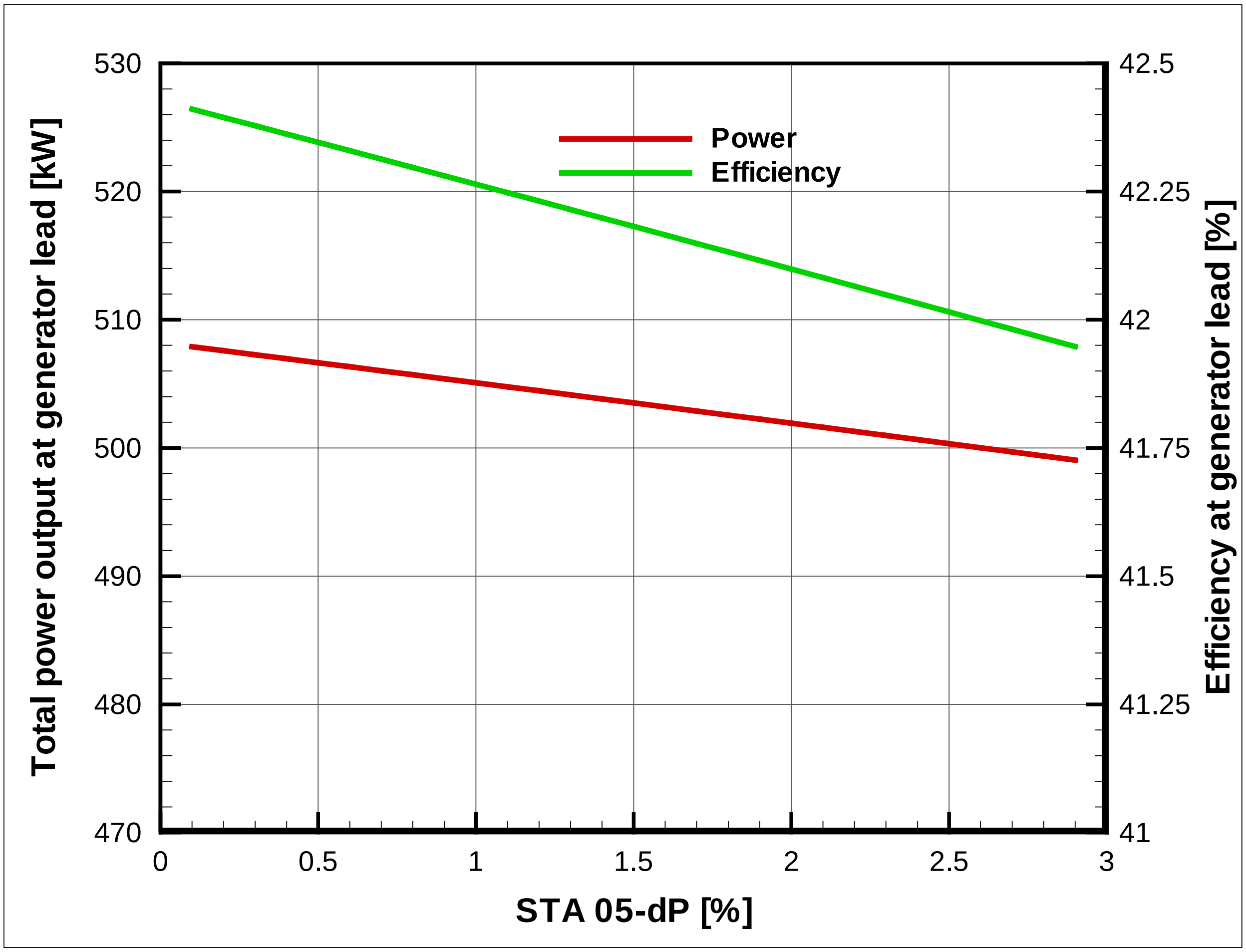

Figure 68: Intercooler Pressure Drop Study

The following observations were made upon revisiting the intercooler design:

1. Intercooler pressure drop of 1.5% is reasonable and should maintain at this level.
2. Intercooler effectiveness of 0.96 is relatively high and a lower number of 0.92 should be adopted.
3. Intercooler inlet fluid temperature can be lower with a running fluid setup or a fan or chiller to cool the fluid. Therefore, a 70 °F fluid temperature at inlet is defined.

Through the study, it was determined that an updated intercooler design target would improve efficiency by 1.13 points and result in about 16 kW increase in power.

Recuperator Design Requirement Study

Initial recuperator effectiveness is 0.89. This effectiveness is inherited from the current C200 recuperator value. However, with the design of a new recuperator, a better technology will be implemented and a higher effectiveness can be achieved. The study of the new recuperator available technology indicates that 0.92 effectiveness is a more reasonable target for development of a new recuperator. The 0.03 point on recuperator effectiveness improvement will increase system efficiency by 0.75 points as shown in Figure 69.

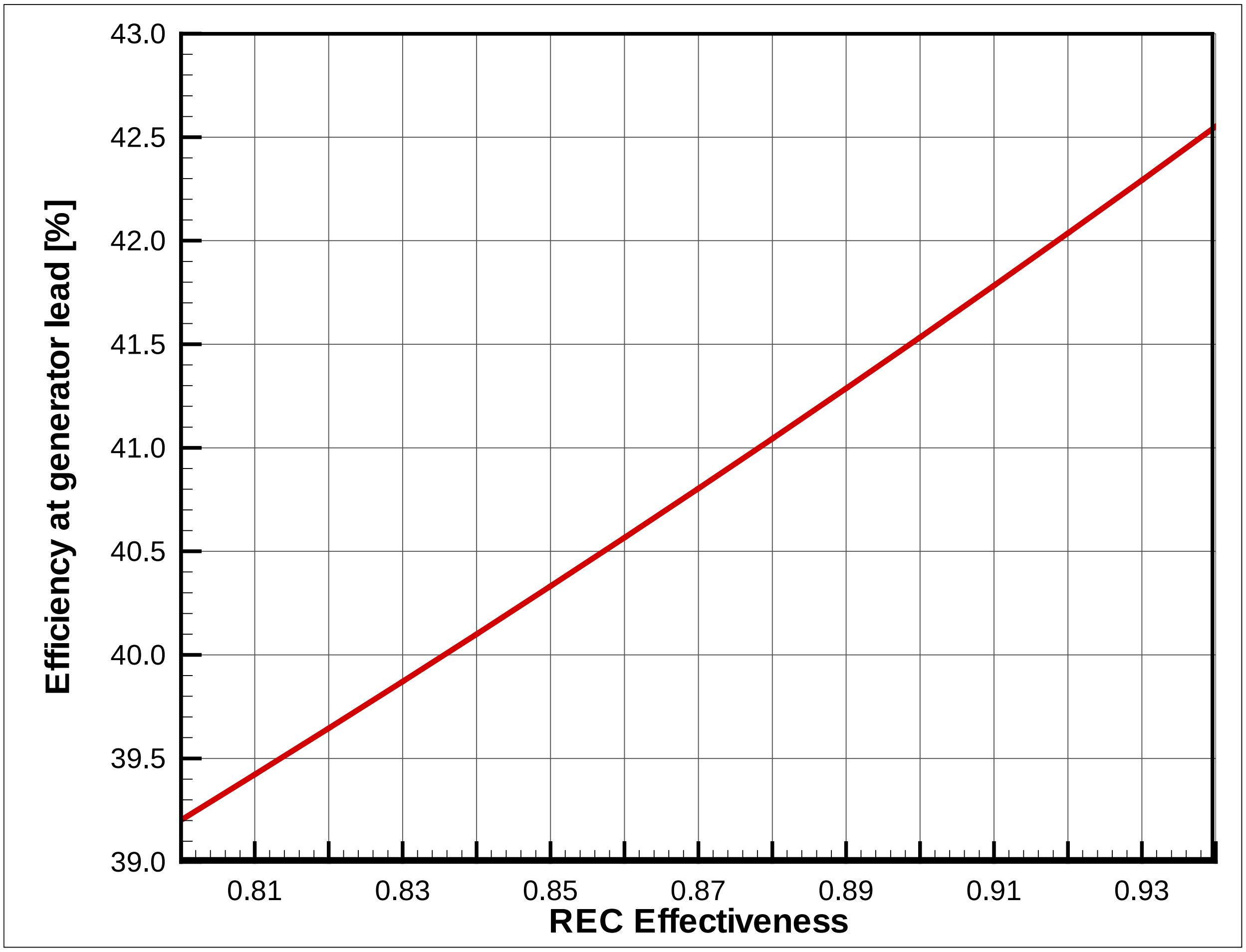

Figure 69: Performance Impact on Recuperator

A performance impact study on the recuperator pressure drop was conducted and results are shown in Figure 70. Current recuperator pressure drop values are reasonable. These results will be maintained as the design target.

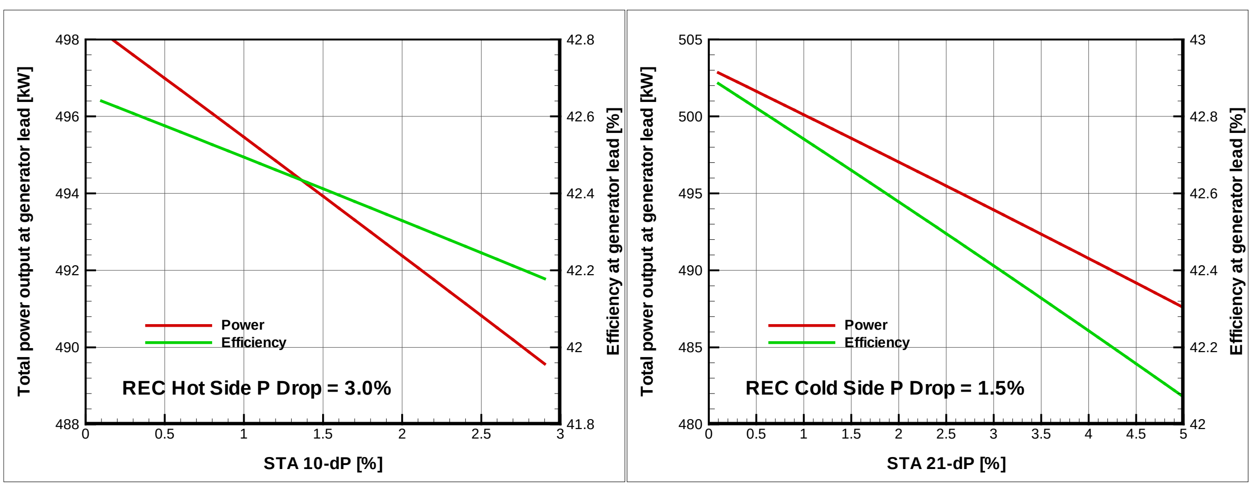

Figure 70: Performance Impact on Recuperator Pressure Drops

6.4.3. Cycle Analysis Design – Design Target

Based on the design study, a C370 cycle model was developed. The cycle is designed to achieve the performance target 370 kW power output at generator lead and 42% electrical efficiency based on generator power. There is also a target to lower TIT as much as possible.

The cycle model was built on initial feedback from component design and system optimization results. After evaluation, an LP pressure ratio of 4 and HP pressure ratio of 2.6 was recommended when the TIT is 2030 °F. This will satisfy both power and efficiency targets and include margins for design discrepancies. It will also operate at lower TIT to generate less thermal stress for parts.

There are two versions of the C370 cycle model, one without HRM — Figure 71 — and one with HRM — Figure 72. The component design targets are extracted from cycle model without HRM. A table of key component design parameters is shown in Table 27.

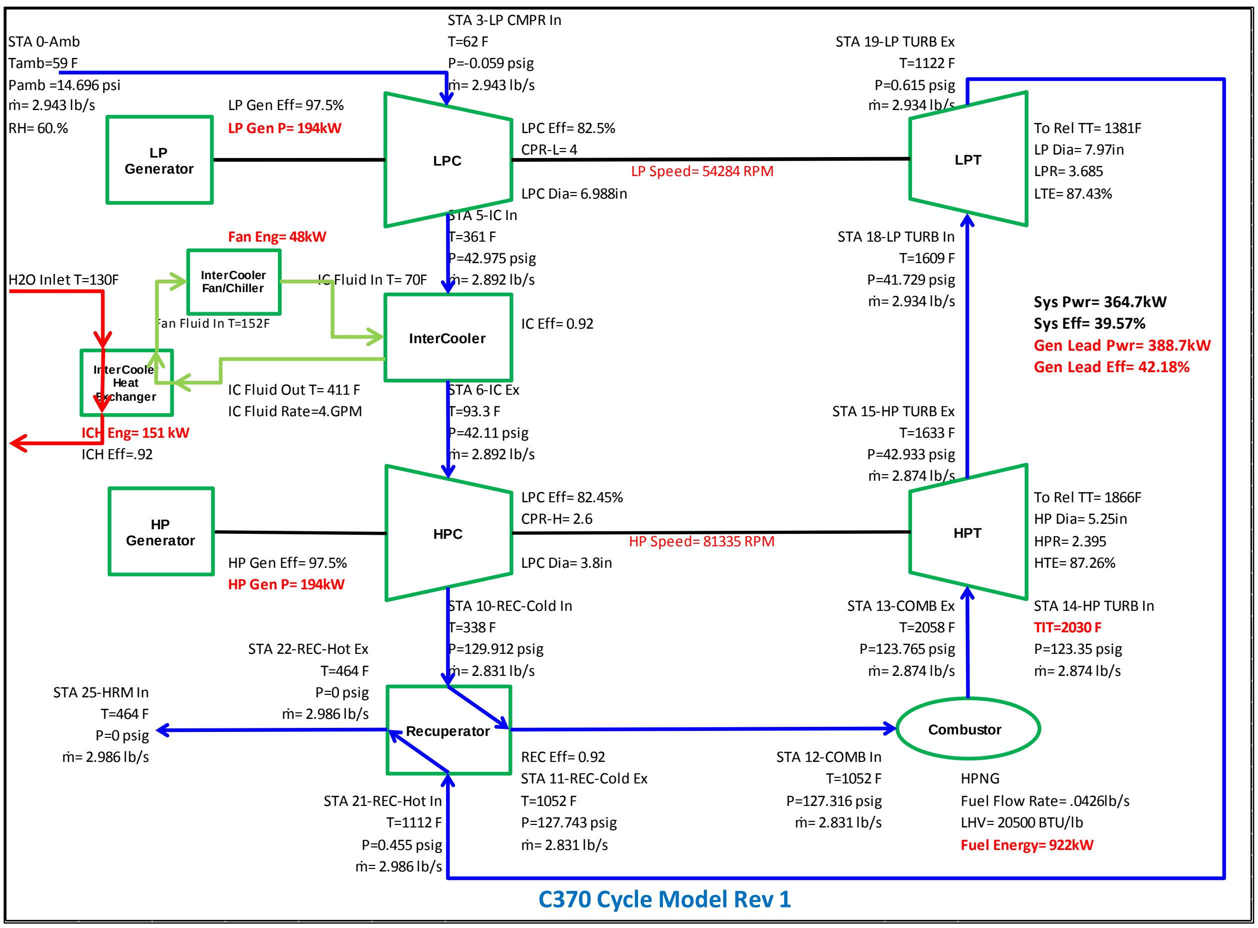

Figure 71: C370 Cycle Design (without HRM)

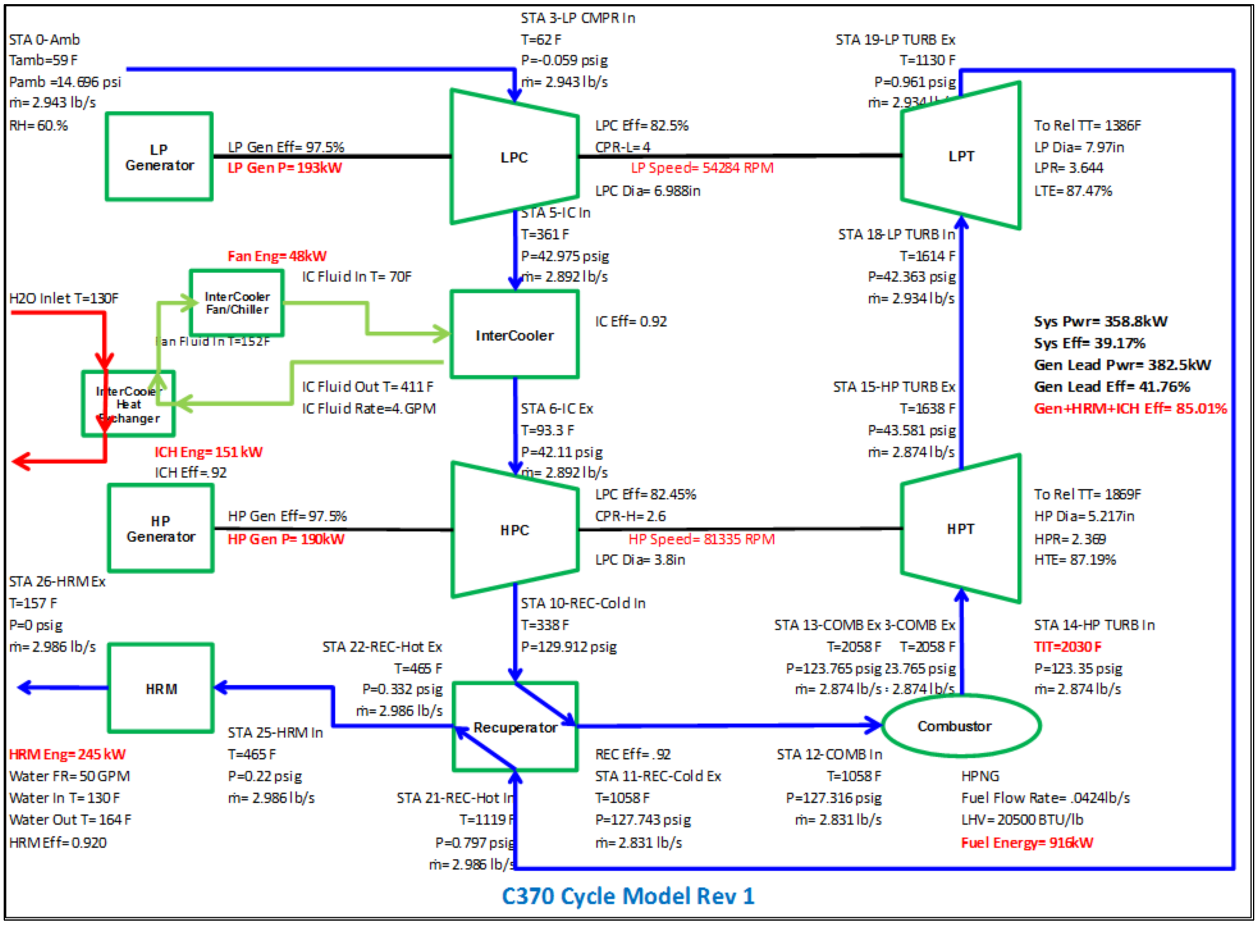

Figure 72: C370 Cycle Design (with HRM)

Key Parameters				
Category	**No.**	**Description**	**Unit**	**Default**
Package	1	Package Inlet Heating	°F	0.0
Generator	2	LE Generator Efficiency	%	97.5
	3	HP Generator Efficiency	%	97.5
	4	Generator Blower Power	kW	1.5
	5	Generator Blower Power	kW	1.5
Leakage	6	Bearing Leakage Mass Flow Rate – LP	lbm/s	≥ 0.05
	7	Bearing Leakage Mass Flow Rate – HP	lbm/s	≥ 0.06
Compressors	8	LP Compressor Pressure Ratio	—	4.0
	9	HP Compressor Pressure Ratio	—	2.6
Intercooler	10	Intercooler Air Exit Temperature	°F	Solution
	11	Intercooler Fluid Inlet Temperature	°F	70
	12	Intercooler Fluid Flow Rate	GPM	4
	13	Intercooler Pressure Drop	%	1.5
	14	Intercooler Effectiveness	—	0.92
	15	Intercooler Heat Exchanger Effectiveness	—	0.92
	16	Intercooler Heat Exchanger Water Inlet Temperature	°F	130
Combustion	17	Combustion Efficiency	%	100
	18	Combustion Pressure Drop	%	2.5
Recuperator	19	Recuperator Effectiveness	—	0.92
	20	Recuperator Pressure Drop – Cold	%	1.5
	21	Recuperator Pressure Drop – Hot	%	3
Internal Heating	22	Temperature Rise across LP Generator	°F	3.0
	23	Temperature Rise across HP Generator	°F	5.0
	24	Temperature Rise from Compressor to Recuperator	°F	30
Mechanical Efficiency	25	LP Spool Mechanical Efficiency	%	99.2
	26	HP Spool Mechanical Efficiency	%	99.2
HRM	27	HRM Effectiveness	—	0.92
	28	HRM Water Inlet Temperature	°F	130
	29	HRM Water Flow Rate	GPM	Ref
	30	HRM Pressure Drop	%	1.5

Table 27: C370 Key Component Design Requirements

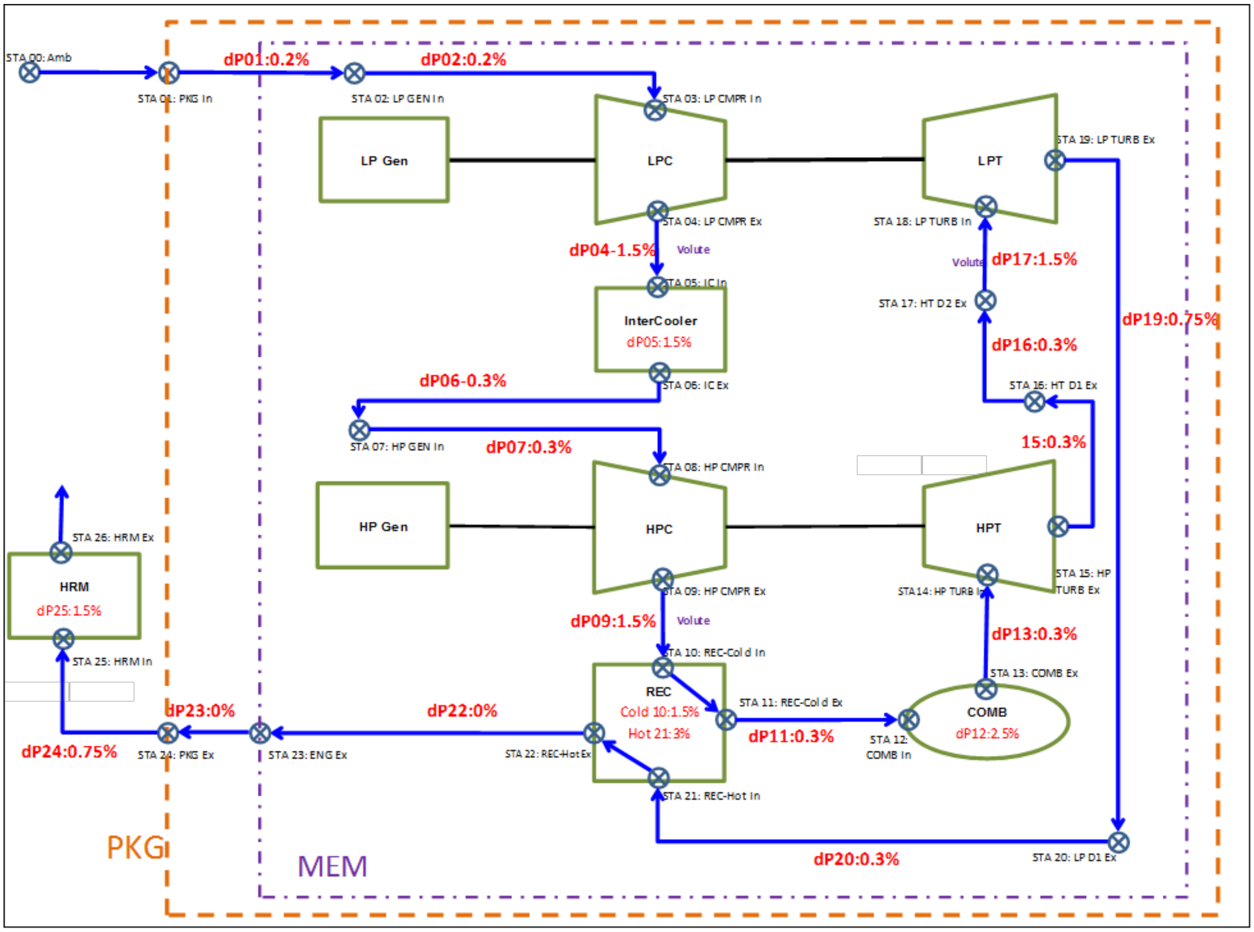

Figure 73: C370 Final Pressure Drop Analysis

6.5. *Bi-Metallic Single Crystal Alloy Turbine Wheel Concept Validation Testing (C65)*

6.5.1. C65 High Temperature Turbine Design

The development of the C370 turbine wheel leverages the C65 turbine wheel due to their similarity in size and blade profiles. However, the temperature and speed requirements of the C370 high pressure spool design are beyond the capability of current C65 turbine wheel material, MarM247. High strength material — such as single crystal CMSX-4 — is a good material candidate for this design. CMSX-4 has significantly higher creep strength than MarM247 as the C65 turbine wheel is creep limited.

It is, however, not practically possible to cast a complete radial turbine wheel out of a single crystal material. A bi-metal wheel design was proposed in which the turbine blade tip is cast as single crystal CMSX-4, while the remaining wheel body — under the scallop radius — will be cast as MarM247. The single crystal tip is then bonded to the wheel body using transient liquid phase (TLP) brazing method. TLP brazing method will be discussed in detail in a later section — including bond interface layer, tooling setup, oven temperature, duration of heat soak, vacuum level. A prototype of this bi-metallic turbine wheel design is shown in Figure 74.

Figure 74: C65 Prototype of a Bi-Metallic Turbine Wheel

In the current preliminary design phase, initial structural analysis has been conducted which focused on back-to-back comparison of creep and rupture life capability of the C65 and C370 bi-metallic turbine wheels based on planned prototype testing conditions. The main focus has been on the development of the TLP bonding process and testing of the bi-metallic turbine wheel.

6.6. Structural Analysis of Turbine Wheel

FEA models for a single passage C65 and bi-metallic turbine wheel have been developed that utilize cyclic symmetry of the wheel to save computational time. Figure 75 shows the cyclic model for the bi-metallic turbine wheel. For the bi-metallic wheel model, the single crystal tip and the MarM247 body are made to share the same interface area to ensure conforming mesh throughout the model and solution fidelity particularly at the TLP bond joint.

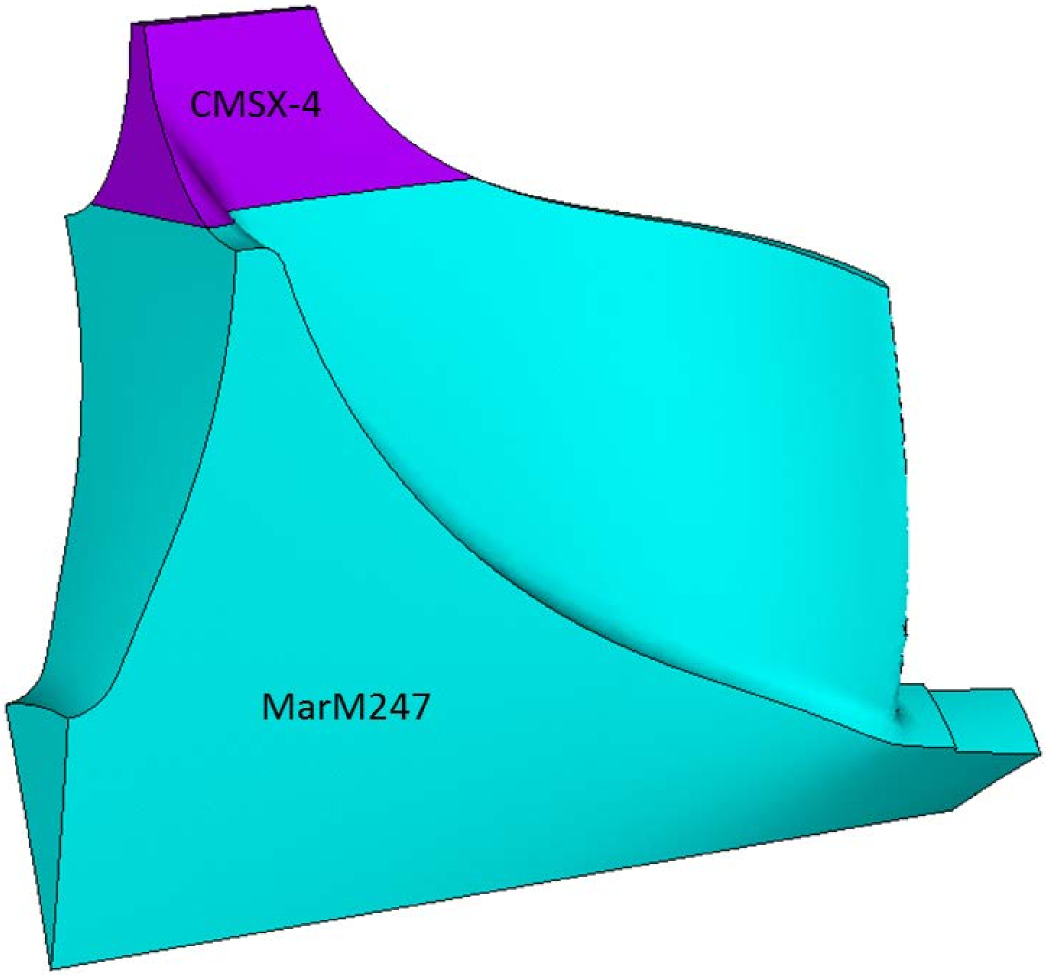

Figure 75: Cyclic FEA Model for Bi-Metallic C65 Turbine Wheel

Turbine wheel operating conditions including TIT and engine speed are based on C65 thermodynamic cycle analysis and estimated C370 turbine wheel tip diameter respectively. TIT is 1823 °F from the thermodynamic cycle analysis results and engine speed is calculated at 88,730 rpm by scaling the C370 speed of 82,780 rpm — from cycle analysis — using the wheel tip diameter ratio of C370 over C65 — i.e., 5.22 instead of 4.87 in. This ensures that the tip speed of the C65 and the bi-metallic wheel remains the same: 1885.5 ft/sec.

The engine speed was later reduced slightly to 81,335 rpm due to rotor dynamics requirements. The results of the analysis here still apply, since the purpose was to look at the relative improvement of the bi-metallic wheel's creep capability over the C65 wheel, not the absolute value. Figure 76 shows the temperature profile for the turbine wheel which was based on the CFX conjugate heat transfer model.

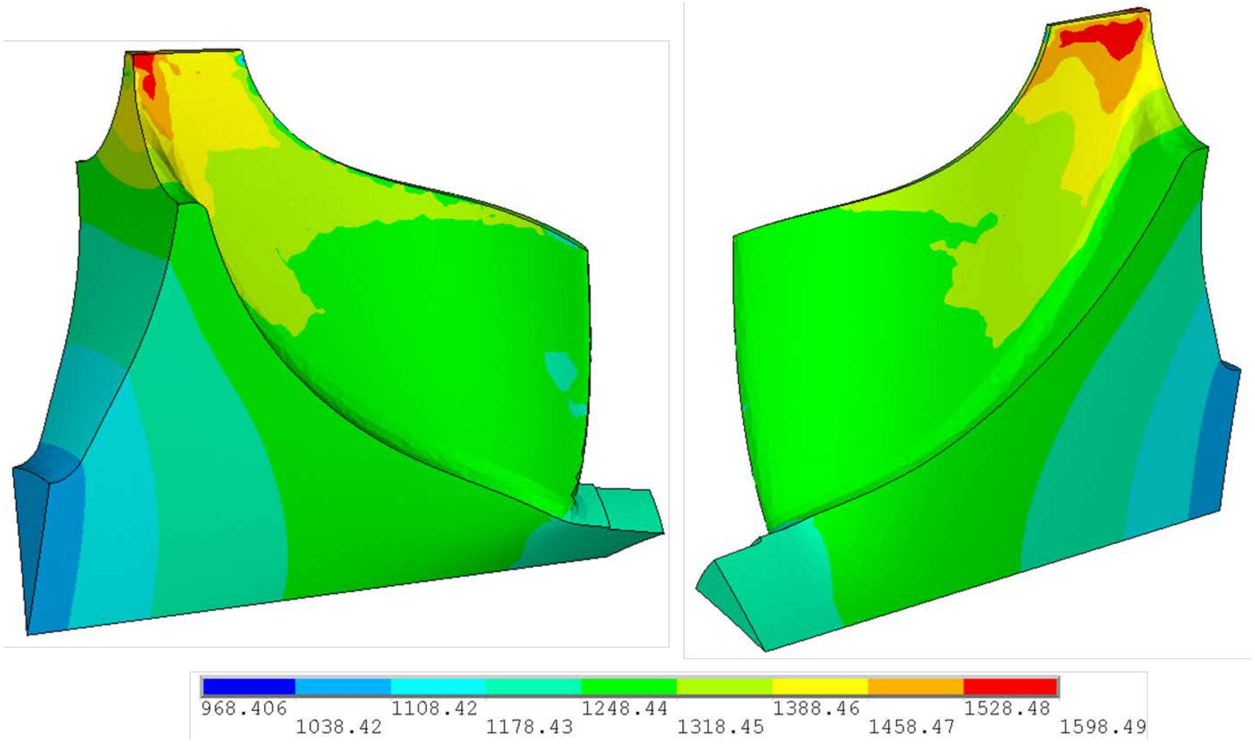

Figure 76: C65 bi-metallic Turbine Wheel Temperature (TIT = 1823 °F, 82780 rpm)

Figure 77 and Figure 78 show an expanded view of the C65 turbine wheel von Mises and the bi-metallic turbine wheel radial stresses respectively. For the C65, the creep life is limited at the blade cross section, perpendicular to the stream line. Therefore, von Mises stress is used for the creep life calculation. For the bi-metallic turbine wheel, the creep life is limited at the TLP bond joint interface which is perpendicular to radial direction. Therefore, radial stress is used to calculate the creep life.

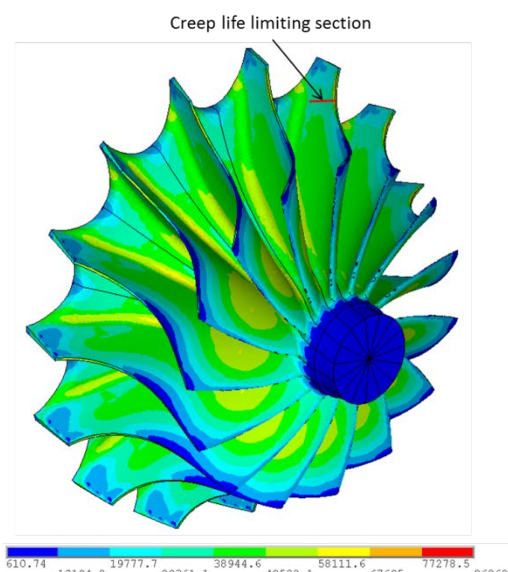

Figure 77: C65Turbine Wheel von Mises Stress

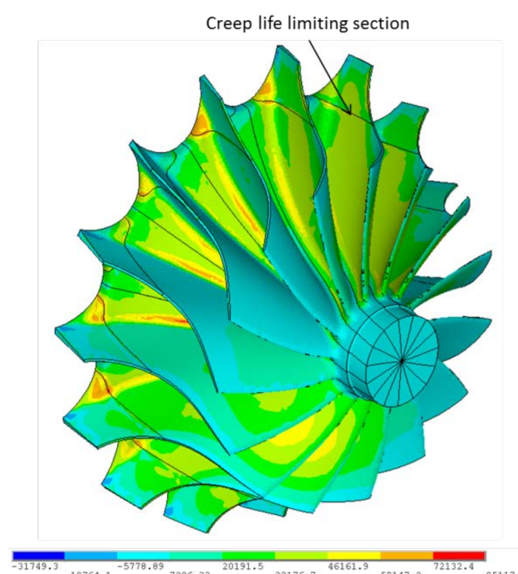

Figure 78: C65 Bi-metallic Turbine Wheel Radial Stress

The life-limiting location of the C65 turbine wheel is identified near the blade tip region, due to combined centrifugal stress and high TIT. For the bi-metallic turbine wheel, the life limiting location is shifted to the bi-metallic bond joint interface on the side of the MarM247 side where the creep and rupture strength of MarM247 is less than that of the single crystal. See Figure 79.

Tensile tests on the bi-metallic bars have confirmed that the bond joint is stronger than either the CMSX-4 or MarM247. Result of tensile test of a sample bi-metallic tensile bar confirms this as shown in Figure 80.

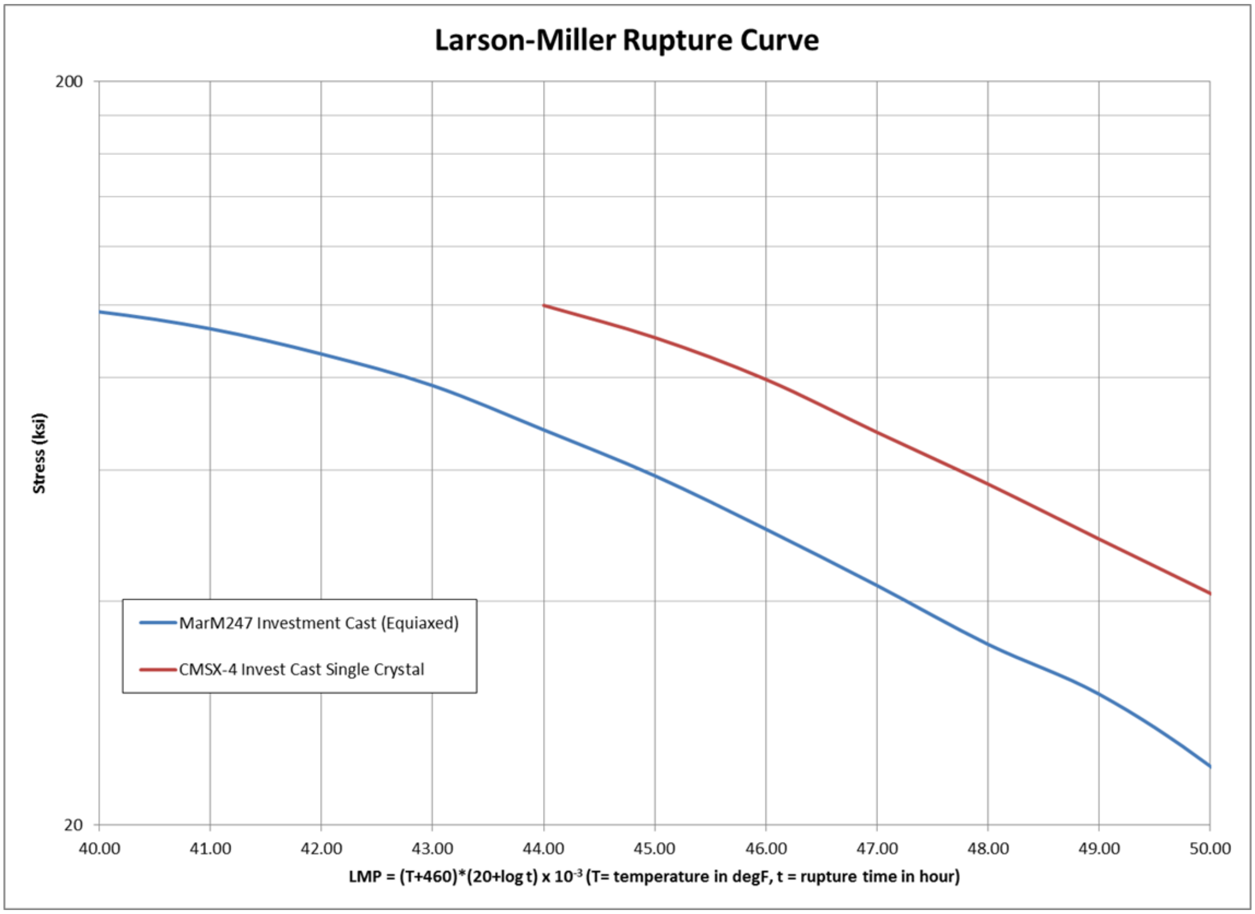

Figure 79: Larson-Miller Rupture Curves for MarM247 and Single Crystal CMSX-4 Investment Cast

From the MarM247 Larson-Miller Rupture Curve — Figure 79 — it was determined that the C65 and bi-metallic turbine wheel creep lives are 2092 hours and 2975 hours respectively, showing more than 40% improvement with bi-metallic turbine wheel. The absolute creep life, however, is significantly below the design requirement. More effort is needed to improve the life capability which may include all single crystal blade, thermal barrier coating, and cooling.

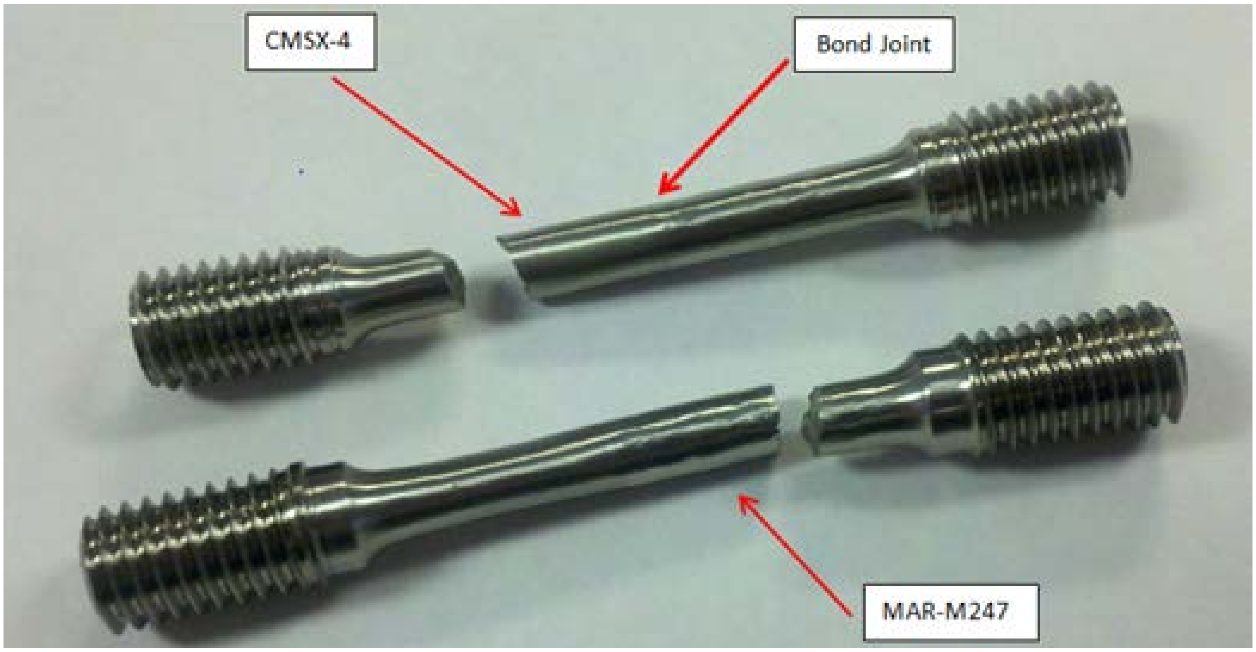

Figure 80: Ruptured Bi-Metallic Tensile Test Bar

Additional creep lives at higher TIT are calculated for both the C65 and bi-metallic wheels. The results are listed in Table 28 and Table 29. For additional creep calculation at higher TIT, metal temperatures are scaled based on TIT value, assuming constant temperature gradient, constant stress, and negligible thermal stress compared to mechanical stress due to centrifugal load. Results show that the bi-metallic wheel has at least 30% more creep life capability than the C65 turbine wheel.

Average radial Stress (ksi)	TIT (F)	Average Metal Temperature (F)	Rupture Life (Khr)
36.3	1823	1589	2.092
36.3	1900	1666	0.299
36.3	1950	1716	0.091
36.3	2000	1766	0.029
36.3	2050	1816	0.01
36.3	2100	1866	0.003
36.3	2200	1966	0.0005
36.3	2300	2066	0.00008

Table 28: Rupture Life for C65 Turbine Wheel

Average radial Stress (ksi)	TIT (F)	Average Metal Temperature (F)	Rupture Life (Khr)
38.5	1823	1562	2.975
38.5	1900	1639	0.409
38.5	1950	1689	0.122
38.5	2000	1739	0.038
38.5	2050	1789	0.0127
38.5	2100	1839	0.0044
38.5	2200	1939	0.00061
38.5	2300	2039	0.0001

Table 29: Rupture Life for C65 Bi-Metallic Turbine Wheel

6.6.1. High Temperature Turbine Design Approach

A C65 turbine is similar to the proposed C370 high-pressure — high-temperature — turbine as described in the above sections. This will be used as a starting point to design and develop a bi-metal turbine prototype. The basic steps for prototype bi-metal turbine development are:

a) A production C65 MAR-M247 turbine has been machined to remove the turbine blade tips similar to the drawing shown in Figure 81.
b) Single crystal CMSX-4 tips to match the C65 turbine blade tip profile were grown and machined to mate to the machined turbine wheel.
c) A TLP bonding process was — and will continue to be — developed to produce a high-temperature bond between the single crystal tips and turbine hub.
d) A prototype turbine will be produced and tested
e) Further refinements to the tip-hub interface and TLP bond will be pursued based on test results.

6.6.2. C65 Bi-Metallic Turbine Wheel Design

A production C65 turbine was wire EDM (electric discharge machined) to remove the blade tips as shown in Figure 81.

Figure 81: C65 Turbine with Blade Tips Removed

Single crystal CMSX-4 tips were grown and EDM cut to match the machined turbine hub. See Figure 82. The joint location was chosen to optimize and reduce stress at the TLP bond and to provide sufficient temperature margins at the tip location as described in above sections.

Figure 82: Single Crystal Tips for Prototype C65 Turbine wheel

The machined turbine hub and tips were joined using a specialized TLP bonding process described in the next section.

6.6.3. Bi-Metallic Transient Liquid Phase Bond Development

A transient liquid phase (TLP) bond is similar to diffusion bonding in that a melting point depressant film or foil promotes bonding between the two adjacent parent materials. It differs from a typical diffusion bonds because the inter diffusion of the eutectic interlay produces an interface that will remain strong at temperatures well above the bonding temperatures. This type of bond differs considerably from a weld or braze as the final bond joint will have no alloyed region between the parent materials.

The process parameters involved in producing a high-quality and high-temperature TLP bond are complex and numerous. For example, the bond temperature, temperature rise rate and cooling rate, bond pressure and bond interlay material are all critical to producing a quality bond. Capstone Turbine has optimized many of the bonding parameters so that high-quality and high-strength bonds have been produced under ideal conditions but further work is still required.

One of the critical requirements for a good TLP bond is correct parent material surface conditions. It was discovered that the EDM process leaves a surface oxide on both the turbine hub and single crystal tips that makes bonds fail at low temperatures and stress conditions. This is partly due to the fact that both MAR-M247 and CMSX-4 have chrome and aluminum that produce oxides during EDM. Aluminum oxide must be mechanically removed from both mating surfaces prior to bonding.

The initial bi-metal turbine prototype was produced using a specialized eutectic interlay foil which produced sufficiently strong bonds as shown in Figure 83.

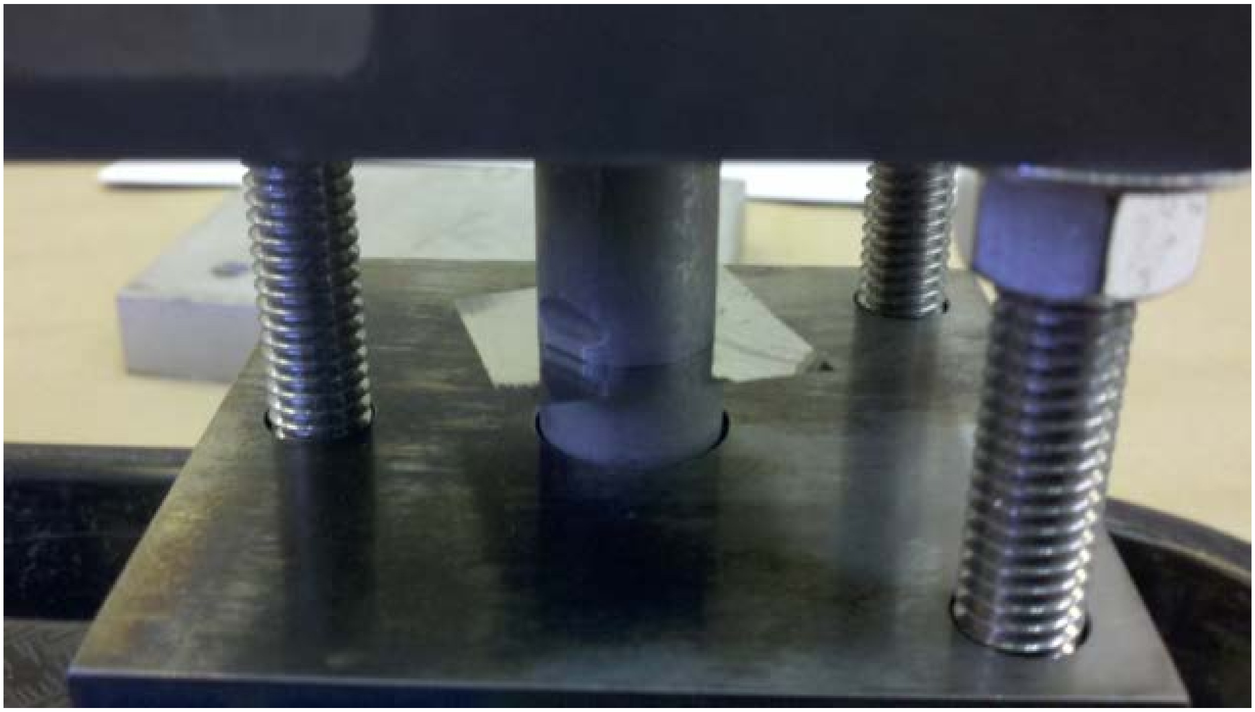

Figure 83 Tensile bars of MAR-M247 and CMSX-4 with interlay foil

A finished tensile sample is shown in Figure 84 along with a mounted sample —

Figure 85 — showing the difference between the polycrystalline MAR-M247 material (left) and CMSX-4 single crystal material (right). Tensile results for bar samples surpassed expected results as well as reported results of similar tests. Room temperature ultimate tensile strength was over 130-140 thousand pounds per square inch (ksi) and one high-temperature tensile test at 1600 °F has yield strength of over 108 ksi. In all cases, the parent materials – not the bond – failed in tensile tests.

Figure 84: Finished Tensile Sample and Sample Mount Showing Material Differences

Material aging or heat treating after bonding is required to relax stress induced during the bonding process. An aging process suggested by Canon-Muskegon and Oak Ridge National Labs has been tested with satisfactory results. More aging and heat treat test are required to produce optimum bond.

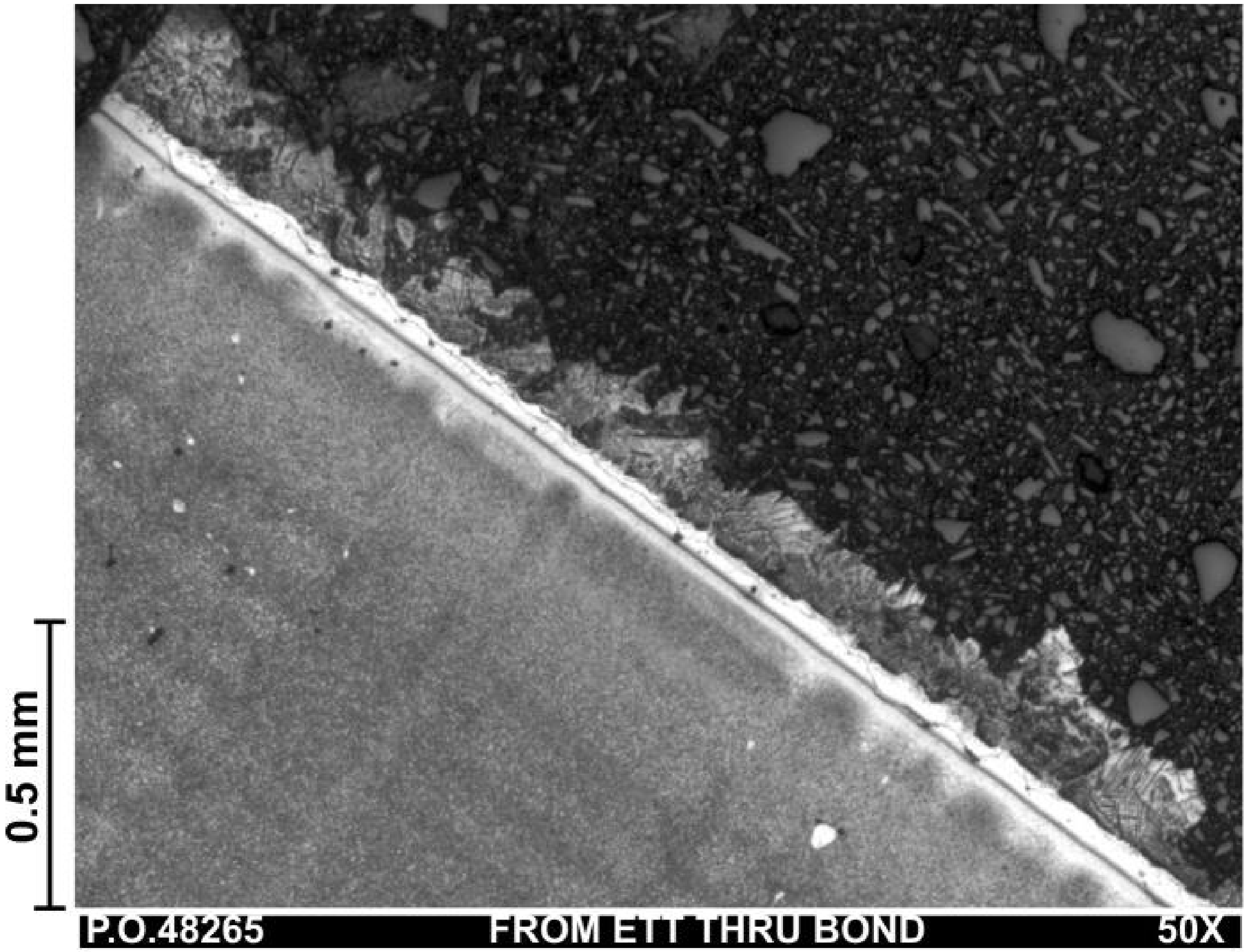

Figure 85: Tensile Sample Showing CMSX-4 and MAR-M247 at Tensile Test Fracture Location

6.6.4. C65 Bi-Metallic Turbine Wheel Prototype Production

Two initial bi-metal turbines were produced using interlay foil as shown in Figure 86. These turbines were bonded and aged in the same way as the previous tensile samples.

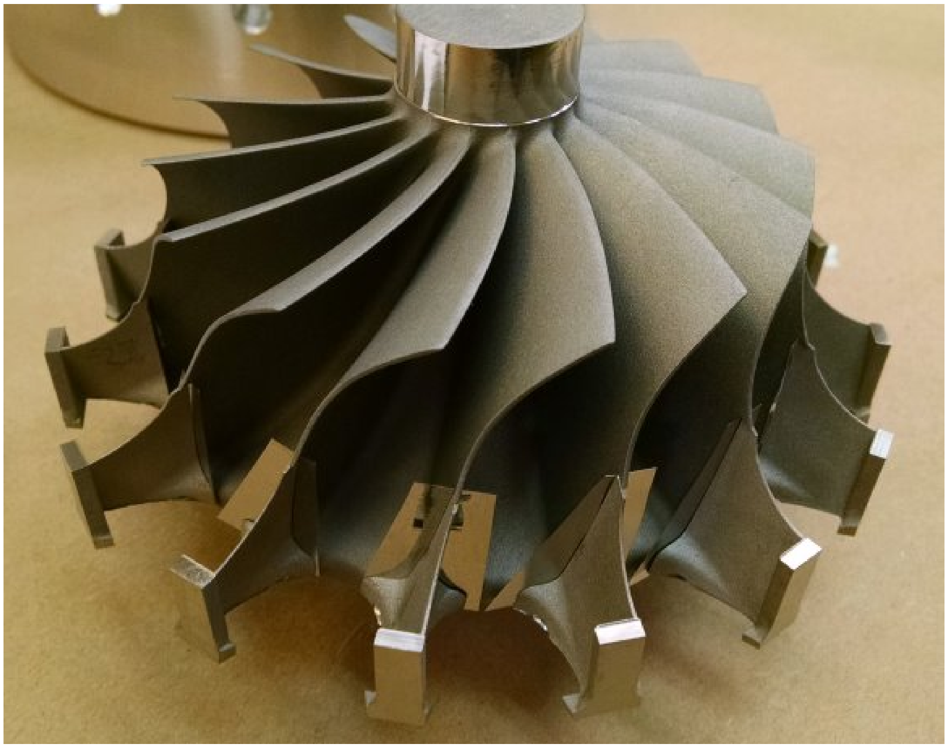

Figure 86: First Prototype C65 Bi-Metal Turbine Showing Hub, Tips and Interlay Foil

One of the two initial prototype bi-metal turbines was used for metallurgical and microscopic analysis. The bond character was excellent and static tensile test showed that the bond withstood tensile forces in excess of 44 ksi which would be the expected radial forces on the bond region due to turbine rotation.

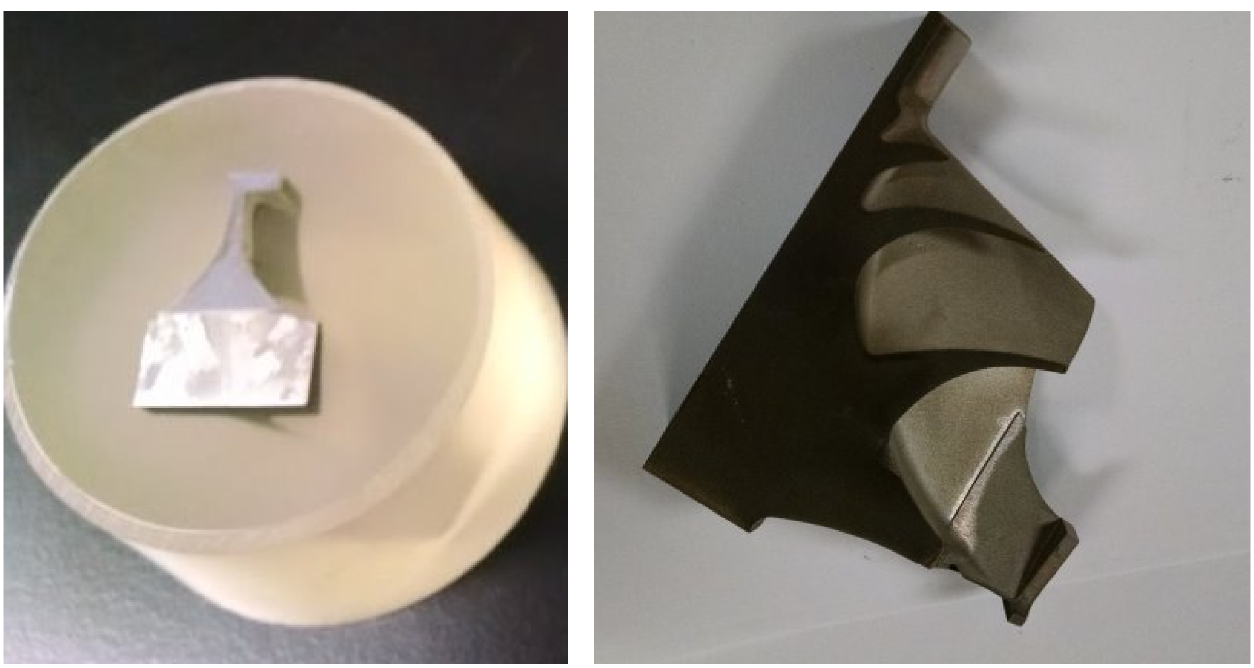

Figure 87: Tensile and Micrograph Analysis of One of the Bonded Prototype C65 Turbines

6.6.5. C65 Bi-Metallic Turbine Wheel Test Results

The finished prototype C65 bi-metal turbine is shown in Figure 88 (left) and the results of the first spin test are shown on the right. The turbine failed at about 25,000 rpm which is well below the desired speed.

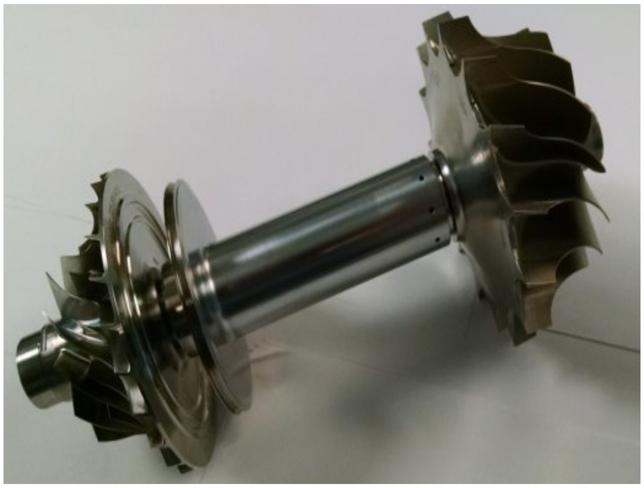

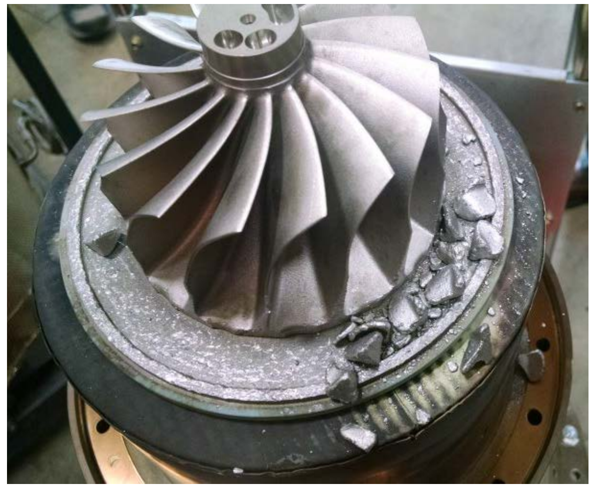

Figure 88: Bi-Metal Turbine Assembly (Left) and Spin Test Results (Right)

Post mortem analysis indicates that one tip bond fractured and the tip became dislodged in the turbine nozzle throat area. The debris from this tip sheared the remaining tips from the hub assembly.

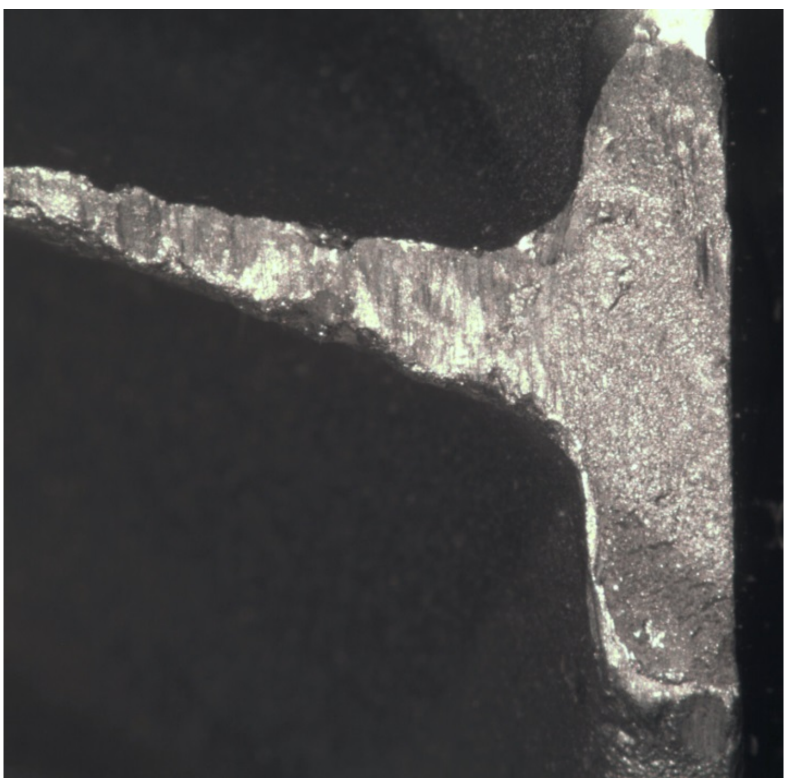

Figure 89: Ductile Fracture of One Turbine Tip

The static tensile testing results of TLP bonds were promising but the blade-tip bonds need to be refined. This will be done as follows:

a) Blade-tip interface will be improved so that surfaces can be machine ground after initial EDM
b) A thin film interlay process is in development so that the foil interlay is not necessary
c) Hand assembly of hub, tips, and foil must be removed
d) A second generation bonding fixture is in development that will hold the turbine hub and tips in better registration under greater bond pressure than was used for the prototype turbines

Initial test of electroplating the interlay onto tensile samples proved to be inadequate and the tensile strength from these samples was far below those produced with interlay foil. Following the electroplating tests, an electron beam thin film coating was produced on tensile sample materials. The tensile results from this interlay were better than those of the electroplated interlay but still not sufficient. Analysis of the electron beam, vacuum thin film coating revealed that a critical component of the interlay material was not present. This component most likely disassociated from the eutectic alloy during the high-temperature evaporation process. Currently, a vacuum sputter deposition process of the interlay material is under investigation. Test results from this process are not currently available.

6.7. C370 Power Electronics Design

The output power difference of the larger C370 generator motor generator drove the target power capacity of the new controllers developed for this engine. Table 30 shows the differences in rated power which drive an increase in amperage capacity for the same motor or generator voltage. The new controller design — capable of running both C370 generators and inverters — was designed to have a 400 A capacity.

	C200 Generator	C370 LP Generator	C370 HP Generator
ISO Max Power Requirement	225 kW	293 kW	246 kW
Percent increase Requirement	0%	30%	10%
Amperage capacity Requirement	300 A	390 A	330 A

Table 30: C200 vs. C370 Generator Power Output

6.7.1. Inverter and Generator Controller Assembly Design

Figure 90 is a schematic of the 400 A power electronic controller. The GCM equivalent of this replaces the output filter with GCM inductors and runs different control software, all other hardware is the same.

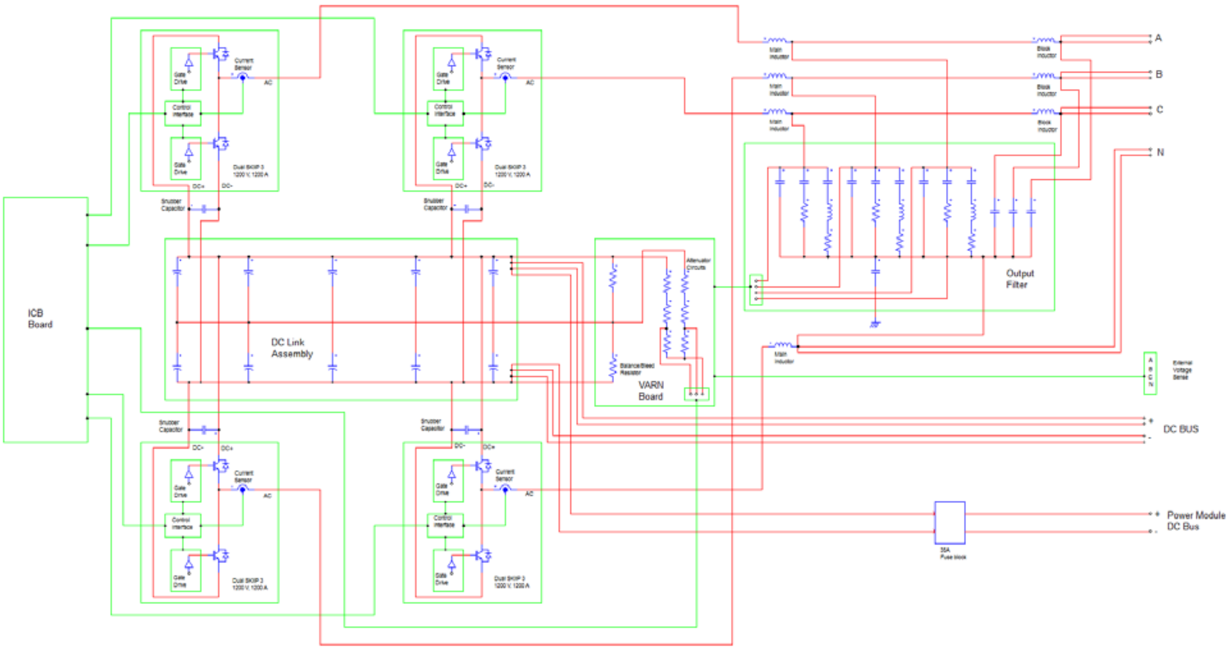

Figure 90: C370 LCM Schematic

Figure 91 is an isometric view of the 3D CAD model of the final inverter controller design. This design was built and qualified for production use for either the C370 or C250 system.

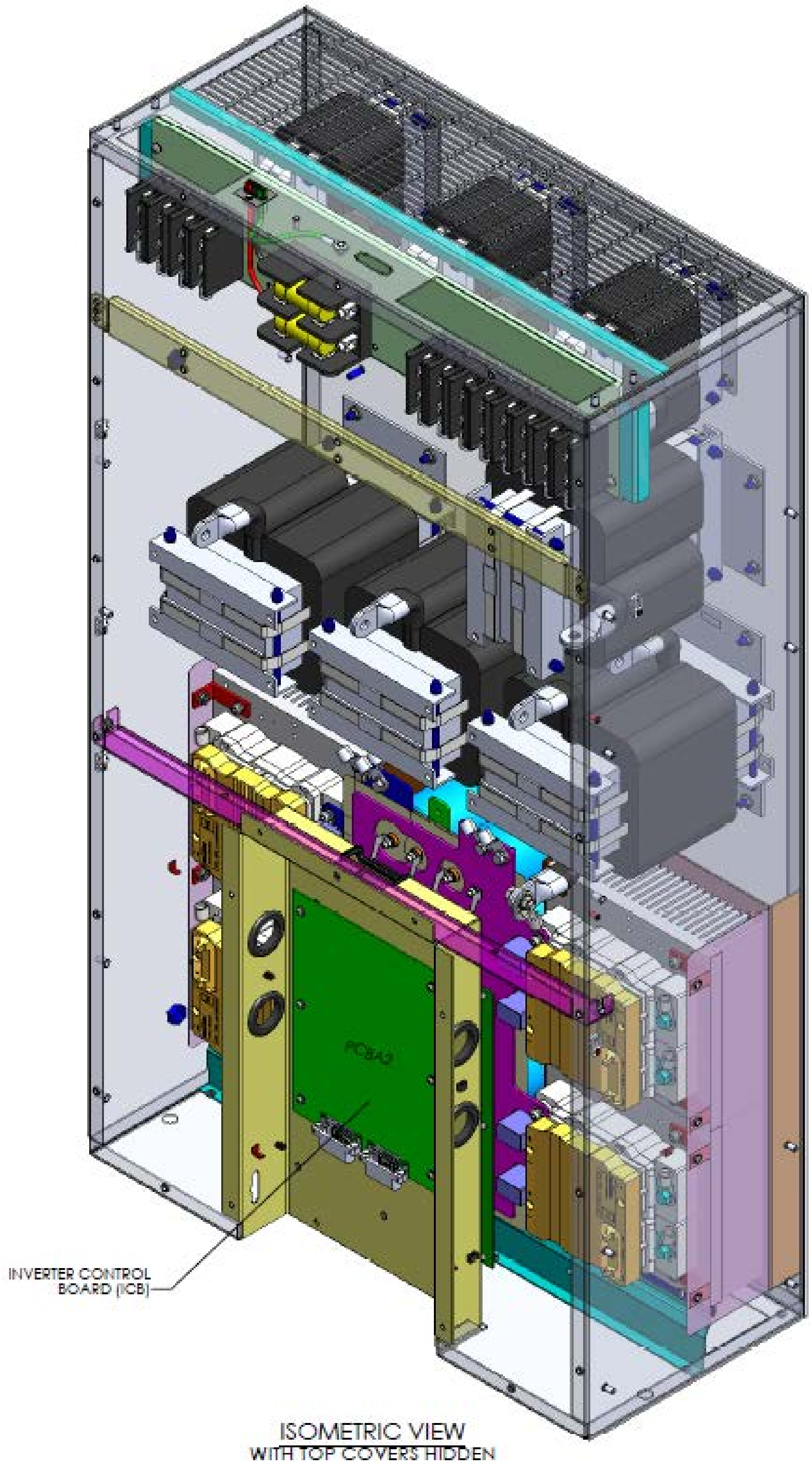

Figure 91: C370 400 A HCI LCM 3D Model (Isometric View)

6.7.2. Primary and Secondary Inductor Design

The 400 A, HCI electrical system design and the calculations of the requirements for the primary and secondary inductors for normal and short circuit conditions were completed as a part of the qualification. The design operating conditions were:

- 400 A inverter continuous output capacity (software limited)
- 25,000 A grid short circuit let through current maximum limited externally to the microturbine

The LCM main output nominal inductance value was determined to be 135 µH and the controller must maintain this inductance at rated maximum current (400 A_{RMS}) without saturation. A model of the C200 LCM PWM waveform and output filter was developed to predict the peak current flowing through the main output inductor. This model is shown in Figure 92.

The model incorporates the following operating conditions:

1.	PWM frequency:	15 kHz
2.	DC Bus Voltage:	760 V_{DC}
3.	Fundamental Load Current:	400 A_{RMS}
4.	Fundamental Load Current Frequency:	50 Hz
5.	Main Inductor Minimum Inductance Value (-7%):	125.6 µH
6.	Block Inductor Minimum Inductance Value (-7%):	31 µH

Components C2, C3, C4, C5, R2, R3, and L3 represent the filter components used in the LCM output filter. The LCM main inductor is identified as L1.

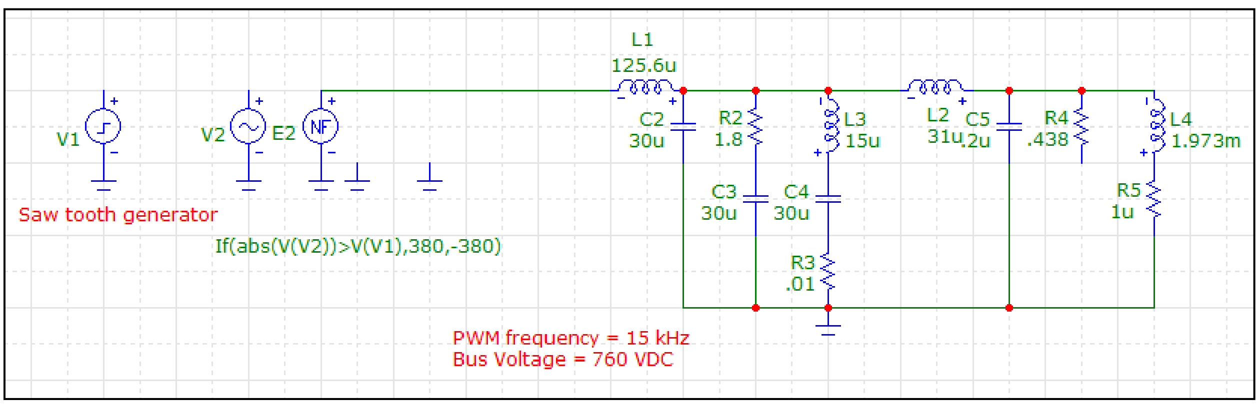

Figure 92: C370 LCM Simulation Model Schematic Diagram

While using the model to define the peak current in the main output inductor, it was discovered that the maximum peak instantaneous current in the main output inductor occurred a zero power factor. Item L4 represents this loading condition.

The main inductor simulation results are shown in Figure 93. The output current waveform at 100% load was predicted to be a peak instantaneous value of 610 A.

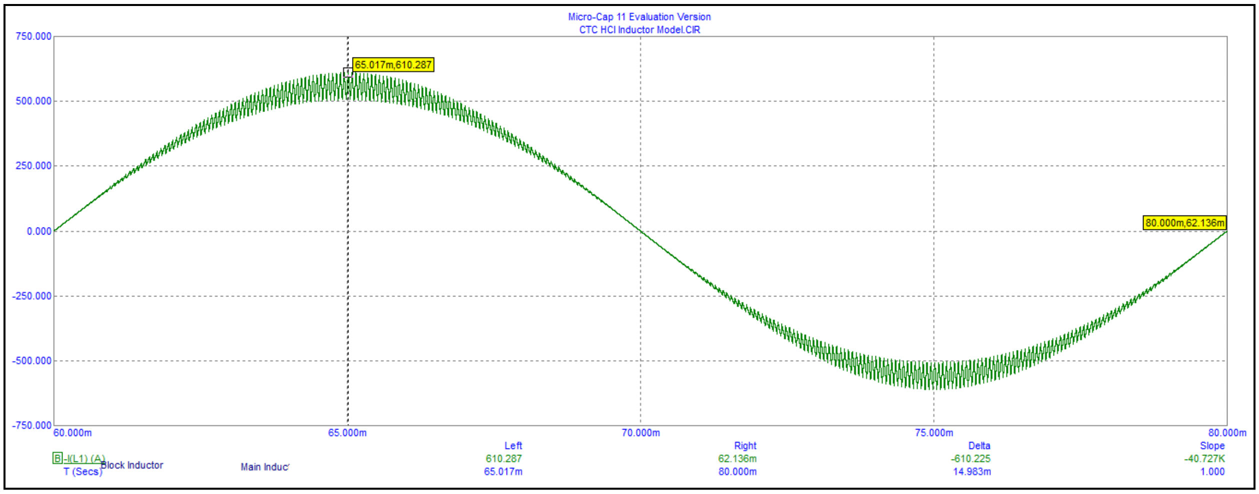

Figure 93: C370 LCM Main Output Inductor Waveform

The LCM block inductor nominal inductance value was determined to be 33 µH. The controller must maintain this inductance at rated current — 400 A_{RMS} — without saturation. The model shown in Figure 92 was also used to predict the peak instantaneous current in the LCM block inductors and is identified as L2 in the model. Due to the relatively low PWM ripple current in the block inductor, the load power factor did not influence the peak instantaneous current. The block inductor current waveform at 100% load — Figure 94 — was predicted to be a peak instantaneous current of 568 A.

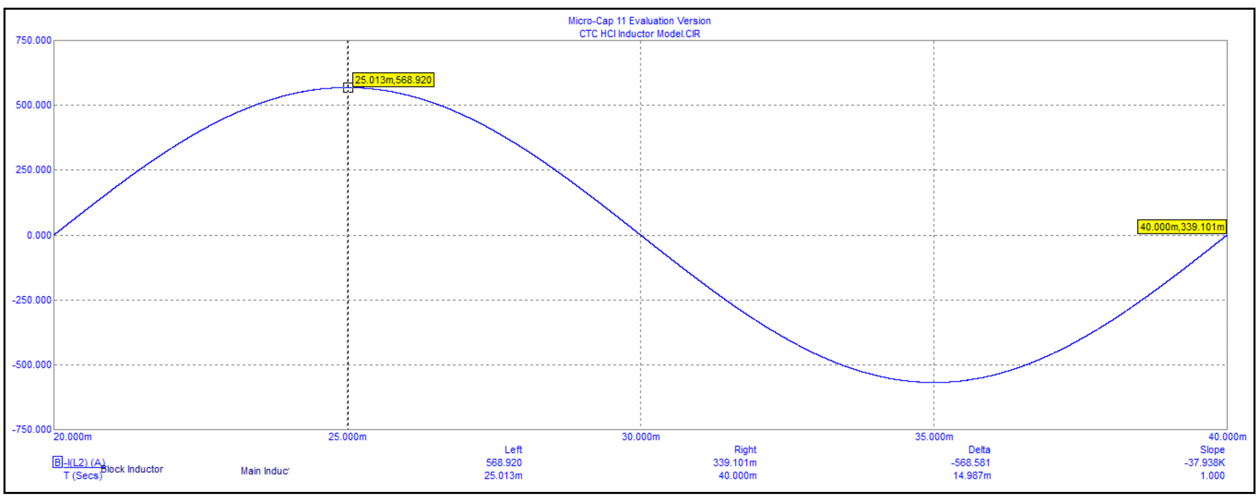

Figure 94: C370 LCM Block Inductor Waveform

Initial Samples of the inductors were procured and qualification testing was done to confirm that both the inductance and onset of saturation met the requirements. Results are shown in Table 31.

	Main Inductor	Block Inductor
Inductance Requirement (µH)	135 ±3%	33 ±1
Inductance Test Results (µH)	132.47	32.04
Saturation Current Requirement (A_{peak})	763 minimum	710 minimum
Saturation Current Test Results (A_{peak})	870	900
Qualification Results	Pass	Pass

Table 31: C370 LCM Main and Block Inductor Qualification Results

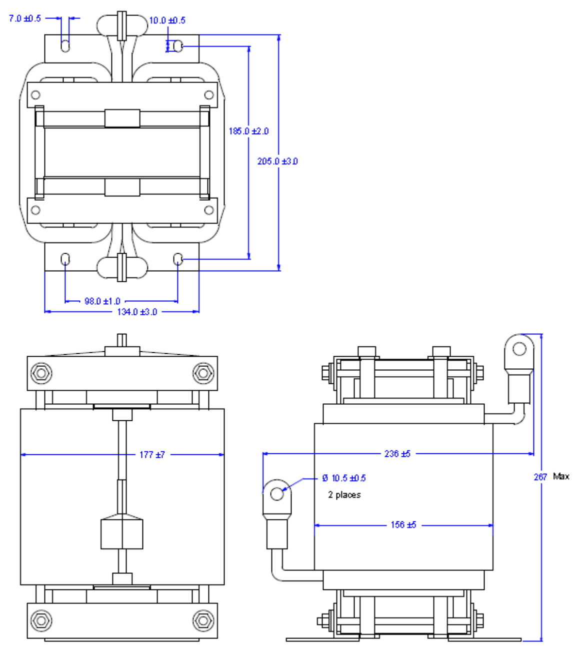

Inductor dimensions [in mm]

Figure 95: C370 LCM Main Inductor Drawing

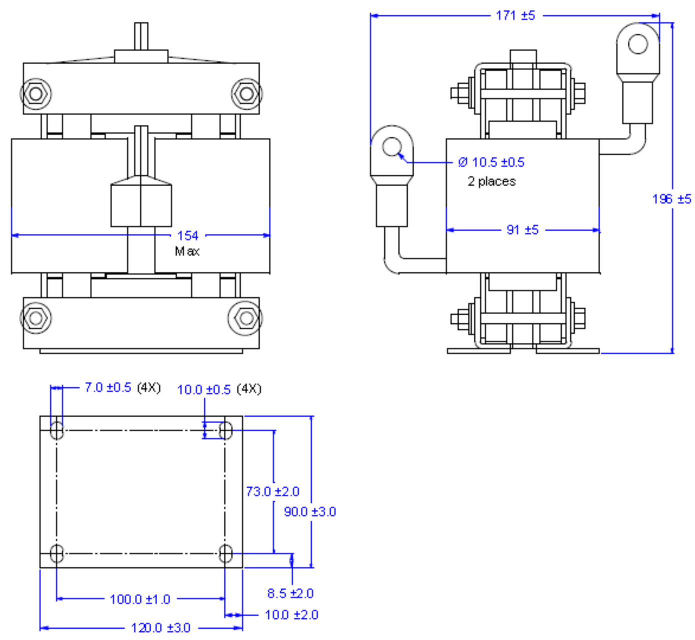

Inductor dimensions [in mm]

Figure 96: C370 LCM Block Inductor Drawing

6.7.3. Output Filter Design

The LCM output filter is designed to filter out the switching harmonics that are created by the LCM inverter bridge. The amount of filtering required is dictated by the allowed power frequency harmonics and inter-harmonics in some requirements. In particular, some VDE harmonics requirements for connections to the low voltage network are above the 40th harmonic. The requirement for the filter was to achieve the same level of filtering as the 300 A inverter filter but at the 400 A power level.

The design of the HCI LCM output filter for the C250/C370 product was approached using two simulation tools: PSIM and Matlab. This was the best approach since the switching frequency is the same in the new LCM as the current LCM. However, the inductances of the LCM main and block inductors are lower — 135 µH versus 165 µH for the main inductor and 33 µH versus 40 µH for the block inductor. Due to the decrease in the inductance of the main inductor, the ripple current through the main inductor — and consequently through the output filter — is increased from the old design. This necessitates obtaining components that can handle more current and more power.

Since the magnitude and phase response of the filter depends on the impedance of connected loads or grids, three cases were examined: infinite bus (zero impedance), base impedance (200 kW, 480 V_{AC} base), 0.01 pu impedance, and infinite impedance (open circuit / no-load). The difference in the magnitude and phase response between the present filter design and the new design was minimized under the constraint of the available component values. There are three main regions of interest in the magnitude response that were examined:

1) The first spike in the magnitude response — approximately 2 kHz
2) The region around the switching frequency — 7.5 kHz
3) Near the second harmonic of the switching frequency — 15 kHz

The magnitude and phase plots that follow are based upon the following values below. The reference designators are defined in Figure 97.

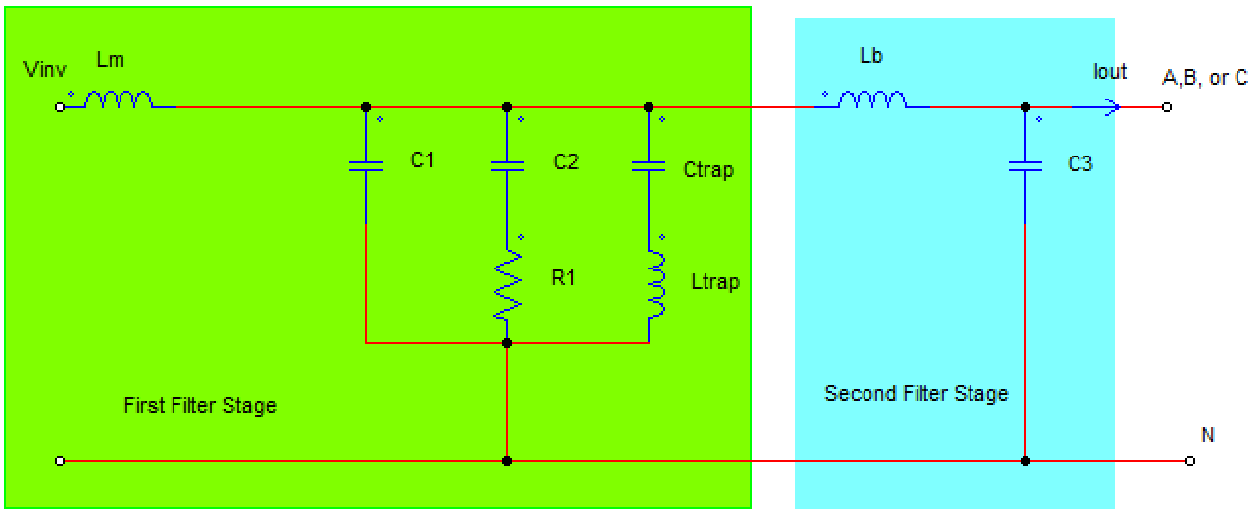

Figure 97: One Phase Leg of the C370 LCM Output Filter

C250/C370 400 A LCM circuit design parameters:

- Inductance of the Main LCM inductor (Lm): 135 µH ±7%
- Inductance of the Block LCM inductor (Lb): 33 µH ±5%
- Capacitance of C1, C2, and Ctrap: 30 µF ± 5%
- Resistance of R1: 1.8 Ω ± 5%
- Inductance of Ltrap: 15 µH ±5%
- Q factor of Ltrap: 39 ±10%
- Capacitance of C3: 0.2 µF (comprised of two 0.1 µF ±10% capacitors in parallel)

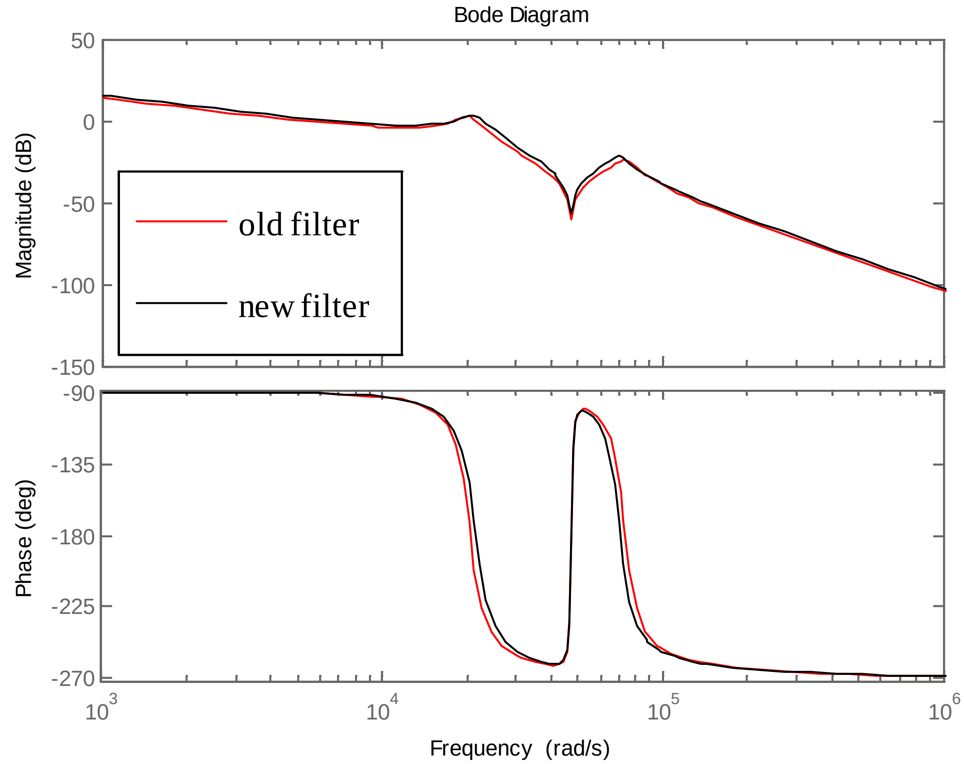

Figure 98: C370 LCM Output Filter Magnitude and Phase Response for Iout/Vinv

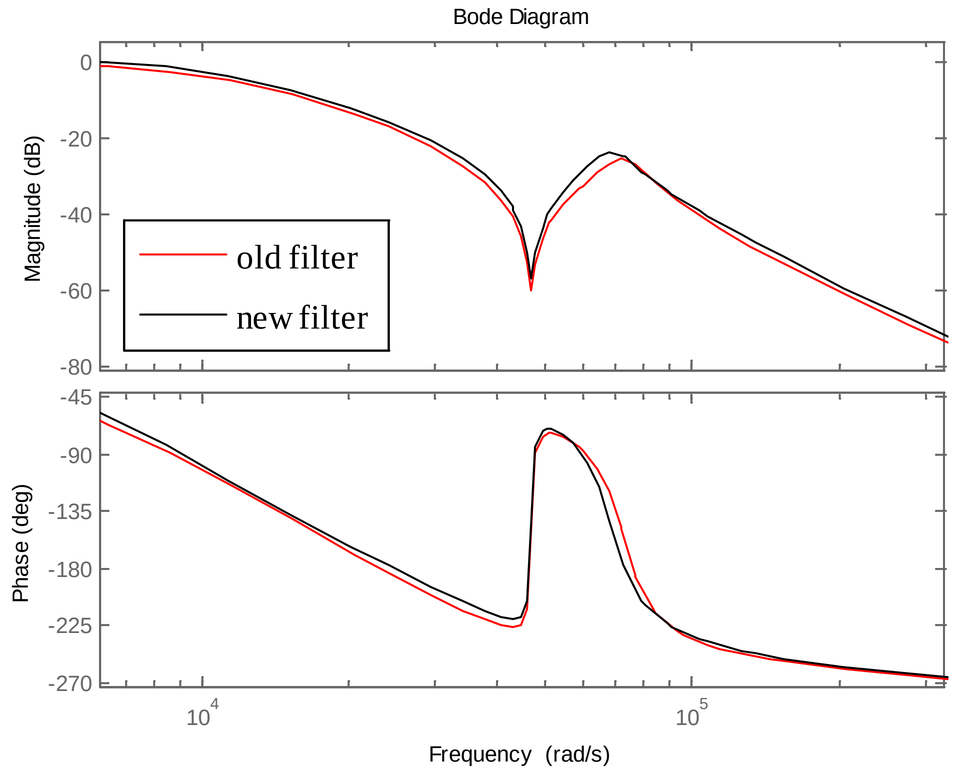

Figure 99: C370 LCM Output Filter Magnitude and Phase Response for VA/Vout

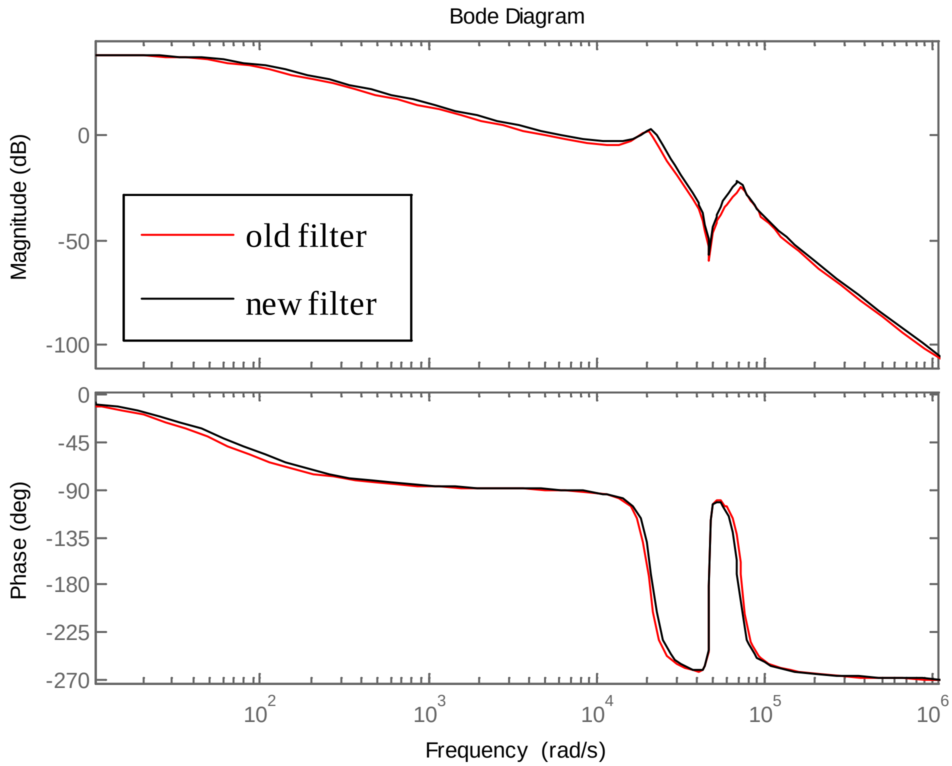

Figure 100: C370 LCM Output Filter Magnitude and Phase Response for Iout/Vinv for 0.01 pu.

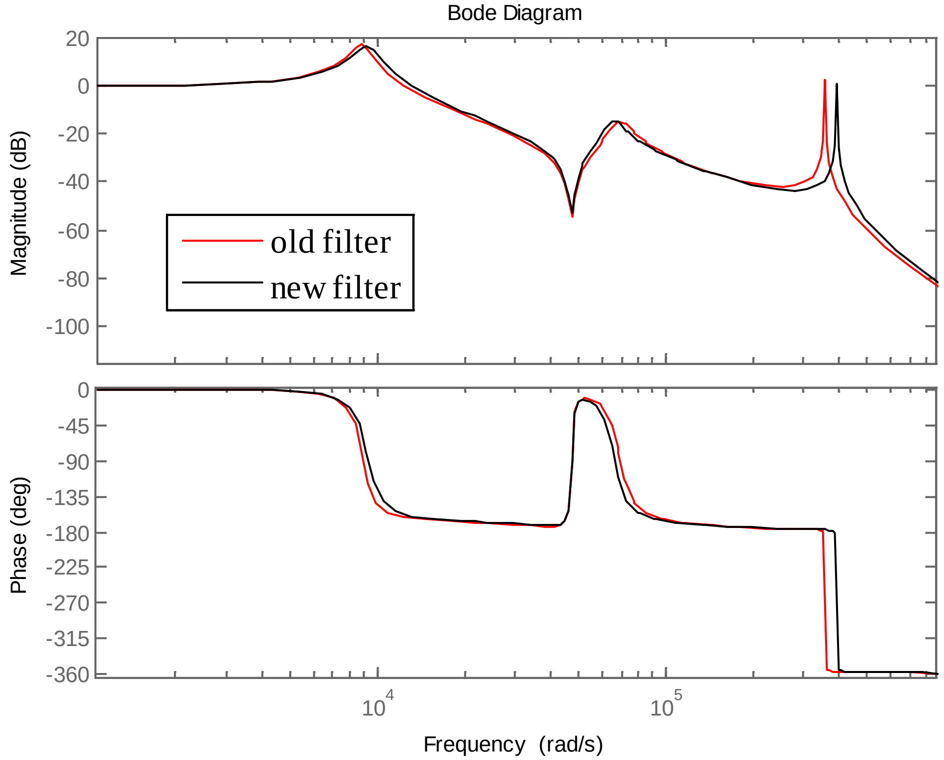

Figure 101: C370 LCM Output Filter Magnitude and Phase response for VA/Vout

As shown in Figure 98 through Figure 101, the magnitude response of the new filter follows the old filter within approximately 5 dB. There is some shifting of the filter frequencies, but this is expected. Note that the high Q value in Figure 101 is due to C3. The second stage filter is used to provide some high frequency filtering.

The LCM was modeled in PSIM in order to predict the current and power requirements of the filter components. In order to correctly predict the filter currents, the bus clamping scheme for the LCM IGBTs was implemented in the simulation. Additionally, the predictive current controllers are modeled and were manually tuned. This tuning allows the modeled inverter to be connected to a simulated grid. Since the purpose of this design activity was to estimate the filter currents — not to provide final controller gains — the tuning was not performed rigorously. The resultant system response is not overly oscillatory; therefore, it is deemed to be acceptable for these purposes.

The behavior of the filter was examined for the entire voltage range — 360 – 528 V_{AC} — and for the entire range of output power factors — 0.8 leading – 0.8 lagging. The effect of the output frequency was also examined for the entire range — 45 – 65 Hz. It was determined that the worst case occurred at maximum line frequency, i.e. 65 Hz. Since the switching ripple current through the main inductor — and through the output filter, as a result — is not strictly dependent on the output current, it is not necessary to sweep the entire output current range. This was confirmed with spot cases. However, the ripple current is dependent on the DC bus voltage. The worst case ripple occurs at maximum DC bus voltage. Due to the product requirement of providing 0.8 lagging power factor at 528 V_{AC}, the DC bus voltage must be increased. At the time of this design activity the new DC bus voltage was not finalized. It is likely that the final value will be in the range of 780 – 800 V_{DC}. For the purposes of this design, a DC bus of 800 V_{DC} was chosen in order to account for the potential worst case ripple current.

Through iterative simulation cases, the worst case ripple current occurs at the lowest line voltage — 360 V_{AC} — and at a load power factor of 0.8 leading. The results of this case are illustrated in Figure 102.

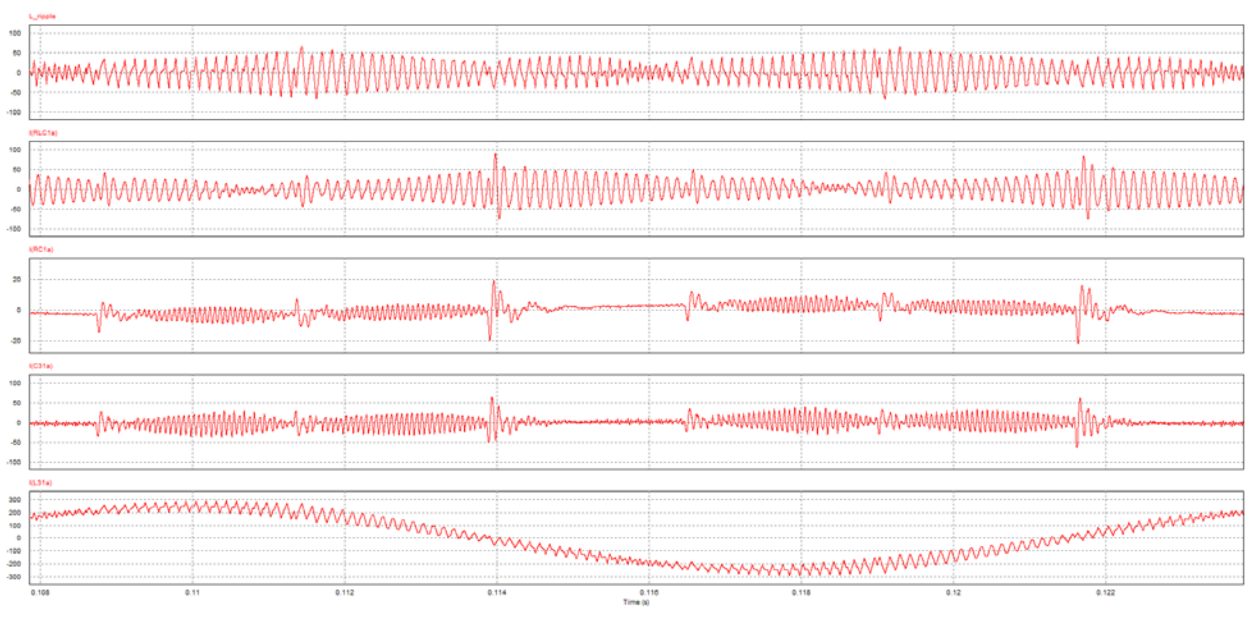

Figure 102: C370 LCM Output Filter Currents

The current through the trap circuit — Ltrap and Ctrap — was larger than through other branches of the filter. For this case the current is 25.3 A_{RMS}. In comparison, the current through the RC branch — R1 C2 — is 4.4 A_{RMS}, whereas the current through the C branch — C1 — is 14.0 A_{RMS}. The total ripple current through the main inductor is 25.7 A_{RMS}. The harmonic spectrum of the currents is different through each branch of the filter, as seen in Figure 103. This comes as no surprise, given the magnitude responses of each branch taken separately. In order to specify the current ratings of the components, it is important to realize that the vast majority of the current for the trap branch is in the neighborhood of 7.5 kHz, whereas the current is more spread out in frequency for the other branches. The selection of a single capacitor for C1, C2, and Ctrap does not present a significant challenge, since the ESR of capacitors decreases with increased frequency. Since the current through Ctrap is considerably larger in magnitude — while also at a lower frequencies — than C1 and C2, it is clear that the current through Ctrap presents the worst case requirement for the selection of C1, C2, and Ctrap. The selection of R1 is based solely on the RMS of the current flowing through the resistor, since a low inductance resistor will be selected. The resistor will likely be chosen from the same series of resistors as the resistor in the current filter design, although the power rating will be increased to 60 W from the 45 W used in the present design. The plots in Figure 102 and Figure 103 are defined from the top to the bottom as listed here:

1. L_ripple = main inductor ripple current
2. I(RLC1a) = trap branch current
3. I(RC1a) = R1 C2 branch current
4. I(C31a) = C1 branch current
5. I(L31a) = total main inductor current

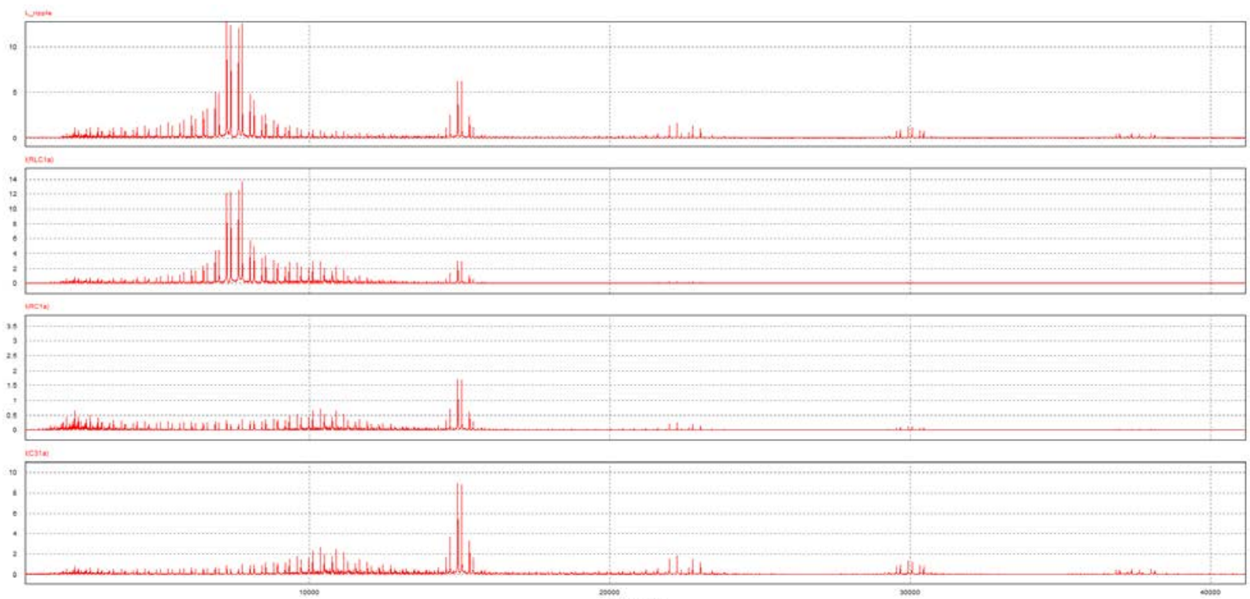

Figure 103: C370 LCM Harmonic Spectrum of Output Filter Branch Currents

The final components that met the design values were selected and an initial test filter was built. Figure 104 shows the 3D CAD design of the final component. Testing was done to qualify the filter to the requirements and the results are shown in Table 32. Test results of the new filter showed high design margin relative to the design targets and was determined ready to be used for full LCM qualification.

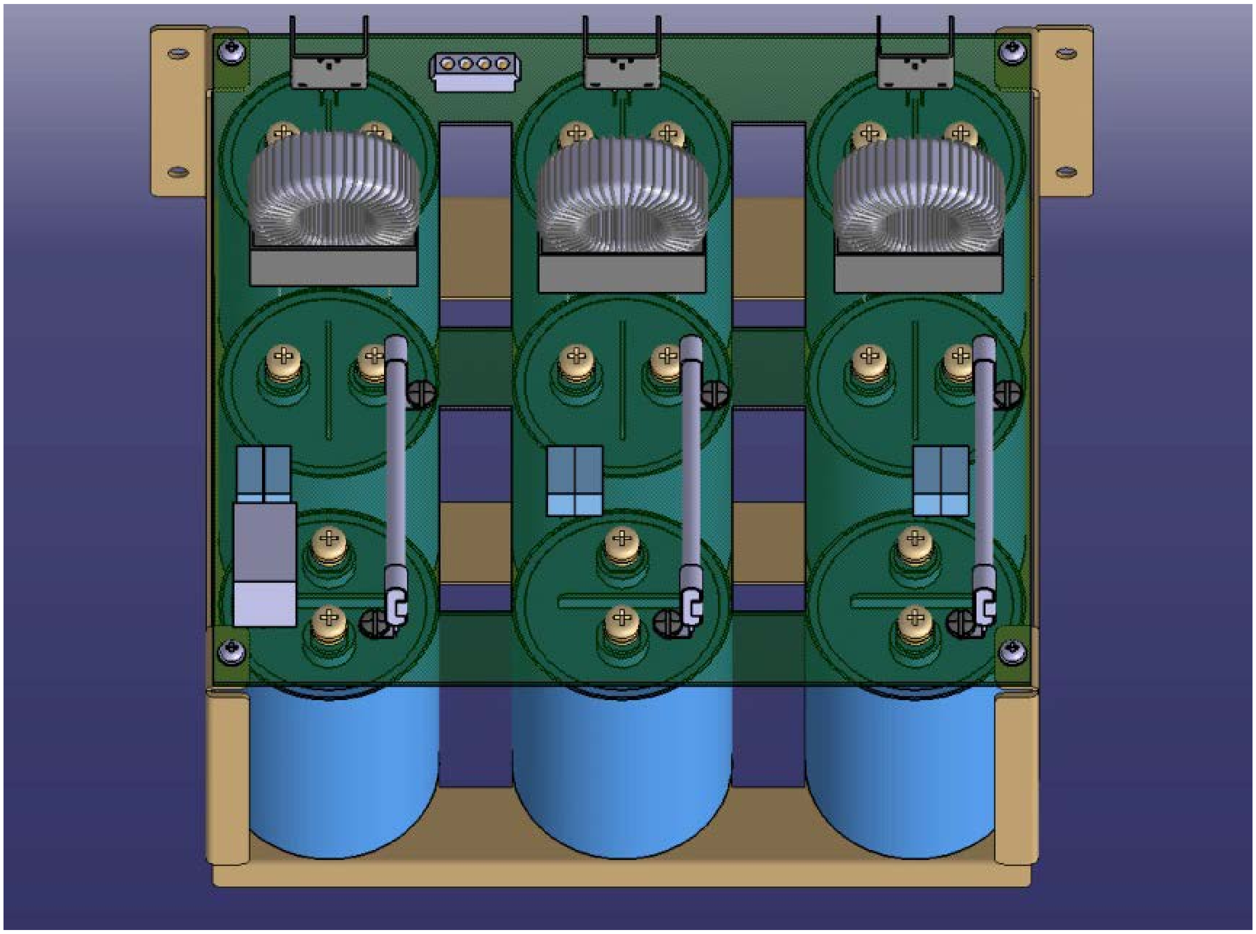

Figure 104: 3D Model of C370 LCM Output Filter Design

Test Parameter	Requirement	Test Results
Open Circuit Gain	± 5dB of existing filter	0 to +4 dB over most of the range*
Short Circuit Gain	± 5dB of existing filter	0 to - 4 dB over most of the range*
Thermal component test (resistor)	230 °C	91 °C
Thermal component test (toroid)	65 °C	40.5 °C
Thermal component test (heatsink)	230 °C	49.7 °C
Thermal component test (Phase A capacitor)	85 °C	35.8 °C
Thermal component test (Phase C capacitor)	85 °C	34.9 °C
THD Phase A (at 65 kW, 415 A)	<5% (per UL1741)	1.77%
THD Phase B (at 65 kW, 415 A)	<5% (per UL1741)	2.43%
THD Phase C (at 65 kW, 415 A)	<5% (per UL1741)	0.57%

* Measurement test error was determined to be the cause of the excursions at certain frequencies above/below the limit

Table 32: C370 LCM Inverter Qualification Results

6.7.4. IGBT Selection Analysis

The IGBT module chosen for this design was the Semikron 1213GB123-2DL. This was chosen for the similarity of electrical connection interface to the IGBT currently used in the production C200 LCM. This minimized the changes needed to the inverter control board and software for the 400 A system. As with the old IGBT module, the internal fault current limiting function protects the IGBT chips from fault currents. The inverse parallel connected diodes are vulnerable, because they are passive and incapable of limiting fault current. The Semikron 1213GB123-2DL data sheet — see Figure 105 — lists the I^2t withstand of the inverse parallel connected diodes as 238 kA^2s. The required high speed semiconductor fuse for grid fault current protection determined through calculations was a Bussmann 170M4014 — 500 A_{RMS}, 170,000 A^2s clearing I^2t.

SKiiP 1213 GB123-2DL V3

SKiiP® 3

2-pack-integrated intelligent Power System

SKIIP 1213 GB123-2DL V3

Features

- SKiiP technology inside
- Trench IGBTs
- CAL HD diode technology
- Integrated current sensor
- Integrated temperature sensor
- Integrated heat sink
- UL recognized File no. E63532

Typical Applications*

- Renewable energies
- Traction
- Elevators
- Industrial drives

Footnotes

[1] With assembly of suitable MKP capacitor per terminal

Absolute Maximum Ratings			T_s = 25°C unless otherwise specified	
Symbol	**Conditions**		**Values**	**Unit**
System				
V_{CC}[1]	Operating DC link voltage		900	V
V_{isol}	DC, t = 1 s, main terminals to heat sink		4300	V
$I_{t(RMS)}$	per AC terminal, $T_{terminal}$ <115°C		400	A
I_{FSM}	T_j = 125 °C, t_p = 10 ms, sin 180°		6900	A
I^2t	T_j = 150 °C, t_p = 10 ms, diode		238	kA^2s
f_{out}	fundamental output frequency		1	kHz
T_{stg}	storage temperature		-40 ... 85	°C
IGBT				
V_{CES}	T_j = 25 °C		1200	V
I_C	T_j = 150 °C	T_s = 25 °C	1145	A
		T_s = 70 °C	882	A
I_{Cnom}			1200	A
T_j	junction temperature		-40 ... 150	°C
Diode				
V_{RRM}	T_j = 25 °C		1200	V
I_F	T_j = 150 °C	T_s = 25 °C	925	A
		T_s = 70 °C	700	A
I_{Fnom}			930	A
T_j	junction temperature		-40 ... 150	°C
Driver				
V_s	power supply		13 ... 30	V
V_{iH}	input signal voltage (high)		V_s + 0.3	V
V_{isolPD}	QPD <= 10pC, PRIM to POWER		1170	V
dv/dt	secondary to primary side		75	kV/µs
f_{sw}	switching frequency		15	kHz

Characteristics				T_s = 25°C unless otherwise specified		
Symbol	**Conditions**		**min.**	**typ.**	**max.**	**Unit**
IGBT						
$V_{CE(sat)}$	I_C = 600 A at terminal	T_j = 25 °C		1.7	2.1	V
		T_j = 125 °C		1.9		V
V_{CE0}		T_j = 25 °C		0.90	1.10	V
		T_j = 125 °C		0.80	1.00	V
r_{CE}	at terminal	T_j = 25 °C		1.3	1.7	mΩ
		T_j = 125 °C		1.8	2.2	mΩ
$E_{on} + E_{off}$	I_C = 600 A, T_j = 125 °C	V_{CC} = 600 V		221		mJ
		V_{CC} = 900 V		390		mJ
$R_{th(j-s)}$	per IGBT switch				0.03	K/W
$R_{th(j-r)}$	per IGBT switch				0.024	K/W

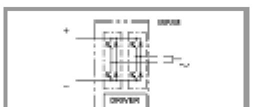

S23

© by SEMIKRON Rev. 2 – 06.10.2012 1

Figure 105: C370 LCM SKiiP 3 IGBT Datasheet

6.7.5. Control Board Design

Control board changes were minimal and only included re-scaling the software to measure the larger amperages for the current sensors that were selected. Board changes can be merged into the existing 300 A design at any time to support a single controller that was compatible with both 300 and 400 A hardware.

6.7.6. Inverter Validation Test Results

The C250/C370 400 A LCM assembly went through full qualification in a C200 microturbine system modified to run at 250 kVA over the 360 – 528 V range and 50 – 60 Hz frequency range. Figure 106 shows an example of a test run data plot.

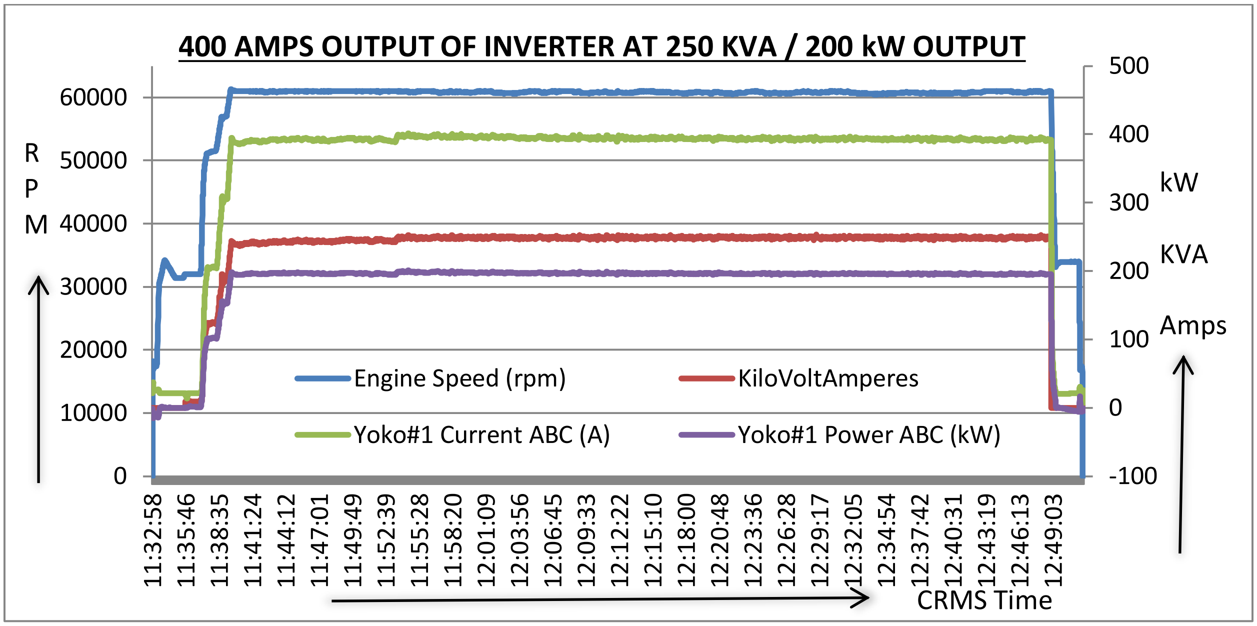

Figure 106: 400 A /C370 LCM Inverter Controller Test Run

The C250/C370 HCI running in a C200 package successfully operated at rated power of 250 kVA and 400 A output current with appropriate cooling for electronics at ambient temperature conditions of 61 °F – 122 °F applying derate at elevated temperatures. Figure 107 shows the qualification unit with Lexan see-through covers. These covers allowed thermal imaging of internal component temperatures while in operation. This configuration required the use of a new system cooling fan with 23% more cooling airflow.

The conditions of operation below the ambient of 61 °F will only be better as the cooling effect will be increased while the electrical contribution to thermal stress will be limited to full capacity already reached at 61 °F. The VFD and fan used for electronics cooling will meet the worst case operating conditions of 360 V_{AC} and 0.8 power factor at 55 Hz operation. With additional intelligence in the fan operation for variable speed operation, the parasitic losses can be reduced for operating conditions where the cooling requirement can be met at lower speeds — e.g. lower power draw by fan. Also, conditions of ambient temperature close to freezing may require reduced cooling flows to avoid freezing of some components — batteries, for example — while maintaining the IGBT temperatures within acceptable range.

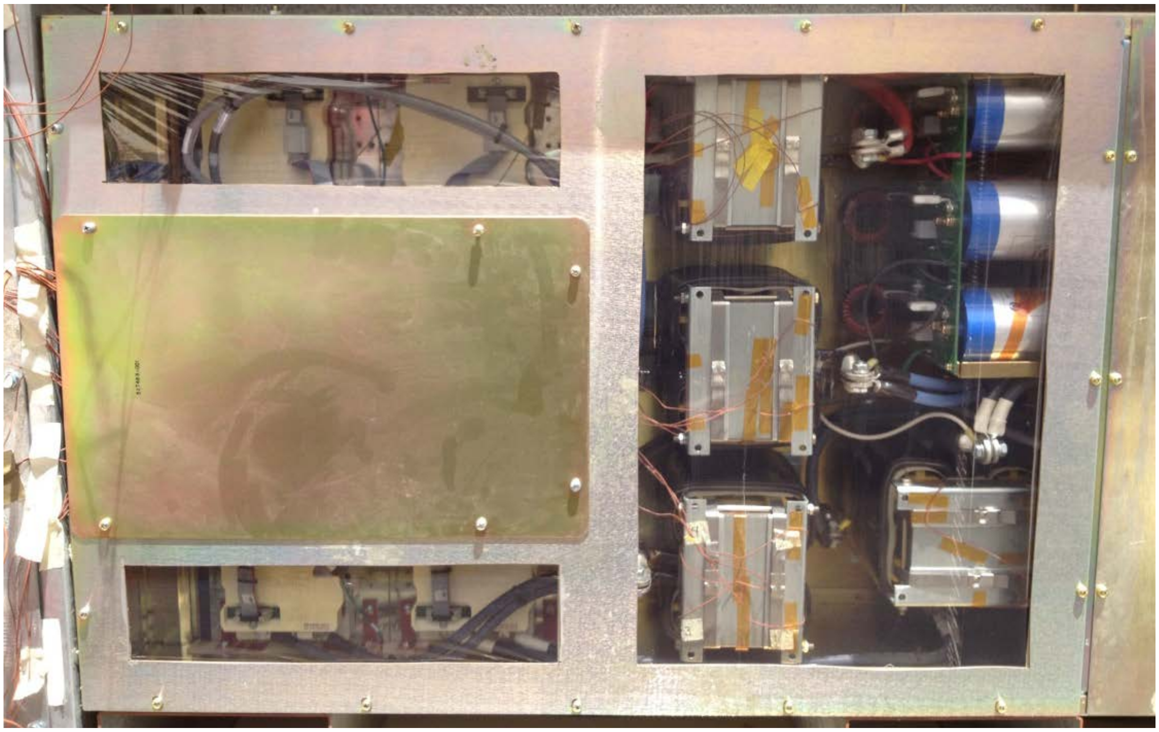

Figure 107: C370 LCM Inverter Qualification Test Unit with Lexan See-Through Covers

6.8. C370 Heat Recovery System Design

The heat recovery system was designed to facilitate the design target of greater than or equal to 85% overall efficiency by capturing as much heat as possible in a liquid. Figure 108 illustrates the thermal system design layout.

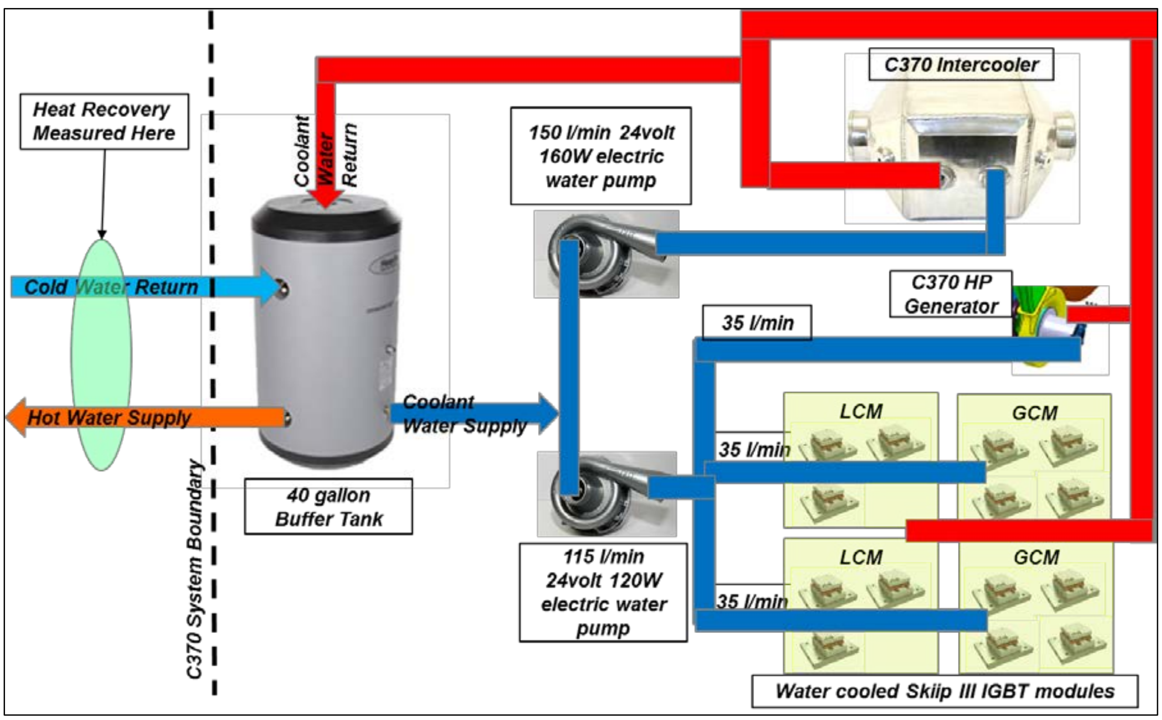

Figure 108: C370 Water Recovery System

In addition to the components shown in Figure 108, an air-to-water heat exchanger would be added on the engine exhaust. Detailed analysis of the impact of each component to the overall thermal efficiency is in the sections below.

6.8.1. Hot Water Recovery System Analysis

Results of the calculated thermal recovery for each component are shown in table 5 below. This analysis assumes 92% effectiveness from the Exhaust heat exchanger and the Intercooler. It is also based on the turbine engine cycle with a TIT of 2030 °F that produces 369 kW of electrical power at the exit of the system.

Component	Heat Recovered	% System Efficiency
Water Cooled IGBTs	20kW	2.2%
High Pressure Spool Generator	5kW	0.6%
Intercooler	146kW	16.1%
Exhaust Heat Exchanger (not shown in figure 10)	213kW	23.4%
Thermal Energy Totals	384 kW	42.3%
Electrical Energy Recovered (@2030 TIT)	369 kW	40.6%
Total Electrical + Thermal Energy Recovered	753 kW	83.9%

Table 33: Thermal Recovery Analysis

With this hot water recovery configuration, the analysis shows that we are 1.1% below the target, but the variation from the target is small relative to the accuracy of the prediction. Given the accuracy of this prediction, all we can say at this point is that we are close at the target value.

6.8.2. Electric Water Pump Selection

The system employs two (2) electric water pumps, one (1) specifically for the intercooler and one (1) for the balance of engine and electronics cooling components. If, at some point, the exhaust heat recovery module were to be included into the assembly, then a third 24 V electric water pump of the EWP brand shown in Figure 109 would be required.

Electric Water Pump - Alloy *EWP®150 150 litres/min*

The world's first universal-fit, automotive Electric Water Pump goers one better with the EWP®150. Suitable for all makes and models – will excel on large six-cylinder engines, V8 engines, heavy-duty 4WDs and most engines over 400HP. Can be a practical alternative to the mechanical belt-driven pump or fitted as an auxiliary pump.

EWP®150

Technical specifications

	Part #8060 - 12 volt pump	Part #8061 - 24 volt pump
Operating voltage	3V DC to 15V DC	10V DC to 27V DC
Maximum current	10A	5.5A @ 24V
Flow rate (max)	150 L/min (39.63 US gal/min) @ 13V DC	150 L/min (39.63 US gal/min) @ 24V DC
Operating temp.	-40° to 130°C (-40° to 266°F)	-40° to 130°C (-40° to 266°F)
Pump design	Clockwise centrifugal with volute chamber	Clockwise centrifugal with volute chamber
Pump weight	1,170 grams (2.6 lb)	1,170 grams (2.6 lb)
Pump material	Aluminium	Aluminium
Burst pressure	500 kPa (72.5 psi)	500 kPa (72.5 psi)
Seal	Ceramic face seal	Ceramic face seal
Fits hose sizes	38mm to 51mm (1½" to 2") Internal thread - inlet: AN-16 - outlet: AN-16	38mm to 51mm (1½" to 2") Internal thread - inlet: AN-16 - outlet: AN-16

Options (both models)

Part #	Description	Qty
8505	90° Hose adaptor	1
1025	Alloy adaptor AN-16 *(2 required)*	1

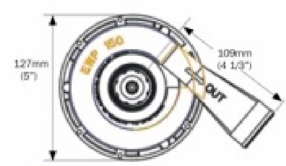

Kit contents

Part #	Description	Qty	#8060 (12V)	#8061 (24V)
8160	EWP®150 Alloy 12V Pump	1	✓	
8161	EWP®150 Alloy 24V Pump	1		✓
8515	Wiring harness	1	✓	✓
8510	Sleeve 3mm rubber adaptors	2	✓	✓
8512	Hose clamps	2	✓	✓
8525	Assorted hardware bag - includes 12V relay #0533	1	✓	
8527	Assorted hardware bag - includes 24V relay #0534	1		✓

Dimensions

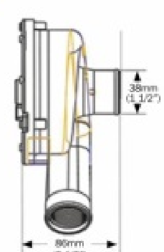

The EWP® is a recirculating pump which is ideal for a 'closed system' similar to an automotive cooling system; it is not 'self-priming'.

Figure 109: C370 Electric Water Pump Component Selection

6.8.3. Thermal Storage Tank Selection

A hydronic buffer tank is necessary to maintain thermal cooling stability in the C370 system. Without this tank, the engine and electronics overheat due to rapid thermal changes in water temperature. The tank size needed was initially determined to be 40 gallons, but an 80 gallon unit is available and could be used if the exhaust heat exchanger water were included in the system. The Heat-Flow Products selection is shown in Figure 110.

Figure 110: C370 Hydronic Water Buffer Tank Component Selection

6.8.4. Water-Cooled Power Electronic Module Analysis and Selection

Semikron makes a 400 A IGBT in a water-cooled package. Inclusion of the water-cooled modules shown in Figure 111 would be a bolt-in replacement of the 400 A air-cooled electronics designed to support the C250/C370 inverter and generator power levels.

SKiiP 1213 GB123-2DW V3

SKiiP® 3

2-pack-integrated intelligent Power System

SKiiP 1213 GB123-2DW V3

Features

- SKiiP technology inside
- Trench IGBTs
- CAL HD diode technology
- Integrated current sensor
- Integrated temperature sensor
- Integrated heat sink
- UL recognized File no. E63532

Typical Applications*

- Renewable energies
- Traction
- Elevators
- Industrial drives

Footnotes

[1] With assembly of suitable MKP capacitor per terminal

Absolute Maximum Ratings			T_s = 25°C unless otherwise specified	
Symbol	**Conditions**		**Values**	**Unit**
System				
V_{CC} [1]	Operating DC link voltage		900	V
V_{isol}	DC, t = 1 s, main terminals to heat sink		4300	V
$I_{t(RMS)}$	per AC terminal, $T_{terminal}$ <115°C		400	A
I_{FSM}	T_j = 150 °C, t_p = 10 ms, sin 180°		6900	A
I^2t	T_j = 150 °C, t_p = 10 ms, diode		238	kA²s
f_{out}	fundamental output frequency		1	kHz
T_{stg}	storage temperature		-40 ... 85	°C
IGBT				
V_{CES}	T_j = 25 °C		1200	V
I_C	T_j = 150 °C	T_s = 25 °C	1145	A
		T_s = 70 °C	882	A
I_{Cnom}			1200	A
T_j	junction temperature		-40 ... 150	°C
Diode				
V_{RRM}	T_j = 25 °C		1200	V
I_F	T_j = 150 °C	T_s = 25 °C	925	A
		T_s = 70 °C	700	A
I_{Fnom}			930	A
T_j	junction temperature		-40 ... 150	°C
Driver				
V_s	power supply		13 ... 30	V
V_{iH}	input signal voltage (high)		15 + 0.3	V
V_{isolPD}	QPD <= 10pC, PRIM to POWER		1170	V
dv/dt	secondary to primary side		75	kV/µs
f_{sw}	switching frequency		15	kHz

Characteristics					T_s = 25°C unless otherwise specified	
Symbol	**Conditions**		**min.**	**typ.**	**max.**	**Unit**
IGBT						
$V_{CE(sat)}$	I_C = 600 A at terminal	T_j = 25 °C		1.7	2.1	V
		T_j = 125 °C		1.9		V
V_{CE0}		T_j = 25 °C		0.90	1.10	V
		T_j = 125 °C		0.80	1.00	V
r_{CE}	at terminal	T_j = 25 °C		1.3	1.7	mΩ
		T_j = 125 °C		1.8	2.2	mΩ
$E_{on} + E_{off}$	I_C = 600 A T_j = 125 °C	V_{CC} = 600 V		221		mJ
		V_{CC} = 900 V		390		mJ
$R_{th(j-s)}$	per IGBT switch				0.03	K/W
$R_{th(j-r)}$	per IGBT switch				0.0425	K/W

Figure 111: C370 Inverter Semikron Water-Cooled IGBT Specification Sheet

6.9. C370 Software and Controls Design

6.9.1. Engine Control Management Analysis

The development of new system controller code will be required to control and effectively operate the C370 twin shaft turbine generator system. The interaction of coupled twin shafts with two (2) generators and two (2) GCMs presents control requirements that are challenging, but manageable using modern software control techniques and hardware processing capabilities. Capstone Turbine will develop new control hardware architectures to support the demanding communications and computational requirements of the C370 control system.

The C370 turbo machinery is a very complex system and will take some time to model accurately and completely. C370 control code development will require that Capstone expand its control code simulation and modeling capabilities as code development must start well before engine hardware will be available to use for algorithm development and testing.

Consider Figure 112. High-pressure shaft combustion requires compressed air from the low-pressure compressor and intercooler. Power for the low-pressure compressor is provided by hot gas from the high-pressure combustor and turbine exhaust. Changes to the high-pressure system affect the low-pressure system, which in turn, affect the high-pressure system. Controlling such an interdependent system is challenging.

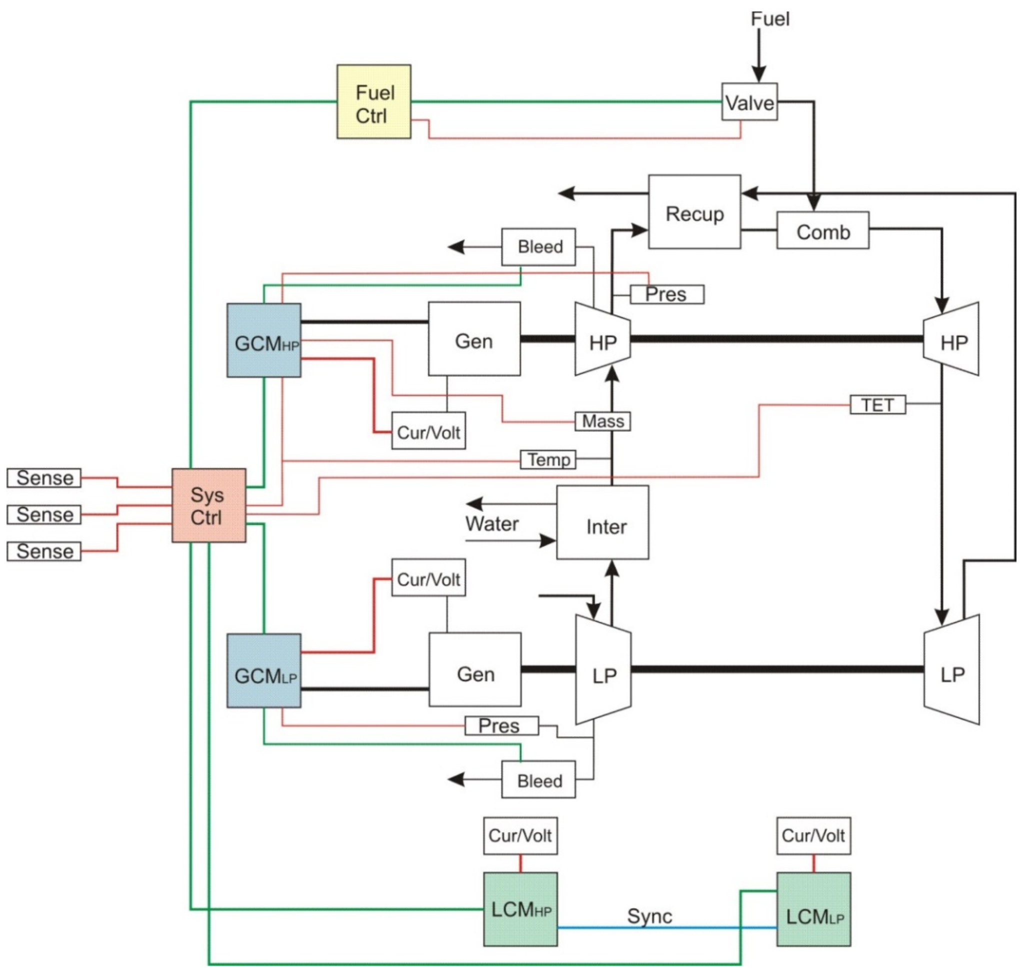

Figure 112: C370 System and Control Model Overview

Overview of Code Development Process

Control specifications were derived from the C370 systems model and informed by the experience gained from the control systems of Capstone Turbine legacy products. Based on this information, a control architecture structure was designed to implement the model. The control architecture is a distributed and networked processing system, incorporating over five (5) high-speed processors. The control system includes a master processor — the system controller — that performs overall control functions and coordinates the subordinate processors. This is similar to control architectures used on current Capstone Turbine products, but the C370 subordinate processors will likely have to have a high-speed communications channel separate from the system controller communication bus.

Control Model Development Overview

Control algorithms were prototyped first in “model form” as basic algebraic equations. These equations were developed in a modeling and simulation language designed to implement mathematics models and — to some extent — control models. These modeling tools — Simulink in this case — offer high-level algebraic tools to support complex algorithm development. These tools are not necessarily available in standard programming languages. In many cases, these modeling programs can export “example C code” that can be used as a starting point for program code development. This process is shown graphically in Figure 113.

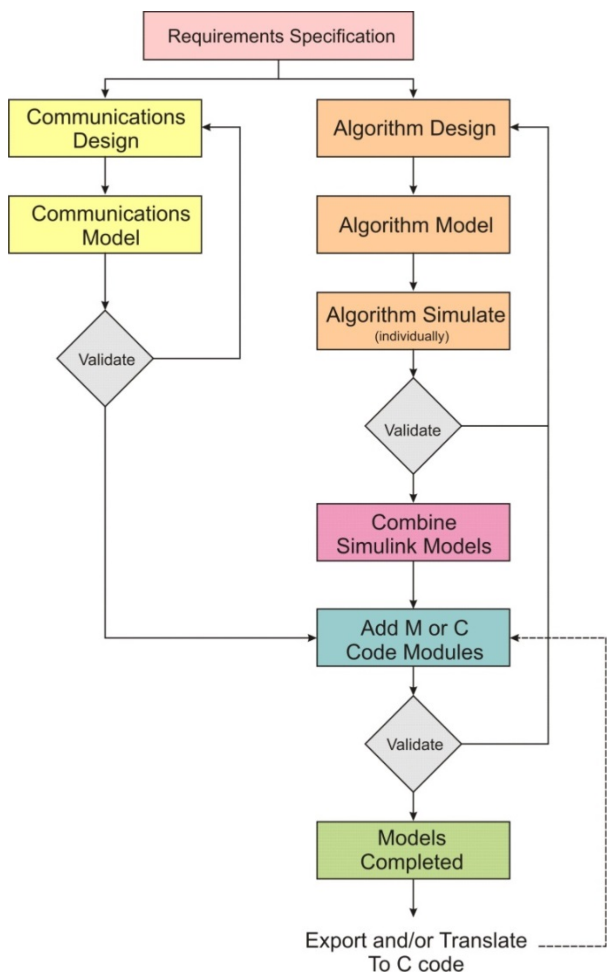

Figure 113: C370 Model Development Workflow

Model Hierarchy and Nomenclature

Control algorithm models will ultimately be translated into C code that runs on controller hardware. This will include (1) system controller code, (2) two copies of generator controller code, (3) two copies of inverter controller code, (4) fuel controller code, and (5) battery controller code, if necessary. Initially, these high-level control code modules can be run against an engine model simulation that allows controller code models to be tested in closed form with an engine model.

6.9.2. Thermal Water System Control Analysis

Water temperature regulation will be accomplished with thermal sensor feedback which will be used to regulate the flow of the variable speed electric water pumps. With this controls approach, the critical engine performance temperatures can be maintained even while the external water heat recovery systems thermal load varies. This is critical to maintain engine life and high overall system efficiency at partial load conditions.

6.9.3. Software Module Architecture Design

Control Processor Code Development

Following algorithm design, model development, and testing as described above, the exported C code from the simulation tool must be translated into operational C code, i.e. the generic exported C code must be targeted and built to execute on particular processor hardware. Most importantly, it must be connected to specific input and output hardware interfaces designed to communicate with the turbine hardware. This is done using the software development environment associated with the processor system incorporated on the controller boards.

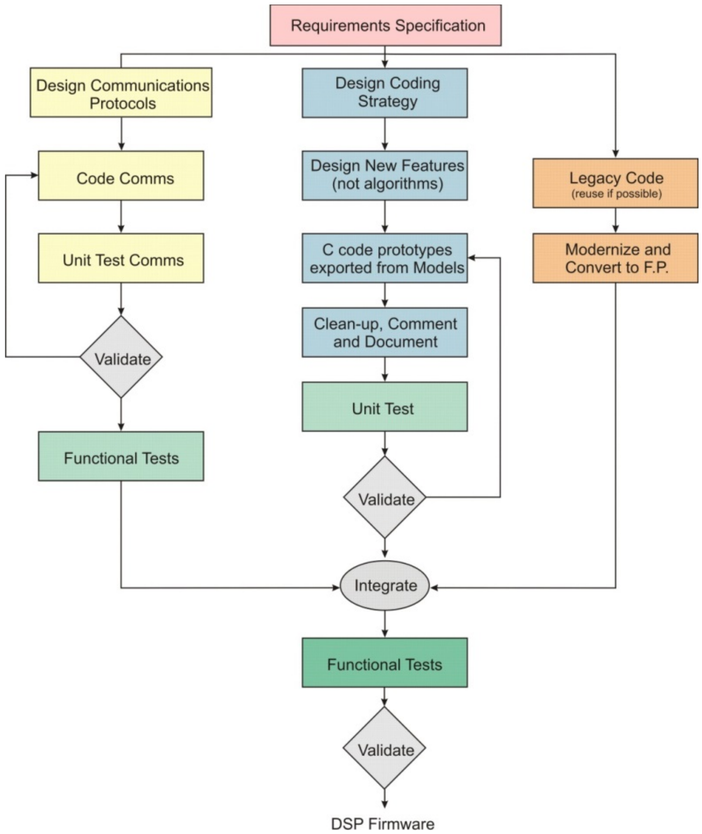

Figure 114: C370 Software Code Development Workflow

Communications Infrastructure Code Overview

A simplified view of C370 controller communications is shown in Figure 115. The uniqueness of the C370 topology is that the system contains two GCMs — each having its own inverter control board (ICB) — and two LCMs — one ICB per LCM. The system will have one fuel controller and fuel control valve feeding the high-pressure turbine combustor. The primary goal of the communications development task for the C370 controller software development effort is to implement the communications protocols necessary to support communications across this topology.

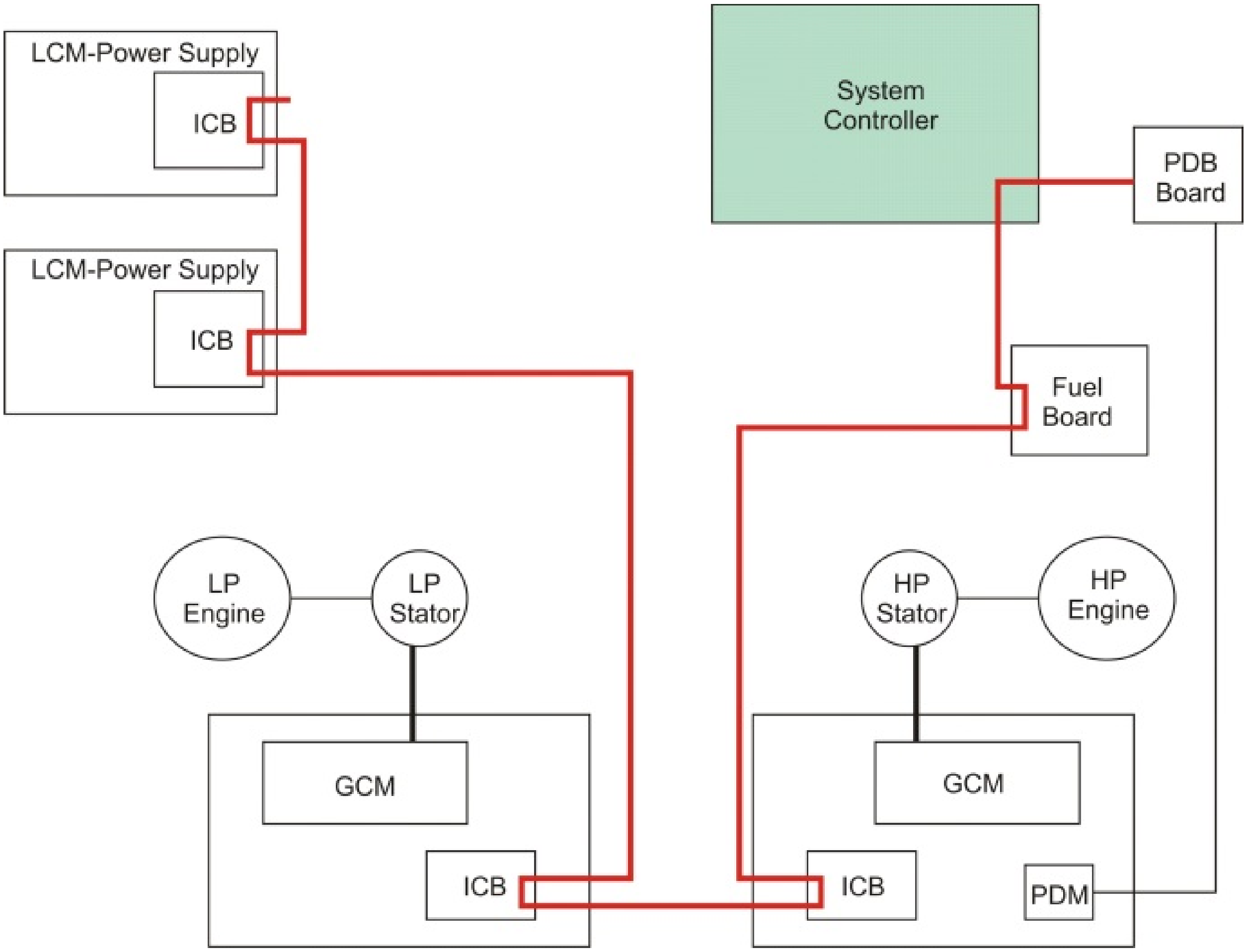

Figure 115: C370 Simplified Communications Topology

Standard Capstone Turbine communications architecture based on RS-485 serial signaling — the CapComm bus — is shown as the red line in Figure 115. Though it is possible that the CapComm bus will support the C370, it is unlikely that it can support the communications messaging bandwidth that will be needed to control the C370 system. A more modern approach — shown in Figure 116 — will support the C370 communications needs.

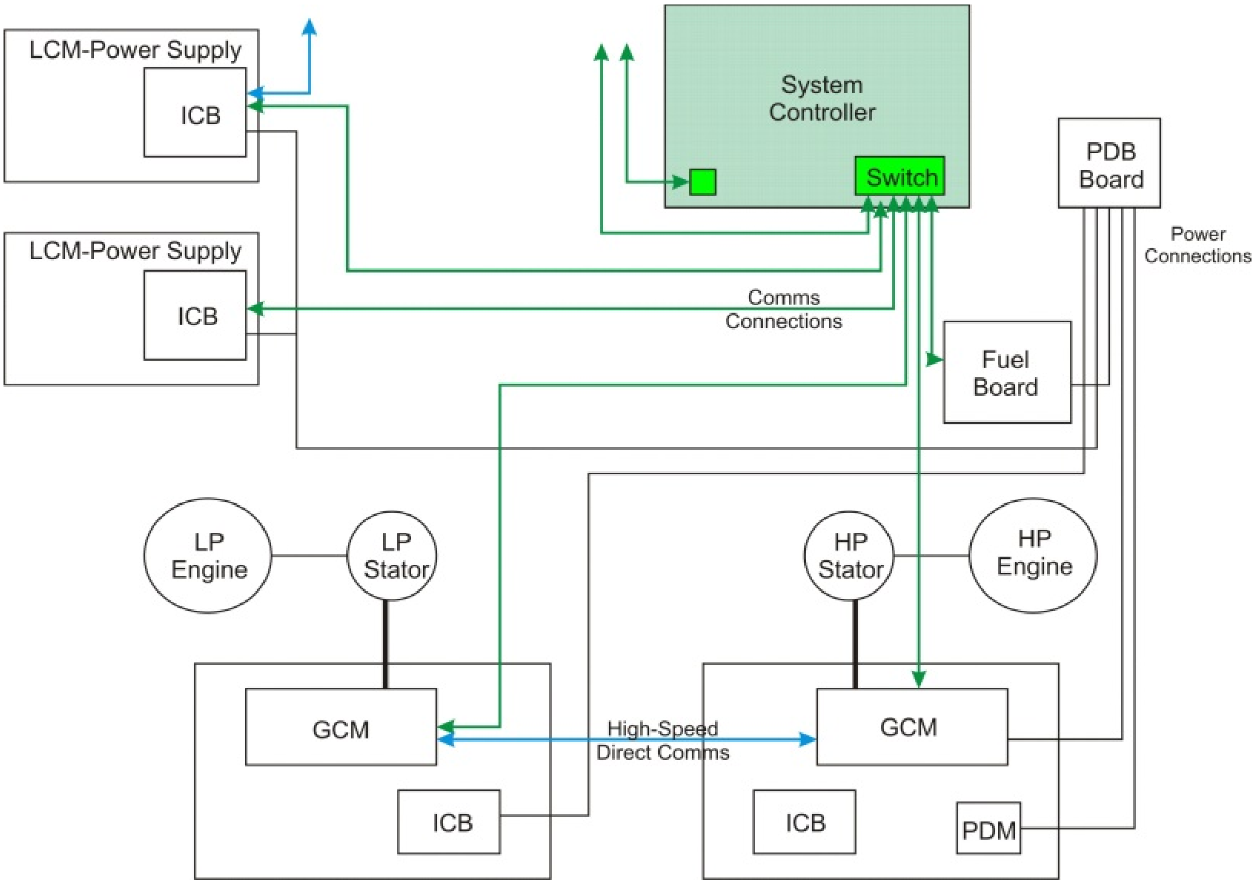

Figure 116: C370 Point-to-Point Communications Architecture

The communication hardware links — shown as green lines in Figure 116 — will be Ethernet physical transport as this technology is simple, fast, and flexible. Ethernet hardware links have the added benefit being transformer or optically coupled, so the grounding problems associated with bussed interfaces can often be avoided. The details of hardware messaging performance are discussed in Part III below.

The CapComm bus operates at 110 kbps and can transfer about 1,000 messages per second. If a particular message requires a response, then the overall message rate or transaction rate is reduced.

An Ethernet message is called a frame and some gigabit Ethernet device manufactures claim as much as 1,500,000 frames per second (fps). For this sort of performance to be realized, the processor must be sufficiently fast to handle frame payload processing.

System-On-Chip (SoC) Architecture

High-end, integrated-circuit manufacturers have recognized the necessity of using the hybrid DSP-FPGA architecture described above and have integrated CPUs — usually two, a large and complex FPGA logic fabric, and an assortment of I/O standards onto a single device.

This architecture has all the advantages of multi-chip circuits, but is less complex and more cost effective since only one large device is needed. The external memory can be connected — internally — to the processor, to the logic fabric, or both. SoC includes a sophisticated cache controller that is optimized to handle both processor instruction and data fetches, as well as to enable FPGA access to external storage. FPGA fabric includes an integrated memory array.

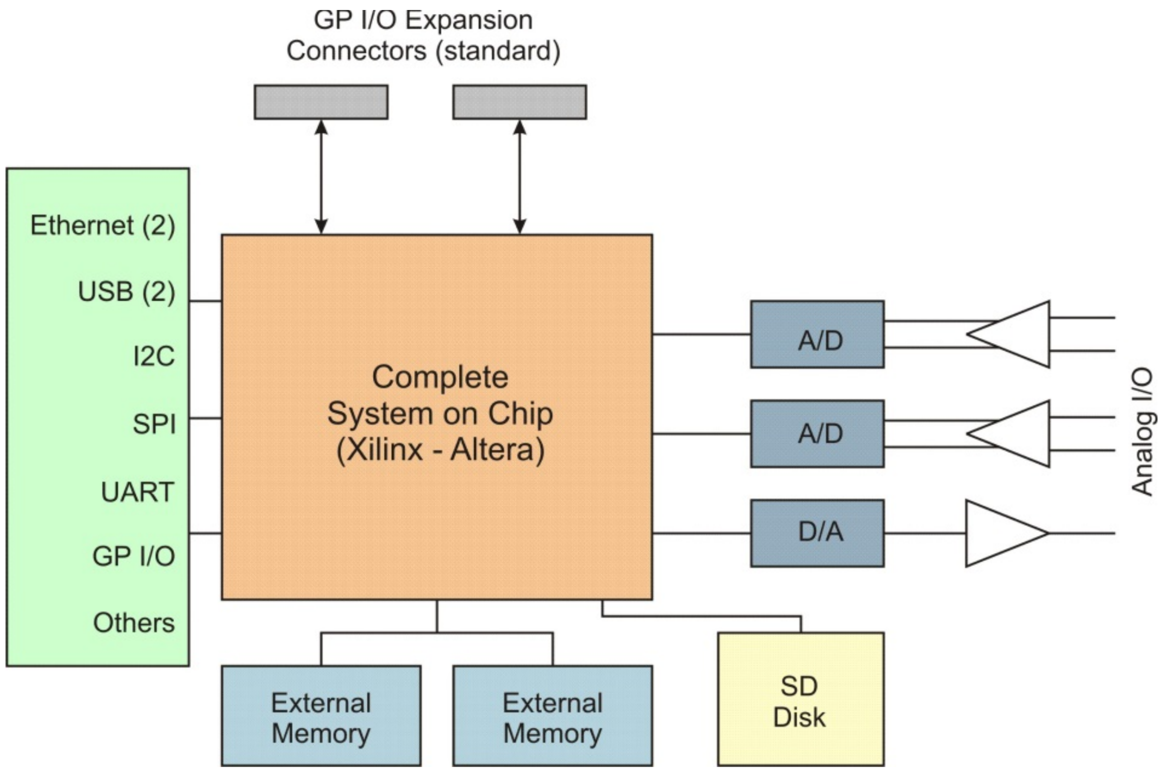

Figure 117: C370 Controller System-on-Chip (SoC) Architecture

6.9.4. Fuel System Controls and Component Design

Major fuel system components and associated capacity were evaluated for prototype engine operation at Capstone's Stagg facility. These components include the fuel gas shutoff valve, fuel pressure sensor, fuel distribution manifold, and fuel gas compression equipment. The fuel control board may also need to be redesigned depending on the control strategy employed.

The given parameters are as follows:

- Environmental Conditions: Capstone Stagg Facility
- Controls: Ability to provide adequate fuel control from idle to full load; may use manual control where practical
- System Thermal Efficiency: 41.76%
- Component Safety Agency Approval: not required for prototype testing

The assumed fuel parameters are as follows:

- Wobbe Index: 1320 BTU/ft^3
- Tfuelnom: 60 °F
- Pinletmin: 160 psig
- Estimated Maximum Transient Fuel Flow Above Steady State: 150%
- Shutoff Valve Allowable Pressure Drop: 1 psi max preferred, 3 psi max acceptable

The required Cv of the shutoff valve was calculated to be 5.2 at 1 psid and 3.0 at 3 psid. The incumbent shutoff valve was found unsuitable due a maximum inlet pressure limitation of 80 psig. An alternate is required.

The incumbent fuel metering valve met the requirements analysis. The Swift 36 and Swift 65 valves should provide the control and capacity the prototype engine requires. Selection of the valve size will depend on suitable engine control and determined by test results.

The incumbent fuel gas booster will not suffice, due to integrated low pressure components. Analysis shows that the compressor has the ability to deliver the fuel required with adequate inlet pressure provided by the facility gas line. Analysis indicates that modification to the incumbent fuel gas booster which addresses the low pressure components would provide viable gas pressure and capacity.

The incumbent fuel distribution manifold and fuel control board will not provide adequate control for the C370. Additional, discrete flow control valves exceed the number provided on the incumbent manifold and valve drivers on the control board. Additionally, the required pressure exceeds the rated capability of the incumbent manifold. Options to address fuel distribution to the engine include a redesigned manifold or a manually operated manifold. These options may allow operation of the prototype C370 without redesigning the control board.

The incumbent fuel pressure sensor does not meet the fuel pressure requirement of 160 psig. A suitable unit is, however, readily available.

6.10. C370 HP Spool Engine Design

6.10.1. Motor/Generator Design

Design Requirements

Design requirements were derived from thermodynamic cycle model predictions. Key requirements identified were:

- Rated Speed = 81,335 rpm
- Rated power = 194 kW
- Desired Over speed Margin = 7%
- Life = 20,000 hours
- Oil free bearings

Generator Design Specifications

Several trade studies were performed on generator design topologies, resulting in the final design specifications in Table 34.

Parameter	Value
Rated Power	194 kW
Rated Speed	81,335 rpm
Maximum Speed	87,000 rpm (7% OS)
Rated Voltage (L-L)	480 V_{RMS}
Fundamental Frequency	1.355 kHz
Generator Type	2 Pole, Synchronous AC
Magnet Type	Rare Earth Permanent Magnet
Efficiency	≥ 98.0%
Life	≥ 20,000 hours
Stator Cooling	Liquid cooled
Rotor Cooling	Air cooled

Table 34: C370 HP Spool Generator Design Specifications

Stator Lamination Design

Due to high frequency conditions, a very thin lamination needed to be selected to minimize the core loss. For this design, Arnon 5 Special, 0.005 in. thickness was considered. Arnon 5 has a density of 7,650 kg/m^3, and a resistivity of 4.8e-7 ohm-m. Figure 118 shows the BH curve and Figure 119 shows the core loss density of Arnon 5.

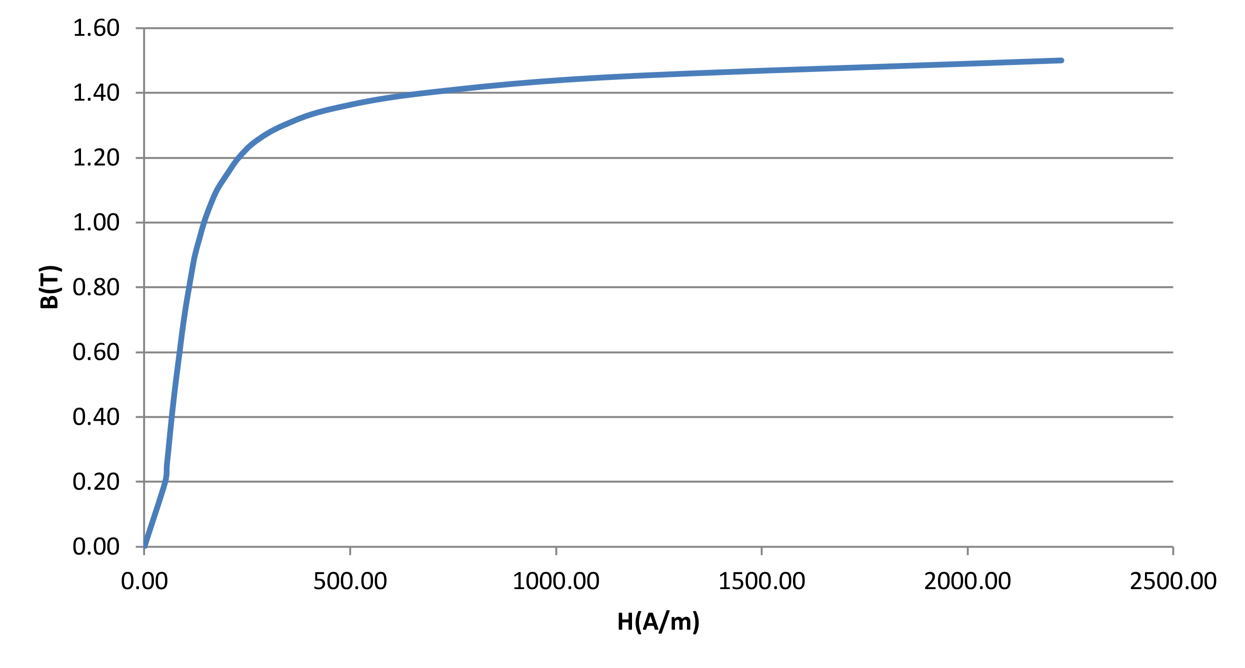

Figure 118: BH Curve of Arnon 5 Special Material

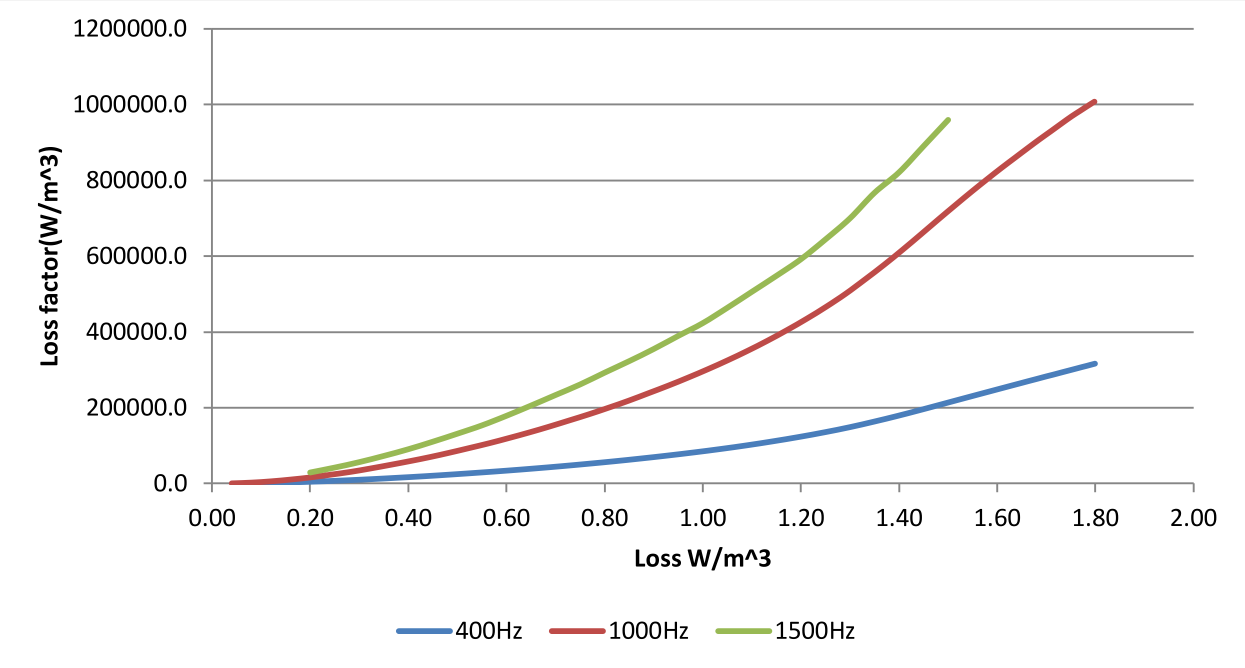

Figure 119: Core Loss Density of Arnon 5 Special Material

Magnet Sizing

Magnet sizing — i.e. length and diameter — was dictated by rotor dynamic analysis — i.e. critical speed margin — of the magnet shaft and magnet retaining sleeve stress. Once the magnet size envelope was established through mechanical analysis — i.e. rotor dynamic analysis and sleeve FEA —trade studies were performed with rotor-stator sizes using Electromagnetic FEA to determine output torque, power, and efficiency. Losses — such as eddy current — were minimized on the sleeve and the magnet for optimal generator performance. Generator rotor design — including magnet assembly — is further discussed in Rotor dynamic Analysis.

Air Gap Sizing

Air gap is a key parameter to design the high speed, high power permanent magnet generators. Although the magnet flux through the gap is increased and the current density is reduced with smaller air gap, it can reduce the air mass flow through the gap and also increases the windage loss. Reduction in the air mass flow and an increase in the windage can make the magnet hotter and the increase chance for demagnetization. Based on current designs, loss calculation, and heat generation, the air gap is selected as 4.572 mm. Figure 120 shows the air gap flux density, which has a maximum of 0.68 T.

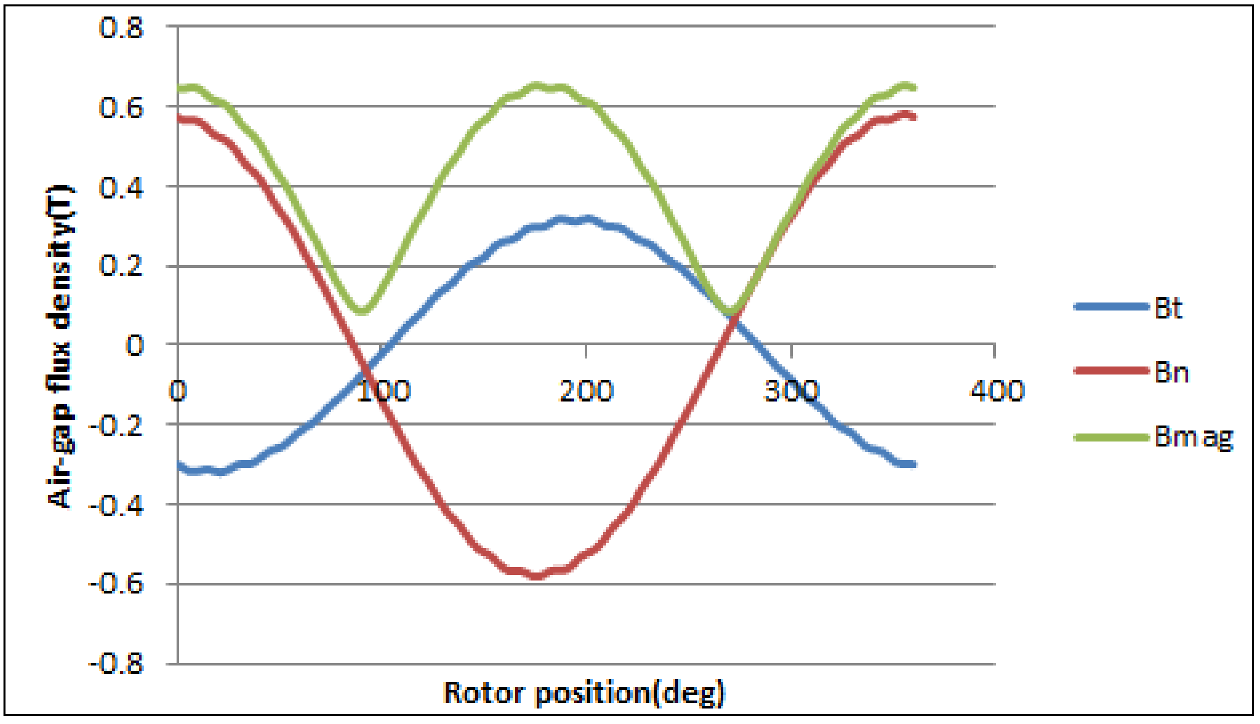

Figure 120: C370 HP Spool Generator Air Gap Flux Density

Winding Design

Based on the design requirements, 24 slot and 36 slot with full pitch and 1 slot short have winding factors greater than 0.95. Higher winding factors generate more torque — Torque α kW. Figure 121 and Figure 122 show the MMF harmonic factor for 24-slot and 36-slot stator stack design.

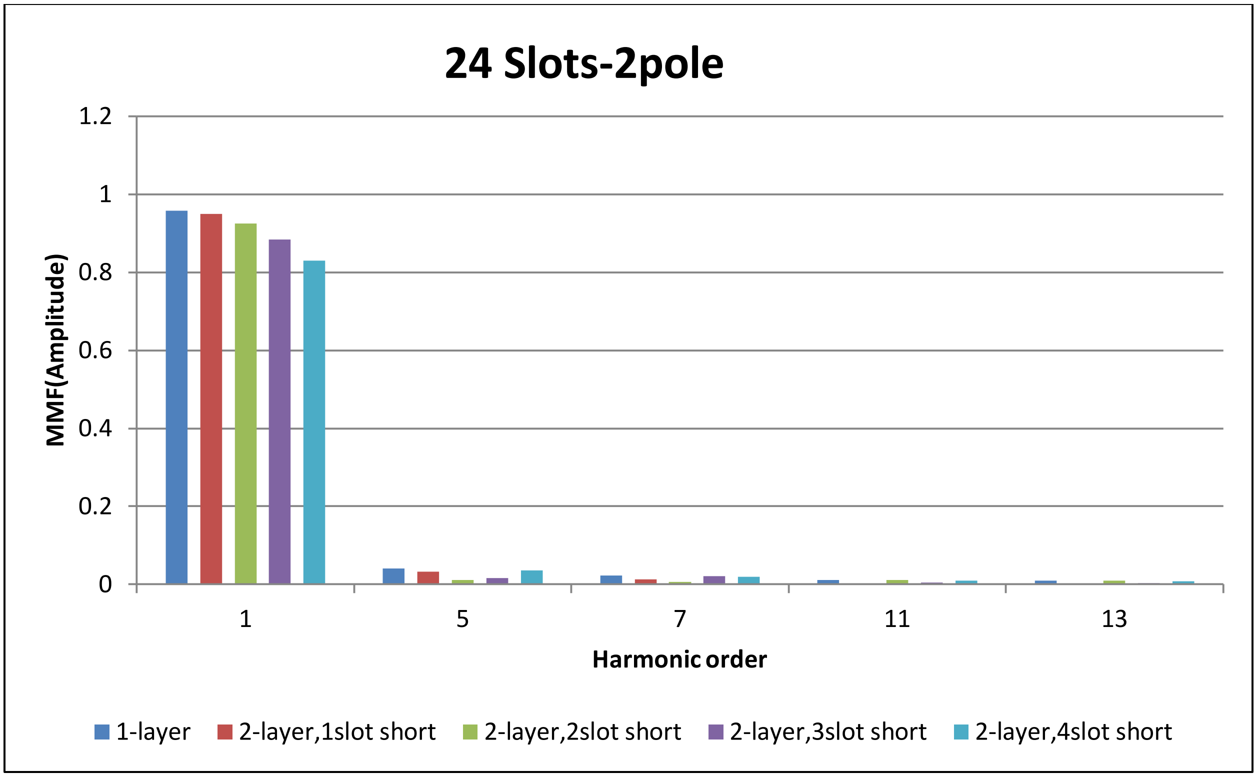

Figure 121: C370 HP Spool Generator Winding MMF Harmonic Factor for 24-Slot, 2-Pole

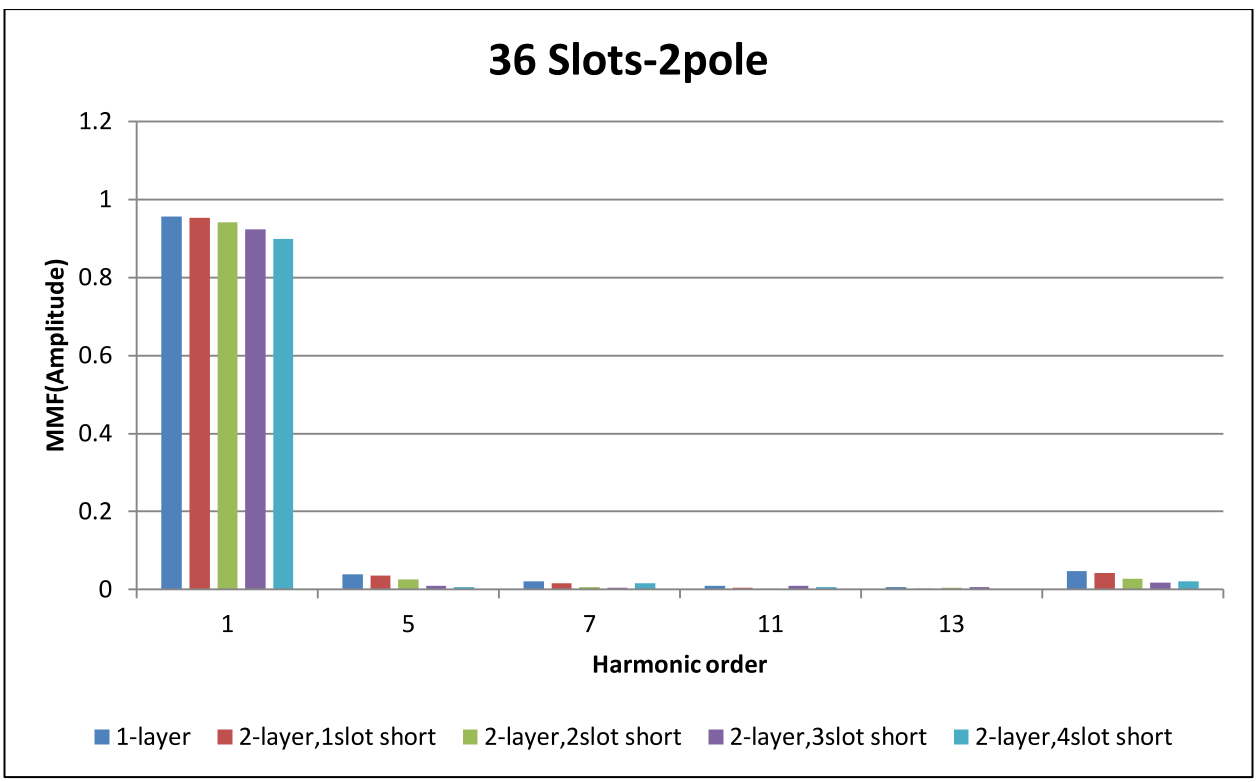

Figure 122: C370 HP Spool Generator Winding MMF Harmonic Factor for 36-Slot, 2-Pole

Another key parameter to the winding layout design is total harmonic distortion (THD) of winding factor. Figure 123 shows a lower THD for 24-slot and 1-slot short pitch. Therefore, 24-slot, double layer, lap winding with adjacent coil layout was selected for the design. Fig. 7 shows the winding layout.

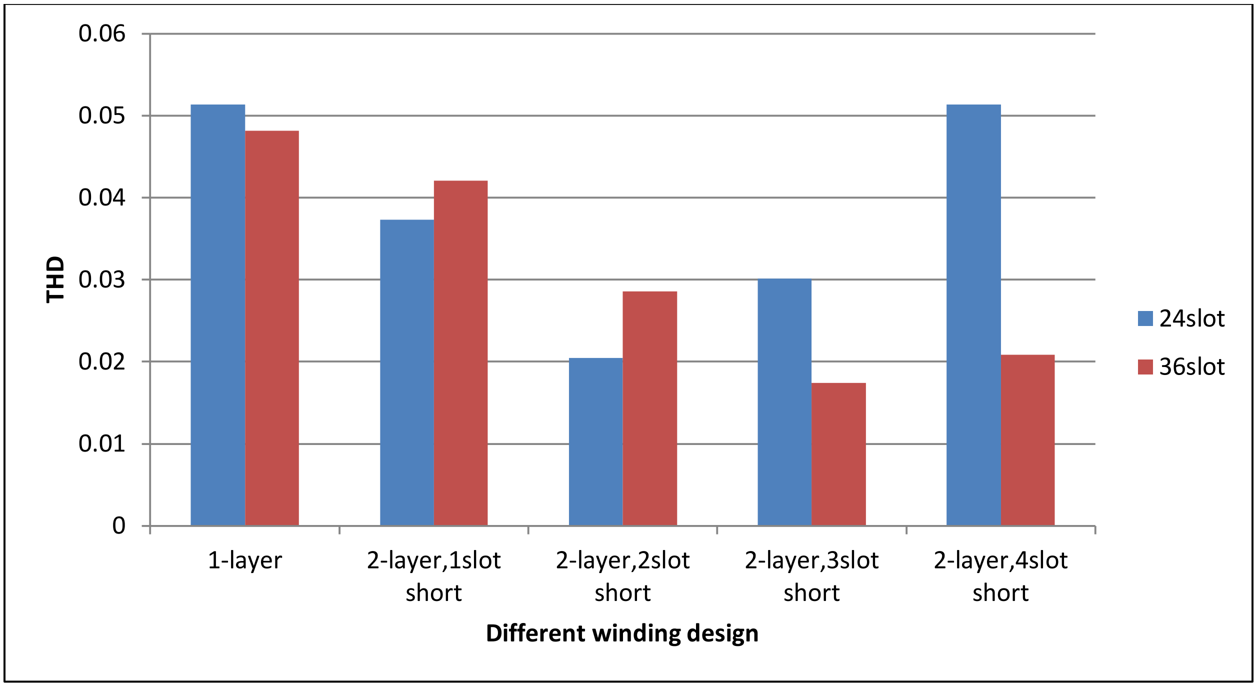

Figure 123: C370 HP Spool Generator THD for Different Winding Patterns

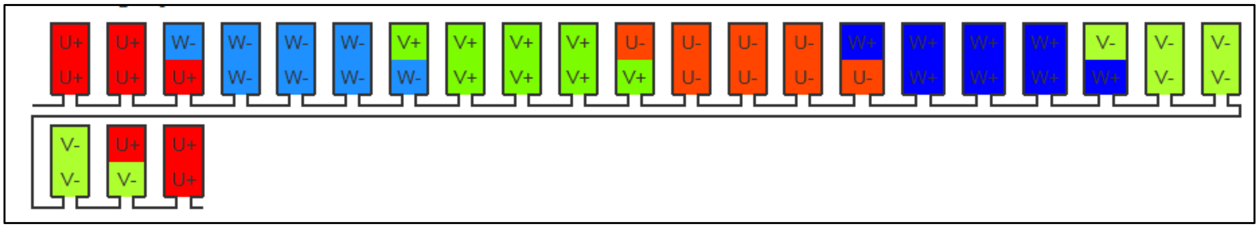

Figure 124: C370 HP Spool Generator Optimal Winding Layout

Two parallel circuits with separated, isolated neutral connections were chosen in order to have higher current capability. Three turns per coil and four coils in series are calculated for the design to meet the voltage capability. Figure 125 shows the winding connections for all three phases. To reduce the skin effect, proximity effect, and overall loss, AWG 26 wire was considered.

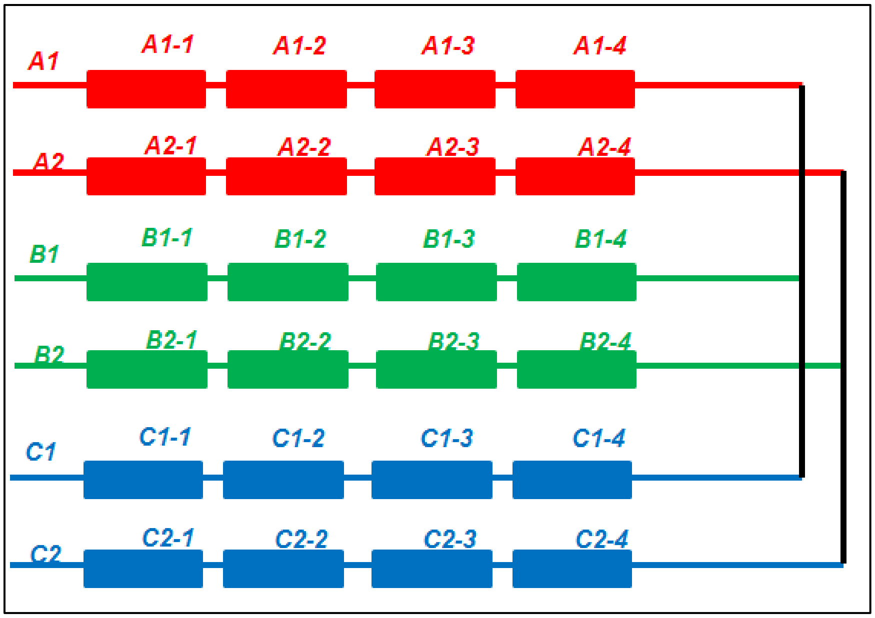

Figure 125: C370 HP Spool Generator Winding Connection

Stator Lamination Sizing

Stator back iron and stator tooth width were the major dimensions designed in this phase. To have a lower core loss and better heat dissipation, fluxes in back iron and tooth are assumed to be 1 T and 1.25 T. The stator back iron (1) and tooth width (2) can be calculated as:

$$h_b = \frac{\frac{OD_{magnet}}{2}\pi B_{gap}}{P B_{sy} k_s} \qquad (1)$$

$$w_t = \frac{\frac{OD_{magnet}}{2}2\pi B_{gap}}{Q_s B_{st} k_s} \qquad (2)$$

Where:

OD	=	magnet outer diameter
B_{gap}	=	air gap flux density
P	=	number of poles
B_{sy}	=	flux in the back iron
K_s	=	stacking factor
Q_s	=	number of slots
B_{st}	=	flux in the tooth

After initial sizing of back iron and tooth width using the equations above, detailed electromagnetic FEA were performed to predict generator performance.

Modeling and Simulation Results

Figure 126 shows the design modeled in Ansys Maxwell.

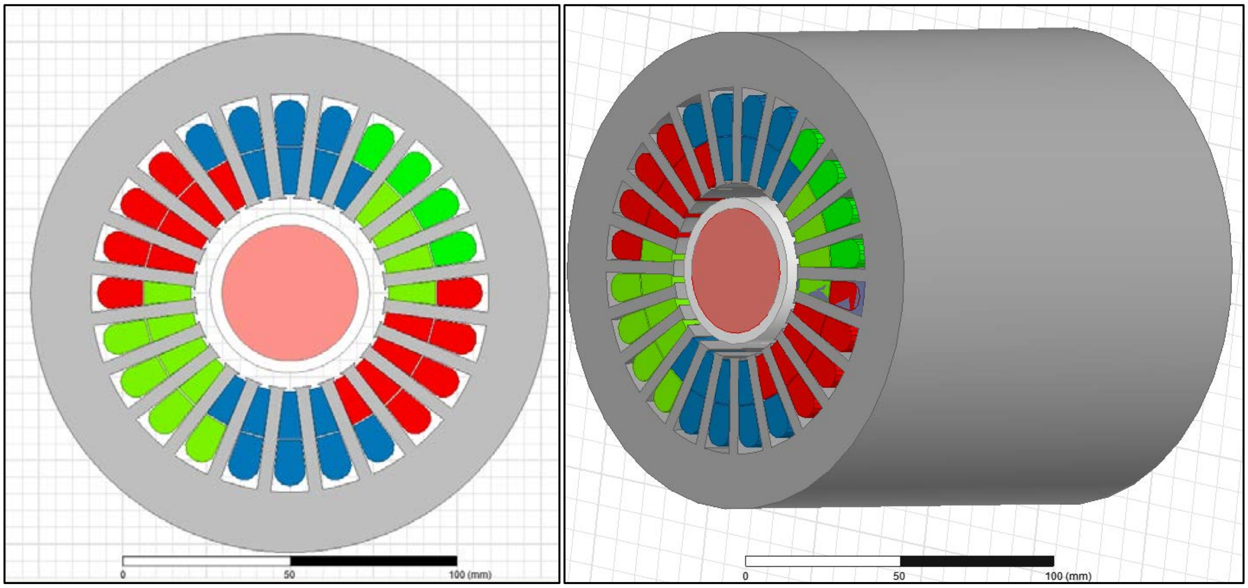

Figure 126: C370 HP Spool Generator Stator Model

The resistance and inductance calculation of the model are shown in Table 35. Since the phase inductance did not meet the required inductance to minimize the current ripple, an external inductor was used in series with the phase inductance. According to Table 35, the proposed design will achieve the required power and is able to produce a peak power of 221 kW for a short period of time. To meet the voltage limit, D-axis current needs to be applied. Figure 127 shows the predicted generator performance curve.

Parameters	Unit	Value	Value	Value	Value
Speed	rpm	81,335	81,335	87,000	87,000
BEMF per phase	V_{RMS}	270.5	270.5	288	288
I_{RMS}	A	258	300	258	300
Id	A	-95	-148	-133	-185
Iq	A	-352.4	-398	340	-382.6
Power output after inductor	W	194,600	221,723	202,346	227,700
Terminal voltage at generator	$V_{L\text{-}L\ RMS}$	449	440	457	443
Terminal voltage after ext. inductor	$V_{L\text{-}L\ RMS}$	500	500	500	500
PF at the generator side	%	97.7	97	99	98.6
PF after inductor	%	87	85	90	87.7

Table 35: C370 HP Spool Generator Design Performance

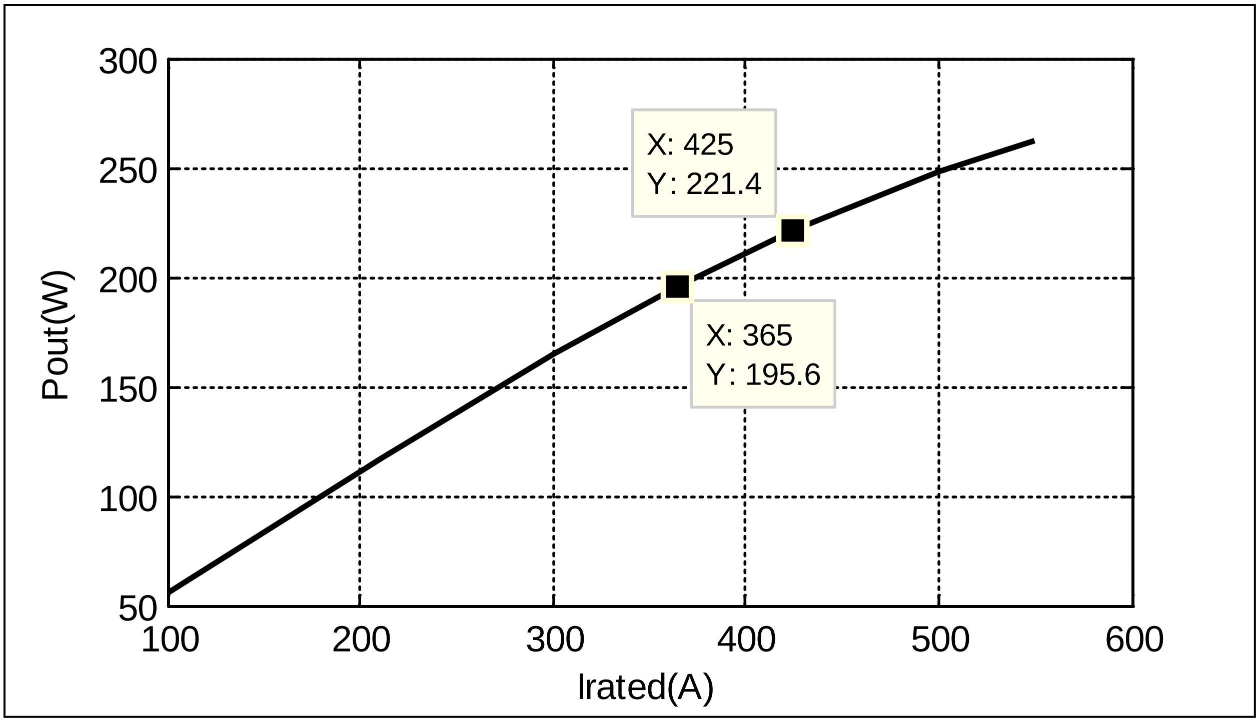

Figure 127: C370 HP Spool Generator Predicted Performance Map

Thermal Investigation and Cooling Design

Winding current density and torque per rotor volume (TRV) are the key indicators to design the cooling. Table 36 shows the parameters for the proposed design.

Speed	rpm	81335	81335	87000	87000
Power output after inductor	kW	194600	220580	202346	227700
TRV	kNm/m^3	71.3	80	68.8	77.42
Current density	A_{RMS}/mm^2	8.14	9.47	8.14	9.47

Table 36: C370 HP Spool Generator Current Density and TRV

A water cooling system for the proposed stator was designed for the following reasons:

- High power-to-dimension ratio needs an effective cooling.
- Water-cooled hardware does not require a large external heat exchanger (air-water), thus the water-cooled hardware can be significantly smaller (lower lamination volume) than air-cooled hardware
- Getting the same power from air-cooled hardware needs lower current density which requires a large volume of copper (effects on the cost and manufacturing)

For the proposed stator, an axial configuration cooling jacket was analyzed and compared to a radial configuration cooling jacket. Figure 128 shows the axial configuration and Figure 129 shows the radial design.

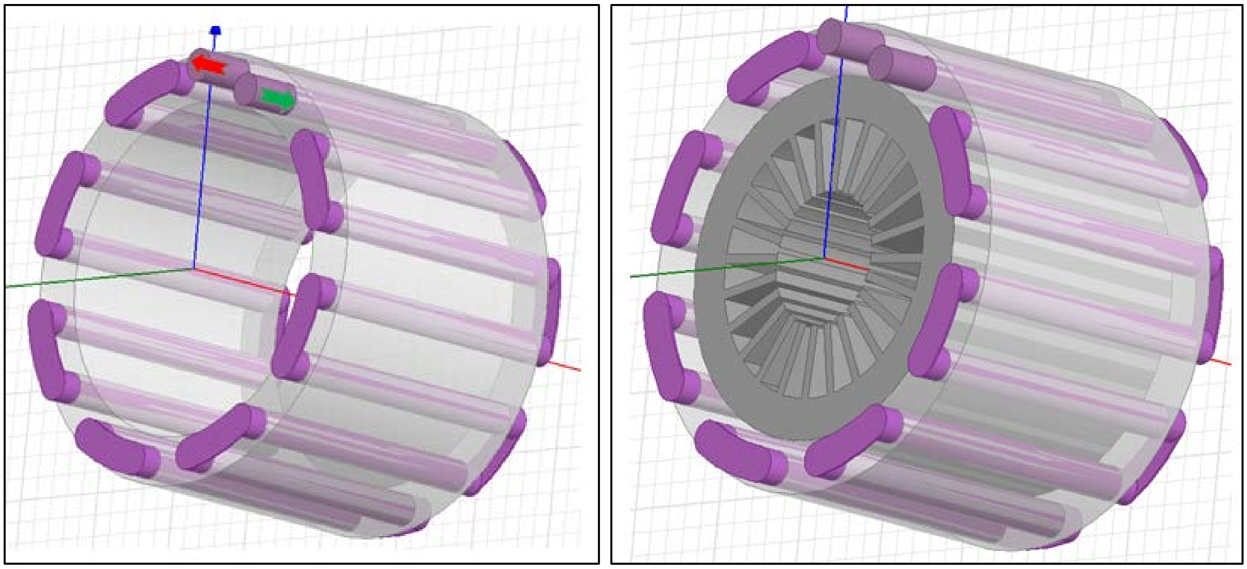

Figure 128: C370 HP Spool Generator Axial Configuration Water Jacket

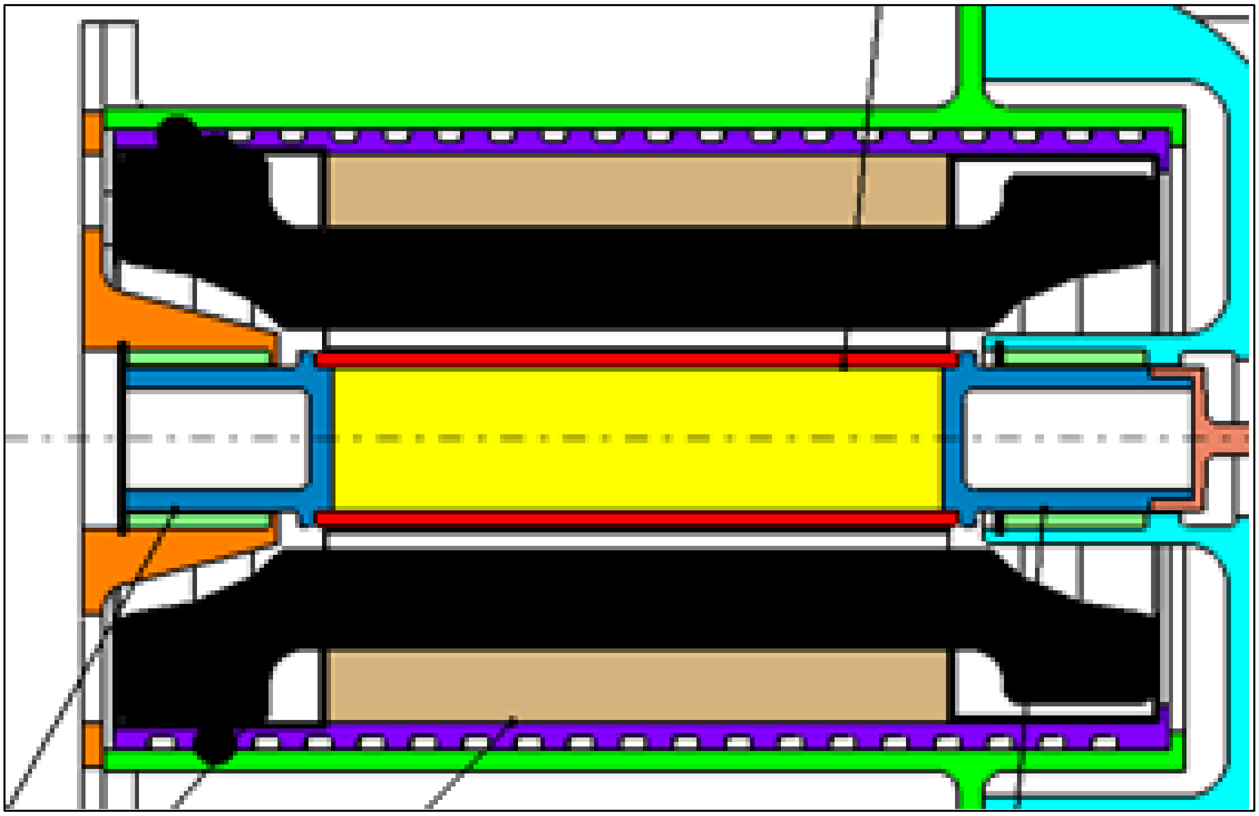

Figure 129: C370 HP Spool Generator Radial Configuration Water Jacket

The radial configuration was chosen as the final design over the axial for the following reasons:

- Industry standard
- Ease of manufacturing
- Effective cooling
- Lower pressure drop

6.10.2. Combustion System Design

This section summarizes the combustion system design work for the C370 POC engine. The design inputs are from C370 system cycle analysis and the combustion system is intended for firing natural gas only. The design work will provide a complete definition of the combustion system, including the architecture, the liner overall sizing and detailed definition —number, location, and dimensions of both the liner dilution holes — as well as injector design.

Design Requirements

The C370 POC emissions high level technical requirements are:

- Emissions Requirements are “based on the California Code of Regulations Law Title 17; Division 3; Chapter 1; Subchapter 8; Article 3; 2007 Fossil Fuel Emission Standards - excluding CHP credit”
- $NO_x \leq 0.07$, $CO \leq 0.1$, $VOC \leq 0.02$ (lb/MW-hr)
- After correction to 15% O_2, $NO_x \leq 1.8$, $CO \leq 4.1$, $VOC \leq 1.44$ ppm at 15% O_2

The C370 POC engine shall operate on high pressure natural gas (HPNG) available at Capstone’s Stagg test site. The higher heating value (HHV) of the fuel shall fall within the range of 825 BTU/scf – 1,275 BTU/scf. The Stagg test site supply of HPNG has an HHV of 1,024 BTU/scf.

For demonstration, the C370 POC engine test environmental requirements are:

- Altitude of 800 ± 50 feet
- Ambient temperature of 75 ± 20 °F
- Demonstrate at Stagg test cell conditions

Design Inputs

The design inputs for the combustion system come from the system level cycle analysis. There are two versions of C370 cycle models: without heat recovery module (HRM) and with HRM, as shown in Figure 130 and Figure 131. The component design targets are based on the cycle model without HRM. For combustion system design, the key inputs are the main air parameters — flow rate, temperature, pressure — as well as fuel information — type, flow rate, energy input, lower heating value. These inputs are listed below.

- Combustion air flow rate: 2.831 lb/s
- Combustion air pressure: 127.316 psig
- Combustion air temperature 1052 °F
- Fuel type: High Pressure Natural Gas (HPNG)
- Fuel flow rate 0.0426 lb/s
- Fuel energy input: 922 kW
- Fuel lower heating values 20,500 BTU/lbm

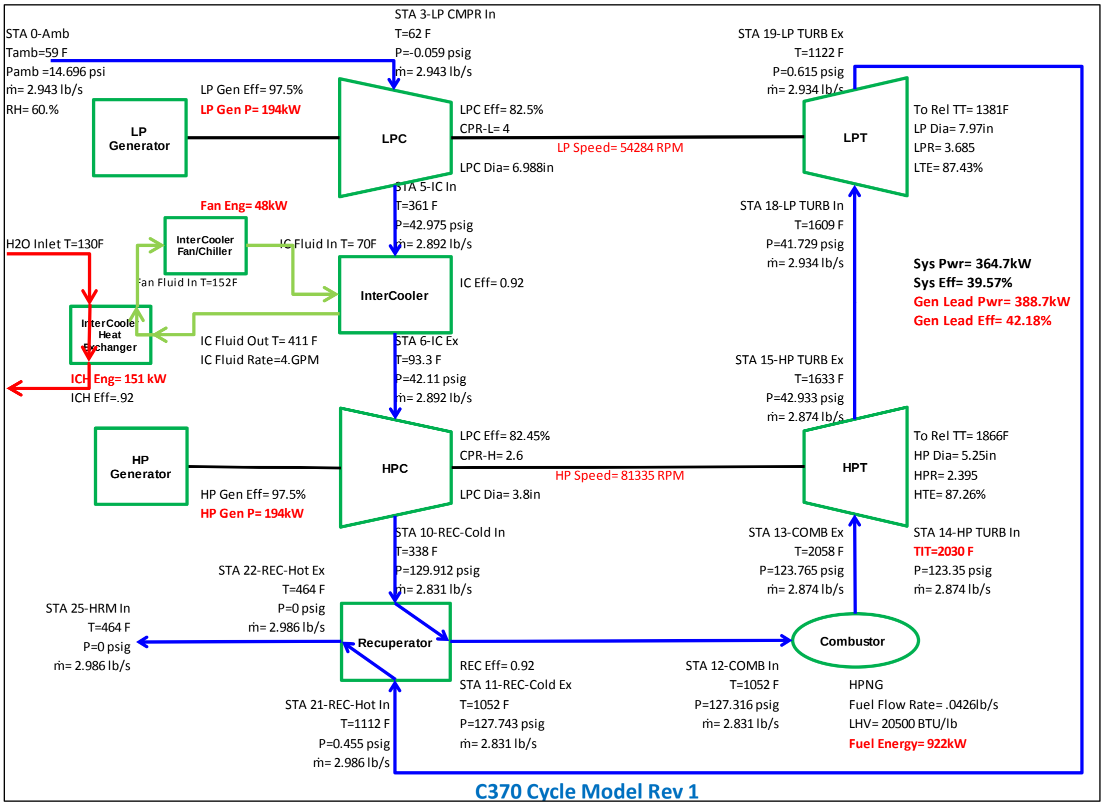

Figure 130: C370 Cycle Design (without HRM)

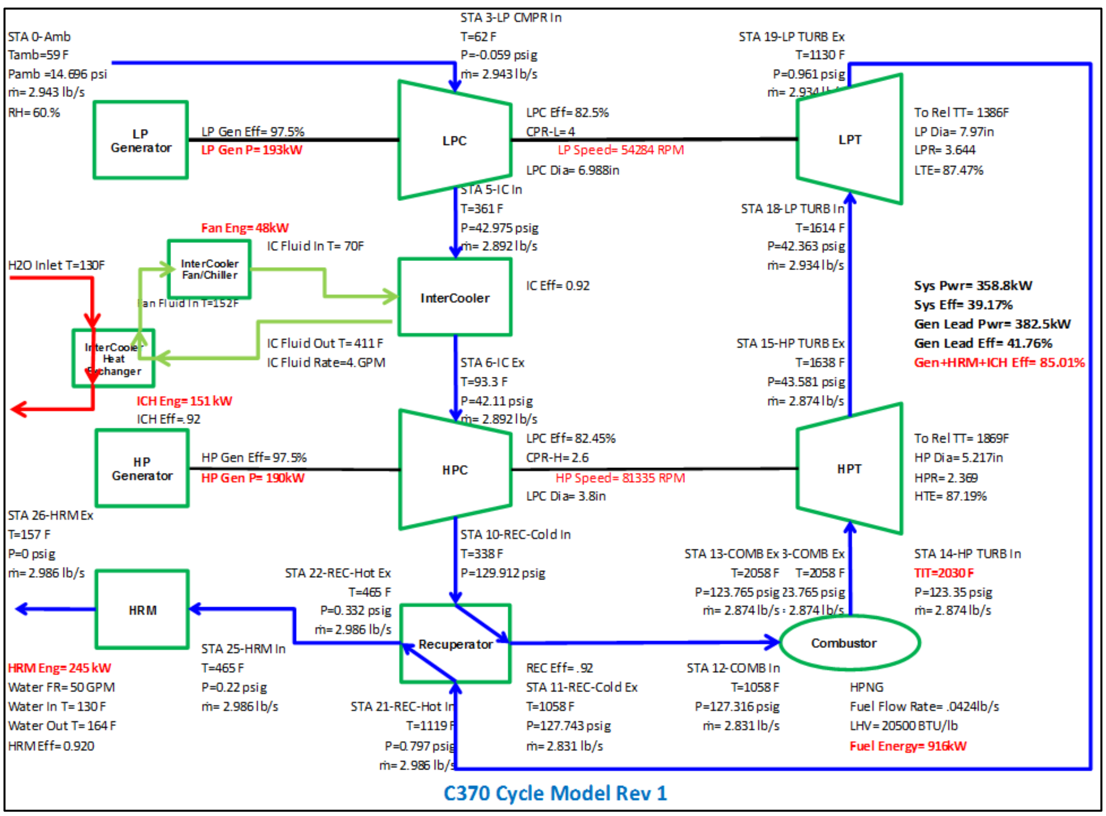

Figure 131: C370 Cycle Design (with HRM)

Combustion System Architecture Considerations

The existing combustion system architectures for Capstone Microturbine systems — including C30, C6X, C200, and C250 POC — are all of the same type, illustrated in Figure 132. These architectures share the following features:

1. Lean premixed injector type
2. Most injectors transport fuel/air mixture tangentially into the combustion PZ
3. Optimal combustion performance is achieved via fuel staging and combustion control

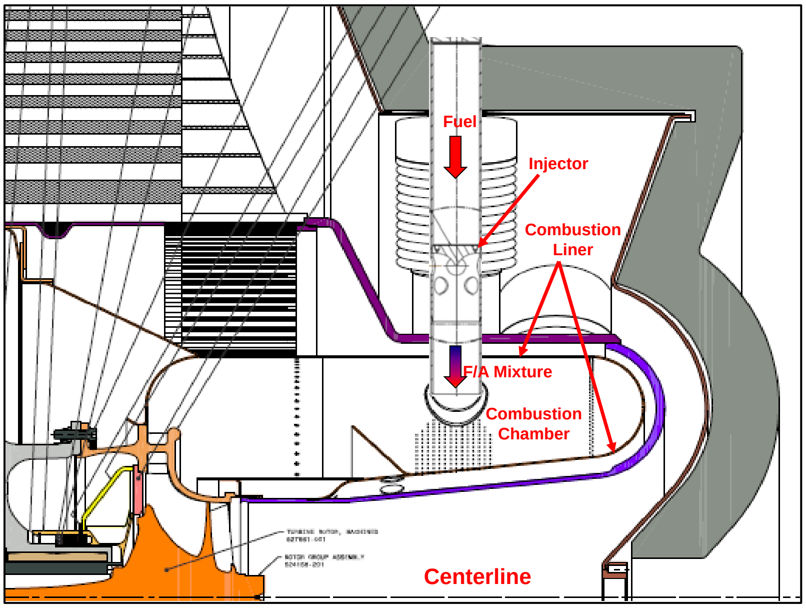

Figure 132: Capstone C200 Combustion System

In the early stages, modifications to C370 combustion design were considered in order to study parameters which may have impacts on combustion performance during design and development test stage with flexible hardware. Potential flexible combustion hardware is shown in Figure 133. The potentially impactful parameters include number of injectors, injector type, tangential injection, axial injection, tangential injection angel, axial injection angle, combustion sizes, as well as combustion control parameters such as TET. With a flexible combustion test bench, the difference variance — Table 37, for example — can be tested or simulated in CFD.

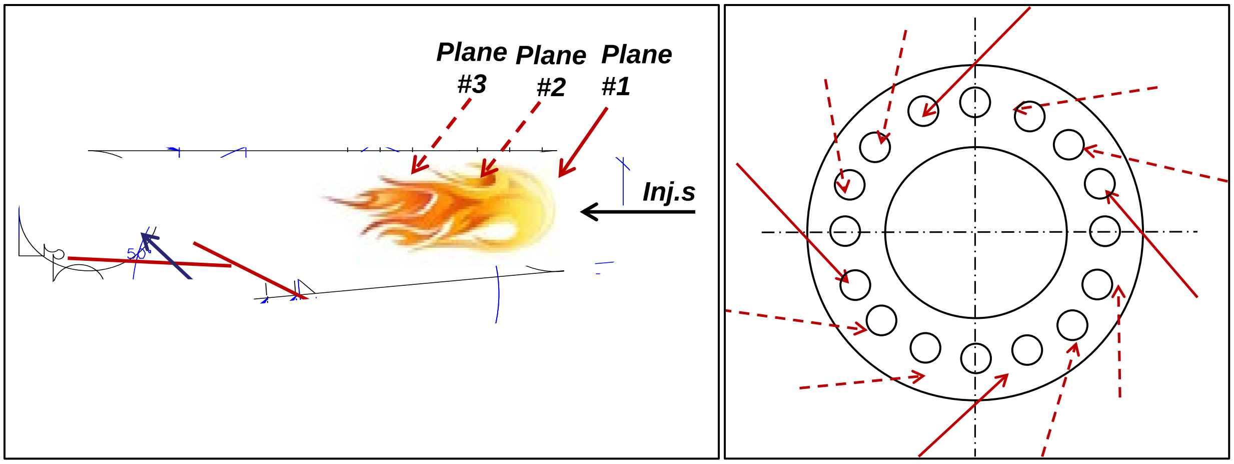

Figure 133: C370 Flexible Conceptual Combustion Architecture

No	Configuration Description	Axial Injector No	Tangential Injectors			
			Plane #1	Plane #2	Plane #3	Subtotal
1	No Tangential Injectors	1 – 16	0	0	0	0
2	One-Plane Tangential Injectors	0 – 16	4, 6, 8, or 12	0	0	4, 6, 8, or 12
3	One-Plane Tangential Injectors	0 – 16	0	4, 6, 8, or 12	0	4, 6, 8, or 12
4	One-Plane Tangential Injectors	0 – 16	0	0	4, 6, 8, or 12	4, 6, 8, or 12
5	Two-Plane Tangential Injectors	0 – 16	0	4, 6, or 12	4, 6, or 12	8, 12, or 24
5	Two-Plane Tangential Injectors	0 – 16	4, 6, or 12	0	4, 6, or 12	8, 12, or 24
6	Two-Plane Tangential Injectors	0 – 16	4, 6, or 12	4, 6, or 12	0	8, 12, or 24
7	Three-Plane Tangential Injectors	0 – 16	2, 3, 4, or 6	2, 3, 4, or 6	2, 3, 4, or 6	6, 9, 12, or 18

Table 37: C370 Combustion Architecture Variance

Combustion Analysis

Chemical Kinetics Analysis

Although there are limitations, chemical kinetics analysis plays a critical role in combustion design by providing the trending information of combustion performance and combustion system sizing such as pollutant emissions — CO, NO_x, and THC — as well as residence time required for achieving designed targets. For C370 combustion design, the design baseline cases are the existing combustion systems which offer satisfactory combustion performance, including the already commercialized C200 and well-demonstrated C250 POC engines. The chemical kinetics analysis for the C370 POC engine design has the following characteristics or features:

- Objective: Use chemical kinetic analysis to guide C370 POC combustor sizing design
    - Chemical kinetics simulation of methane and air mixture
    - Study impact of pressure and pre-heat temperature
    - The simulation is for trending informational purposes only and may not be accurate
- Reactor: Perfect Stirred Reactor (PSR)
- Reaction Mechanism: GRI-Mech 3.0® for CH_4 combustion
    - GRI-Mech 3.0 is an optimized mechanism designed to model natural gas combustion, 325 reactions, and 53 species
- Simulation Cases:
    - Case #1: CH_4 and air, φ = 0.50, T = 1129.50 °F, Constant P = 0 psig
    - Case #2: CH_4 and air, φ = 0.50, T = 1129.50 °F, Constant P = 46.642 psig, which is typical C200 full power condition at ISO
    - Case #3: CH_4 and air, φ = 0.50, T = 1129.50 °F, Constant P = 157.80 psig
    - Case #4: CH_4 and air, φ = 0.50, T = 990 °F, Constant P = 157.80 psig

The chemical kinetics simulation results are presented in Figure 134, Figure 135, and Figure 136. These results show the impacts of residence time and air temperature on the performance of the combustion system. While the C370 conditions were not directly simulated, data obtained can be interpolated.

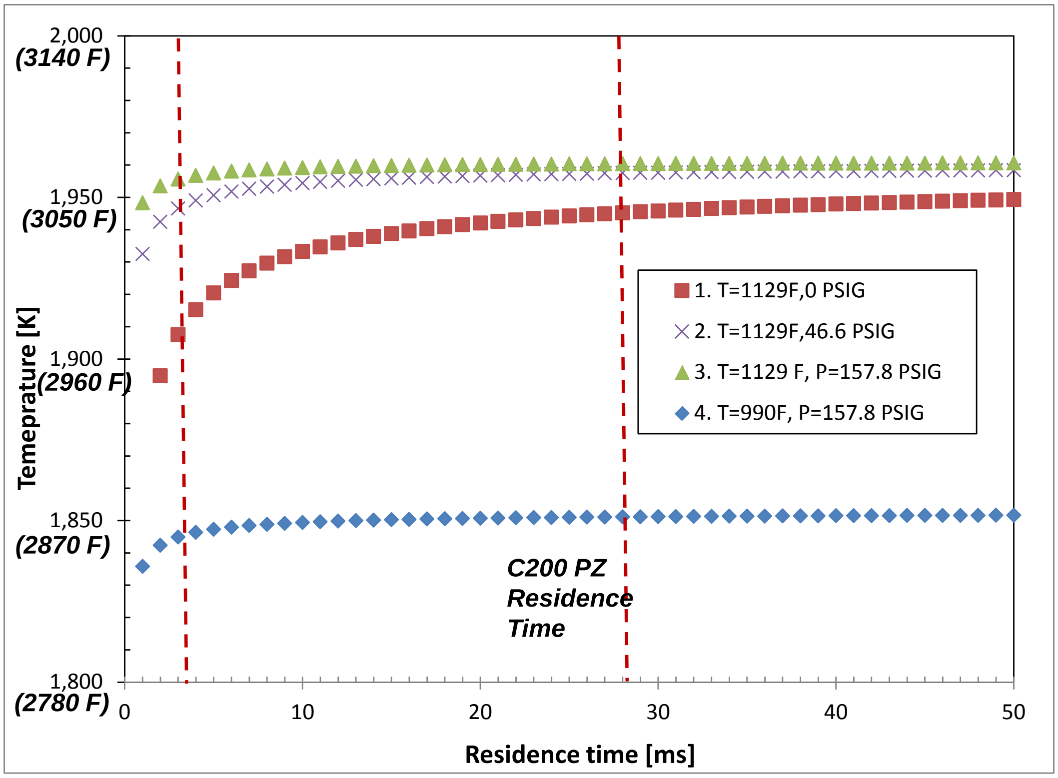

Figure 134: C370 Combustor Adiabatic Flame Temperature as Function of Residence Time

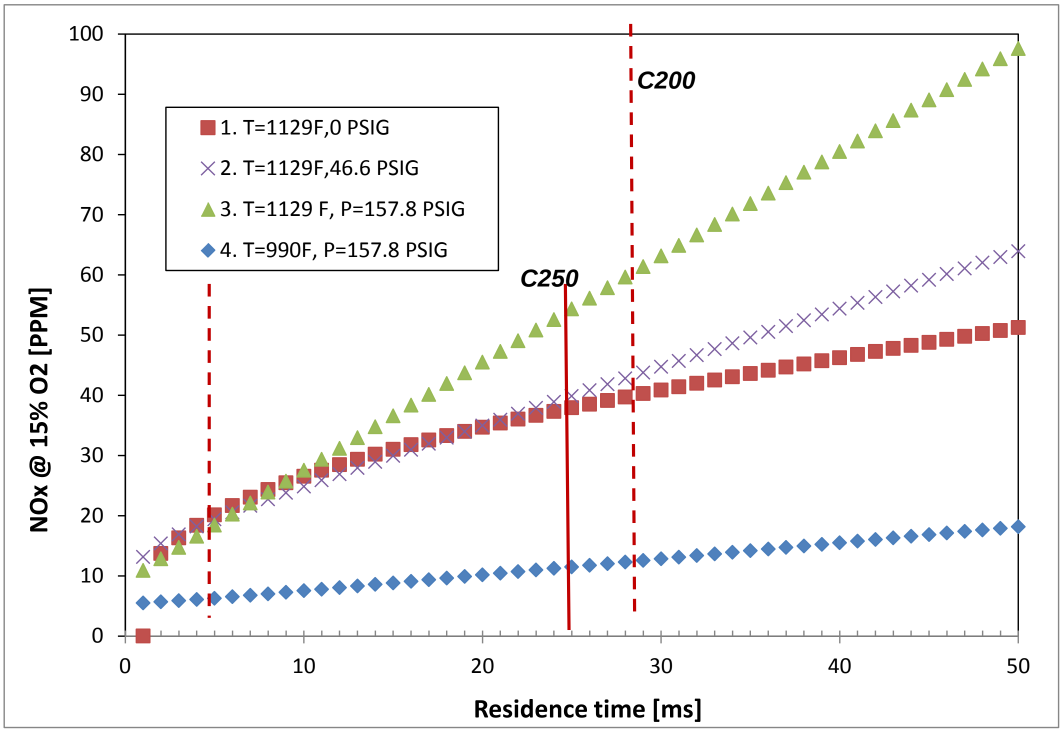

Figure 135: C370 Combustor NO_x Emission as Function of Residence Time

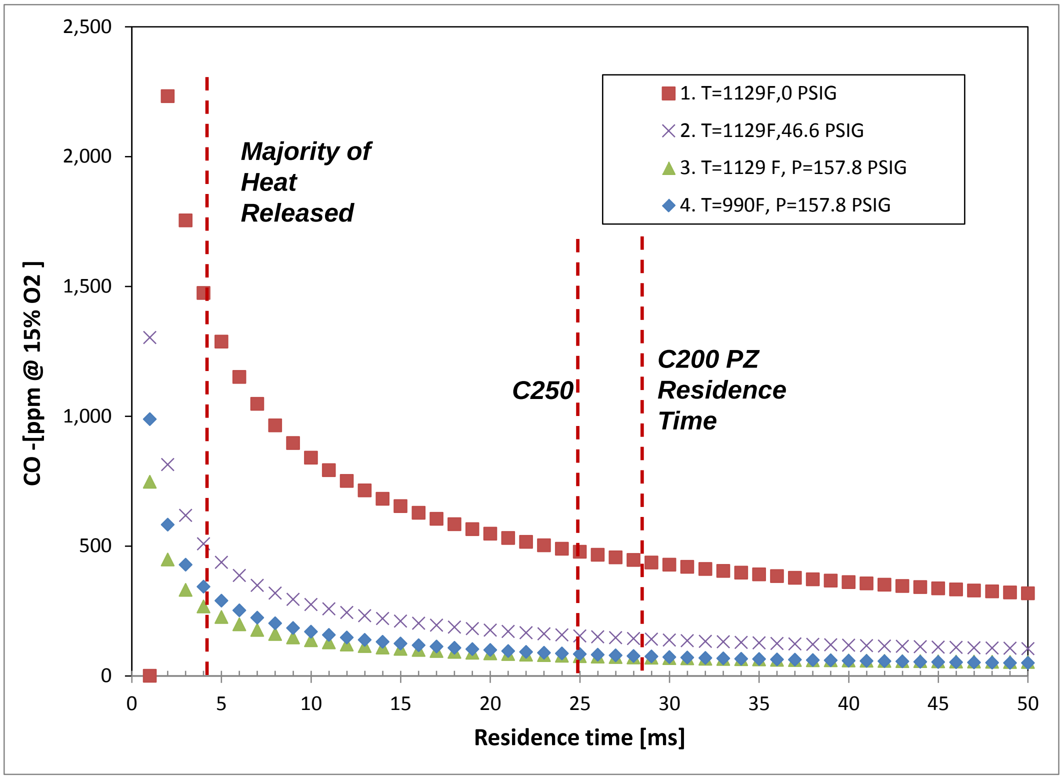

Figure 136: C370 Combustor CO Emissions as Function of Residence Time

Issues of Premixed Combustion Systems

In order to achieve the design goals for the C370 combustion system, a lean premixed combustion is still the best technical approach. For a lean premixed combustion system like that employed in Capstone microturbine systems, combustion design challenges and possible issues include flashback, lean blowout, and autoignition. The design criteria used for current design was based on Capstone's existing technologies and is a "scaling" of the C200 and C250 POC systems.

Auto-Ignition

Auto-ignition is a spontaneous chemical reaction between fuel and air without an external ignition source. Higher temperature, higher pressure, and longer residence time make it easier for a fuel-air mixture within the flammability range to auto-ignite. At a fixed temperature, pressure, and fuel-air mixture, there is a minimum amount of residence time that is needed for the mixture to auto-ignite, which is called auto-ignition delay time. For Capstone microturbine engines, auto-ignition within the injector must be prevented because it leads to injector hardware damage and combustion system failure. Chemical kinetics simulations revealed that at the full power condition of C370 operation, the air-fuel mixture has a predicted autoignition delay time of more than 80 ms while the residence time of the fuel/air mixture in the injector is much less — 2 to 3 ms. As a result, even at C370 conditions — higher temperature, higher pressure — the risk of autoignition within the injector is low and there is no concern of auto-ignition in the injector.

Flashback

With fuel variation and certain other operational variations, flashback has been a great concern for a premixed system. The general methods of combatting flashback include:

1. Injector mixture design optimization to avoid or minimize a recirculation zone
2. Increase bulk velocity within the injector to give higher flashback resistance margin
3. Reduce fuel concentration in low velocity zone

Figure 137 is a recent literature review of the methane/air laminar flame speed, which can be used as a reference to design desired average velocity inside the injectors.

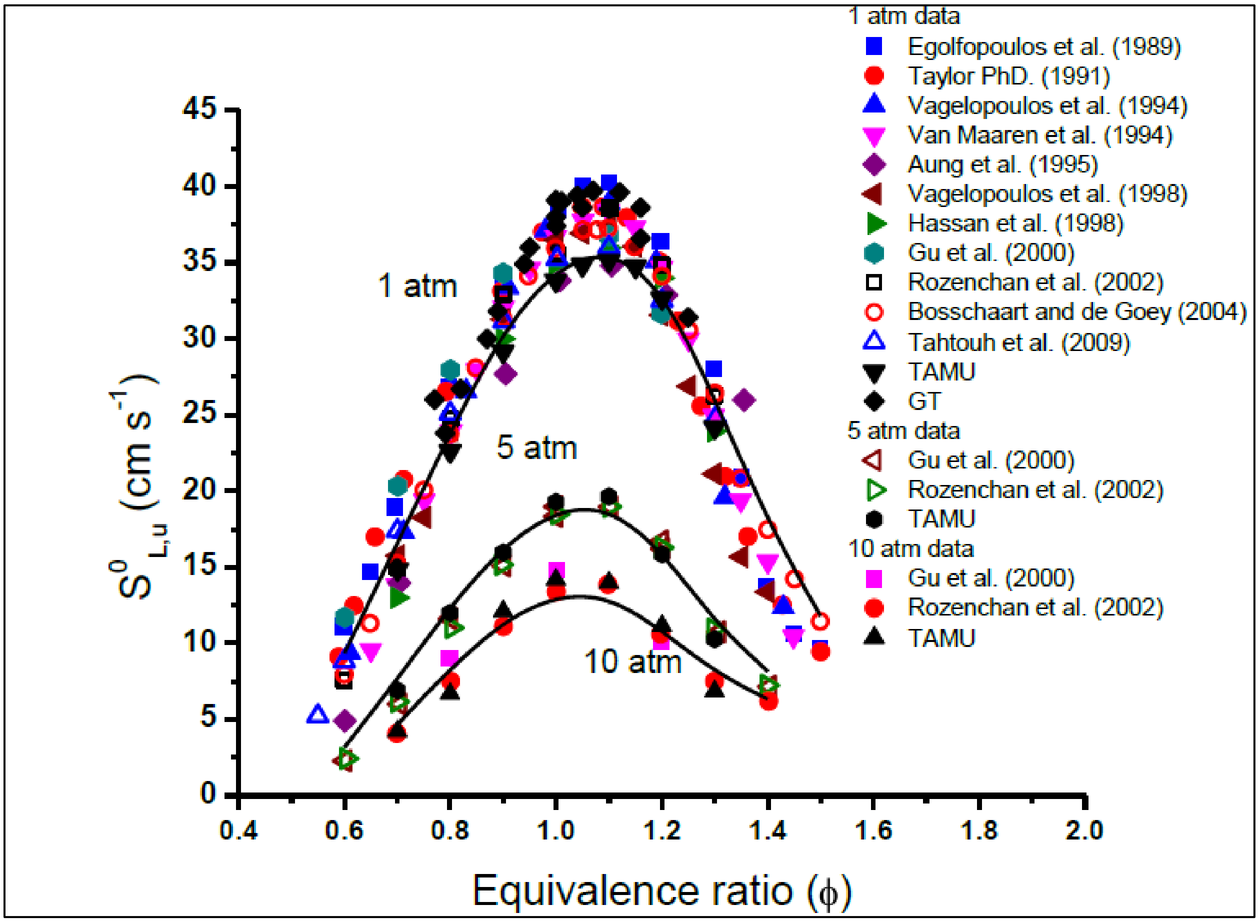

Figure 137: Methane/Air Laminar Flame Speed (GT2011-45122)

Since the existing Capstone gaseous injector design was selected for the C370 POC engine, the characteristics and performance will be inherited. However, the new C370 injector shall be designed to have the mixture velocity magnitude and profile give a higher flashback resistance margin. From past C30/C60/C65/C200 experience, it has been established that when the average velocity of fuel/air mixture in the injector is at least 50 times the laminar flame speed of the fuel/air mixture in order to have a good flashback-resistance margin. By scaling the C200 injector, 40 m/s bulk velocity in the injector was found be desirable to have a good flashback resistance margin.

Combustion Liner Trade-Off Studies

Based on combustion analysis and existing engine performance, it was estimated that the combustion PZ size should be about 200 – 250% of the current C65 liner, the residence time 20 – 25 ms, and the average AFT should be maintained at 2650 – 2700 °F at full power. The average of PZ temperature (T_{pz}) is a function of the amount of air introduced to the PZ; this relationship is shown in Figure 138. As a result, the PZ air split ratio is approximately 58%.

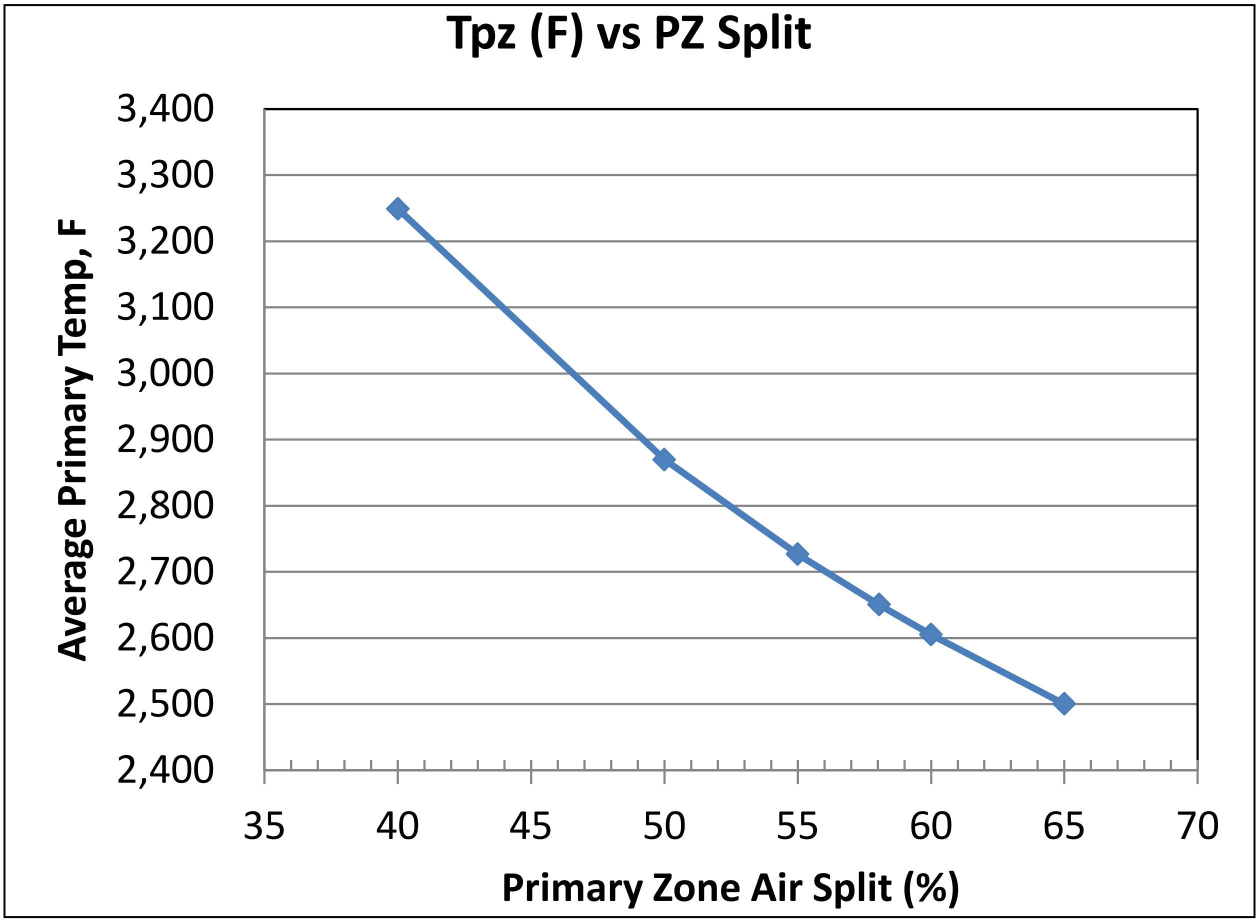

Figure 138: C370 Combustor Average Primary Zone Adiabatic Flame Temperature as a Function of Air Split Ratio

Combustion Injector Design Trade-Off Studies

At a given primary zone air ratio, to further quantify the inner diameter (ID) and the quantity of injectors, a series trade-off such as those shown in Figure 139 was conducted. The five studied IDs of injector design were 0.87”, 0.926”, 1.057”, 1.25” and 1.37”, which include the sizes of existing C30, C65 and C200 systems. On the other hand, at C370 full power conditions, an average flow speed of ~40 m/s is desired to reduce flashback risk.

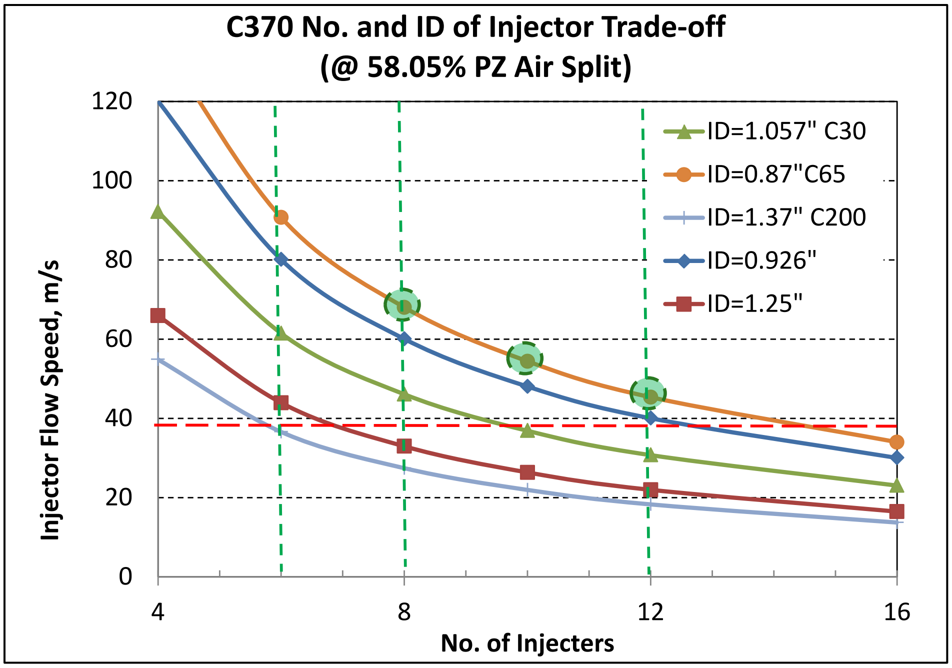

Figure 139: C370 Combustor Quantity vs. Flow Speed for Injectors by Size

Based on the injector sizing trade-off studies — Figure 139 — the following injector configurations are recommended:

1. Injector of the same size as C60/C65, which is an ID of 0.87 in.
2. Number of injectors is between 8 and 12.

Based the past Capstone experience, both the existing C65 injector — Figure 140 — and the injector for high flame speed fuels are candidate injectors for C370 high pressure spool combustion system.

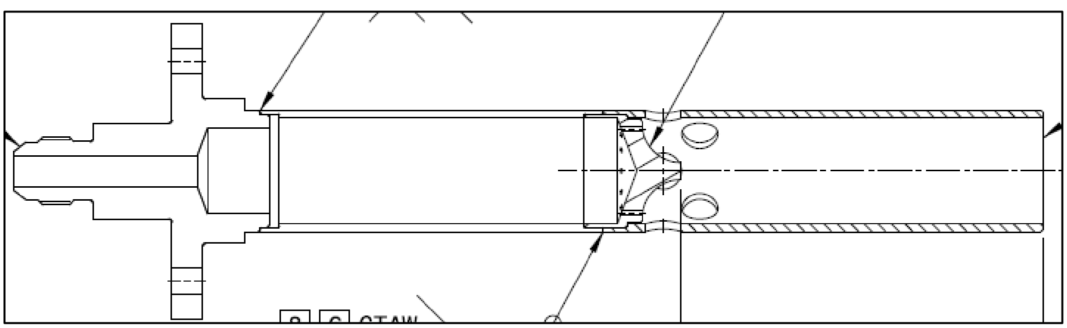

Figure 140: C65 Injector for Gaseous Fuels

Combustion System Detailed Definition

Based on analysis introduced in the previous sections and Capstone experience, the following preliminary key combustion system specifications for C370 high pressure spool were established:

- The PZ volume of combustor is to be 200 – 250% of C65, which was further evaluated in CFD simulation and / or prototype tests
- Injector ID is to be the same as the C65

- Total 10 – 12 injectors. The number of injectors at plane A is to be determined based on CFD simulation results.
- Three planes — each with four injectors — of injectors tangentially injected into PZ with a 45° injection angle. Injectors may also have axial tilting.
- Each injector plane has a 30° offset from the neighboring plane(s)

The overall layout and injector arrangement are schematically shown in Figure 141 and Figure 142 respectively. Figure 143 illustrates the 3-D view of the preliminary C370 combustor concept.

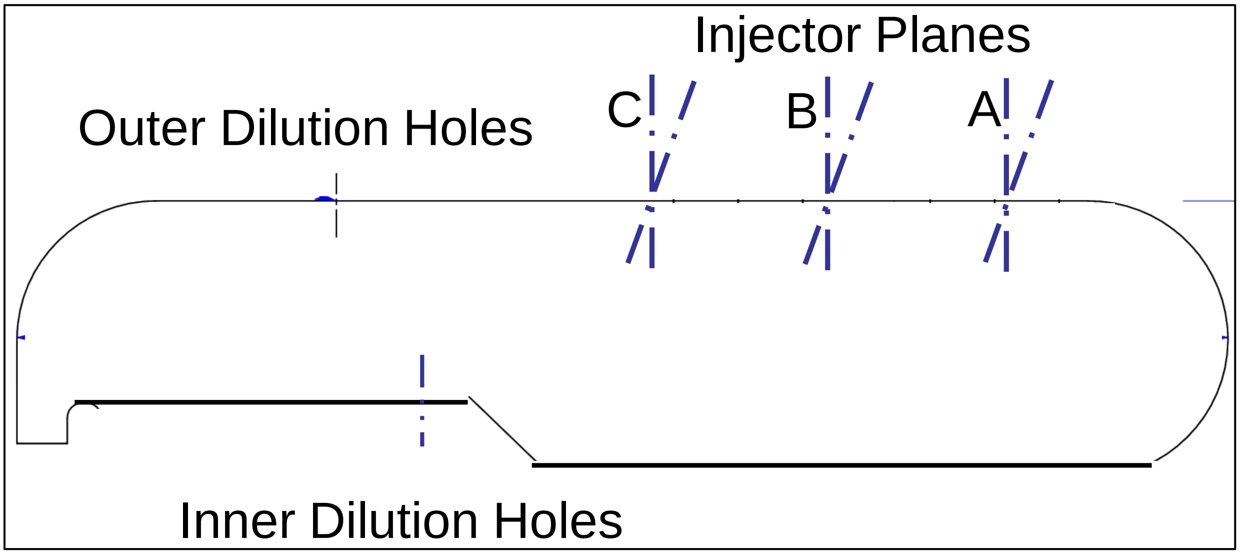

Figure 141: C370 Combustor Overall Layout (Section View)

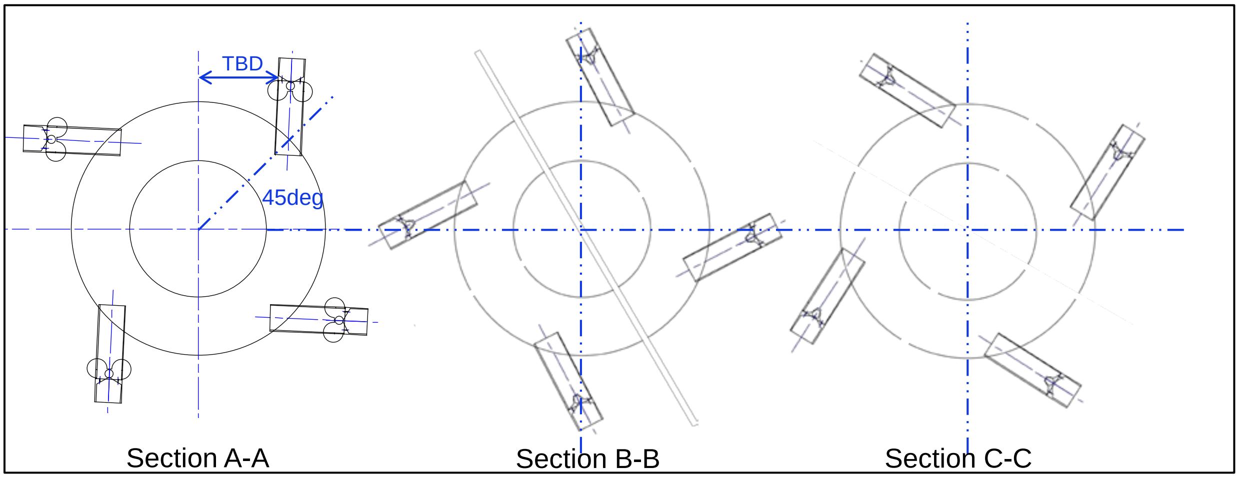

Figure 142: C370 Combustor Layout of Injector Planes

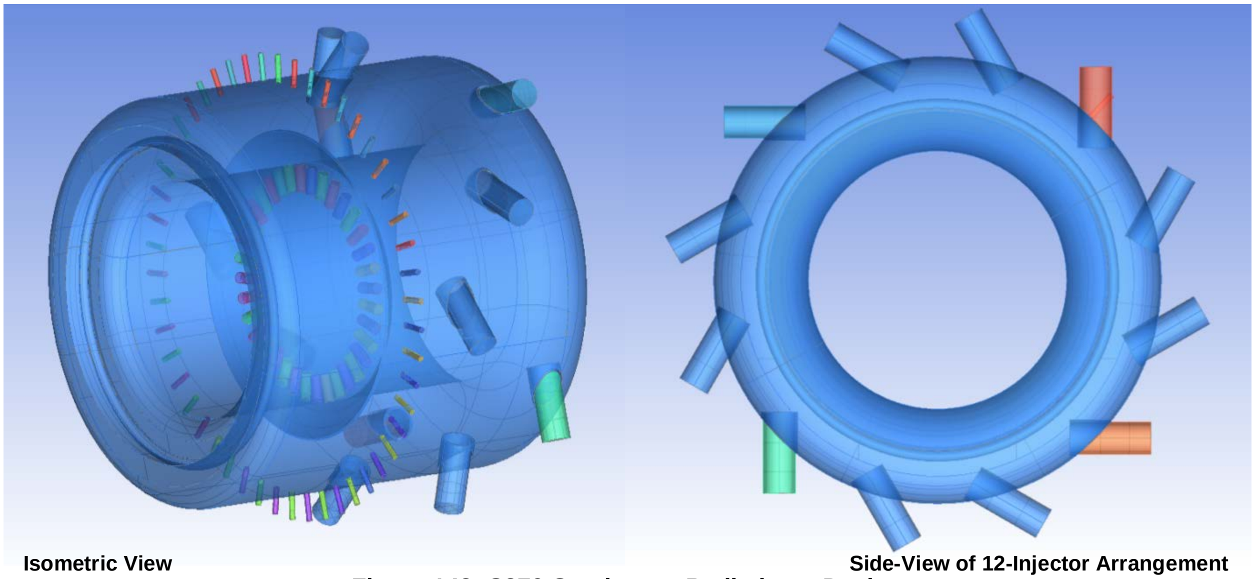

Figure 143: C370 Combustor Preliminary Design

The detailed sizing and geometric definitions of the C370 combustor are further defined in Figure 144. While keeping the inner diameters of the combustor unchanged for both inner — 7.12 in. — and outer liner — 12.32 in. — two different configurations of combustors are under consideration for the C370 with varying spacing between injector planes and dilution holes. The dimensions of the shorter combustor are labeled in black, those of the longer in red.

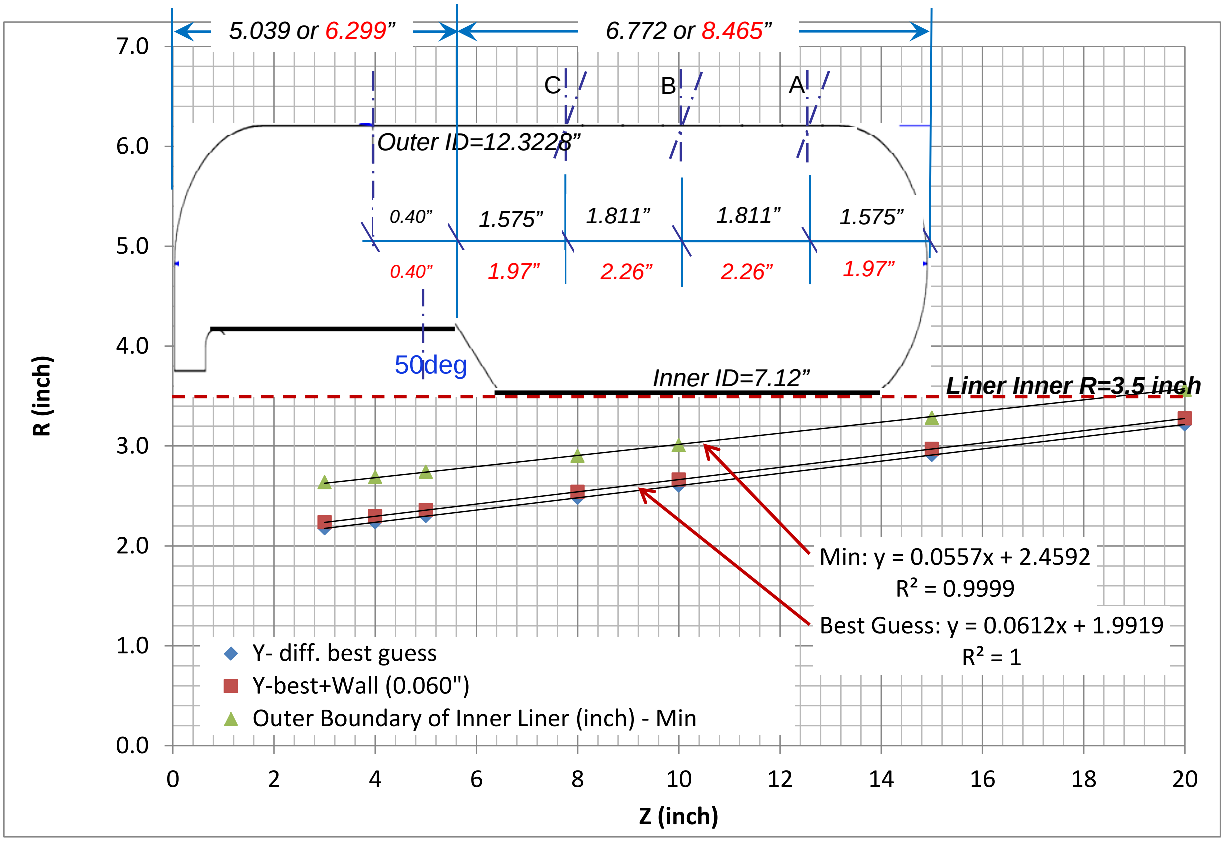

Figure 144: C370 Combustor Dimensions

To further define the combustion liner, geometric dimensions of the effusion holes, outer dilution holes, and inner dilution holes are needed. These parameters are listed in Table 38. The relative offsets of the inner and outer dilution holes are further illustrated in Figure 145.

6.0 Total Eff. Opening Area	in.^{2}	11.070	100.00%
Effusion Holes	in.^{2}	0.550	4.97%
Outer Dilution Holes	in.^{2}	1.025	9.26%
Area-All Injectors	in.^{2}	6.420	58.00%
Inner Dilution Holes	in.^{2}	3.075	27.78%

Table 38: C370 Combustor Liner Geometry

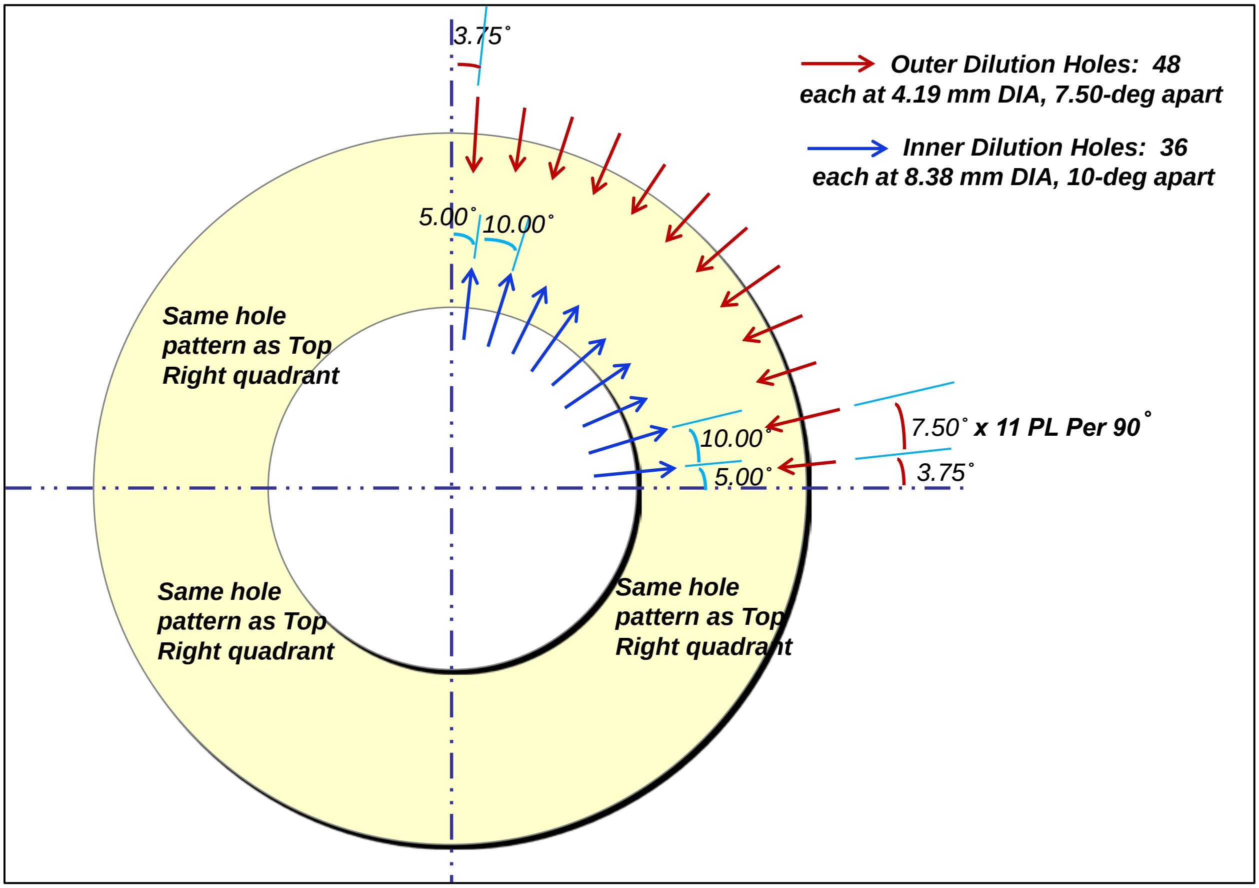

Figure 145: C370 Combustor Inner and Outer Liner Dilution Arrangement

Combustion System Down-Selection with CFD Simulation

As mentioned previously, there were two different lengths for different combustion PZ volumes which maintained the inner and outer IDs of the liner. The dilution zone has two different styles as well, which are labeled “big” and “small” dilution zones. As a result, there were four combustor candidate configurations as shown in Table 39.

	SHORT	LONG
Big Dil. Zone	Config.1 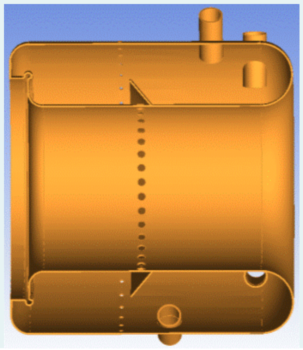	Config.2 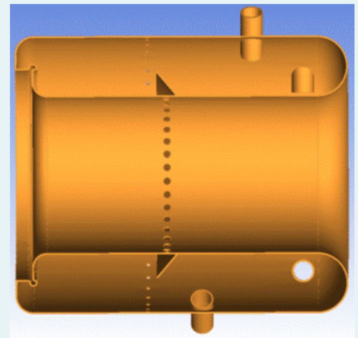
Small Dil. Zone	Config.3 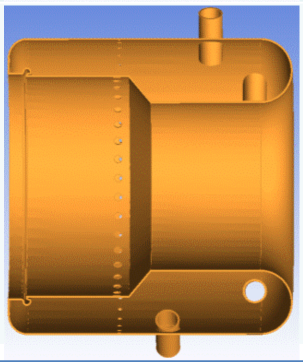	Config.4 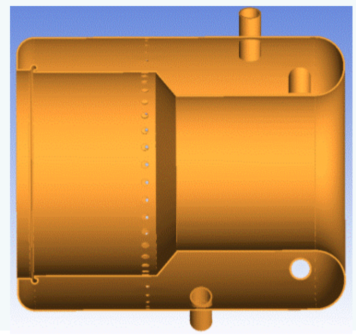

Table 39: C370 Combustor Candidate Configurations

To further compare the performance of these candidate combustor configurations, CFD simulations for Configurations 2 and 3 were performed to evaluate key combustion characteristics at the outlet of the combustor, such as peak temperature, pattern factor, pressure drop and NO_x emissions.

Meshing

The CFD modeling was performed for a 180° periodical section. As shown in Figure 146, based on geometry complexity, the combustion liner was divided to multiple modules for hybrid meshing as follows

- Each of the six injectors was meshed with hexahedral cells
- Combustion main domain was meshed with hexahedral cells
- Inner dilution hole regions were meshed with tetrahedral cells with prism layers
- Outer dilution hole regions were meshed with tetrahedral cells with prism layers
- Injector exit zone (PZ) was meshed with tetrahedral cells with prism layers

Some of the meshing details can be found in Figure 147.

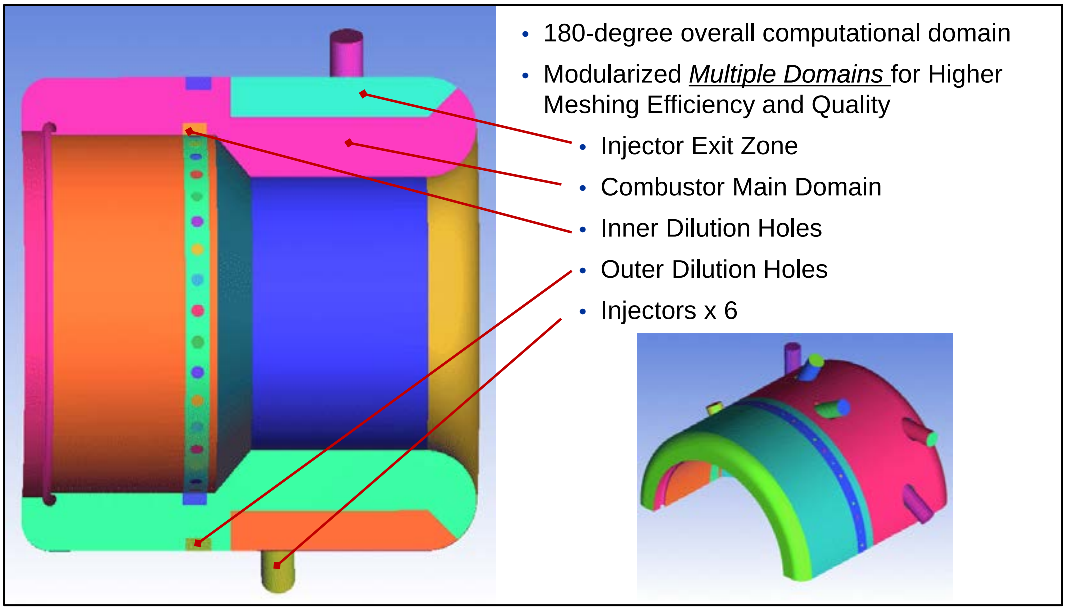

Figure 146: C370 Combustor Modularized Meshing Strategies

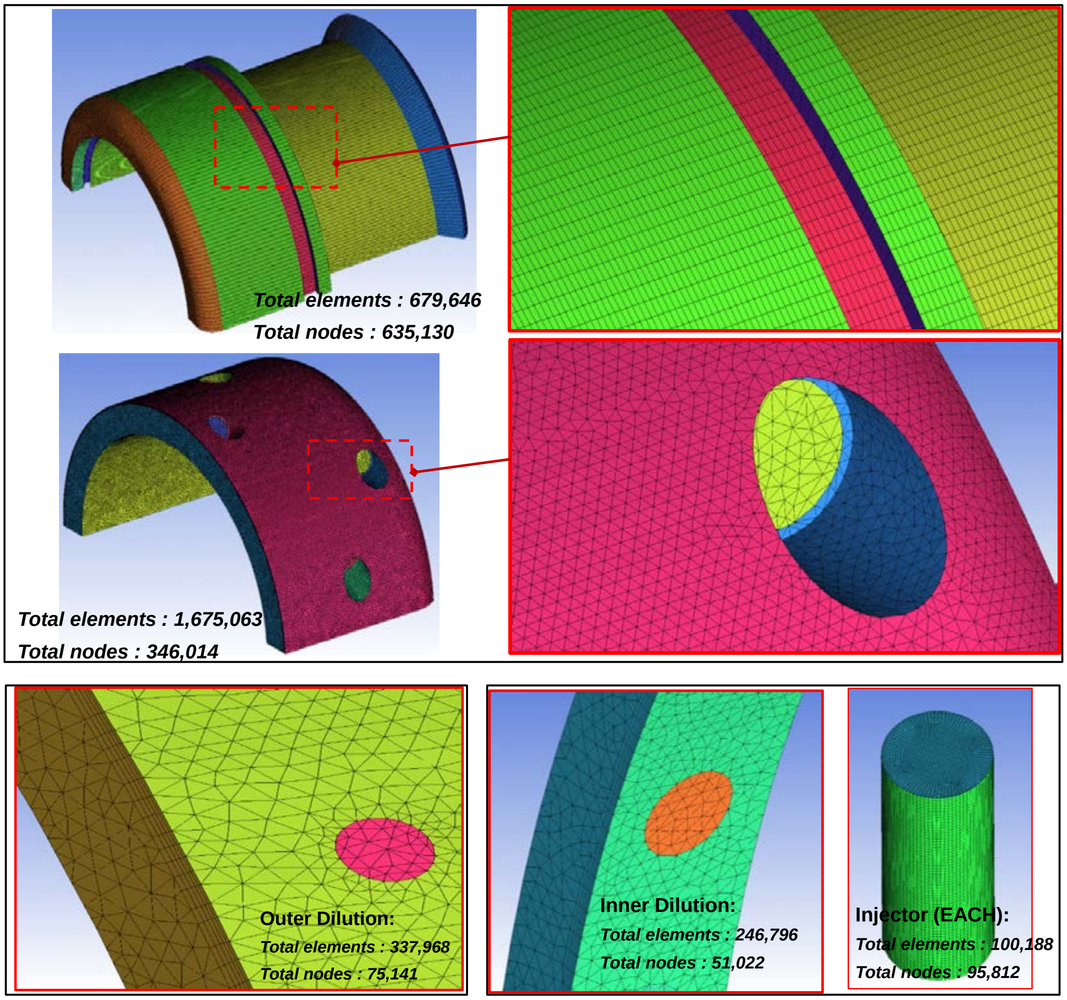

Figure 147: C370 Combustor Example Mesh Details

CFD Model Setup

The combustor is an important module in a gas turbine system. The combustor is designed to maintain balance between the combustion performance parameters such as emissions, combustion efficiency, and flow pattern. Due to the fact that the natural gas fuel — assumed to be 100% methane — and oxidizer — air — undergo rapid combustion in which combustion rate is dominated by the rate of mixing of the materials, the Eddy Dissipation model was applied to all the simulations referred in this report.

The chemical mechanism used was a one-step reaction "Methane Air WD1 NO PDF" in the CFX library. NO was modeled with thermal-NO formation mechanism and the O-radical was estimated based on O_2 concentration and temperature. Radiation was simulated with the P1 model.

While the outlet of the combustor is simulated with an average static pressure of 127.316 psig —defined by the C370 Cycle Deck — other boundary conditions are defined as mass flow rate inlet with appropriate speciation. The air splits to PZ via injectors, outer dilution holes, inner dilution holes, and effusion holes are 58%, 9.26%, 27.78%, and 4.96% respectively. The CFD setup in the CFX-Pre is illustrated in Figure 148.

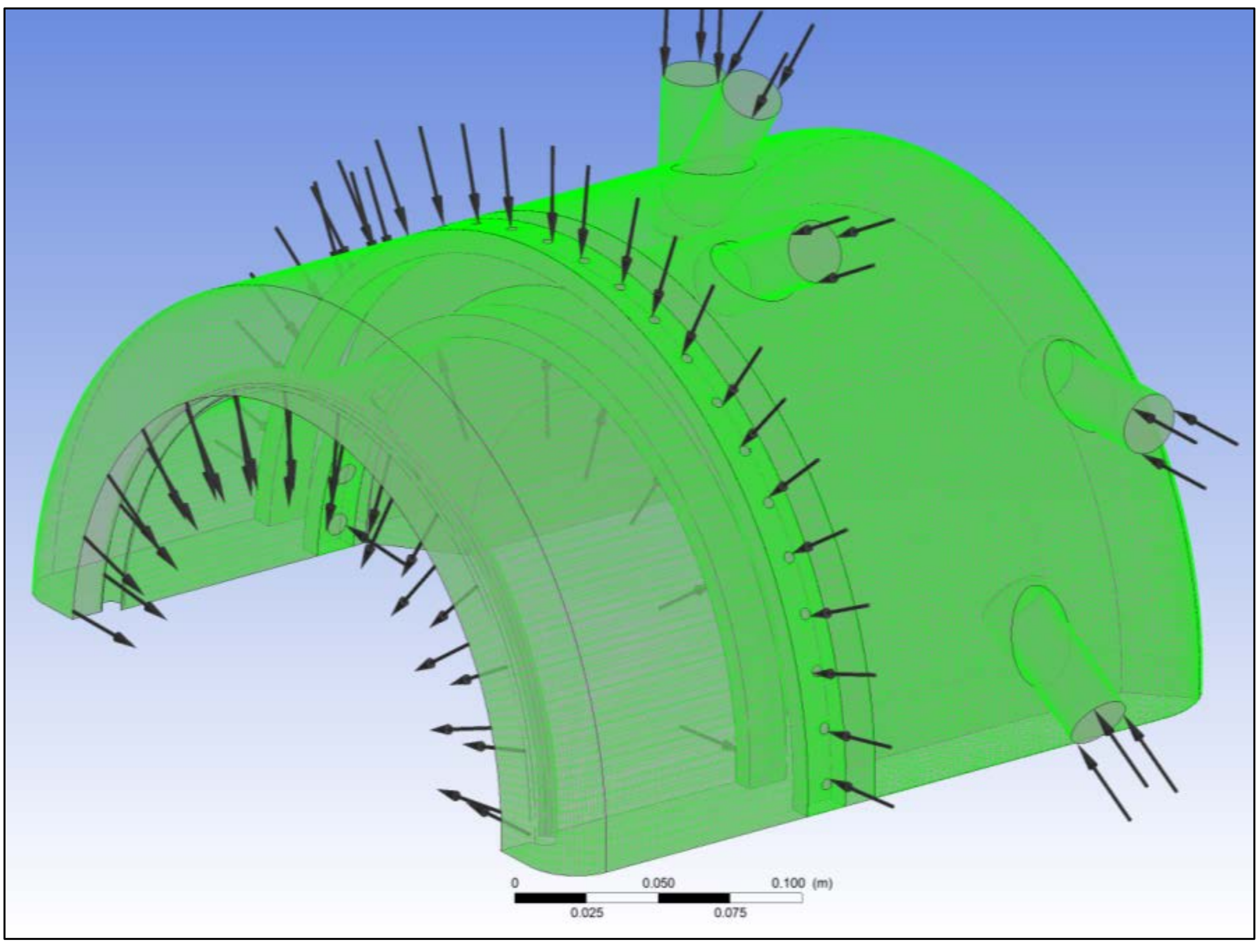

Figure 148: CFD Model Setup in ANSYS CFX-Pre

Combustion CFD Results

CFD simulations were performed for Configurations 2 and 3. Each of the configurations was examined for the different combination of injectors; a total of eight CFD cases were completed. The results are shown in Table 40.

Case No	Number of Injectors			dP	NO	Exit Avg. Temp	Exit Peak Temp	Pat Factor
	Plane C	Plane B	Plane A	%	ppm@15%O_2	°F	°F	—
208	4	4	2	0.88	1.66	2031	2276	0.23
207	4	2	4	0.76	1.57	2033	2280	0.23
206	2	4	4	0.87	1.52	2033	2254	0.21
205	4	4	4	0.87	1.59	2031	2276	0.23
309	4	4	2	0.86	1.56	2028	2321	0.28
308	4	2	4	0.86	1.46	2029	2299	0.25
307	2	4	4	0.86	1.45	2029	2299	0.25
311	4	4	4	0.86	1.56	2026	2343	0.30

Table 40: C370 Combustor Summary of CFD Results

The important results for the current phase of studies include the impact of the injector arrangement and the combustion volume on the performance the combustion process, which include combustor pressure drops, NO emissions, average temperatures, peak temperatures, and pattern factors at the exit of the combustor. The CFD results show that:

1. The overall pressure drop allowance for the combustion system is 3.3%. While the pressure drop of the combustor at full power operating point is less than 0.9% for all cases, the balance of the pressure drop allowance — 2.4% — can be used to further optimize combustion performance via further liner and/or injector optimization.
2. For NO_x emissions, the design target is 1.8 ppm @ 15% O_2. All eight design cases were able to reach the design targeted, ranging from 1.45 to 1.66 ppm at 15% O_2, with reasonable margin based on the simulations.
3. While the average combustor exit temperatures are close to the desired 2030 °F, the peak temperature of the combustion products varies from 2254 to 2343 °F. In general, the gas peak temperatures of the four different design cases for Configuration 3, as well as the pattern factor, are higher than those of the Configuration 2 cases. As a result, the Configuration 2 design cases are deemed to be superior to Configuration 3.
4. Staging capability consideration: Among the four design cases of Configuration 2, Case 205 has 12 injectors while the other three cases have only 10 injectors. The extra injectors give the combustion system extra air/fuel staging capability.

As a result, although Case 205 — Configuration 2 with 12 C65-sized injectors — does not have the lowest peak temperature or pattern factor, it is the most desirable C370 combustion configuration among the simulated cases because of its overall combustion performance and the flexibility in fuel and air staging.

6.10.3. Rotor dynamics and Bearing Design

7. HP Spool RBS Requirements

Design requirements were derived from thermodynamic cycle model predictions. Key requirements identified were:

- Oil free bearings
- RBS Life = 20,000 hours
- Rated Speed = 81,335 rpm @194 kW Net Output Power at HP Generator Lead
- Desired Over speed Margin = 7%
- RBS to provide dynamic load support at all engine operating conditions such as during start/stop, steady state and transient load cycles

8. Generator Rotor-Bearing System Design

8.1. Rotor Sizing

Generator rotor sizing was dictated by the following factors:

- Bearing surface speed
- Magnet retaining sleeve stress
- Retaining sleeve manufacturing process
- Generator electromagnetic design
- Rotor windage

Due to new HP Spool Generator design with high output power, the magnet shaft needed higher torque per unit rotor volume, resulting in increased magnet diameter. This necessitated different diameters at the magnet shaft and bearing journals to keep bearing DN number low and reasonable. Trade studies were performed by varying some of the factors described above to identify optimal rotor design with sufficient bending critical speed margin. The dimensions chosen were:

- Generator Shaft Journal Diameter = 1.65 in.
- Generator Shaft Sleeve Diameter = 1.875 in.
- Shaft Surface Speed = 665.42 ft/s (or 202.82 m/s)
- Radial Bearing Surface Speed = 585.57 ft/s (178.50 m/s)

8.2. Retaining Sleeve Sizing Analysis

The magnet size was dictated by the electromagnetic design which in turn fixed the magnet diameter. Magnet material has low tensile strength — at high speed it is prone to cracking due to centrifugal loading — and requires a retaining sleeve for magnet retention. This retaining sleeve must have high tensile strength, low electrical resistivity, and good thermal conductivity. In order to address design challenges, two nickel-based materials — Material A and Material B — were considered during the design phase. Trade studies were performed at various operating speeds, temperatures, and diametrical press fit values for both materials.

Numerical analyses were performed using a commercial FEA tool to estimate rotor stress for design verification. Figure 149 shows magnet stress and sleeve stress for Material A at operating conditions — high speed and temperature for a given value of press fit. The magnet stress is below the tensile stress limit of the magnet and the sleeve stress is below yield stress limit of Material A, providing sufficient design margin.

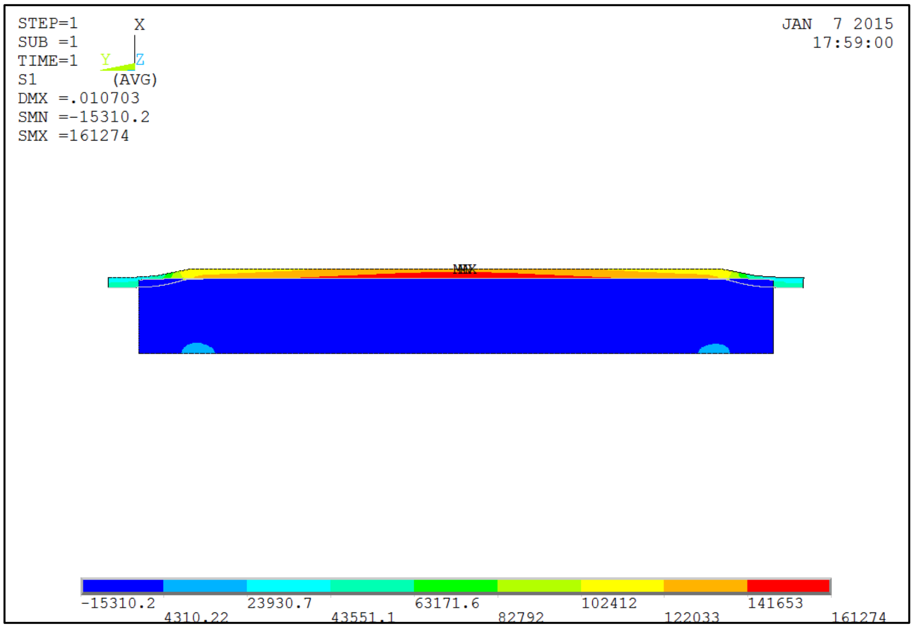

Figure 149: HP Spool Magnet and Sleeve Stress, Material A

Similarly, Figure 150 shows magnet stress and sleeve stress for Material B at operating conditions — high speed and temperature for a given value of press fit. The magnet stress is below the tensile stress limit of the magnet and the sleeve stress is below yield stress limit of Material B, providing sufficient design margin. The green stress band in the middle of the magnet is due to 29% higher press fit value chosen for this case.

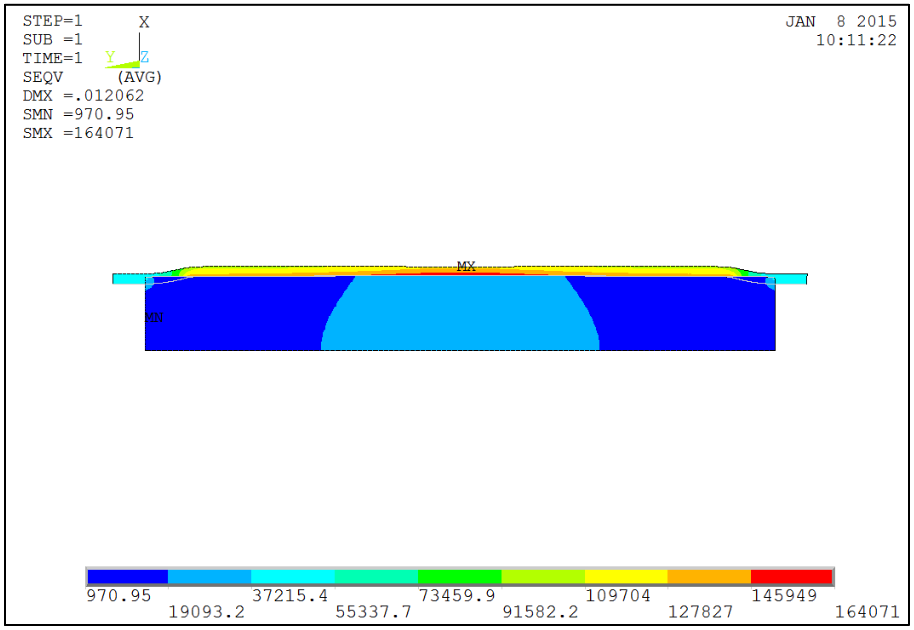

Figure 150: HP Spool Magnet and Sleeve Stress, Material B

Thermoplastic polymer matrix materials were also studied for this effort since they have high tensile strength and good weight-to-strength ratio, but were not analyzed due to low temperature rating of the material.

8.3. *Rotor dynamic Analysis*

8.3.1. UCS Model

An undamped critical speed (UCS) rotor dynamic model was constructed at various bearing stiffness values, using commercial FEA code to identify

- rigid body modes
- 1st bending critical

Figure 151 plots predicted rigid body modes — depicted in black and red lines — are below 30,000 rpm, which is below HP Spool operating speed of 81,335 rpm. The 1st bending mode — depicted by the green line — is at 120,568 rpm, thus providing 48% critical speed design margin. Free-Free natural frequency analysis was performed to identify the true natural frequency of the rotor group, which will provide a baseline for rotor dynamic model verification via Rap test on the physical hardware. This predicted free-free natural frequency is calculated as 111,820 rpm.

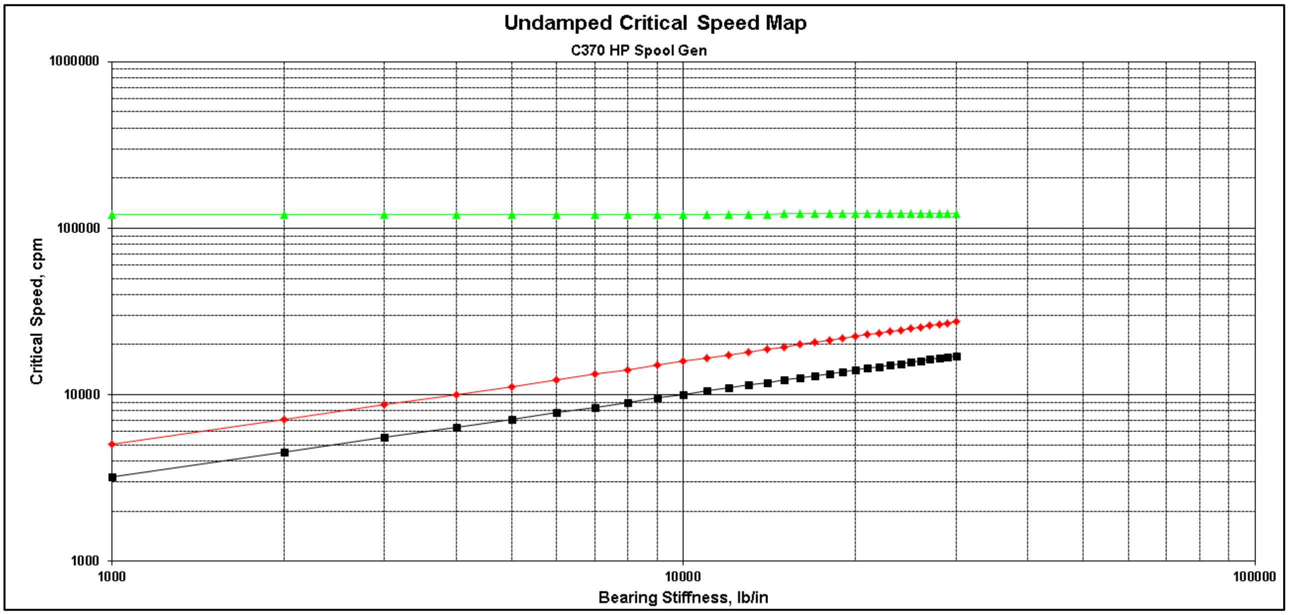

Figure 151: Generator Rotor Group UCS Map

8.3.2. Damped Eigen Value and Synchronous Forced Response Analysis

After bearing design, calculated dynamic force coefficients were used in the rotor dynamic model as an input to perform stability analysis — Damped Eigen Value. Additionally, synchronous forced response analysis was performed per ISO G2.5 balance standard for in and out of phase imbalance conditions for synchronous response and bearing dynamic loads. All results showed satisfactory rotor group performance at all operating conditions.

8.4. Generator Radial Bearing Sizing

Radial bearings were sized based on the following factors:

- DN number
- psi load
- power loss

Generator rotor speed was chosen based on fixed DN number for the bearing based on prior experience with similar foil bearing-supported Capstone microturbines. Once rotor mass was determined based on electromagnetic analysis of the generator, psi load on the bearing was calculated. Using in-house bearing design code, dynamic force coefficients were calculated at different operating conditions and bearing loads to create a bearing performance map. Bearing design was optimized based on stiffness and damping needed to provide load support and acceptable levels of rotor synchronous response in rotor dynamics code.

The bearing performance map also included power loss, which is needed to size secondary cooling flow to dissipate heat from the bearings for stable rotor-bearing system operation. Sizing is as follows:

- Generator Shaft Journal Diameter = 1.65 in.
- Bearing Surface Speed = 585.57 ft/s (178.50m/s)

9. Turbine Rotor-Bearing System Design

9.1. Rotor Sizing/Scaling

Sizing of the turbine rotor group was dictated by the aerodynamic design of the turbine and compressor wheels. Aerodynamic blade profile for the wheels changed, but the tip diameters were comparable to Capstone C65 microturbine wheels, i.e. the psi loading on the radial bearings is similar to C65. No new bearing design is needed. Similarly, axial loads were comparable to C65; hence no new thrust bearing design is needed. Therefore, the HP spool turbine section uses the same radial and thrust bearings as a C65 microturbine. The rotor group grew axially, due to slightly longer wheel base, but the effect of loading is minimal on the bearings. Rotor group sizing is as follows:

- Turbine Shaft Journal Diameter = 1.40in
- Bearing Surface Speed = 496.84 ft./s (151.43m/s)

9.2. Rotor dynamic Analysis

Since the rotor group grew axially — due to slight changes in the wheel's base — re-evaluation of the rotor dynamics of turbine rotor-bearing system became necessary. A similar approach was taken to that described in Rotor dynamic Analysis section of Generator Rotor-Bearing System Design.

9.2.1. UCS Model

An undamped critical speed (UCS) rotor dynamic model was constructed at various bearing stiffness values, using commercial FEA code to identify

- rigid body modes
- 1st Bending Critical

Predicted rigid body modes — depicted in black and red lines in Figure 152 — are below 20,000 rpm, which is below the HP Spool operating speed of 81,335 rpm. The 1st bending mode — depicted as a green line — is at 181,742 rpm, providing 123% critical speed design margin. Use of existing bearing design allows much stiffer rotor group. Free-Free natural frequency analysis was also performed to identify true natural frequency of the rotor group, which will provide a baseline for rotor dynamic model verification via Rap test on the physical hardware. This predicted free-free natural frequency is calculated as 111,172 rpm. Adding bearing stiffness to the Free-Free model significantly increases the critical speed margin for UCS.

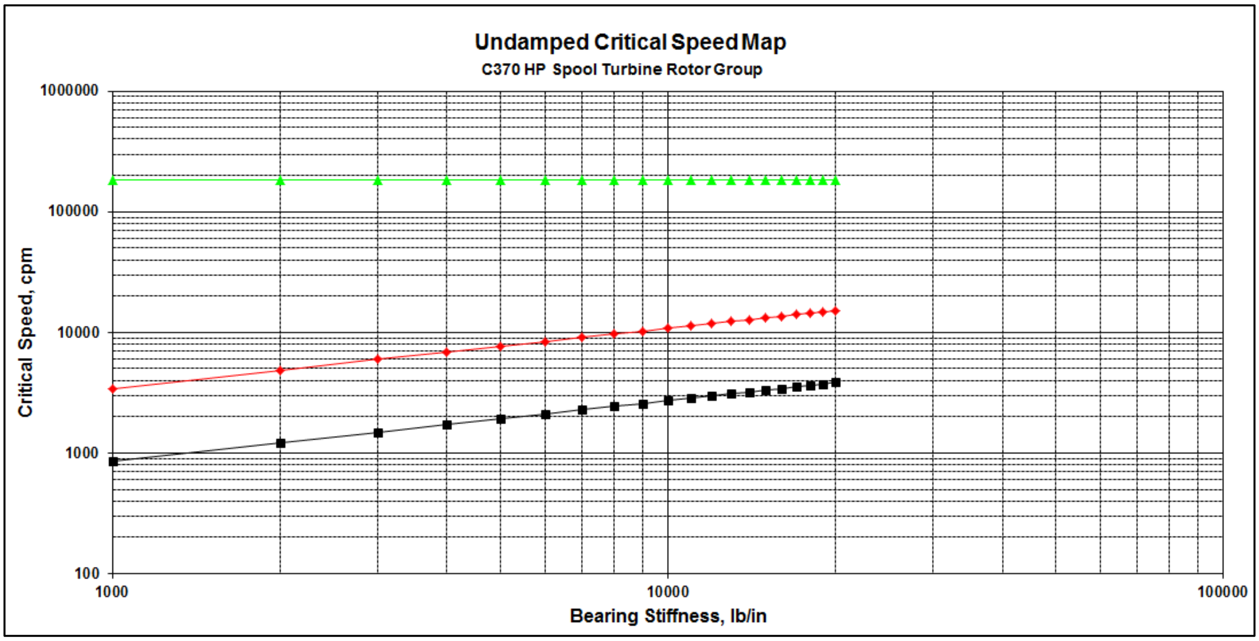

Figure 152: HP Spool Turbine Rotor Group UCS Map

9.2.2. Damped Eigen Value and Synchronous Forced Response Analysis

Bearings dynamic force coefficients were used in the rotor dynamic model as an input to perform stability analysis — Damped Eigen Value. Additionally, synchronous forced response analysis was performed per ISO G2.5 balance standard for in and out of phase imbalance conditions for synchronous response and bearing dynamic loads. All results showed satisfactory rotor group performance at all operating conditions.

9.3. Turbine Radial and Axial Bearing Sizing/Analysis

No change in bearing size, due to similar radial and thrust loads as Capstone C65 microturbine.

10. HP Spool Fully Assembled Rotor Group

Figure 153 shows the fully assembled HP Spool Rotor Group, comprised of generator and turbine rotor groups coupled via flexible coupling. The coupling is designed for lateral and torsional stiffness needed to keep both rotor groups vibrations isolated from each other yet spinning in synchronous fashion with respect to each other.

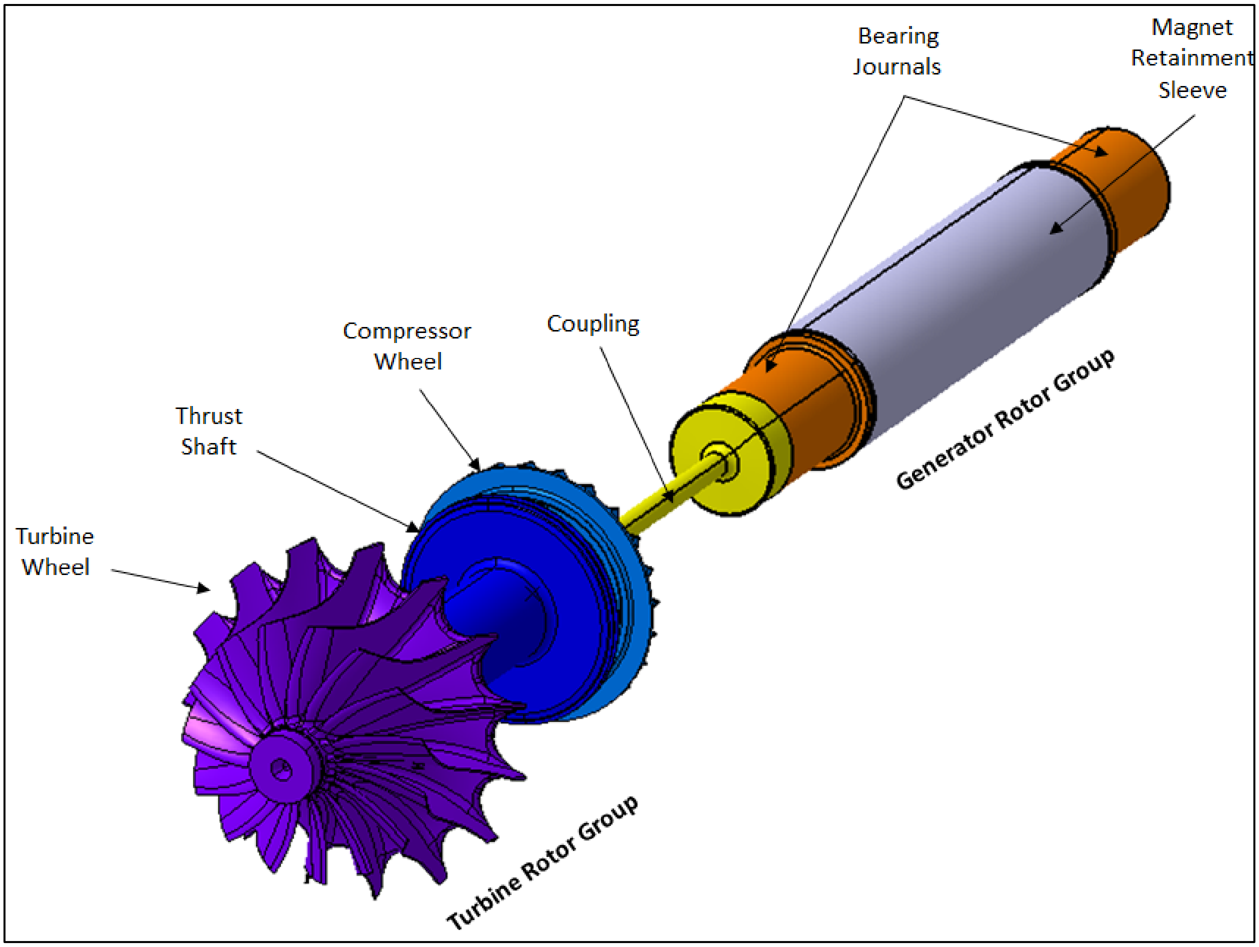

Figure 153: HP Spool Rotor Group Assembly Diagram

10.1.1. Compressor Design

Compressor Stage Design Objectives and Requirement

The design point operating conditions and performance goals for the compressor are summarized in Table 41. These were unchanged from those stated in the preliminary design exercise. The C370 high pressure stage design is targeted to have a single stage centrifugal impeller and a diffuser. The upstream interface to the high pressure compressor stage is a radial inlet duct and the downstream interface is a volute.

Parameter	Unit	Value	Remarks
Pressure Ratio		2.6	Total-Static
Rotational Speed	rpm	81,335	NOM Speed
Mass Flow	lbm/s	2.89	Pure Dry Air
Inlet Total Temperature	°F	98.3	At Compressor Inlet
Inlet Total Pressure	psia	56.465	
Surge Margin	%	10	
Choke Margin	%	12	
Stage Poly. Efficiency	%	84.60	Total-Static
Running tip clearance	in	0.005	Axial
	in	0.01	Radial

Table 41: C370 High Pressure Compressor Stage Aerodynamic Requirements

Compressor Stage Design – Impeller

To fulfill the design target, a compressor stage was developed. The compressor impeller has 8 main blades and 8 splitter blades as shown in Figure 154. To increase the primary blade flapping mode, the impeller has an increasing blade thickness on the hub, near the leading edge, and canting the leading edge back about 5°. The main and splitter blade lead edge angles were set to keep the blade loading at reasonable levels at both the design point and lower flows. The back-sweep angle was set at -47.5° and the exit lean at 30° to balance design point performance while maximizing flow range and lowering blade root stresses near the exit.

Compressor Stage Design – Diffuser

The chosen diffuser is a low-solidity airfoil diffuser with 10 vanes — shown in Figure 154 — used to avoid interference with the impeller blade natural frequencies. The diffuser is predicted to stall before the impeller. Therefore, the blade setting angle chosen maximizes the flow range without reducing design point performance significantly.

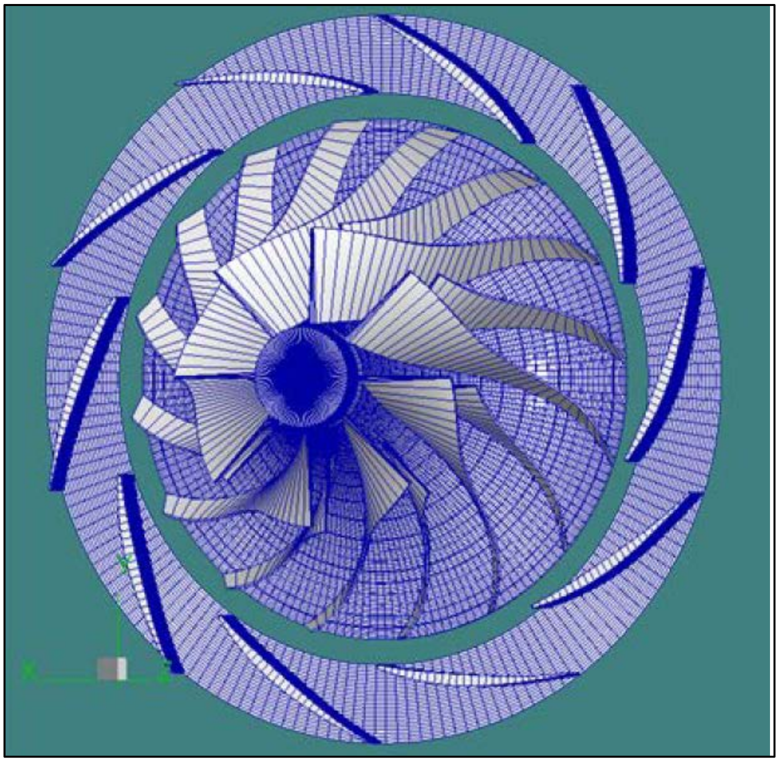

Figure 154: C370 High Pressure Compressor Stage Design

Compressor Stage Performance

The compressor stage performance was evaluated using two different approaches: mean line performance prediction and CFD simulations. The mean line prediction results are shown in Table 42. A comparison of mean line and CFD predictions are shown in Table 43 and Figure 155. The results of both approaches meet design target. CFD predictions achieve a stage total-to-static pressure ratio of 2.64 and 84.9% for stage polytropic efficiency. A compressor performance map was generated based on the mean line prediction and corrected by CFD prediction as shown in Figure 156.

Mass Flow (lbm/s)	2.89	Impeller Exit Mach Number	0.744
Shaft Rotational Speed (rpm)	81,335	Impeller Flow Angle (deg – mrd)	72.940
Stage Aerodynamic Power (hp)	211.34	Impeller Tip Speed (ft/s)	1394
Stage Pressure Ratio T-T	2.655	Diffuser Pressure Recovery Coefficient	0.651
Stage Pressure Ratio T-S	2.642	Diffuser Loss Coefficient	0.166
Stage Efficiency T-T Poly-Real	0.853	Volute Pressure Recovery Coefficient	0.459
Stage Efficiency T-S Poly-Real	0.849	Volute Loss Coefficient	0.463
Rotor Efficiency	0.913	Compressor Exit Mach Number	0.083
Inlet Relative Mach Number	0.831	Specific Speed (NSUS)	107.4
		Machine Reynolds Number	1.06E+07

Table 42: C370 HP Compressor Mean line Design Point Performance Prediction

	Mean line	Pushbutton CFD
Mass Flow	2.890	2.868
ETAtt, End of Diffuser	0.869	0.883
PRtt, End of Diffuser	2.730	2.907
PRts, End of Diffuser	2.569	2.688

Table 43: C370 HP Compressor Performance Comparison between Mean line and CFD Approaches

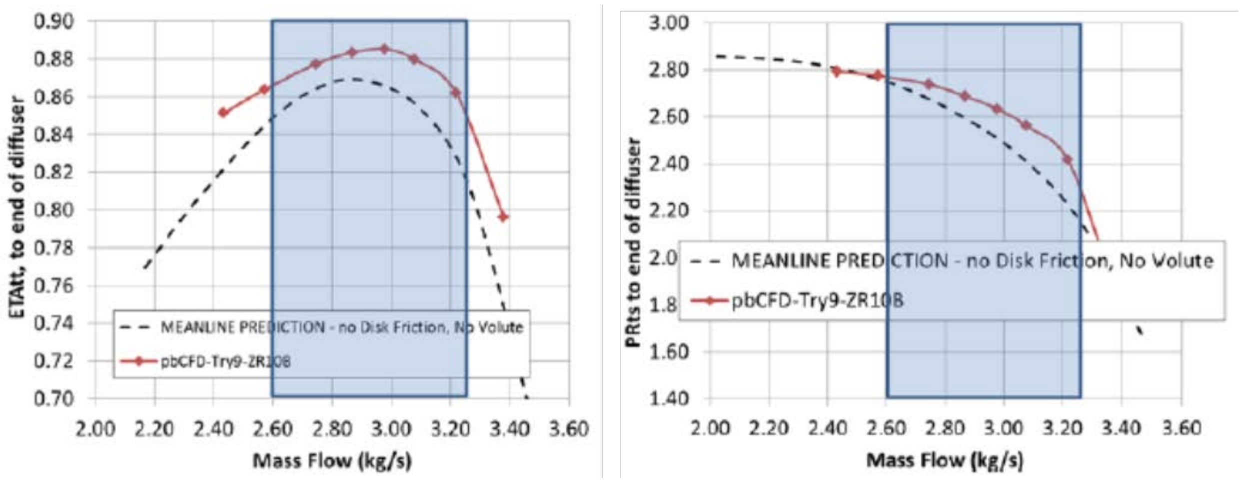

Figure 155: C370 HP Compressor Comparison of Mean line and CFD Prediction at Design Speed

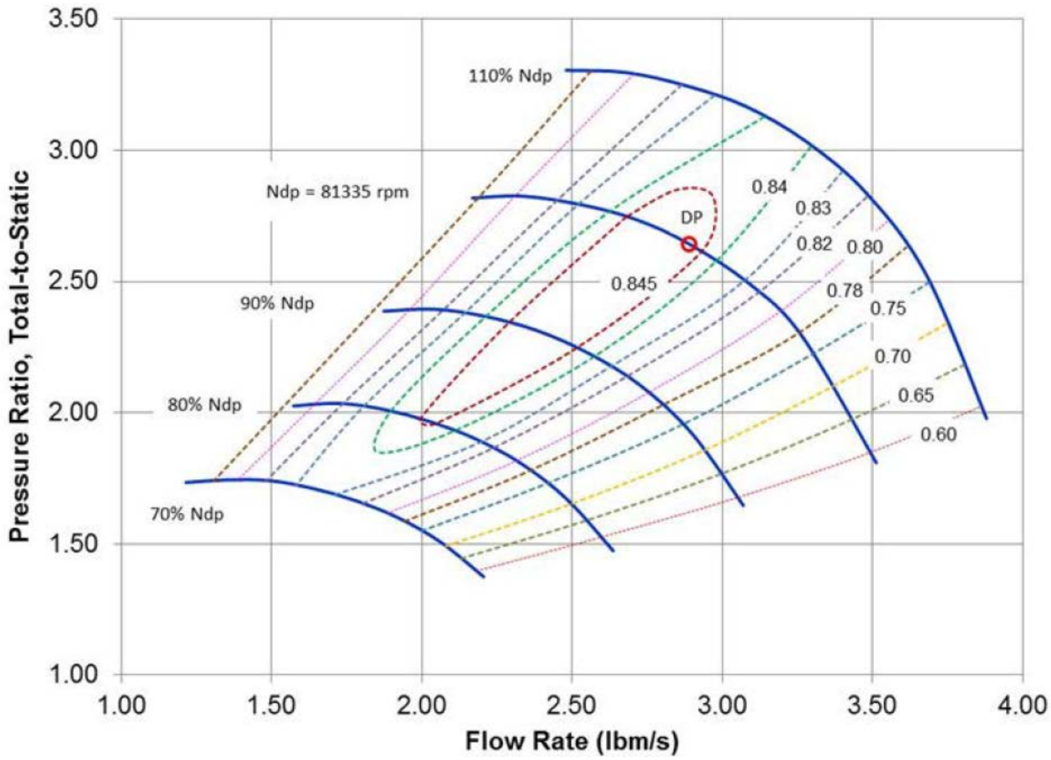

Figure 156: C370 HP Compressor Performance Map

The pressure loadings from three of the pushbutton CFD runs — representing near surge, design point, and near choke — are presented in Figure 157. Both the impeller blades and the diffuser vanes were set in order to keep the loading levels reasonable for even the lowest flow rate expected. On the shroud, the loadings near the leading edge of the main blade are slightly negative at the design point.

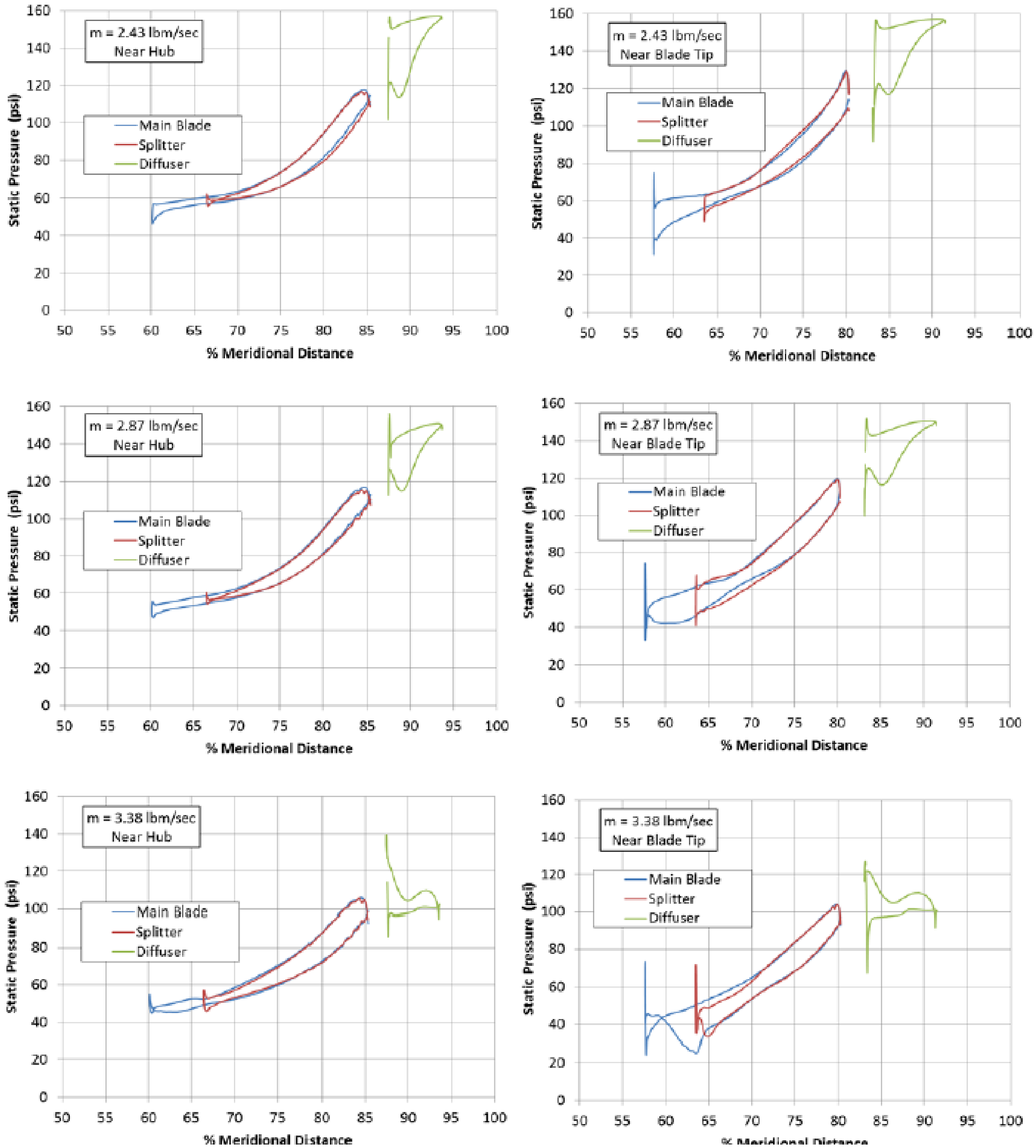

Figure 157: C370 HP Compressor Blade Loading Distribution from CFD

The mid-passage meridional velocity at the design point is shown in Figure 158. There appears to be an area of recirculation in the knee region of the impeller — which seems to be contained within the tip clearance gap — and some near the leading edge of the diffuser. Neither is expected to be an issue. Overall, the compressor stage meets design target. The CFD analysis also suggested a flow range of 10% surge margin and 12% choke margin.

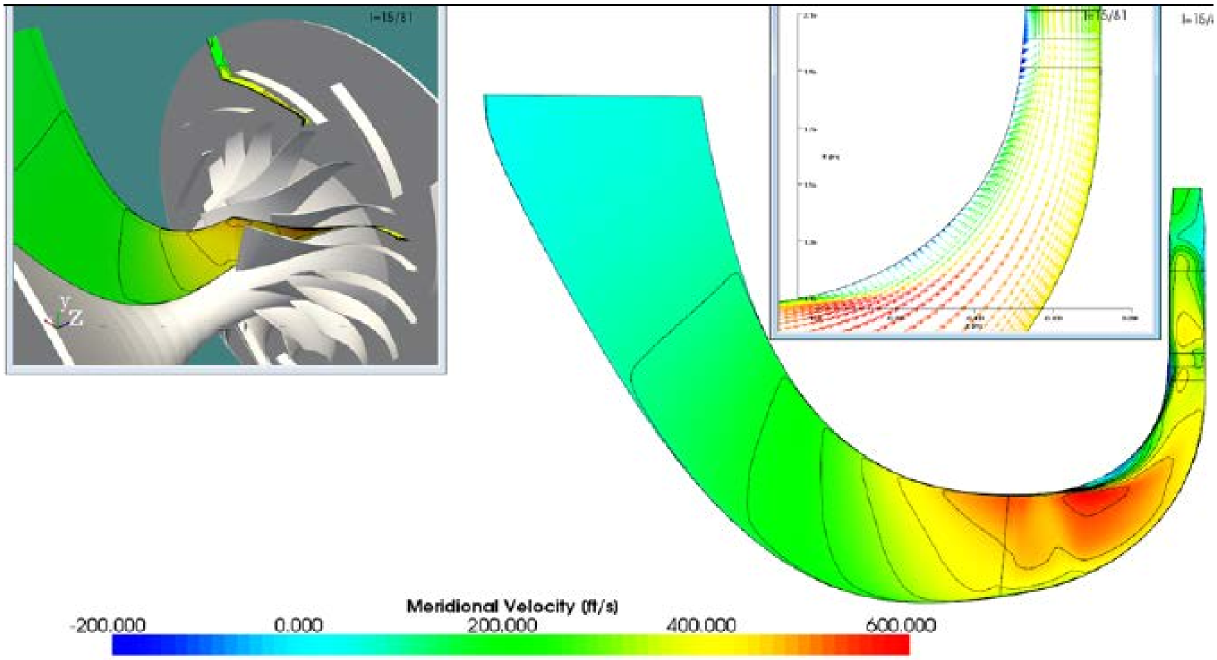

Figure 158: C370 HP Compressor Stage Mid-Passage Meridional Velocity Profiles at the Design Condition

10.1.2. Turbine Design

Turbine Stage Design Objectives and Requirement

The design of the high pressure turbine stage included three major components: (1) a turbine nozzle, (2) a turbine rotor, and (3) an exhaust diffuser. A performance target of the turbine stage is listed in Table 44.

Parameter	Unit	Value	Remarks
Stage Inlet Total Temperature	°F	2,030	
Rotor Relative Tip Total Temperature	°F	1,866	Max temperature allowed
Inlet Total Pressure	psia	138.046	
Mass Flow Rate	lbm/s	2.87	
Expansion Ratio		2.40	Total-Static
Rotational Speed	rpm	81,335	
Blade Speed Ratio		0.716	
Turbine Diameter	in	5.25	Max diameter allowed
Stage Isen. Efficiency	%	87.89	Total-Total
Stage Isen. Efficiency	%	87.26	Total-Static
Running tip clearance	in	0.040	Axial
	in	0.012	Radial

Table 44: C370 HP Turbine Design Requirement

Turbine Stage Design – Turbine Nozzle

The nozzle blade for the C370 HP turbine stage is a 2D design. It has a constant section in the span-wise direction. It is designed to have good passage area contraction and smooth variations in surface curvatures. The nozzle blade profile is shown in Figure 159.

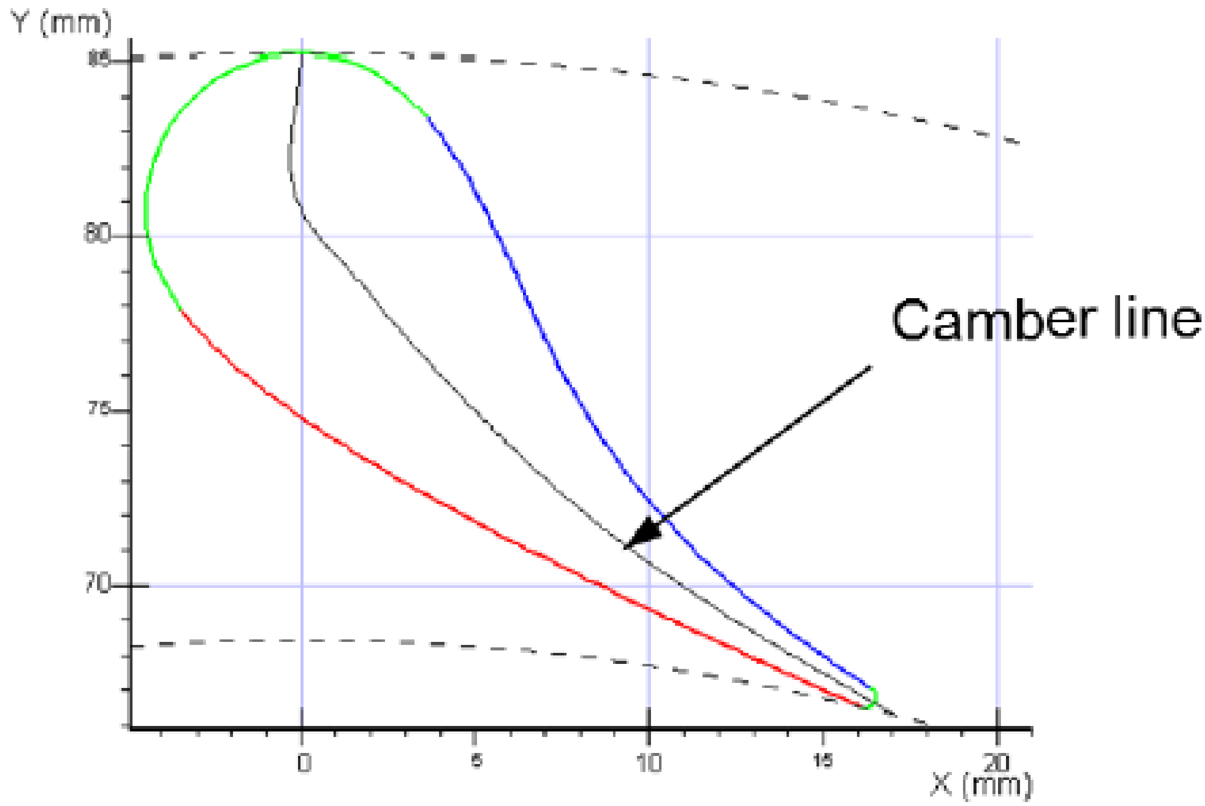

Figure 159: C370 Turbine Nozzle Blade Profile for HP Turbine Stage

Turbine Stage Design – Turbine

The rotor blade is defined using radial elements for minimum stress. The camber line is defined on a cylinder of arbitrary radius. The blade angle variation is defined on any contour — such as the hub, mid-span, or tip — and is calculated from that contour. The mid-span blade angle is plotted as a function of axial distance — as shown in Figure 160 — which also shows the passage-average relative flow angle.

The blade angle variation controls the blade loading and, in an effort to reduce the loading near the trailing edge and alleviate the problem due to secondary flow and tip leakage in the tip-suction surface corner of the blade, the turning was reduced as far as possible near the trailing edge. Figure 160 indicates that the maximum blade angle occurs not at the trailing edge, but some small distance upstream. This is an acceptable solution if not taken to extremes.

The differences between the blade and flow angles at the leading edge and the trailing edge are measures of the incidence and deviation angles respectively.

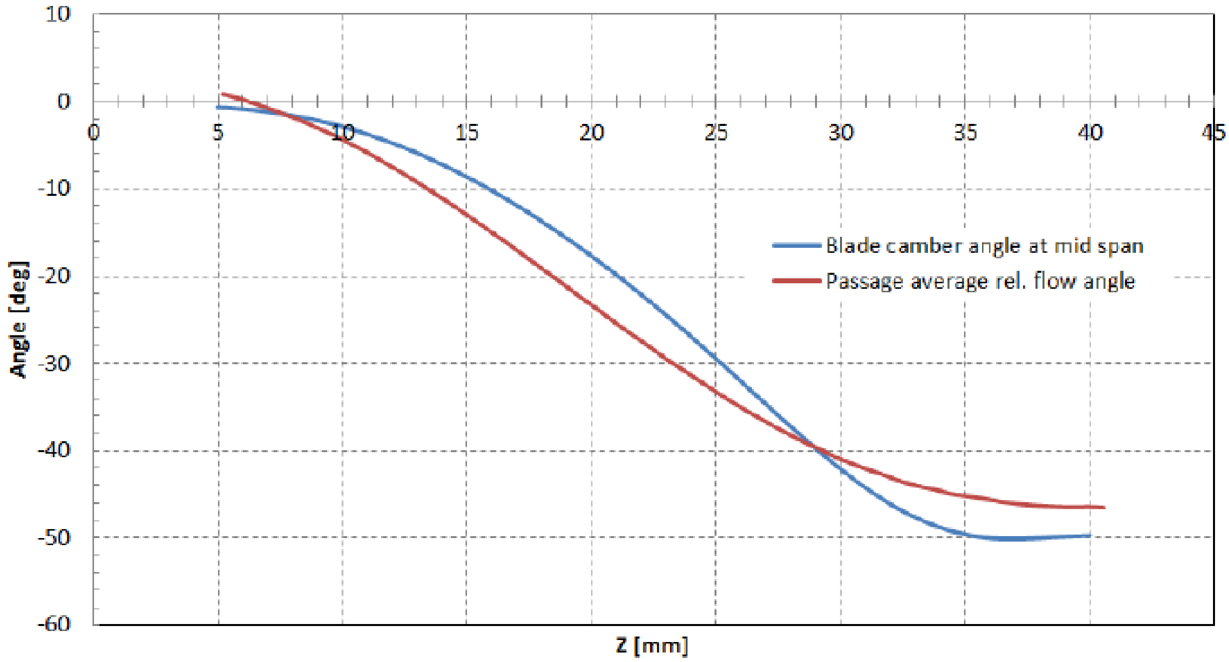

Figure 160: C370 HP Turbine Blade Camber and Flow Angles for HP Turbine Stage

Turbine Stage Design – Exhaust Diffuser

The development team recognized need for an exhaust diffuser to achieve the target total-to-static efficiency. It was important to determine the space required for the diffuser, since the performance of a diffuser depends strongly on size. Extensive information about the performance of conical diffusers is available from laboratory testing, but this is not always directly applicable to turbines because the flow field leaving the turbine rotor and entering the diffuser may be considerably different from the well-controlled and uniform flow field obtained in the laboratory. Therefore, a 2-step process was developed. First, use published lab test data to estimate exhaust diffuser size. Second, use CFD for the complete turbine stage simulation to predict and validate the exhaust diffuser performance.

The lab test data used exit and inlet area ratio, the length to inlet radius ratio, and diffuser divergence angle to estimate pressure recovery coefficient. An estimated efficiency of the turbine stage is shown in Figure 161 which is based on the lab test data. Through the process, it is suggested that a minimum exhaust diffuser length of 16 in. is required.

The exhaust diffuser was designed to have a 0.47 in. (12 mm) length of straight just downstream of the rotor trailing edge, a 15.75 in. (400 mm) length of straight conical section with a divergence angle of 6.4°, and a 5.9 in. (150mm) length of straight downstream of the conical section.

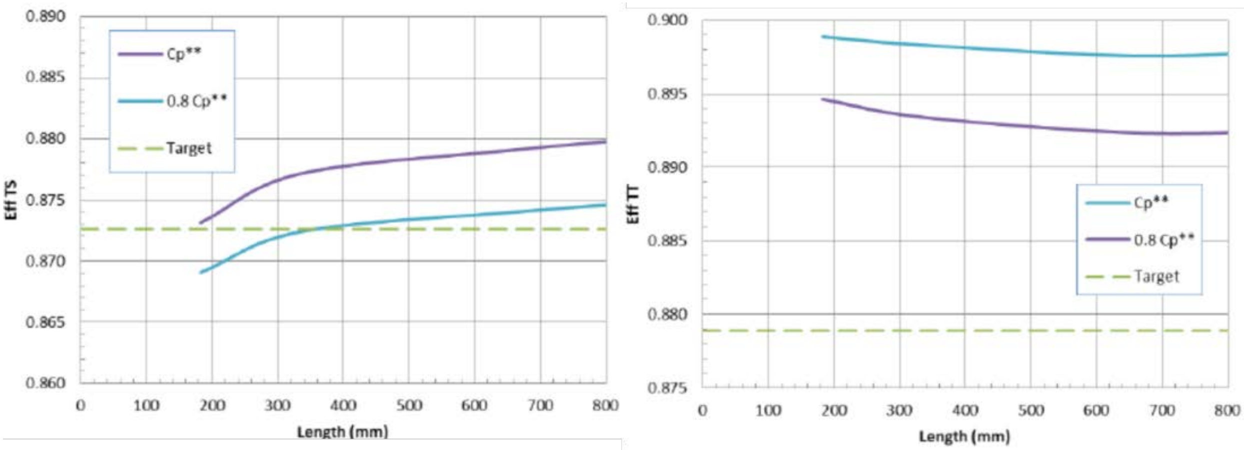

Figure 161: C370 HP Turbine Efficiency vs. Diffuser Length

Turbine Stage Design – Stage Performance

An initial turbine stage CFD simulation was conducted. The simulation was first run without the diffuser, and the total-to-total (t-t) and total-to-static (t-s) efficiencies were compared to simulation with the diffuser as shown in Table 45. The CFD result indicates 2.5 points of total-to-static efficiency gain is observed due to the diffuser.

	Without Diffuser	With Diffuser
$\eta_{t\text{-}t}$	90.4%	89.2%
$\eta_{t\text{-}s}$	85.9%	88.4%

Table 45: C370 HP Turbine Stage CFD Prediction

The design was then coupled with structural considerations. The resulting design that met all of these requirements was run through CFD to determine the impact on performance. It was found that the structural changes caused a decrease in T-S efficiency to 87.1%. This is slightly lower than the design goal of 87.26%.

10.1.3. Recuperator Internal vs External Tradeoff Analysis

For the initial prototype system, it was determined that the first lab prototype would use an external recuperator rather than our current integrated recuperator. Figure 163 shows the difference in the concept designs of an integrated versus externally-recuperated C370 engine. A 2-step approach was determined to be the safest path. Performance would be easier to measure with an externally-recuperated prototype that would be eventually being built into a more compact integrated design at the next prototype stage.

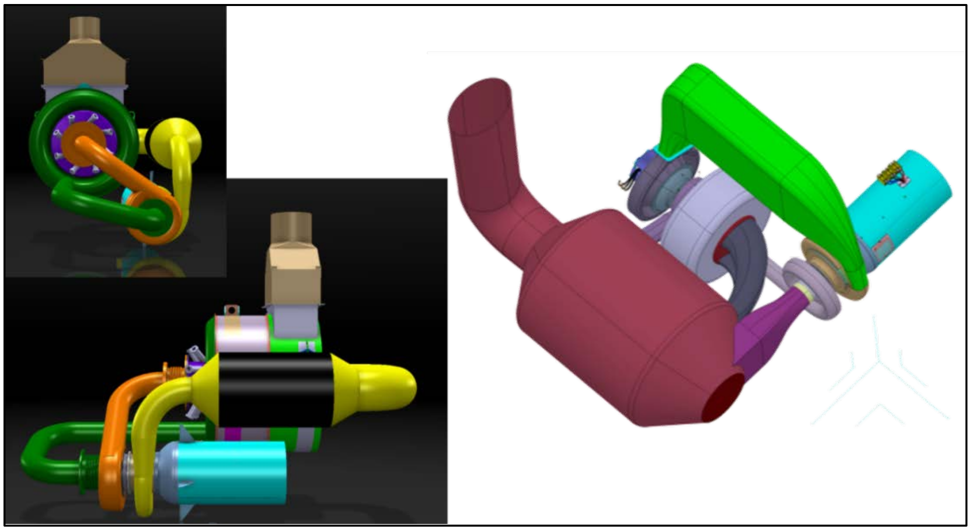

Figure 162: C370 Integrated vs. External Recuperator Prototype Configurations

Performance calculations of existing C200 integrated recuperator versus an external design were completed. Figure 164 details the results of these calculations. Performance was very similar and only varied by 0.8% effectiveness, which would be almost unmeasurable at the system level. Since performance was not an issue, the only other item to address was the higher pressure ratio.

	ACTE Core	C200 Core	C370 (C200 Core)
Air Mass Flow (kg/sec)	1.284	1.42	1.284
Air Tin (° F)	338	383	338
Air Pin (psig)	129.912	44.1	129.912
Gas Mass Flow (kg/sec)	1.354	1.44	1.354
Gas Tin (° F)	1114	1195	1114
Gas Pin (psig)	0.455	0.424	0.455
Effectiveness (%)	92	90.3	91.2
Air delta P (psi)	0.96	1.01	0.92
Gas delta P (psi)	0.33	0.44	0.41
Length (ft)	4	3	3
Diameter (ft)	3.2	3	3

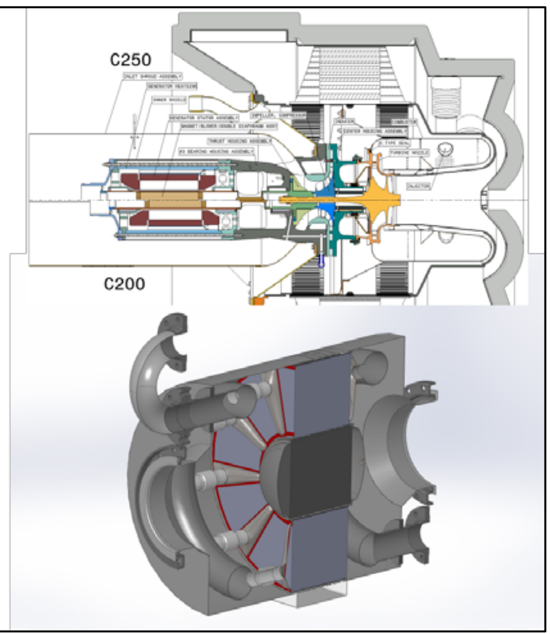

Figure 163: C370 Integrated vs. External Performance Predictions and Cross Sections

A study was done to determine the stress on the recuperator cells and the 11:1 pressure ratio. Figure 165 shows the results of the stresses at the higher stress levels.

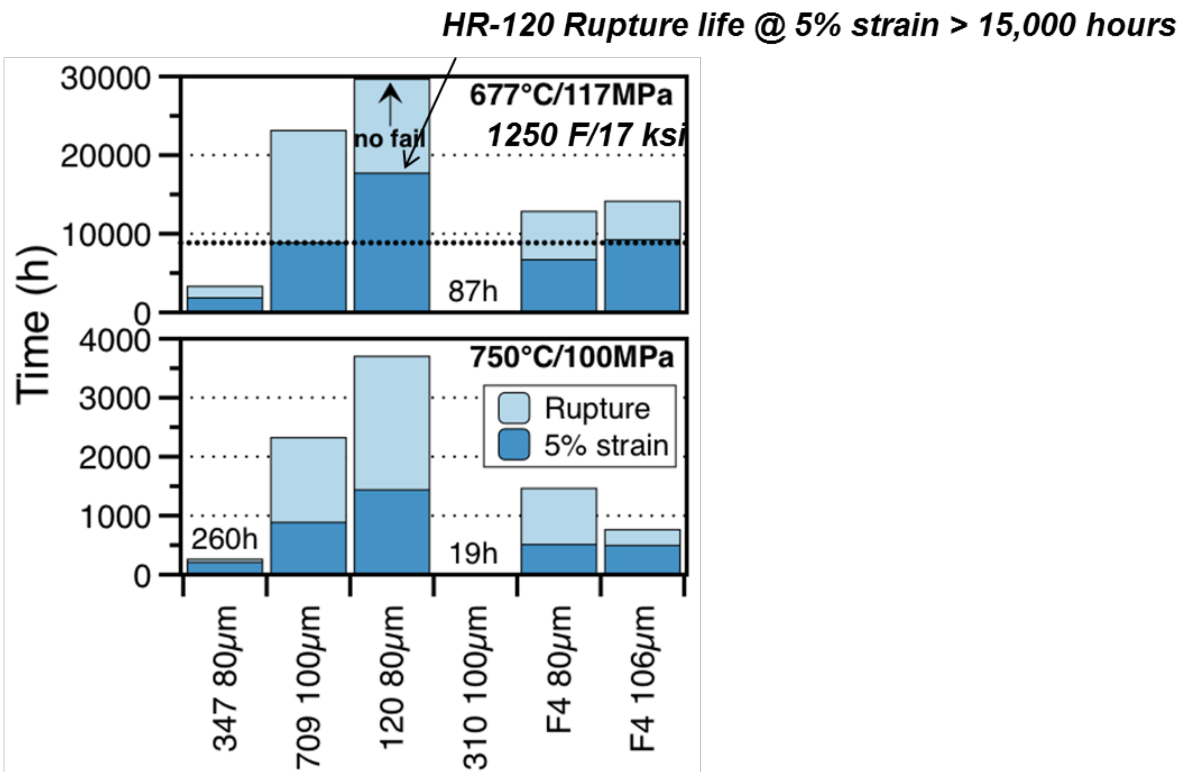

	Pressure Ratio	Peak Stress (ksi)	Peak Contact Pressure (ksi)	Max. Displacement (.001")
C200	4	3.8	3.9	.011
C370	10	13.4	13.6	.31

Figure 164: C370 Integrated Recuperator Strain Life Predictions

The results of the analysis showed that the existing C200 recuperator would have a life greater than 15,000 hours, but may have issues meeting the current C200 life requirements of 80,000 hours. Given this potential life issue and the fact that an external design made prototype testing performance measurement easier, the decision was made to go forward with an external design. This option would be designed and manufactured by external vendor.

10.1.4. Recuperator Design

A high pressure recuperator was designed by an external supplier, under the supervision of the Capstone Turbine technical team. Key aspects of the design activities — including design layout, sizing, CFD and heat transfer analysis, and material selection and life analysis — are discussed and summarized below.

Recuperator Layout and Initial Sizing

An existing compact annular recuperator with primary surface recuperator core was selected for this design and is shown in Figure 166. A high level of performance and extended mechanical life can be achieved with this design.

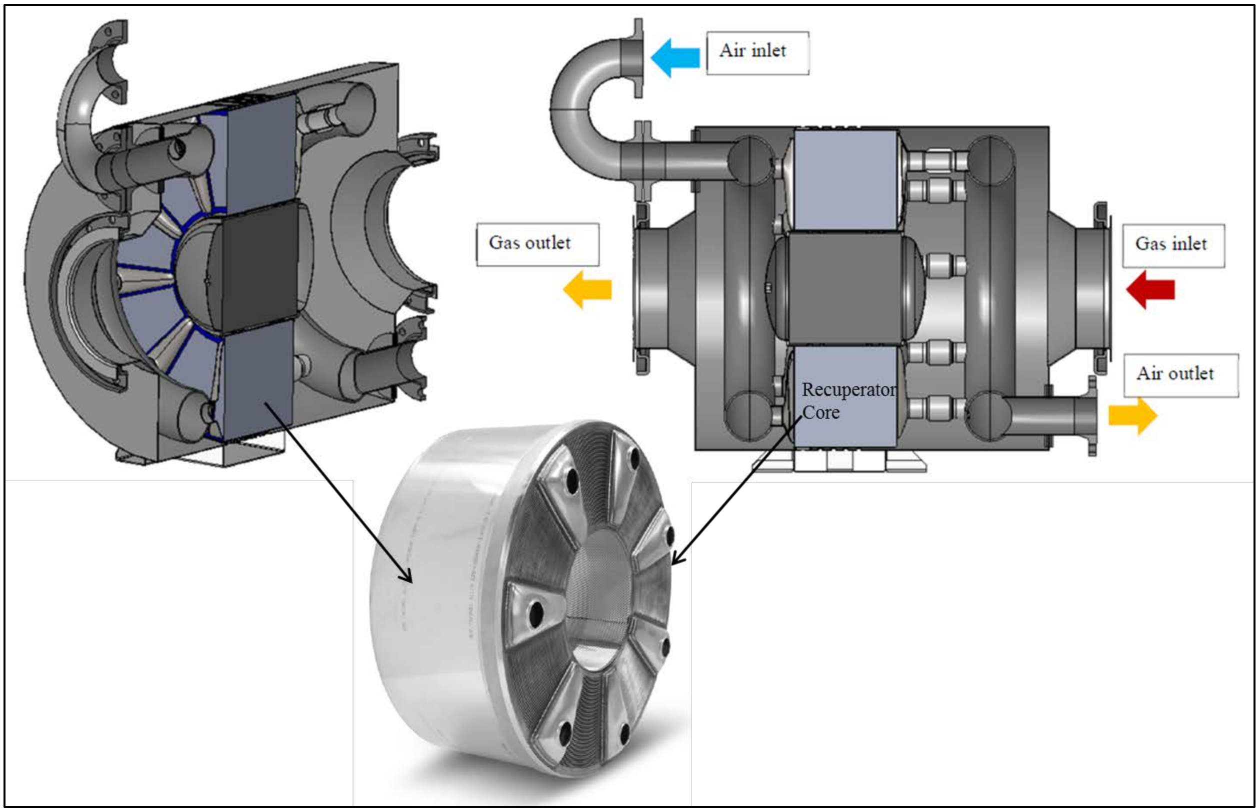

Figure 165: C370 Annular Recuperator Design with Primary Surface Heat Exchanger Core

Based on the operating condition and design requirements — shown in Table 46 — recuperator initial sizing — i.e., core and overall size — are given in Table 47. The choice for the dimensions depends on the expected performance and cost pertaining to the casing manufacturing and assembly procedure.

Parameter	Unit	Value
Air Mass Flow Rate	lbm/s	2.831
Air Inlet Temperature	°F	338
Air Inlet Pressure	psig	129.912
Gas Mass Flow Rate	lbm/s	2.986
Gas Inlet Temperature	°F	1114
Gas Inlet Pressure	psig	0.445
Recuperator Effectiveness	%	> 0.92
Air Side Pressure Drop	%	< 1.5
Gas SISE Pressure Drop	%	< 3

Table 46: C370 Recuperator Operating Parameter and Design Requirement

Dimension/Feature	Unit	Value
Inner Active Diameter	in.	15.16
Outer Active Diameter	in.	35.67
Core Length	in.	11.89
Number of Header		9.00
Equivalent Header Angle	°	11.42
Recuperator External Casing Diameter	in.	37.48
Overall Length	in.	47.24

Table 47: C370 Recuperator Sizing

CFD and Heat Transfer Analysis of the Recuperator Core

A 2D computational domain at the RMS diameter taken between half of a cold header and half of an adjacent hot header was selected. By means of cyclic symmetry, the computational solution is applicable to the remaining cold and hot headers of the recuperator core. The flow domain is discretized into 20 and 30 cells in the tangential and axial directions respectively. Uniform inlet flow velocity and temperature profiles are assumed for boundary conditions.

The resulting flow velocity vectors, pressure, flow and heat exchange foil temperature is presented below. Figure 167 shows the flow velocity vectors which illustrate the counter flow characteristics of the heat exchanger core.

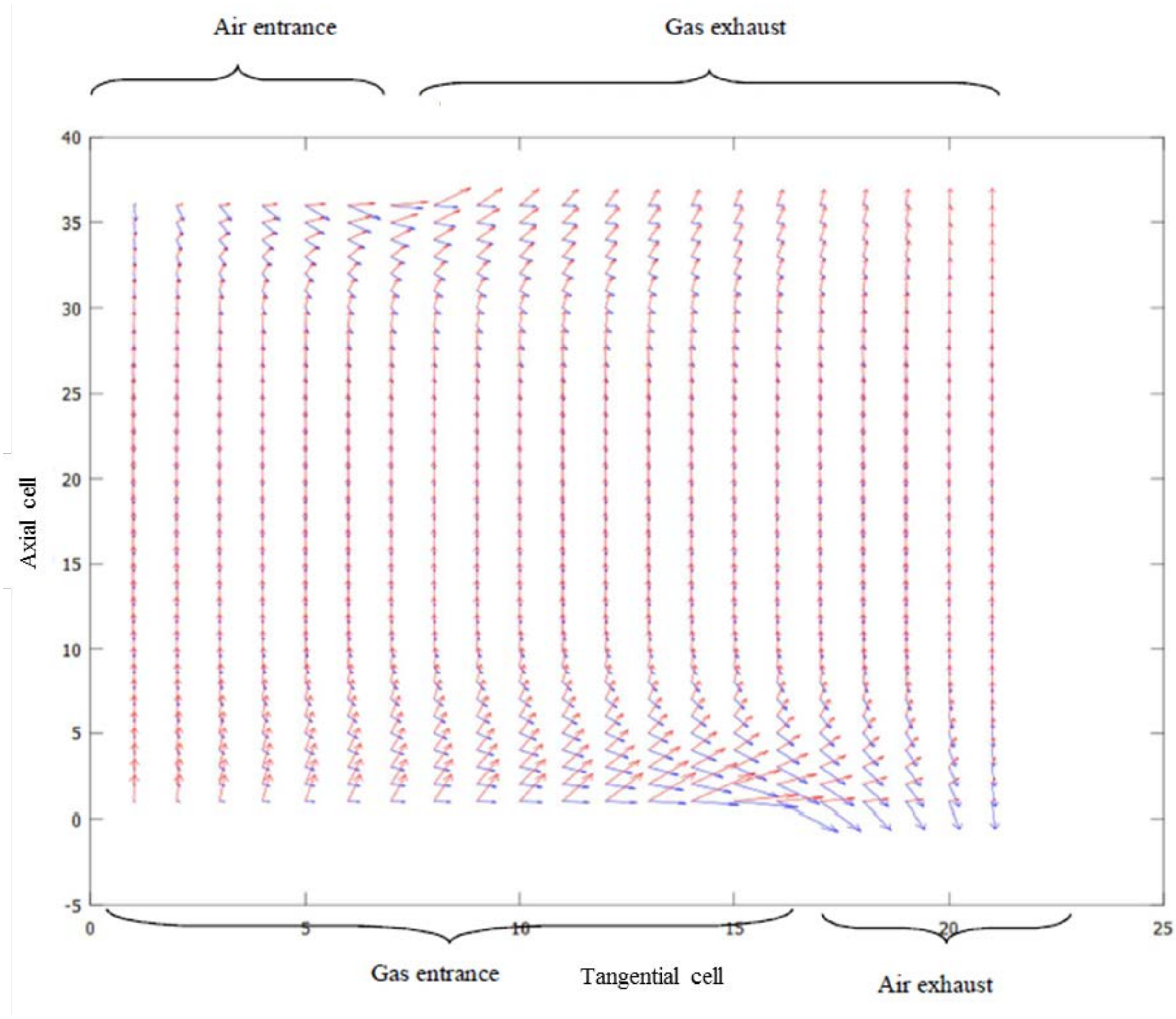

Figure 166: C370 Recuperator Air and Gas Flow Velocity Vector Plot

Figure 168 shows the air side velocity iso-curves in the axial and tangential directions respectively. Figure 169 shows the gas side velocity iso-curves, which is higher than those on the air side due to higher pressure effect causing lower gas density and thus higher velocity.

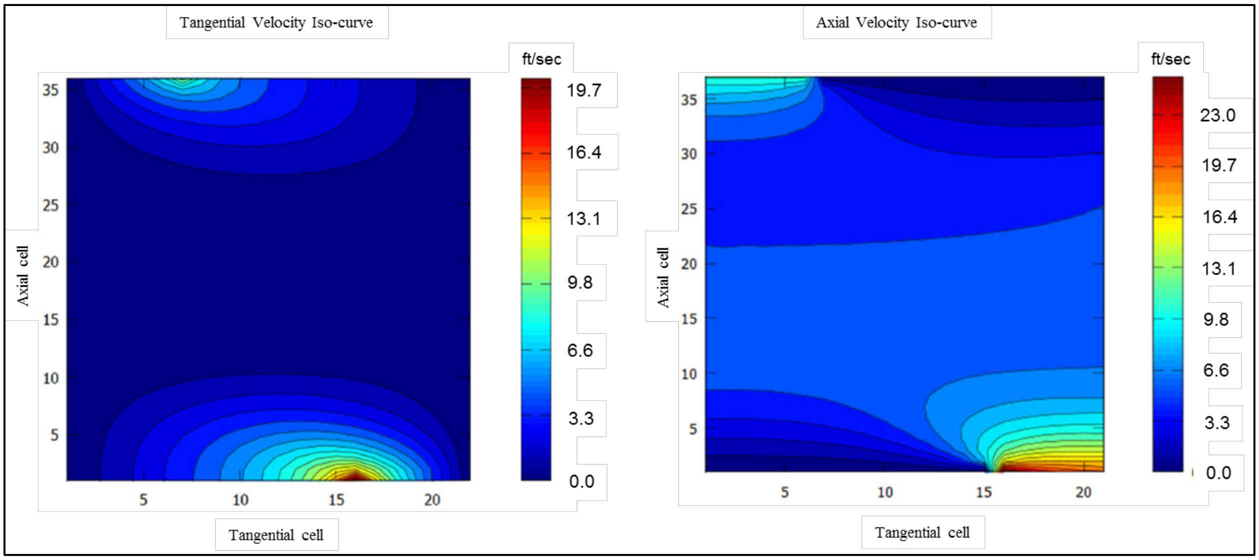

Figure 167: C370 Recuperator Air Side Velocity Iso-Curve

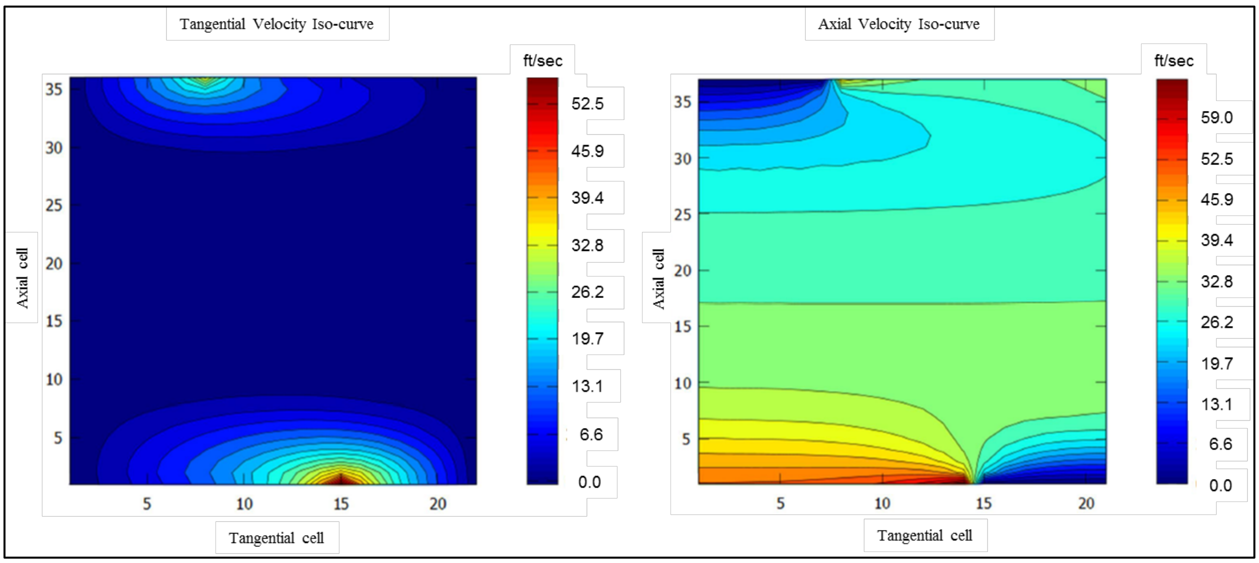

Figure 168: C370 Recuperator Gas Side Velocity Iso-Curve

Figure 170 shows the comparison of the air and gas side pressure loss, which indicate slight high pressure loss on the gas side due to higher velocity.

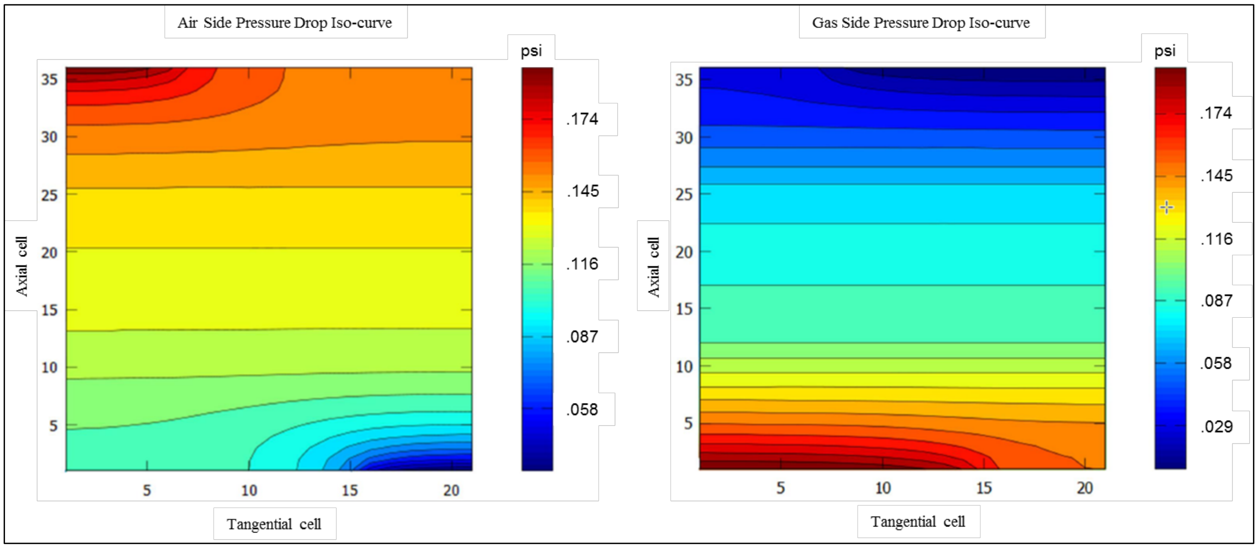

Figure 169: C370 Recuperator Air and Gas Side Pressure Drop Iso-curves

Figure 171 shows the air and gas side temperature distribution, which — compared to temperature distribution of the heat exchanger metal foil shown in Figure 172 —indicates effective heat transfer by convection between the flow and metal.

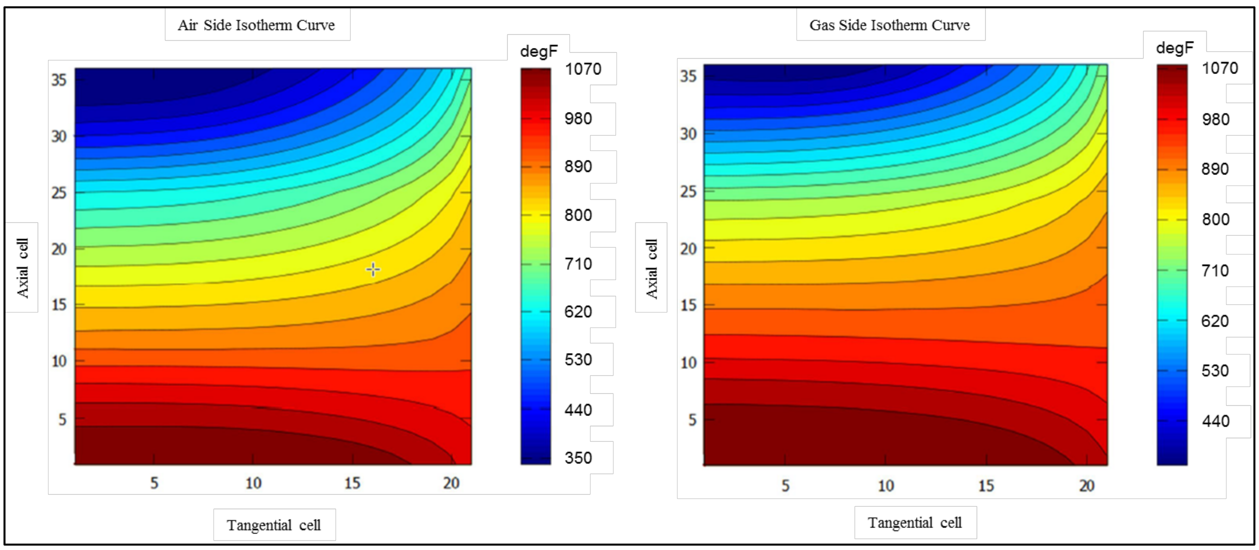

Figure 170: C370 Recuperator Air and Gas Temperature Distribution

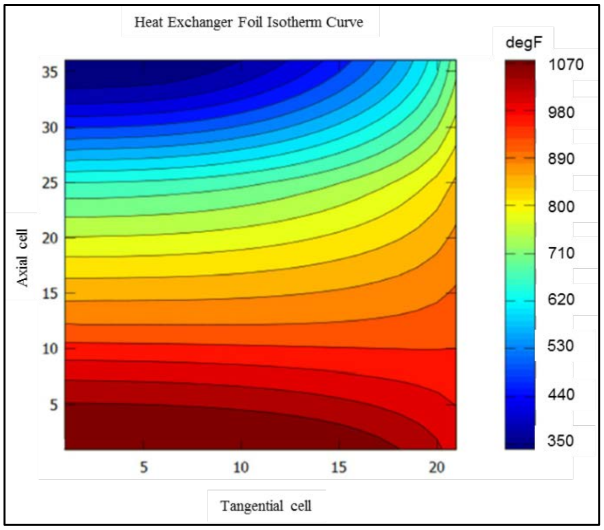

Figure 171: C370 Recuperator Heat Exchanger Metal Foil Temperature Distribution

Heat Exchange Metal Foil Material Selection and Life

A high temperature, high strength and oxidation-resistant alloy was selected to handle high pressure load due to 10:1 pressure ratio and thermal load due to 1114 °F turbine exhaust gas temperature.

Stress analysis shows that the low cycle fatigue (LCF) life limiting location is at the heat exchange core outer diameter with a predicted LCF life greater than 50,000 cycles. The rupture life limiting location is located at the recuperator header, with a predicted rupture life greater than 65,000 hours — or creep life of greater than 10,000 hours. The LCF and rupture lives are deemed acceptable for the recuperator mechanical requirement.

10.2. C370 Integrated Engine Design

10.2.1. Stationary Flow Path Component Design Approach

A comprehensive model of the C370 engine aerodynamic flow path was developed in the CATIA commercial computer aided design (CAD) software. The model incorporated the following components:

- Low Pressure (LP) Spool Compressor Stage Generator and Compressor Inlet
- LP Spool Compressor Stage
- LP Spool Compressor Exit Volute
- Intercooler Inlet Duct
- Intercooler
- High-Pressure (HP) Spool Compressor Inlet Duct
- HP Spool Compressor Stage
- HP Spool Compressor Exit Volute
- Recuperator Cold Side Inlet Duct
- Recuperator
- Combustion Chamber Inlet Duct
- Combustion Chamber Case
- HP Turbine Stage

- HP Turbine Outlet Duct
- LP Spool Turbine Inlet Volute
- LP Spool Turbine Stage
- Recuperator Hot Side Inlet Duct
- Atmospheric Exhaust Duct

The flow path geometry was developed in CATIA as a single volume to maintain continuous connectivity and consistency between components. This model is shown in Figure 173.

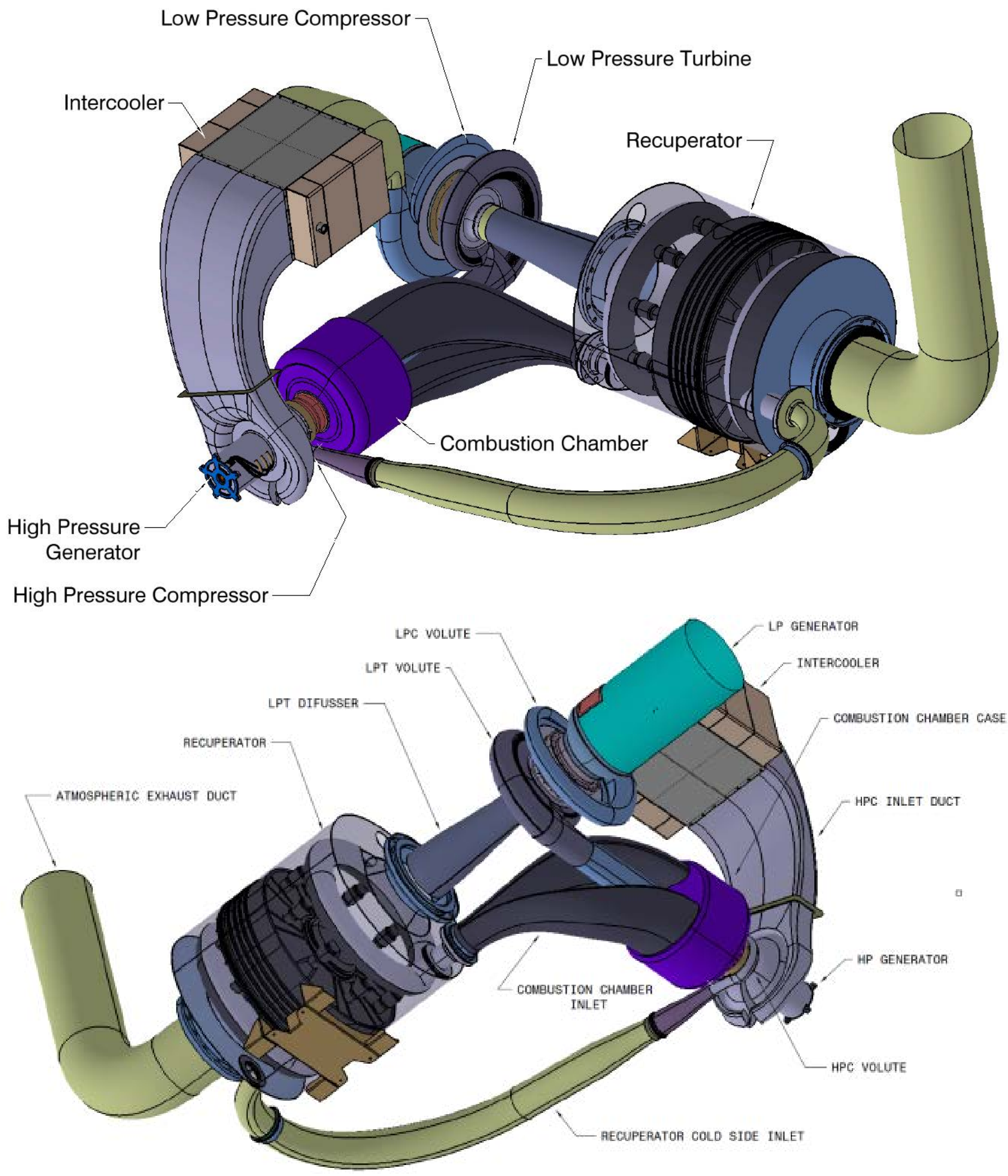

Figure 172: C370 CATIA Model

Performance predictions for each component were generally obtained from steady, 3D CFD analyses at the engine design point cycle conditions using the Ansys CFX Version 16 commercial software. The modeling approach can be summarized as follows:

1. The fluid volume was discretized using hybrid tetrahedral/prismatic meshes with inflation layers adjacent to solid wall surfaces

2. Turbulence was modeled using the shear stress transport (SST) turbulence model with the Ansys Automatic wall treatment to adapt the near-wall physics model to the local mesh density
3. Where surface roughness was deemed significant, walls were modeled as rough with an appropriate roughness height
4. The gas was modeled as an ideal gas with constant specific heats
5. Inlet flow boundary conditions were normally specified as Total Temperature/Total Pressure/Flow Angle
6. Mass flow rate was imposed at outlet boundaries

Where possible, the flow solutions at the outlets of individual components were used directly to specify inlet boundary conditions for the corresponding connected downstream component to fully capture component interactions and the effect of upstream flow non-uniformities on the performance of downstream components.

The following subsections detail the design and analysis results for each stationary flow path component.

10.2.2. HP Spool Compressor Inlet Duct Design

Flow exiting the intercooler core must be transported — with minimum pressure loss and maximum flow uniformity — to the inlet face of the HP compressor. Since the intercooler exit and HP compressor inlet are in opposite directions, the transition ducting connecting them must efficiently reverse the direction of flow. Two general arrangements are possible for this ducting — shown in Figure 174:

a. A gradual 180° “U-bend” ending in an axial compressor inlet. This is referred to as the “Axial” arrangement.
b. A shorter, more highly curved flow path incorporating a radial-to-axial transition plenum immediately upstream of the compressor. This is referred to as the “Radial” arrangement

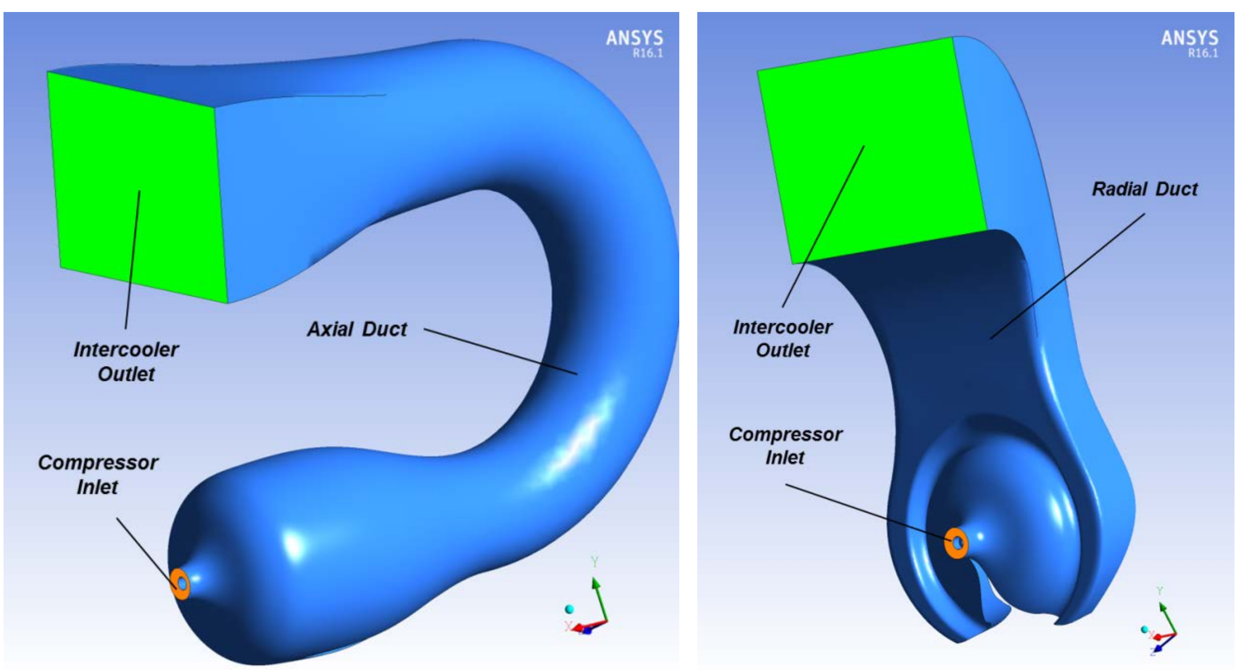

(a) **(b)**

Figure 173: C370 HP Spool Axial (a) and Radial (b) Inlet Duct Geometries

The primary advantage of the axial inlet is the potential for higher flow uniformity due to the relatively low flow path curvature and long axial ducting upstream of the compressor face. However, the longer flow path could result in higher pressure losses. More importantly, the generator design is complicated by its location within the high-pressure flow path. The radial inlet simplifies the generator design by locating it outside the flow path, but careful design of the flow path is required to assure circumferentially uniform flow at the compressor face.

To quantify the advantages — both mechanical and aerodynamic — of each approach, a tradeoff study was completed. Four iterations of both the axial and radial flow path were completed in parallel — with limited generator mechanical design efforts — to identify the principal mechanical challenges associated with each approach. Figure 175 illustrates the history of total pressure loss predictions from CFD analyses of all design iterations. After some fine-tuning of the area distributions in the initial iterations, the minimum pressure loss of the axial configuration was found to be 0.32% and that of the radial configuration was 0.29%. This made it apparent that either configuration will comfortably meet the pressure loss target of 0.6%.

To quantify the flow distortion at the outlet — which would impact the compressor performance — a Distortion Coefficient (DC) was defined as:

$$\mathrm{DC} = \frac{\iint mv^2}{\mathrm{m}\bar{v}^2}$$

Where:

- $\bar{v}$ is the area-averaged velocity at the outlet a
- m is the mass flow rate.

A DC value of unity implies a uniform flow. Values for the axial and radial configurations were 1.020 and 1.013, respectively. Although no target value was set, these values are low and the effect of inflow non-uniformity on the compressor performance is believed to be negligible.

The generator mechanical design investigation validated the perceived advantages of the radial approach. The radial configuration was consequently selected as the go-forward approach.

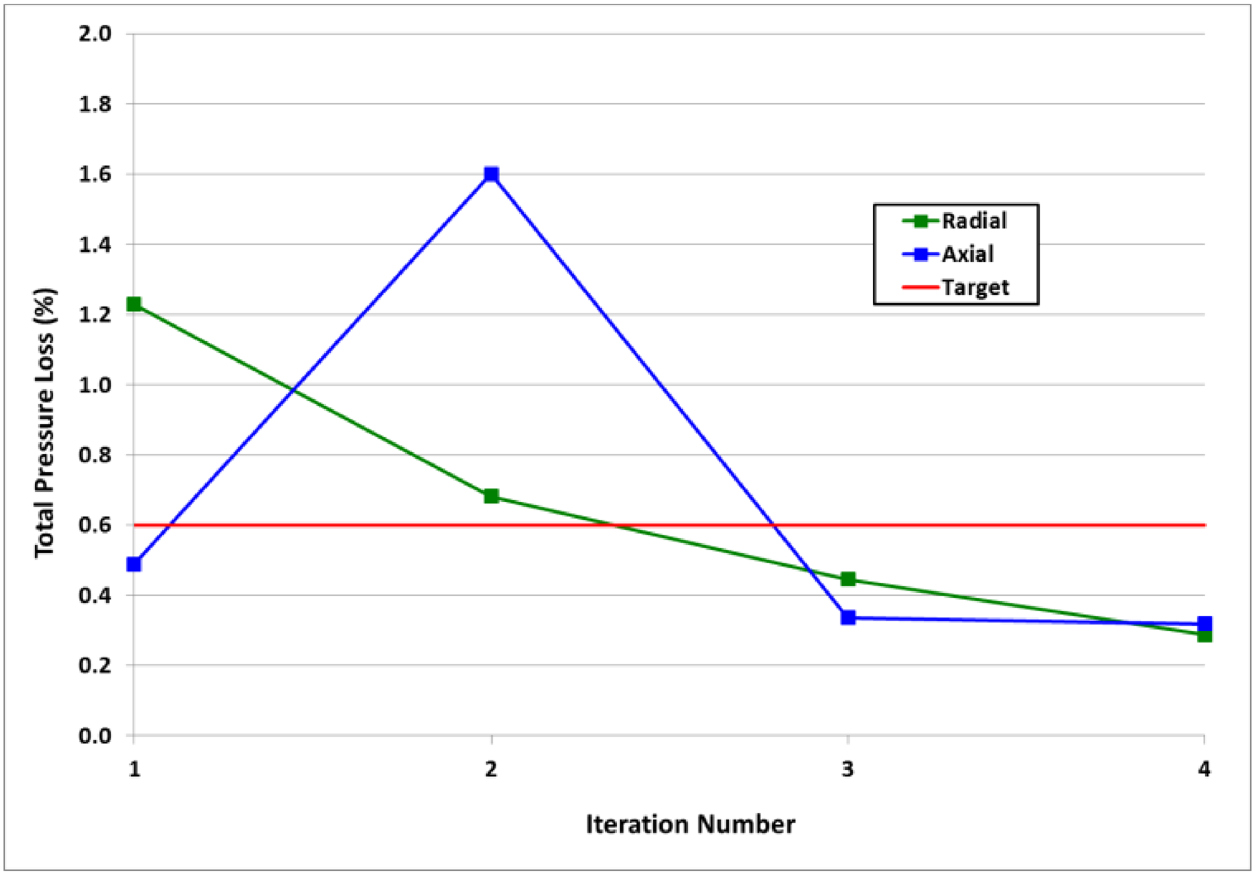

Figure 174: C370 HP Compressor Inlet Duct Pressure Loss History

Flow solution streamlines and velocity contours at several axial locations for the final radial inlet design — iteration 4 — are illustrated in Figure 176 (a). Initial iterations revealed that a splitter was necessary at the bottom of the duct to prevent swirl generation, even with symmetric geometries. Careful control of the area distribution and strong acceleration near the outlet resulted in very good circumferential uniformity and low losses. The majority of the losses are produced near the outlet due to the higher flow velocities and the flexible coupling, as illustrated in Figure 176 (b). To minimize flow separation in the gap between the ends of the flexible coupling, a fairing was added over the aft portion. Slight additional improvements in flow uniformity are possible by adding vanes in the radial-to-axial transition, but these were deemed unnecessary.

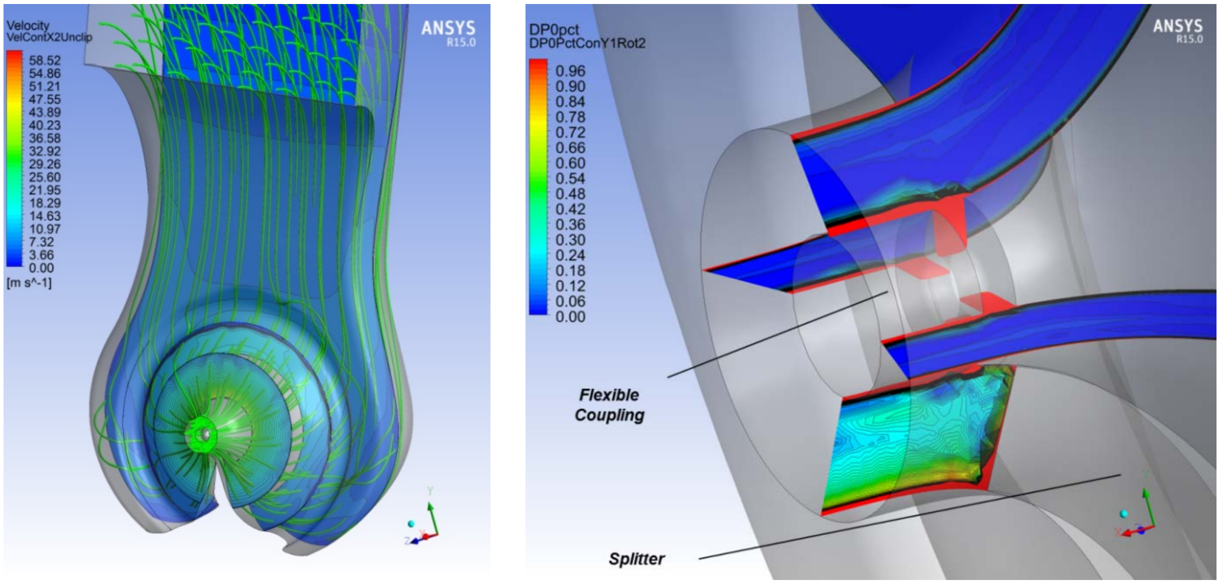

(a) Solution Streamlines and Velocity Contours **(b) Total Pressure Loss Contours Near Outlet**

Figure 175: C370 HP Compressor Inlet Duct Flow Visualization

10.2.3. LP Spool Compressor Inlet Involute Design

Similar to the high pressure compressor discharge, the low pressure compressor diffuser outlet flow must be collected and efficiently transported to the intercooler inlet face. In addition to the lowest possible pressure losses, high flow uniformity is required to maximize the intercooler performance. The complete transition ducting from the diffuser discharge was developed as a connected assembly of a circular cross-section volute and circular-to-rectangular duct connecting the volute outlet and intercooler inlet planes.

The design procedure developed for the HP compressor volute and recuperator cold side inlet duct was applied to the LP compressor volute and intercooler inlet duct designs with two primary modifications.

One — since the C250 compressor diffuser was previously developed with a wedge-type diffuser with a thick “cut-off” trailing edge — the diffuser required some modification near the trailing edge for adequate flow around the volute tongue. It is well known that rounding of the vane pressure side trailing edge can reduce the wake size and subsequent flow losses. Furthermore, since the C370 design speed is below that of the C250 engine, some performance improvement potential exists to modify the base diffuser vane shape for the new operating condition. For these reasons, a wedge diffuser design procedure, including controls to tailor the shape of the trailing edge, was incorporated into the 1D volute design tool. Figure 177 illustrates the user interface.

Design Description	Sample Diffuser	

PRIMARY INPUTS		
Axis of Rotation	+Z	
Contour Trailing Edge?	No	
Rotation	Clockwise	
Auto Turbogrid Output	On	
Leading Edge R (R3)	in	4.0748
Trailing Edge R (R5)	in	11.5
Leading Edge Radius	in	0.015748
Vane Stagger Angle Alpha	deg	16.6750919
Gas Path Divergence Angle (2*Theta)	deg	8.94766
Total Throat Area	in^2	2.813256
Number of vanes	---	19
CFD Inlet R (< R3)	in	3.4
CFD Outlet R (> R5)	in	11.61417
Hub Z	in	0
CFD Inlet Width	in	0.38
Number of points along vane surface for Turbogrid output	---	201
Number of leading edge points for Turbogrid output	---	21

Trailing Edge Contour Bezier Control Point Inputs	
Pt 1 % L	70
Pt 2 % L	75
Pt 3 %L	90
Pt 3 % Thickness	70
Pt 4 % Thickness	10

OUTPUT

Summary		
Throat Diameter	in	0.4701
Vane Height	in	0.3150
Vane Divergence Angle	deg	9.9997
Vane Stagger Angle at LE Center	deg	72.604
Vane Outlet Stagger Angle	deg	19.764
L/W	---	18.0454
Area Ratio	---	3.8532
Throat Aspect Ratio	---	1.4926

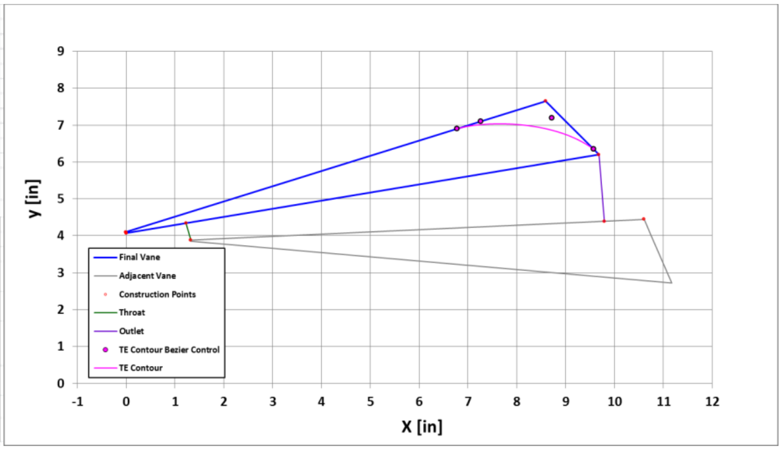

Figure 176: Wedge Diffuser Design Tool Example

Two, the intercooler was incorporated into the flow model. The intercooler was expected to have a significant effect on the upstream flow field due to the high flow resistance associated with the array of narrow flow passages required for adequate heat transfer. This made it important to include the intercooler for an accurate estimate of the intercooler inlet duct pressure loss and flow distribution. Furthermore, incorporating the intercooler directly would allow the most accurate determination of the intercooler pressure loss.

The intercooler was modeled as a porous medium using a simple directional loss model, which applies an appropriate resistance coefficient in the primary flow direction and a much higher resistance coefficient in the transverse direction. This allows a simulation of channel flow whereby the flow direction is constrained to the direction of the channels. Since the intercooler is sized assuming relatively uniform flow, the porous medium modeling coefficients were initially determined using an intercooler-only CFD model with uniform inlet boundary conditions. The porous medium coefficients were adjusted until the predicted pressure loss from the CFD model matched the design target. These coefficients were then used in the full model. This resulted in the pressure loss predicted in the full model representing a direct estimate of the as-designed — or operating — pressure loss.

The porous medium model does not resolve the details of the heat transfer surfaces, so the heat transfer effectiveness of the intercooler could not be directly estimated using this approach. In lieu of direct modeling, an indirect approach was taken using Capstone's proprietary heat transfer model for the C250 recuperator. Since any pressure loss above the design target implies an additional flow blockage, the model was used to determine the area reduction necessary to achieve the same relative increase in pressure loss from the nominal operating condition. This area reduction was then used in the effectiveness calculation to estimate the change in effectiveness.

Similar to the HP compressor volute approach, a single blade passage model of the LP compressor impeller and diffuser was developed and run at the design flow conditions. The model is illustrated in Figure 178. The calculated pressure ratio and efficiency were 4.03 and 82.77%, respectively, both of which exceed the design targets. A second model was then developed incorporating the compressor diffuser, volute, intercooler inlet duct, intercooler core, and a short outlet volume, as shown in Figure 179. This model was then run at the design flow conditions using diffuser inlet conditions obtained from the single blade compressor stage CFD results. Due to the higher pressure ratio — hence greater impeller tip flow distortion — than the HP compressor stage, a fluid profile inlet condition was used, in which the total pressure, total temperature, and flow angle varied from hub to tip for an accurate representation of the impeller outlet flow field.

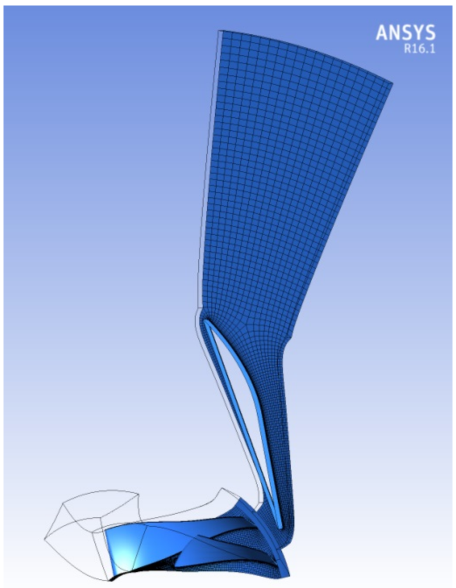

Figure 177: C370 LP Compressor Stage CFD Model

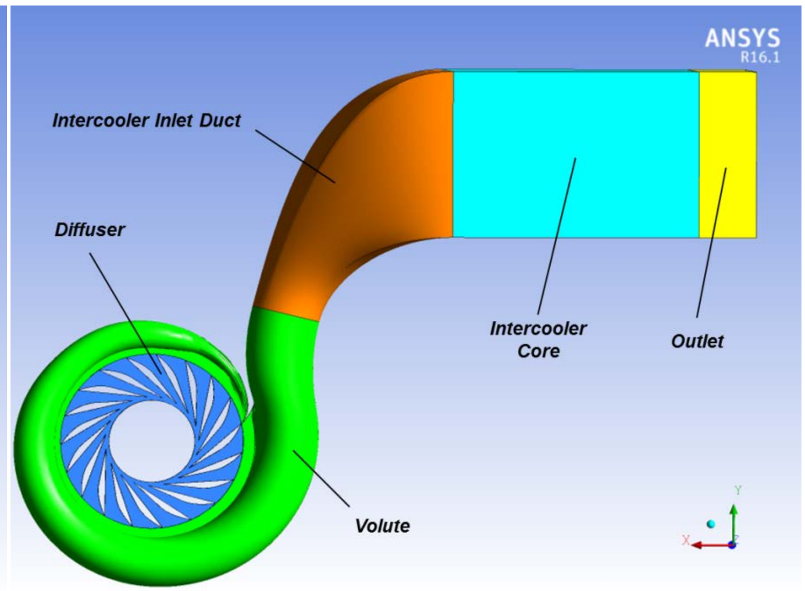

Figure 178: C370 LP Compressor Volute and Intercooler Model

The volute and intercooler inlet duct flow solutions are illustrated in Figure 180. The volute flow field is exhibits significantly higher non-uniformities than the HP compressor volute and a strong "jet-wake" pattern at the discharge of the diffuser, due to the generally higher velocities associated with the higher pressure ratio compressor as well as the thicker vane. Although the diffuser vane trailing edge contouring does appear to allow the flow to remain attached for some of the vanes, sizeable wakes are present for most vanes. The high-speed jets at the diffuser discharge impinge on the outer wall of the scroll and mix with the swirling scroll flow to generate higher than expected losses.

An attempt was made to reduce the volute losses by increasing the diffuser length approximately 50% to lower the diffuser outlet velocities. Unfortunately, the losses were not found to be measurably lower. Since this had the negative effect of increasing the volute size significantly — due to the lower diffuser outlet circumferential velocities — this idea was abandoned. The calculated pressure loss for the volute only was 2.91%.

The short distance from the volute outlet to the intercooler inlet face requires a circular-to-rectangular transition duct with relatively high curvature and rapid area increase. Solution streamlines for this geometry — shown in Figure 180 — indicate that significant flow separation is present.

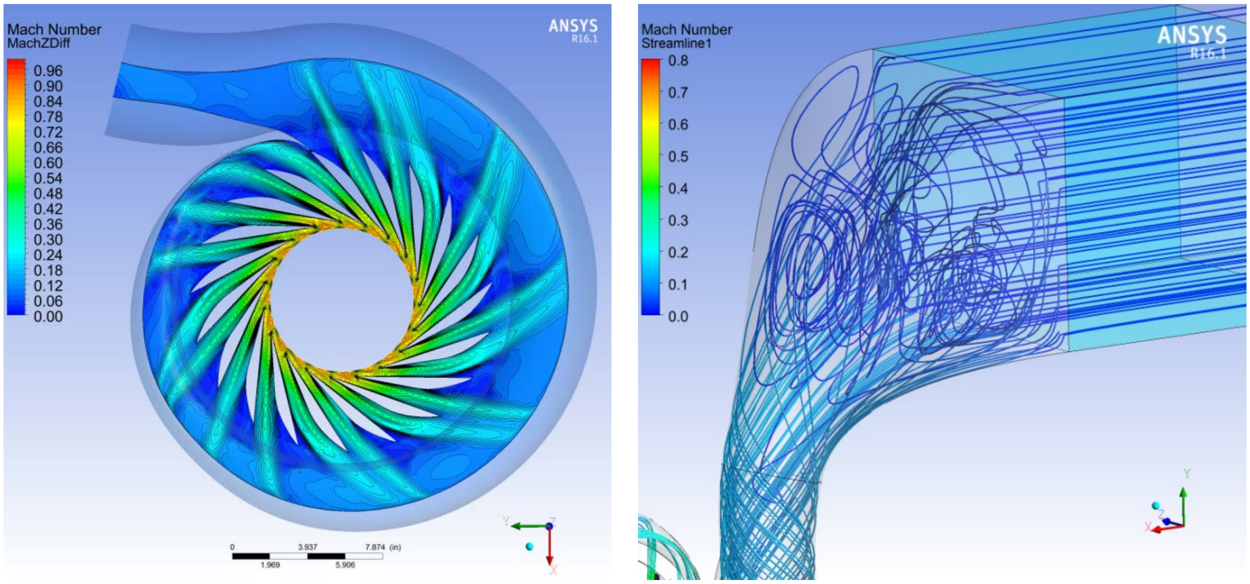

Figure 179: C370 LP Compressor Volute and Intercooler Inlet Duct Flow Solution Visualizations

Table 48 summarizes the volute and intercooler inlet duct performance estimates.

		Target	As-Designed
Compressor Stage Total-to-Total Pressure Ratio	**---**	4.0	4.03
Compressor Stage Total-to-Total Efficiency	**%**	82.5	82.77
Volute Total Pressure Loss	**%**		2.91
Intercooler Inlet Duct Total Pressure Loss	**%**		0.61
Total Volute + Intercooler Inlet Duct Total Pressure Loss	**%**	1.5	3.52

Table 48:C370 LP Compressor Volute and Intercooler Duct Performance Summary

10.2.4. LP Spool Turbine Inlet Involute Design

The approach taken for the LP turbine volute design differed substantially from that of the HP and LP compressor volute approaches. There was a strong desire to use the existing C250 turbine nozzle unmodified to minimize design effort and cost. Typical turbine nozzles mated with volutes have non-zero leading edge blade angles for compatibility with the swirl generated by the volute scroll. Since the C250 nozzle was developed for the minimally swirling combustor exit flow field, the leading edge blade angle is near zero which is not optimum for a typical turbine volute. To address this issue, flow velocities near the nozzle leading edge were minimized by substantially increasing the scroll flow areas, thereby reducing the sensitivity to any flow mismatch (non-optimum incidence).

This proved to be a very successful approach. Figure 181 illustrates the geometry and solution Mach number contours at an axial plane corresponding to the nozzle mid-span. The Mach number is circumferentially uniform and generally below 0.1 within the entire scroll volume, resulting in a very low predicted pressure loss of 0.052% from the inlet to the nozzle leading edge radius. Since the simulations were run with uniform inlet boundary conditions, a conservative factor of 5 was applied to the calculated pressure loss for cycle modeling purposes in order to account for additional losses due to upstream flow non-uniformity. Hence, the maximum design point pressure loss is believed to be 0.26%.

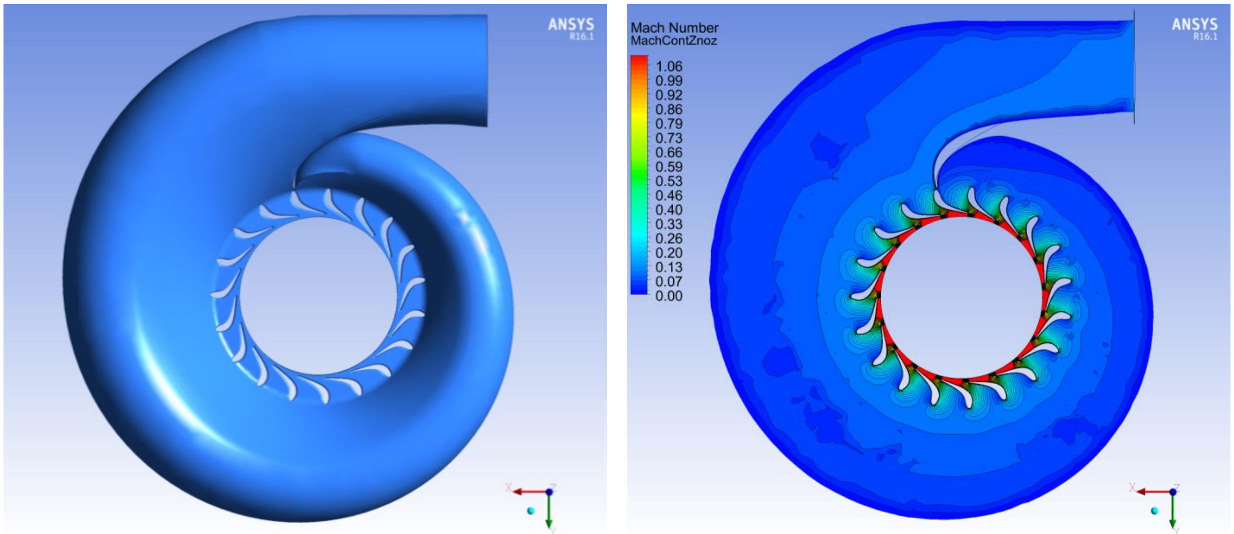

(a) Geometry (b) Mach Number Contours

Figure 180: C370 LP Turbine Volute Geometry (a) and Flow Visualization (b)

10.3. C370 Prototype Engine Analysis Results

10.3.1. Predicted Performance of Prototype

The as-designed performance estimates discussed above for each flow path component were used as inputs to the design cycle model to estimate the as-designed engine performance. Use of the design cycle model assured complete consistency of the as-designed performance estimate and the design target.

Design Summary				
Component	Unit	Target	As-Design	
LPC Stage Pressure Ratio		4.0	✔	4.0
LPC Stage Efficiency	%	82.5	✔	82.8
LPC Volute and IC Inlet Duct P Drop	%	1.50	✘	3.52
IC P Drop	%	1.50	✔	1.50
IC Effectiveness		0.92	✔	0.92
IC to HPC P Drop	%	0.60	✔	0.29
HPC Stage Pressure Ratio		2.6	✔	2.6
HPC Stage Efficiency		84.60	✔	84.90
HPC Volute and REC Inlet Duct P Drop	%	1.50	✘	2.89
REC Cold Side P Drop	%	1.50	✔	0.66
REC Effectiveness		0.92	✔	0.92
REC to Combustor P Drop	%	0.30	✔	0.04
Combustor P Drop	%	2.50	✘	3.30
HPT Stage Pressure Ratio		2.4	✔	2.4
HPT Stage Efficiency		87.26	✘	87.1

HPT to LP Turbine Duct P Drop	%	0.60	✔	0.18
LPT Volute P Drop	%	1.50	✔	0.26
LPT Stage Pressure Ratio		3.7	✔	3.7
LPT Stage Efficiency		87.4	✔	87.4
LPT to Recuperator Duct P Drop	%	1.05	✔	0.24
Recuperator Hot side P Drop	%	3.00	✔	2.18
LP Generator	%	97.5	✔	97.5
HP Generator	%	97.5	✔	98.0

Table 49 summarizes the component performance values for the flow path stationary ducts, turbomachinery stages, and heat exchangers, respectively.

Design Summary				
Component	**Unit**	**Target**	**As-Design**	
LPC Stage Pressure Ratio		4.0	✔	4.0
LPC Stage Efficiency	%	82.5	✔	82.8
LPC Volute and IC Inlet Duct P Drop	%	1.50	✘	3.52
IC P Drop	%	1.50	✔	1.50
IC Effectiveness		0.92	✔	0.92
IC to HPC P Drop	%	0.60	✔	0.29
HPC Stage Pressure Ratio		2.6	✔	2.6
HPC Stage Efficiency		84.60	✔	84.90
HPC Volute and REC Inlet Duct P Drop	%	1.50	✘	2.89
REC Cold Side P Drop	%	1.50	✔	0.66
REC Effectiveness		0.92	✔	0.92
REC to Combustor P Drop	%	0.30	✔	0.04
Combustor P Drop	%	2.50	✘	3.30
HPT Stage Pressure Ratio		2.4	✔	2.4
HPT Stage Efficiency		87.26	✘	87.1
HPT to LP Turbine Duct P Drop	%	0.60	✔	0.18
LPT Volute P Drop	%	1.50	✔	0.26
LPT Stage Pressure Ratio		3.7	✔	3.7
LPT Stage Efficiency		87.4	✔	87.4
LPT to Recuperator Duct P Drop	%	1.05	✔	0.24
Recuperator Hot side P Drop	%	3.00	✔	2.18
LP Generator	%	97.5	✔	97.5
HP Generator	%	97.5	✔	98.0

Table 49: C370 Stationary Duct Component Pressure Losses

To update the performance with the latest design parameters of individual components, following processes were applied:

1. All duct design information was updated and included in the performance prediction
2. All stationary components — such as intercooler, recuperator, and generators — were included in the performance update
3. Through design analyses, most of compressor and turbine stage performance was predicted to be better than target, but the actual component performance should be evaluated at the component level. Without doing component level tests, a more conservative approach was adopted. The performance update used the target value for compressor and turbine stages except high pressure turbine stage. This information will be updated as soon test data is available.

Description	Unit	Target	As-Design
Gen Power	kW	370	✓ 390.4
Gen Efficiency	%	42	✓ 42.9

Table 50 summarizes the estimated engine performance. The efficiency is expected to meet the design target of 42.0%, while the power is expected to exceed the design target of 370kW.

Description	Unit	Target	As-Design
Gen Power	kW	370	✓ 390.4
Gen Efficiency	%	42	✓ 42.9

Table 50: C370 Estimated As-Designed Engine Performance

11. Attachment 1: List of Acronyms

AFR: Air-to-Fuel Ratio. See FAR.

AFT: Adiabatic flame temperature.

AMTS: Advanced microturbine system.

ATP: Acceptance test procedure. Test(s) that is/are used to verify that components, assemblies, modules, or Microturbine system meets specified requirements within a prescribed range. This term is also used generically to refer to the test itself. One of these tests is designed for each major subassembly in the Microturbine. The test is performed on each instance of the subassembly after its final assembly and before the subassembly is approved by Capstone for customer use.

BTU: British thermal unit. A measure of heat energy; the amount of heat energy necessary to raise the temperature of one pound-mass of water one degree Fahrenheit (1 °F).

CARB: California Air Resources Board.

CDR: Critical design review; a review that is held to determine whether or not the product is ready to enter the next stage of production.

CFD: Computational fluid dynamics. **CFD** is a branch of fluid mechanics that uses numerical analysis and algorithms to solve and analyze problems that involve fluid flows

CHP: Combined heat and power; a system which produces both thermal and electrical energy.

CRMS: Capstone Remote Monitoring Software. Software tool used to configure microturbine system software settings.

DG: Distributed generation.

DN: Non-dimensional bearing performance characteristic number

DOE: Department of Energy.

dP: Pressure drop.

DSP: Digital signal processor.

EDM: Electrical discharge machining

ER: Equivalence ratio.

ES: Engineering Specification.

ESR: Equivalent series resistance.

FAR: Fuel-to-air ratio; the ratio of fuel to air in the gas mixture — on a mass basis —that is burned in the combustor. This ratio will vary according to operating requirements such as load demand.

FE: Finite element.

GCM: Generator control module; assembly — ICB, IGBTs, and other hardware —used to control the MEM and convert power produced at generator leads into DC loaded on system bus.

HCI: High current inverter; a 400 A inverter system based on Capstone microturbine technology.

HEV: Hybrid electric vehicle.

HHV: Higher heating value.

HP: (1) High pressure, as gas or fuel; (2) Horse power; generally abbr. hp.

HPC: High pressure compressor (wheel); component of the high pressure spool

HPT: High pressure turbine (wheel); component of the high pressure spool

HRM: Heat recovery module; a module designed to recover thermal energy from exhaust gases.

IC: Intercooler

ICB: Inverter control board; printed circuit board used to control electrical modules such as GCM and LCM.

iCHP: Integrated combined heat and power; an integrated system that generates both thermal and electrical power, e.g. an integrated microturbine and heat recovery module.

ID: Inner diameter

IGBT: Isolated gate bipolar transistor; used bi-directionally in power electronics modules to convert input AC to system DC and to convert system DC to output AC waveform.

ISO: International Organization for Standardization.

LCF: Low cycle fatigue

LCM: Load control module; assembly — ICB, IGBTs, and other hardware —used to convert power on DC bus into AC output to connected loads.

LE: Leading edge; front edge of a rotor blade

LP: Low pressure; applies to gas or fuel

LPC: Low pressure compressor (wheel); component in the low pressure spool

LPT: Low pressure turbine (wheel); component in the low pressure spool

MEM: Microturbine engine module; assembly consisting of engine, generator, associated hardware, and frame.

MW-hr: Megawatt hour

MRD: Market Requirements Document.

NG: Natural gas.

NO_x: Oxides of Nitrogen; the sum of NO and NO_2.

Pamb: Ambient pressure

POC: Proof of concept; syn. prototype.

PSR: Perfect stirred reactor

PZ: Primary zone

ppm: Parts per million; used to define the concentration of gaseous pollutant species.

ppmVd: Parts per million on a dry volumetric basis; used to define the concentration of gaseous pollutant species.

PSIA: Pounds per square inch absolute; equal to psig (gage) + atmospheric pressure.

PSIG: Pounds per square inch gage. 0 psig = atmospheric pressure (14.7 at sea level). 1 psig = 27.707 in. of water.

PWM: Pulse Width Modulation; a control technique that varies the duty cycle of a digital electrical waveform to effect a change in an average value of an analog variable.

RBS: Rotor-bearing system

RMS: Root-mean-square; the square root of the sum of the squares. AC voltage or current: The square root of the mean of the square of the voltage or current, during a complete cycle. AC voltages are expressed as RMA unless otherwise specified. Also abbr. rms.

RPM: Revolutions per minute. Also abbr. rpm.

scf: Standard cubic feet; cubic feet at 1 atmosphere, 68°F.

SoC: System-on-chip; a CPU architecture that integrates ancillary system parts into the main chipset.

SST: Shear stress transport

T-S: Total-to-Static. Also abbr. t-s.

T-T: Total-to-Total. Also abbr. t-t.

Tamb: Ambient temperature; measured by a sensor at the turbine inlet

TE: Trailing edge; rear edge of rotor blade

TET: Turbine exit temperature; the temperature of the exhaust gas, as measured by the thermocouple at the exit of the turbine rotor.

THC: Total hydrocarbons; measure of emissions content

THD: Total harmonic distortion

TIT: Turbine inlet temperature; the temperature of the combustion gases at the entrance to the turbine nozzle.

TLP: Transient liquid phase

TRV: Torque per rotor volume

UCS: Undamped critical speed

UL: Underwriter's Laboratory.

VDE: Verband der Elektrotechnik; German grid interconnect governing body

VFD: Variable frequency drive

VOC: Volatile organic compounds; measure of emissions content